PLACEMENT OF TRAFFIC BARRIERS ON ROADSIDE AND MEDIAN SLOPES

A Dissertation

by

MD RUBIAT FERDOUS

Submitted to the Office of Graduate Studies of
Texas A&M University
in partial fulfillment of the requirements for the degree of

DOCTOR OF PHILOSOPHY

May 2011

Major Subject: Civil Engineering

PLACEMENT OF TRAFFIC BARRIERS ON ROADSIDE AND MEDIAN SLOPES

A Dissertation

by

MD RUBIAT FERDOUS

Submitted to the Office of Graduate Studies of
Texas A&M University
in partial fulfillment of the requirements for the degree of

DOCTOR OF PHILOSOPHY

Approved by:

Chair of Committee,	Harry L. Jones
Committee Members,	Jose Roesset
	Stefan Hurlebaus
	Make McDermott
	Akram Abu-Odeh
Head of Department,	John Niedzwecki

May 2011

Major Subject: Civil Engineering

ABSTRACT

Placement of Traffic Barriers on Roadside and Median Slopes. (May 2011)
Md Rubiat Ferdous, B.S., Bangladesh University of Engineering and Technology;
M.S., Louisiana State University
Chair of Advisory Committee: Dr. Harry L. Jones

Cross median crashes have become a serious problem in recent years. Most of the median cross sections used for divided highways have terrains with steep slopes. Traffic barriers, frequently used on slopes, are generally designed based on the findings obtained from crash tests performed on flat terrain. For barriers placed on roadside and median slopes, vehicle impact height varies depending on the trajectory of the vehicle along the ditch section and lateral offset of the barrier. Thus depending on the placement location on a relatively steep slope, a barrier can be impacted by an errant vehicle at height and orientation more critical compared to those considered during its design. Hence, detailed study of performance of barriers on roadside and median slopes is needed to achieve acceptable safety performance.

In this study, performances of modified G4(1S) W-beam, Midwest Guardrail System (MGS), modified Thrie-beam, modified weak post W-beam, and box-beam guardrail systems on sloped terrains are investigated using numerical simulations. A procedure is developed that provides guidance for their placement on roadside and median slopes. The research approach consists of nonlinear finite element analyses and multi-rigid-body dynamic analyses approach. Detailed finite element representation for each of the barriers is developed using LS-DYNA. Model fidelity is assessed through comparison of simulated and measured responses reported in full scale crash test studies conducted on flat terrain. LS-DYNA simulations of vehicle impacts on barriers placed on flat terrain at different impact heights are performed to identify performance limits of the barriers in terms of acceptable vehicle impact heights. The performances of the barriers are evaluated following the guidelines provided in NCHRP Report 350. Multi-

rigid-body dynamic analysis code, CARSIM, is used to identify trajectories of the vehicles traversing various roadside and median cross-slopes. After analyzing vehicle trajectories and barrier performance limits, a guideline has been prepared with recommendations for the placement of barriers along roadside and median slopes. This guideline is then verified and refined using the responses obtained from full-scale LS-DYNA simulations. These simulations capture the full encroachment event from departure of the vehicle off the traveled way through impact with the barrier.

DEDICATION

To my parents.

ACKNOWLEDGMENTS

I would like to express my deepest gratitude to my advisor, Dr. Jones, and my committee member, Dr. Abu-Odeh, for their excellent guidance, invaluable wisdom, and constant support, encouragement and patience throughout the course of this research. The completion of this dissertation would not have been possible without their support. I express my deepest and sincere thanks to Dr. Roesset, Dr. Hurlebaus, and Dr. McDermott for accepting to serve on my advisory committee. This dissertation has been improved by their comments and fruitful discussions. I also thank Dr. Fry for his fruitful comments and discussions during my defense.

I would like to extend my sincere appreciation to Dr. Bligh for his support, suggestion, discussion, and invaluable wisdom throughout this research. I also like to thank Nauman M. Sheikh for his suggestions and help. I sincerely thank the researchers at Midwest Roadside Safety Facility, in particular Dr. Ronald K. Faller, and at Worcester Polytechnic Institute, in particular Dr. Malcolm H. Ray, for sharing data and answering many questions. I would like to acknowledge the contributions made by researchers and staff at the Texas Transportation Institute. Without them, this achievement would not have been possible. I would also like to acknowledge the Texas A&M Supercomputing Facility's role for allocating enough computing hours to perform large number of simulations on both HYDRA and EOS.

I am greatly indebted to my parents, Mr. Khorshed Alam and Mrs. Ferdous Ara Begum, for their loving care and support throughout my life and especially throughout my academic pursuit. I would like to especially thank my beloved wife, Gul-E-Rukh Ferdousi, for her constant patience and love. This wouldn't have been possible without her support.

Last but not least, I would like to thank everyone at Texas A&M University who played their roles in making this work successful.

TABLE OF CONTENTS

Page

Page

Page

Page

LIST OF FIGURES

Page

Page

Page

Page

Page

Page

Page

Page

Page

Page

LISTS OF TABLES

Page

Page

Page

Page

1. INTRODUCTION

1.1. GENERAL BACKGROUND

Cross median crashes have become a serious problem in recent years. Most of the median cross sections used for divided highways have terrains with steep slopes. In the late 1970s, an analysis of barriers placed on slopes indicated that most guardrails do not perform well when placed on 6:1 or steeper slopes (*1*). Since then, the vehicle fleet has changed dramatically, with significant increase in the percentage of light trucks and sport utility vehicles. Designs of roadside barriers have changed based on the findings obtained from crash tests performed on flat terrain. However, it is unclear how these changes affect the performance of roadside barriers on sloped terrain.

Roadside safety hardware including barriers are evaluated following the guidelines provided in NCHRP Report 350, prepared by TTI researchers (*2*). The Federal Highway Administration (FHWA) mandated the use of NCHRP Report 350 approved barriers on National Highway System (NHS) by October 1998 (*3*). The barriers on NHS are required to successfully pass the safety evaluation criteria for the test conditions specified in Report 350. The basic test condition, defined in the Report 350, consists of a 2000-kg pickup truck (2000P) impacting a barrier at 100 km/h (62 mph) and 25 degrees and an 820-kg (1,800-lb) passenger car (820c) impacting the barrier at 100 km/h (62 mph) and 20 degrees. Structural adequacy, post-impact vehicle trajectory, and occupant risk factors are three categories of safety evaluation criteria defined in Report 350 guidelines. There is a large body of full-scale crash tests performed following NCHRP Report 350 guidelines to demonstrate acceptable impact performance of commonly used barrier systems on flat, level ground. However, a very limited number of crash tests have been performed to evaluate the performance of these barriers systems on sloped terrain.

This dissertation follows the style of *Journal of Transportation Research Record.*

In addition to full scale crash tests, finite element techniques are widely used to evaluate the performance of roadside safety devices. Due to the availability of powerful computers, roadside safety researchers are overwhelmingly using LS-DYNA, a commercially available finite element software package, to simulate vehicular impacts with roadside safety features. Public domain finite element models of 2000P and 820c test vehicles, specified in the NCHRP Report 350, are available in LS-DYNA. These models were originally developed by the National Crash Analysis Center (NCAC). Other than being state-of-the-art impact analysis software, the availability of public domain models (vehicles and hardware) with adequate modeling details makes LS-DYNA the finite element code of choice for this research.

In this study, the performances of five widely used guardrails and barriers placed on roadside and median slopes are investigated using computer simulations. To properly evaluate these guardrail systems, suitable FE representations must first be developed in LS-DYNA. A significant component of the current study addresses preparing quality FE guardrail LS-DYNA models. While public domain FE models for the needed vehicles exist, this is not the case for some of the selected guardrail systems. Although FE models for most of the components used in selected guardrail systems are readily available, preparing quality FE model for each system requires component assembly, defining contact algorithms, and modifications to attain satisfactory simulation results. To ensure reliable results, model fidelity is assessed through comparison of simulated and measured responses reported in full scale crash test studies conducted on flat terrain. The methodology used in drawing comparisons between simulated and actual behavior is addressed later in the dissertation.

Vehicle impact height is one of the most important factors in evaluating performance of barriers. For barriers placed on roadside and median slopes, vehicle impact height varies depending on the trajectory of the vehicle along the ditch section and lateral offset of the barrier. LS-DYNA simulations of vehicle impacts on barriers placed on flat terrain at different impact heights are performed to identify performance limits of the barriers in terms of vehicle containment heights. A commercially available

multi-rigid body dynamic analysis software package, CARSIM, is used to determine trajectories of the vehicles traversing along various roadside and median cross-slopes. Setup for the vehicle dynamic analysis and median configurations, vehicle types, encroachment angles and speeds selected for this study are shown in Figure 1.1. After analyzing vehicle trajectories and barrier performance limits, a guideline has been prepared with recommendations for the placement of barriers along the roadside and median slopes. This guideline is than verified and refined using the responses obtained from full-scale LS-DYNA simulations that capture the full encroachment event from departure of the vehicle off the traveled way through impact with the barrier.

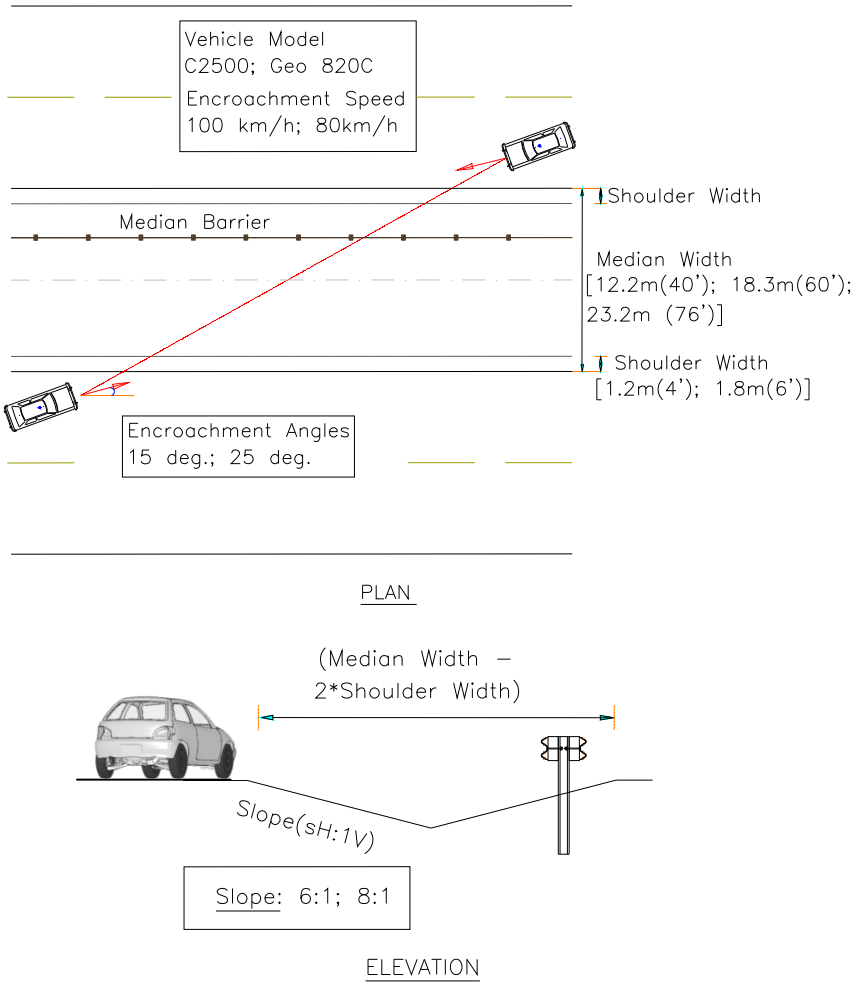

Figure 1.1 Vehicle dynamic analysis setup with parameters selected for the study.

1.2. OBJECTIVE

The primary objective of this study is to develop comprehensive recommendations for the placement of five widely used guardrails and barriers on roadside and median slopes. This objective is attained through the creation of a good quality LS-DYNA FE model for each barrier system and to use them in simulated impacts of NCAC vehicles with the barriers under conditions which mimic those occurring in the collisions of a vehicle on the guardrail on sloped terrain.

1.3. SCOPE OF STUDY

The study focuses on the placements of Modified Strong-post G4(1S) W-beam, Midwest Guardrail (MGS), Modified Thrie-beam, Modified Weak-post W-beam, and Box-beam guardrail Systems on sloped terrain. It investigates performance limits of theses guardrails when impacted by a pickup truck and a passenger car at different impact heights following the NCHRP report 350 guidelines. Trajectories of the pickup truck and the passenger car along various roadside and median slopes are then investigated to determine acceptable guardrail placement locations.

1.4. ORGANIZATION

This dissertation is organized into nine major sections.

Section 1 gives a general introduction to the problems related to the placements of existing barrier systems on roadside and median slopes. The objectives, scopes and organization of the dissertation are also presented.

Section 2 presents a literature review of commonly used barrier types, existing guidelines for performance evaluation of barriers, previous crash tests performed on guardrails placed on flat terrain, and past studies and existing recommendations related to the placements of barriers on sloped terrain. The section also provides an overview of

past studies related to the development of quality guardrail FE models and trajectory analyses of vehicles traversing sloped terrains.

Section 3 describes various parameters selected for the study and research methodology used for the evaluation of performance of barriers on roadside and median slopes.

Brief description of the NCAC developed vehicle models and the modifications to these models made for this study is presented in Section 4. Material models and properties used for various components of each guardrail systems are also discussed. The section also provides detailed description of the development process and validation approach used in developing quality FE models for five guardrail systems.

Numerical impact simulations performed to determine override and underride limits for each of the selected guardrail systems are presented in Section 5.

Section 6 discusses the methodology used to analyze the trajectories of vehicles traversing various ditch configurations using multi-rigid-body dynamic analysis code, CARSIM. Description of the vehicle properties used in the CARSIM deck and validation approach used for the vehicle trajectory analyses are also discussed.

Section 7 presents the results obtained from the barrier performance limit analysis and vehicle trajectory analysis discussed in Section 5 and 6, respectively. Preliminary guidelines for the placement of guardrails on roadside and median slopes, developed using these results, are also presented.

Several Full scale LS-DYNA simulations of selected preliminary guideline scenarios, where vehicle impacts the guardrail placed on foreslope or backslope of a depressed median, are performed in Section 8. The preliminary guidelines are validated and fine-tuned using the results obtained from these simulations. Finally, the comprehensive recommendations for the placement of five selected guardrail systems on roadside and median slopes are presented in this section.

In Section 9, conclusions are drawn from the study and directions for future research are recommended.

2. LITERATURE REVIEW

2.1. INTRODUCTION

A comprehensive literature review is presented in this section to acquire an overall view of what has been accomplished in developing guidelines for the placement of traffic barriers on slopes. The literature review presented herein can be divided into three main sub-sections. The first part includes a review of five widely used barrier types, existing guidelines to evaluate the performance of these barriers, and existing recommendations for their placement on sloped terrain. A list of crash tests performed on these barriers on flat terrain and past studies related to their performance evaluations on sloped terrain are discussed in the next part.

For many years, computer codes have been used to simulate vehicle handling, vehicle impacts with roadside objects, and vehicle encroachments over roadside geometric features such as slopes, ditches, and driveways. Use of an explicit non-linear finite element solver has become a standard in the simulation of vehicle impacts with roadside objects. To reduce the computation costs, multi-rigid-body dynamic analysis codes can be used to simulate vehicle encroachments over slope terrains prior to the impacts. The final part of this section provides an overview of past studies related to the development and validation of quality finite element guardrail models. This part also introduces a multi-rigid-body dynamic analysis code, which was used in this study to determine trajectories of vehicles traversing various roadside and median slopes.

2.2. BARRIER TYPES

Longitudinal barriers are placed on roadsides to prevent vehicles from leaving the roadway and striking a fixed object or terrain feature when the incident is considered more hazardous than hitting the barrier itself (*3*). Guardrails and median barriers can be classified into three general categories: weak post systems, strong post systems, and

rigid concrete barriers (*4*). Weak post systems are the most flexible and have the greatest dynamic deflection. Provided there is adequate space to accommodate the deflection, these barriers impose lower deceleration on an impacting vehicle. Thus, these systems are more tolerant and less likely to cause injury. Box beam and weak-post W-beam guardrails are examples of weak post systems. After the adoption of NCHRP report 350(*2*) by the Federal Highway Administration (FHWA) as the official guidelines for crash testing of roadside safety features, the performance of the standard weak post W-beam guardrail system was judged to be unsatisfactory. The modified weak post W-beam guardrail was then prescribed to improve the performance under test conditions defined in NCHRP report 350(*2*). Figure 2.1(a) and (b) show typical modified weak post W-beam (G2) and box beam (G3) guardrail, respectively.

Strong-post barriers incorporate larger and stronger posts. These posts absorb significant energy as they rotate through the soil during an impact (*4*). The combined action of higher post and soil stiffness causes reduced dynamic deflection and increased deceleration rates. Spacer blocks are used to offset the rail element from posts to minimize vehicle snagging on the post, which can impart high decelerations to the vehicle. Strong post W-beam and Thrie-beam guardrails are two examples of strong post systems. The Modified Strong post (G4(1S)) W-beam guardrail, shown in Figure 2.1(c), is the result of improvements to the Standard G4(1S) W-beam guardrail system making its performance satisfactory in accordance with the evaluation criteria set forth in NCHRP report 350. In 2000, The Midwest Roadside Safety Facility (MwRSF) developed a new strong-post W-beam guardrail system to improve barrier performance for higher center-of-gravity light truck vehicles, to provide reasonable barrier height tolerance, and to reduce the potential for W-beam rupture (*5*). The system, as shown in Figure 2.1(d), is called the Midwest Guardrail System (MGS). Thrie-beam guardrails were developed to extend the performance of strong post systems. The Modified Thrie-beam guardrail, shown in Figure 2.1(e), is the result of improvements to the standard Thrie-beam and was specifically designed to reduce the rollover incidences for larger vehicles (e.g school bus).

(a)

(b)

(c)

(d)

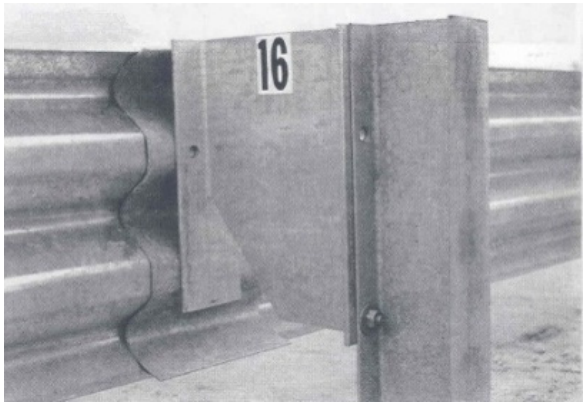

(e)

Figure 2.1 (a) Modified weak post W-beam guardrail (*3*) (b) Box beam guardrail (*6*) (c) Modified G4(1S) W-beam guardrail (*7*) (d) Midwest guardrail system(*5*), and (e) Modified Thrie beam guardrail(*6*).

2.3. EXISTING BARRIER PERFORMANCE EVALUATION GUIDELINES

Roadside safety hardware, including barriers, are evaluated following the guidelines provided in NCHRP Report 350(*2*). The report, prepared by TTI researchers, was adopted by Federal Highway Administration (FHWA) in 1997. Since that time, roadside safety hardware must satisfy standards provided in the NCHRP Report 350 to be accepted by FHWA for use on National Highway System (NHS). According to Test Level 3 of NCHRP Report 350, roadside barrier systems must be subjected to two full scale crash tests:

- Test designation 3-10: An 820-kg (1806 lb) passenger car (820c) impacting the barrier at nominal speed and angle of 100 km/h (62 mph) and 20 degrees, respectively.
- Test designation 3-11: A 2000-kg (4406 lb) pickup truck (2000P) impacting the barrier at nominal speed and angle of 100 km/h (62 mph) and 25 degrees, respectively.

NCHRP report 350 warrants three categories of safety evaluation criteria for full scale crash testing: (1) structural adequacy, (2) post-impact vehicle trajectory, and (3) occupant risk factor. To pass the structural adequacy criteria, the test vehicle should be contained and redirected by the test article and the vehicle should not penetrate, underride, or override the test installation. The vehicle trajectory after impact is an indicator of the potential of post-impact trajectory to cause subsequent multi vehicle collisions, or secondary collisions with fixed objects. The vehicle trajectory and final stopping position should intrude a minimum distance, if at all, into adjacent or opposing traffic lanes (*2*).

The occupant risk evaluates the degree of hazard to the occupant in the impacting vehicle. In 1981, Michie (*8*) developed the flail space model to evaluate occupant risks in roadside safety hardware crash tests. The model assumes that the occupant injury severity is related to the velocity at which occupant impacts the interior and the subsequent acceleration experienced by the occupant. As shown in Figure 2.2, the

occupant is allowed to flail 0.6 m (2 ft) in longitudinal direction (parallel to the typical vehicle travel direction) and 0.3 m (1 ft) in lateral direction before impacting the vehicle interior. Difference in velocity between the occupant and vehicle interior at the instant the occupant reach either 0.6 m longitudinally or 0.3 m laterally is computed using measured vehicle kinematics (*9*). The largest difference in velocity, at the instant of occupant impact, is termed as occupant impact velocity (OIV). OIV in lateral and longitudinal directions are calculated independently. The expressions for occupant impact velocities in longitudinal and lateral directions are:

$$V_{I|x} = \int_0^{t^*} a_x dt \tag{2.1}$$

$$V_{I|y} = \int_0^{t^*} a_y dt \tag{2.2}$$

where, $V_{I|x}$ and $V_{I|y}$ are the occupant-car interior impact velocity in longitudinal and lateral direction, and a_x and a_y are the vehicular acceleration in longitudinal and lateral direction, respectively. t^* is the time when the occupant has traveled either 0.6 m longitudinally or 0.3 m laterally, whichever is smaller. The time t^* can be determined using following expressions:

$$X = \int_0^{t_x^*} \int_0^{t_x^*} a_x dt^2 \tag{2.3}$$

$$Y = \int_0^{t_y^*} \int_0^{t_y^*} a_y dt^2 \tag{2.4}$$

where, X and Y are 0.6 m and 0.3 m, respectively. Acceleration in the longitudinal direction is integrated twice with respect to time to find the value of t_x^*, at which the double integration equals 0.6 m. Similarly, the acceleration in the lateral direction is integrated twice to find the value of t_y^*, at which the double integration equals 0.3 m. Time t^* is the smaller of t_x^* and t_y^*. Once the occupant impacts the vehicle interior, the occupant is assumed to remain in contact with the interior and experience subsequent vehicular accelerations. The maximum 10-ms average of the acceleration (lateral and longitudinal directions are calculated independently) subsequent to the occupant impact is termed as ride down acceleration. TTI developed the Test Risk Assessment Program

(TRAP)(*10*) to evaluate these occupant risk factors using the procedure discussed above. Using the vehicular accelerations data obtained from the accelerometer placed at vehicle CG during a crash test, the program calculates the OIV and RDA in both longitudinal and lateral directions. NCHRP report 350 prescribes threshold values, shown in Table 2.1, for both occupant impact velocity and occupant ride down acceleration to minimize the risk of occupant injury. To pass the occupant risk criteria, occupant impact velocities and ride down accelerations in both longitudinal and lateral directions obtained from a crash test must not exceed the maximum values specified. These maximum values correspond to serious but not life-threatening occupant injury (*11*).

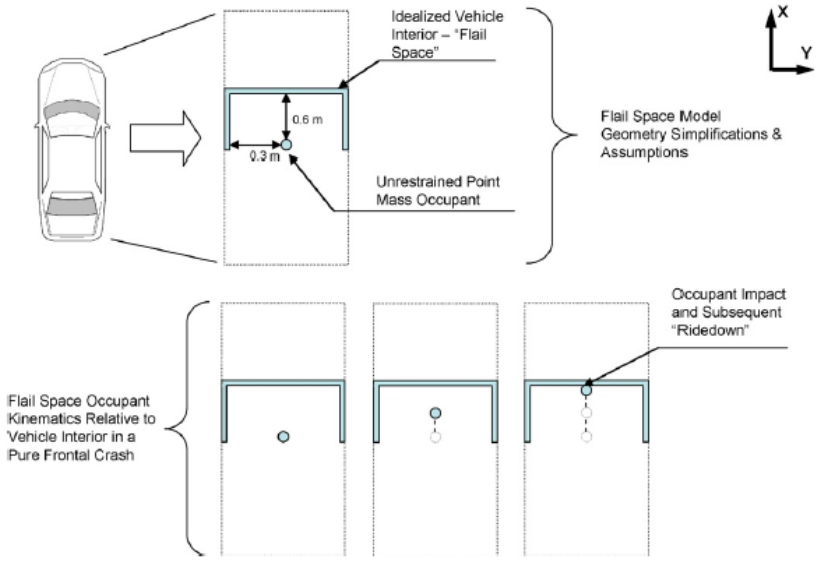

Figure 2.2 Flail space model assumption and simplifications as described by Michie (*9,11*).

Table 2.1 NCHRP Report 350 specified flail space model threshold values used for occupant risk evaluation criteria(*2*).

Occupant Risk Factors: (Longitudinal and Lateral direction)	Preferred Value	Maximum Value
Occupant Impact velocity (OIV)	9 m/s (30 ft/s)	12 m/s (40 ft/s))
Occupant Ridedown Acceleration (RDA)	15 g's	20 g's

2.4. EXISTING RECOMMENDATIONS FOR THE PLACEMENT OF BARRIERS ON SLOPED TERRAIN

Barriers are generally designed and tested for placements on flat terrain. However, they are also placed on various sloped terrains. The American Association of State Highway and Transportation Officials (AASHTO) Roadside Design Guide (RSDG)(*12*) provides guidelines for the placement of roadside barriers on a slope steeper than 10:1. These barrier placement guidelines are based on classifying the sloped medians into three categories: (a) Depressed medians or medians with ditches (Section I) (b) Stepped medians (Section II), and (c) Raised medians or medians berms (Section III). Figure 2.3 from RSDG (*12*) depicts these three categories with the recommendations for barrier placements. According to the guideline, if both slopes in a depressed median (Section I) require shielding, a roadside barrier should be placed near the shoulder on both sides of the median. However, if only one slope requires shielding, e.g. S_3 in Illustration 1, a median barrier should be placed at "d". If neither slope requires shielding but either one or both are steeper than 10:1, a median barrier should be placed on the side with steeper slope (Illustration 2). If both slopes are relatively flat, barrier should be placed at or near the center of the median (Illustration 3). For stepped medians (Section II), if embankment slope is steeper than 10:1, a median barrier should be placed at "b"(Illustration 4). For a non traversable slope, barrier should be placed near the shoulder on each side of the median (Illustration 5). . If the slope is flatter than 10:1, barrier should be placed at or near the center of the median (Illustration 6). The cross section of a raised median (Section III), if wide and high enough, can itself act as a barrier. However if the cross section is inadequate to redirect an errant vehicle, a median barrier should be placed at the top of the cross section.

Although the AASHTO guidelines for barrier placement on sloping terrain have been in place for over 5 years, there remain concerns about their effectiveness. As a result, the National Cooperative Highway Research Program (NCHRP) commissioned a study “Placement of traffic barriers on median and roadside slopes” to address these

concerns. This work is being performed by TTI and much of the data needed to meet the objective of this dissertation has been drawn from that work.

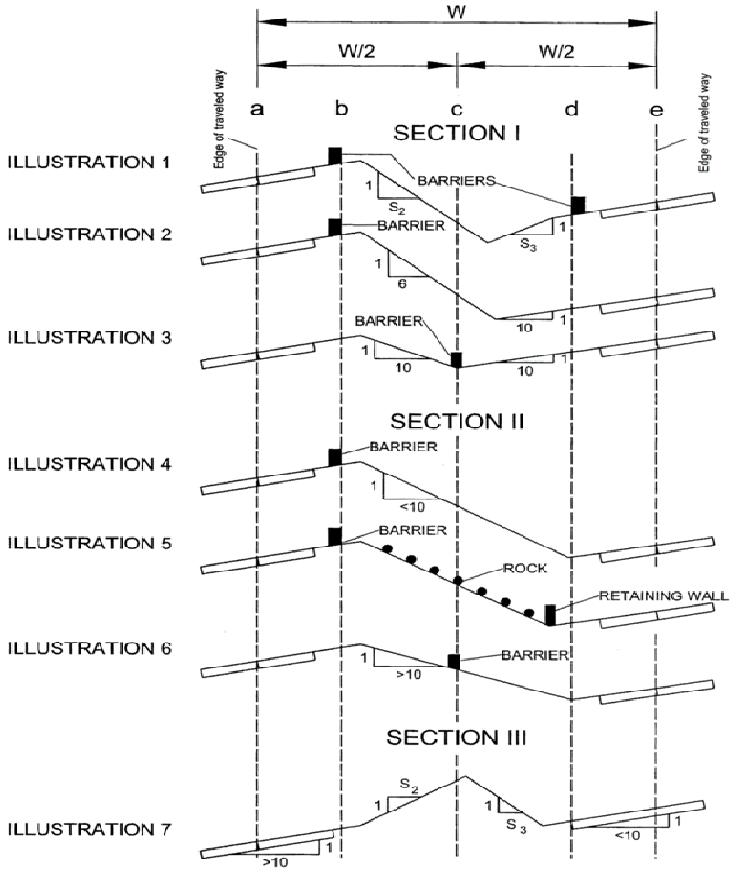

Figure 2.3 Recommended barrier placements in non-level medians (*12-13*).

2.5. CRASH TESTS ON FLAT TERRAIN

In the mid 1990s, TTI researchers conducted full-scale crash tests of all commonly used guardrail systems placed on flat terrain in accordance with NCHRP Report 350 test conditions (*3,6-7*). Under these testing programs, performance issues with the strong steel-post W-beam guardrail (G4(1S)), weak-post W-beam guardrail (G2), and strong steel-post Thrie-beam guardrail (G9) were first identified (*6*). Summaries of the tests are

presented in Table 2.2. As can be seen, the Box beam guardrail successfully passed the test. However, the standard weak post W-beam (G2), strong post W-beam (G4(1S)), and strong post Thrie-beam (G9) guardrails failed to pass the required acceptance criteria. These standard guardrails were modified to perform satisfactorily in accordance with the evaluation criteria set forth in NCHRP report 350. As shown in Table 2.2, all three modified systems successfully contained and redirected the 2000P test vehicles impacting the systems at nominal speed and angle of 100 km/h (62 mph) and 25 degrees, respectively.

Table 2.2 Lists of crash tests performed at TTI on the barriers on flat terrain(*3,6-7*).

Test Number	Barrier System	Test Condition	Result and Comments
471470-21(*6*)	W-Beam, Weak-Post (G2)	3-11	Vehicle overrode barrier.
471470-33(*6*)	Box-Beam (G3)	3-11	Successful containment & redirection.
471470-27(*6*)	W-Beam, Strong Steel-Post (G4(1S))	3-11	Vehicle rolled over on its side.
471470-31(*6*)	Standard Thrie-Beam (G9)	3-11	Vehicle rolled over two and a quarter revolutions.
471470-30(*6*)	Modified Thrie-Beam	3-11	Successful containment & redirection.
405421-01(*7*)	Modified (G4(1S)) with timber blockout	3-11	The rail system considered passed. However, it was considered marginally failed the preferable post impact vehicle trajectory.
473750-3(*3*)	Modified Weak-Post W-beam guardrail	3-11	Successful containment & redirection.

The Midwest Guardrail System (MGS) was developed to improve performance of strong-post W-beam guardrail system for higher center-of-gravity light truck vehicles (*5*). A series of six full scale crash tests were conducted at Midwest Roadside Safety Facility (MwRSF) to develop the MGS for standard and reduced post spacing (*14*). In

the fourth test (NPG-4), the modified system with standard post spacing met all the evaluation criteria set forth in NCHRP report 350 for Test Level 3 conditions.

Thus, the crash tests performed on five guardrail systems, selected for this study, passed the safety evaluation criteria set forth in NCHRP report 350 for Test Level 3 conditions. Results of these crash tests were used to validate the FE models of each guardrail system created in this study following the procedures described in Section 4.

2.6. PAST STUDIES RELATED TO PLACEMENT OF BARRIERS ON SLOPES

The barrier placement guidelines in AASHTO Roadside Design Guide (*12*) were derived from the research conducted by TTI in the early 1980s (*1*). The study investigated the impact performance of roadside barriers installed on sloped terrain. Seven full scale crash tests, as shown in Table 2.3, coupled with an extensive computer simulation effort using Highway Vehicle Object Simulation Model (HVOSM), a vehicle handling code, was used to develop guidelines for placement of barriers on non-level terrain. Crash tests were performed on standard W-beam G4(1S), three-cable (G1), and Thrie-beam (G9) guardrails. Barrier offsets of 1.8 m (6 ft) and 3.7 m (12 ft) from slope break were evaluated. The tests were performed before the adoption of NCHRP report 350 guidelines. Hence, the vehicles used for the test were a 2043 kg (4500 lb) sedan and 1021 kg (2250 lb) passenger car. As can be seen from Table 2.3, both standard G4(1S) W-beam and standard Thrie-beam (G9) guardrails failed to successfully contain and redirect the 2043 kg (4500 lb) passenger car as it impacted the guardrail at a nominal speed and angle of 100 km/h (62 mph) and 25 degrees, respectively. The use of pickup truck test vehicle, as specified in report 350, would have further aggravated the problems encountered during these tests. The higher C.G., higher bumper height, and shorter front overhang of the pickup make it inherently less stable compared to passenger cars in barrier impacts. The shorter front overhang of the pickup truck tends to result in more severe post snagging and higher impact loads on the rail, resulting in a greater probability of rail rupture compared to a similar test with a passenger sedan.

Table 2.3 Full-scale crash tests on barriers placed on 6:1 slope (*1*).

Barrier System	Test Vehicle	Impact Speed	Angle (deg.)	Barrier Offset (from slope break)	Structural Adequacy
Standard G4(1S)	2043 kg (4500 lb) 1974 Plymouth Sedan	101.3 km/h (62.8 mph)	25	1.8 m (6′)	Fail
Standard G4(1S)	2043 kg (4500 lb) 1974 Plymouth Sedan	101.3 km/h (62.8 mph)	25	3.7 m (12′)	Fail
Standard G4(1S)	2043 kg (4500 lb) 1974 Plymouth Sedan	102 km/h (63.3 mph)	14.75	1.8 m (6′)	Pass
Standard G4(1S)	1021 kg (2250-lb) 1974 Chevrolet Vega	93.8 km/h (58.2mph)	14.75	3.7 m (12′)	Pass
Standard G1 (Cable)	2043 kg (4500 lb) 1974 Plymouth Sedan	100 km/h (62.0 mph)	26.0	1.8 m (6′)	Pass
Standard G1 (Cable)	1021 kg (2250-lb) 1974 Chevrolet Vega	94.2 km/h (58.4 mph)	17.25	1.8 m (6′)	Pass
Standard G9 (Thrie-beam)	2043 kg (4500 lb) 1974 Plymouth Sedan	100 km/h (62.0 mph)	26.0	1.8 m (6′)	Fail

To supplement crash test results in developing barrier placement guidelines, Ross and Sicking used HVOSM to determine the bumper trajectory of a vehicle encroaching onto various terrain configurations(*1*). This data was combined with barrier containment criteria to establish acceptable and unacceptable (i.e. override or underride) regions. Ross and Sicking (*1*) found W-beam and Thrie-beam barriers to be more sensitive to the effects of sloping terrain compared to other barriers. They selected the barrier containment criteria based on a limited number of crash tests and engineering judgment. The criterion used for G4(1S) W-beam and Box-beam guardrail placed on a median barrier is shown in Figure 2.4. For W-beam and Thrie-beam guardrail systems, Ross and Sicking (*1*) assumed that acceptable barrier behavior is expected when mid-height of the bumper impacts between the upper and lower corrugation centers of the "W-beam" or "Thrie-beam" rail. For box-beam guardrail system, the acceptable barrier behavior is expected when mid height of the bumper impacts below the top of the box beam rail and upper front corner of the vehicle fender impacts above the rail base(*1*). The authors

presented Figure 2.5 to illustrate the method used to establish acceptable and unacceptable (i.e. override or underride) barrier placement regions. The plotted curve in the figure is the HVOSM generated right front bumper profile of a 2043 kg (4500 lb) passenger car traversing a 4:1 embankment slope and the two horizontal lines represent the W-beam's upper and lower corrugation centers.

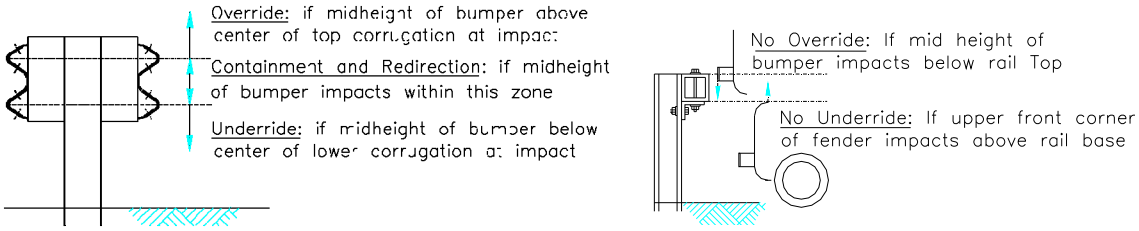

(a) (b)

Figure 2.4 Containment criteria for (a) G4(1S) W-beam barrier (b) Box-beam barrier(*1*).

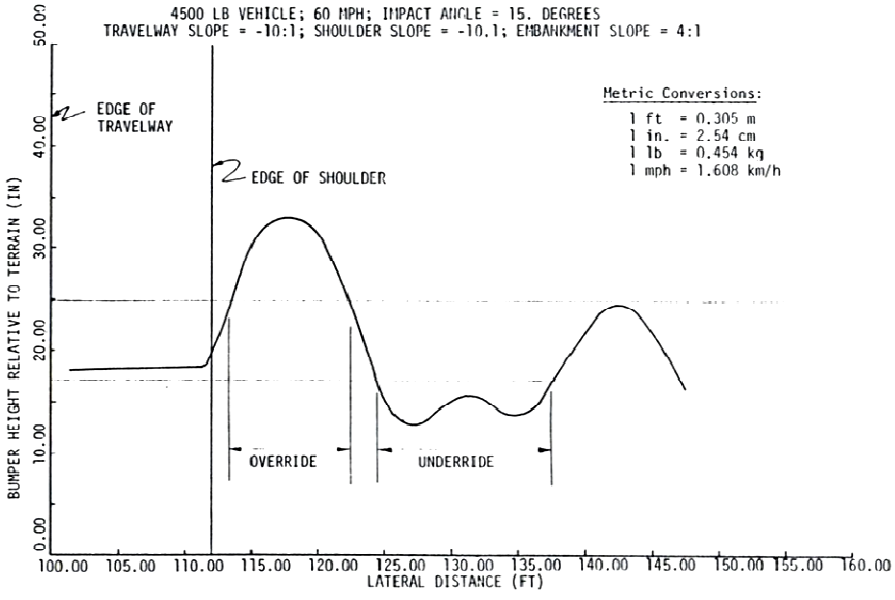

Figure 2.5 Plot of a 2043 kg (4500 lb) vehicle right front bumper relative to terrain(*1*).

There are three limitations to this work that were addressed in the current study. First, due to the composition of the vehicle fleet and the design test vehicles used in the late 1970s and early 1980s, light pickup trucks were not considered in the analysis and testing program. Second, the research did not include the scenario in which barrier was impacted on the back slope of a depressed median. Finally, certain assumptions were made with regard to the barrier containment criteria based on engineering judgments. Effectiveness of these assumptions has not been verified.

In the mid 2000s, TTI investigated the performance of concrete barriers placed on roadside and median approach slopes using finite element analysis and two full scale crash tests (*15-16*). Initially, finite element simulations were performed, using LS-DYNA, to determine bumper trajectory of the vehicle along the ditch cross section as it freely traversed a 6:1 slope in absence of a barrier. As shown in Figure 2.6, this trajectory was used to identify critical barrier offset locations, considering the point of maximum bumper height above local terrain elevation and the point where the vehicle suspension was compressed to its greatest extent. Even though the vehicle's suspension undergoes maximum compression at the point of minimum bumper height, a short distance beyond this point was identified as a more critical case (i.e. Case 2). The already rebounding vehicle suspension at this point would give the vehicle a tendency to move upward, which can induce more vehicle climb and greater vehicle instability as it interacts with a barrier(*15*). Finally, two full scale crash tests were performed to evaluate a permanent cast-in-place F-shape barrier and a free standing, precast F-shape barrier placed at the critical offset locations on 6:1 cross-slopes. Both the concrete barriers successfully contained and redirected the 2000P truck impacting at nominal speed and angle of 100 km/h (62 mph) and 25 degrees, respectively.

Marzougi et al. (*17*), in 2007, performed vehicle dynamic analysis, finite element analysis, and full-scale crash tests to study the effect of sloped terrain on the safety performance of cable barriers. Two full scale crash tests were performed to validate the simulation results. In the first test, the three-strand cable barrier was placed at 1.22 m (4 ft) offset from the center of the 6:1 slope V-shape median(*17*). In the second test, the

barrier was placed 0.3 m (1 ft) offset from center of the median. The tests were performed following the NCHRP Report 350 Test Level 3 conditions but using a large sedan (Ford Crown Victoria) rather than a pickup as the test vehicle. Although the large sedan underrode the cable barrier in the first test, the vehicle was successfully redirected by the barrier in the second test. The test results confirmed the behavior obtained from the FE simulations and vehicle dynamic analyses.

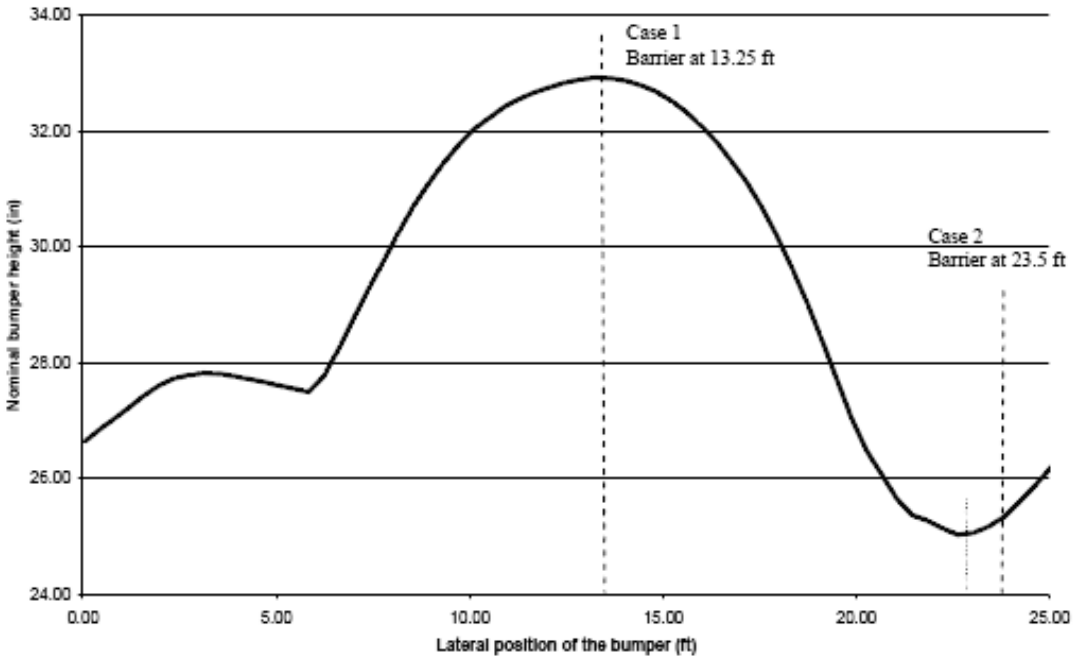

Figure 2.6 Height of a 2000 kg (4409 lb) truck bumper relative to local terrain elevation(*15*).

Researchers at National Crash Analysis Center (NCAC) recently investigated the performance of a three-strand cable barrier placed on sloped terrains(*18*). The researchers used Human vehicle Environment (HVE), a multi-rigid body vehicle dynamics analysis package, to study the trajectory of a large sedan (Ford Crown Victoria), a small sedan (Mitsubishi Mirage), and a pickup truck (Chevrolet C2500)

traversing median slopes at various approach angles and speeds. They identified two points, labeled 1 and 2 in Figure 2.7(a), to represent the primary interface region on the vehicle. The effective interface conditions for the cable barrier were determined by assessing relative positions of the vehicle to the barrier such that (a) lower critical point on the vehicle (labeled 1 on Figure 2.7a) should impact below the top cable to minimize the potential for override, and (b) upper critical point on the vehicle (labeled 2 on Figure 2.7a) should impact above the bottom cable to minimize the potential for underride. Using vehicle dynamic simulation results, the trajectories of points 1 and 2 for both directions of vehicle crossing the median were plotted, as shown in Figure 2.7(b). These curves are normalized to relate the relative heights of individual cables in the barrier to a horizontal plane. For any position along the ditch section, the ordinate of the normalized plot is equivalent to the vertical height of the trajectory with respect to the actual sloped surface. The shaded area in the figure represents the barrier interface envelope that surrounds all of the trajectories for different classes of vehicles traversing the median at various encroachment angles and speeds. The dark solid override limit line represents the upper projection of individual plots of lower critical point (labeled 1) on the vehicle across the ditch profile. Similarly, the gray solid underride limit line represents the lower projection of individual plots of upper critical point (labeled 2) on the vehicle across the ditch section. The three dash-dot lines, shown in Figure 2.7(b), represent coverage of a generic three cable barrier. To ensure successful containment, the override limit line should fall below the top dash-dot line and the underride limit line should fall above the bottom cable line. The shaded areas presented at the bottom of the figure identify the acceptable and unacceptable lateral placement locations for the barrier.

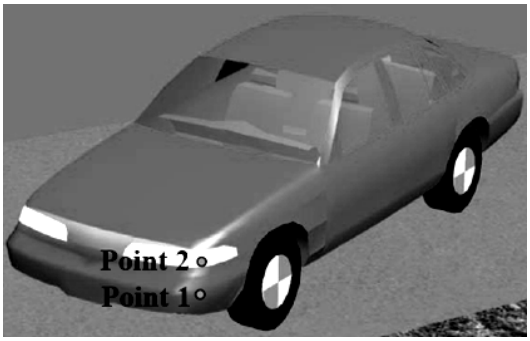

(a)

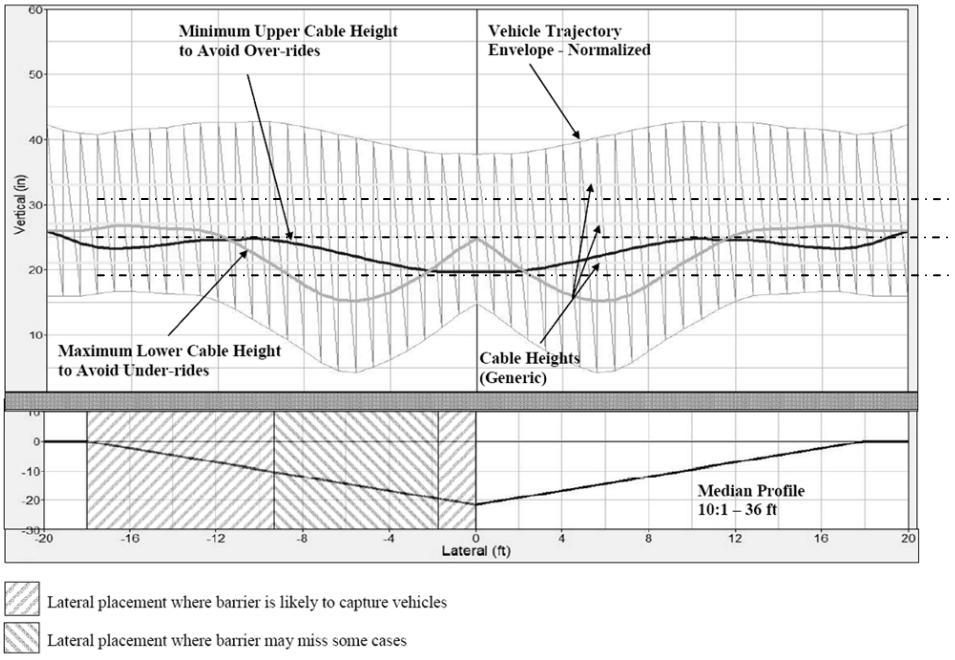

(b)

Figure 2.7 (a) Critical interface points on the vehicle (b) Acceptable barrier placement locations obtained from the vehicle dynamic analyses results(*18*).

Recently, the researchers at the Midwest Roadside Safety Facility (MwRSF) investigated the performance of Midwest Guardrail System (MGS) placed on approach slopes(*19-20*). LS-DYNA simulations were performed to determine the critical slope and associated offset for placement of MGS off the roadway. After a parametric analysis, a slope of 8:1 was found to be the steepest slope on which an MGS could be safely placed anywhere on the slope. It was also concluded that the critical offset location for the MGS

on this slope would be 1.5 m (5 ft) from slope break. The MGS placed on 8:1 slope at 1.52 m (5 ft) offset from slope break was then subjected to two full scale crash tests as shown in Figure 2.8. In the first test, a 2036 kg (4485 lb) Chevrolet 2500 pickup truck impacted the system at a speed and angle of 100.4 km/h and 25.9 degrees, respectively. In the second test, a 912 kg (2009 lb) Geo Metro impacted the system at a speed and angle of 99.6 km/h (61.75 mph) and 21.6 degrees, respectively. Both the vehicles were successfully contained and redirected by the system and the tests met the safety evaluation criteria set forth in NCHRP report 350. Researchers concluded that the MGS may be placed anywhere on an 8:1 or flatter slope.

Figure 2.8 MGS system on 8:1 slope as impacted by a pickup truck (right) and a small car (left)(19).

2.7. USE OF NUMERICAL ANALYSIS IN ROADSIDE SAFETY

For many years, computer codes have been used to simulate vehicle handling, vehicle impacts with roadside objects, and vehicle encroachments over roadside geometric features such as slopes, ditches, and driveways. In addition to the expensive full scale crash tests, finite element techniques are widely used for simulating vehicular impacts with roadside objects. Due to the availability of powerful computers, roadside safety researchers are overwhelmingly using non-linear finite element techniques to evaluate

performance of roadside safety features. Examples of general-purpose finite element analysis (FEA) codes include ADINA, ABAQUS/EXPLICIT, MSC-DYTRAN, PAM-CRASH, RADIOSS, and LS-DYNA. These explicit nonlinear finite element programs are capable of simulating complex nonlinear dynamic impact problems. During the 80's DYNA3D, a finite element solver especially tailored to simulate crash events was developed at Livermore National Laboratories and was soon after followed by its commercial counterpart, LS-DYNA. The roadside safety community soon adopted LS-DYNA as their code of choice for analyzing the performance of roadside safety hardware under impact loading. LS-DYNA incorporates explicit and implicit algorithms for the integration of the equation of motion in the time domain. It incorporates state-of-the-art contact algorithms that can be used to model vehicular collisions with roadside objects. Tires interactions with the ground can also be simulated in a more realistic manner using the contact library available in LS-DYNA rather than using other assumed behavior models incorporated into some of the other codes. Public domain models of the 2000P and 820c test vehicles specified in the NCHRP Report 350 are available in LS-DYNA. These models were originally developed by the National Crash Analysis Center (NCAC) under the FHWA sponsorship. Other than being state-of-the-art impact analysis software, the availability of public domain models (both vehicles and hardware) with adequate modeling details was the reason the finite element code, LS-DYNA, was selected for this research.

Ideally, a single finite element code would simulate the vehicle traversing the slope and impacting the barrier. However, the total encroachment event is relatively long in duration and large computational times are required to capture both events. The research approach used for this work engages LS-DYNA to simulate the crash event at the instant of contact between vehicle and guardrail. However, considering the large number of parametric runs needed to address the variables of interest, LS-DYNA is too computationally expensive to simulate events from beginning to first contact. Instead, a multi-rigid-body dynamic analysis code was used to simulate events during that time. The output from this simulation is attitude and dynamic state of the vehicle at the instant

of impact. Many previous studies have focused only on encroachment on the ditch foreslope (assuming use of two barriers or barrier placement at the bottom of a symmetric ditch). In the current study, the complete ditch traversal was captured, including the traversal through the ditch bottom and up the ditch backslope. This is critical for achieving guidelines that are applicable for non-symmetric barrier placement along the ditch side slope. Using a multi-rigid-body code significantly reduced the time needed to complete this phase of the study.

An overview of past studies related to the development and validation of quality finite element guardrail models and an introduction to the multi-rigid-body dynamic analysis code used for this study are presented next.

2.7.1. Development of Quality FE Guardrail Models

Each of the five guardrail systems proposed for study in this work have numerous components that must be modeled. The features of LS-DYNA allow for multiple ways for modeling each component. A sampling of some of these issues and how they have been addressed by others follow.

Bolted connections for different systems may require different modeling techniques. For example, study revealed that the bolts used in splice connections for guardrail systems should not fracture during the collision. Bolts used in the post to rail connections for strong post systems are also strong enough to withstand fracture. Plaxico et al. (*21*) conducted a series of quasi-static laboratory tests of the post to rail connections used in strong post G4(1S) W-beam systems. In each of these tests, the connection failed as the head of the bolt was pulled through the slot deforming the surrounding region of w-beam material. Researchers at NCAC used nodal-rigid-body constraints, null shell elements, and piecewise linearly plastic beam elements to model the post-rail connections for a strong post G4(1S) W-beam guardrail system (*22*). Beam elements were used to represent the tensile, shear and bending stiffness of the bolts. Shell elements with null material properties were used to represent the geometry of the

bolt for contact purpose. Null elements have no effect on the stiffness of the bolts and therefore do not affect the time step. The beam elements were connected to the surrounding shell elements by nodal rigid body constraints.

The rails of weak post systems, on the other hand, should detach easily and reliably from the posts prior to the vehicle impacting the posts (*23*). Connections that are too strong can cause the rail to be carried to the ground allowing the vehicle to override. Ray et al. (*23*) investigated the performance of weak post w-beam connection in a realistic manner by applying the load to the connection through guardrail and flange. The connection was positioned at several angles to replicate the bending and twisting that may occur in a typical collision. For all the cases the connection failed due to fractures in the bolt. Engstrand (*24*) later modeled the post-rail connection for weak post w-beam system using nodal rigid body spotweld option available in LS-DYNA. The connections were set to fail at a load of 17.8 kN (4 kips).

Sonnenschein (*25*) showed three techniques for modeling bolts in LS-DYNA. In the first technique, the bolt shank was modeled using beam elements. A spider mesh containing stiff beam elements was used to connect the bolt shank to its clamping partners. Since loads are transferred circumferentially to the hole, setting contact between bolt shank and hole and the bolt head and outside components is not necessary in this technique. Second technique used solid elements for modeling the bolt. Contacts between the bolt and the surrounding components were defined. A more realistic bearing stress on the hole edge is possible with this technique. The third technique combined the advantages of first two techniques. Here, bolt shank was modeled with spot-weld beams, bolt heads were modeled with shell elements, and null beams were used around the holes to define contacts between the bolt shank and surrounding hole.

In 1996, Hendricks and Wekezer (*26*) developed the model of a weak post W-beam G2 guardrail using LLNL-DYNA3D, a nonlinear, explicit finite element code. Model details for different components such as W-beam end anchorage, post-soil interaction, post to W-beam connection were explained. To reduce the number of elements, the guardrail system outside the impact region was modeled using elastic

springs. An elastic spring constant of 14 N/m (79.9 kips/in) was derived from axial stiffness of five spans of the 19.05 m (62.5 ft) long W-beam rail. Instead of including the finite element model for the soil, depth of fixity for the post, a distance below the ground at which the post could be fixed and could produce the same resistance of a post embedded soil, was calculated. Bolts, in the post to W-beam connections, were modeled using elastic-plastic spring elements. The plastic spring constant was set to 0.0 to allow the bolt to separate without any applied force after the failure. The 820C model, developed by FHWA, was used to mimic a full scale crash test scenario.

Ray et al. (*23*) investigated the problems associated with the standard weak post W-beam guardrail as it failed to pass the safety evaluation criteria set forth in NCHRP report 350. They developed finite element guardrail models to explore design modifications to the standard system. Various components of the guardrail system were tested in the laboratory to develop quality FE sub-models. Qualitative and quantitative comparisons were made between the crash tests results and simulations to validate the accuracy of the FE model. Modified weak post (G2) W-beam guardrail system, developed from this study, successfully passed the safety evaluation criteria set forth in report 350.

To develop an accurate and computationally efficient FE model for the modified G4(1S) W-beam guardrail, Plaxico (*27*) investigated both the simplified and more complete and geometrically explicit modeling techniques. In one case, post-soil interaction was modeled using the sub grade reaction approach where post was supported by an array of uncoupled springs as shown in Figure 2.9(a). In the other case, the continuum finite element approach was used where the post was embedded in a soil continuum of solid elements. It was concluded that the continuum FE approach to model post to soil interaction would be inappropriate due to immense computational requirements of such an analysis. To develop the post-rail connection, explicit FE models with different mesh refinements were investigated. The models with finer mesh were found impractical for use in the complete guardrail model due to the small time-step required to perform an explicit FE analysis with this model. The model with coarser

mesh, with an element size of 5.6 mm (0.22"), required very little computation time but was inadequate because of its overly stiff response. To increase the accuracy of this model, the thickness of the W-beam material in the slotted hole region were modified to achieve a connection stiffness equivalent to that obtained in a laboratory test. Non-linear spring elements were used to model the end terminals for the modified G4(1S) W-beam guardrail model. The FE sub-model of a Modified Eccentric Loader Terminal (MELT) section, developed by Patzner et al. (*28*), was used to determine force-displacement relationship for the rail-end springs. Vehicle impact simulation on the final guardrail model was validated using the results obtained from a previously performed crash test.

Marzougui et al. (*22*) developed FE model for the G4(1S) W-beam guardrail to investigate the effect of rail height on its safety performance. Modeling techniques used for different guardrail components were explained. Explicit geometry of all components including W-beam rail, post, blockouts, soil, and bolted connection were incorporated. All posts and rail elements were modeled using quadrilateral Belytschko-Lin-Tshay (*29*) shell elements. Wooden blockouts were modeled using eight-node reduced-integration hexahedral solid elements. The soil, as shown in Figure 2.9(b), was modeled as a cylindrical block of eight-node hexahedral solid elements. The "soil_and_foam" model (Type 5) in LS-DYNA was used to represent the soil material. Non-reflection boundary constraints were used at the outer boundaries of the soil model to prevent the stress wave from reflecting at the fixed boundary. The shape of the post, with appropriate web and flange thicknesses, was incorporated into the soil mesh. The guardrail model was validated against several full-scale crash tests performed following NCHRP report 350 TL-3 guidelines.

Uddin (*30*) used the non-linear finite element analysis technique to analyze crashworthiness of the modified Thrie-beam guardrail. As shown in Figure 2.9(c), non-linear springs were used to simulate the soil response. Based on the results obtained from a field-test study, a pivot point on the post was set at 813 mm (32") below grade to simulate the post rotation. Splice connections and rail overlaps were not simulated in the guardrail model. Post-to-blockout connections were modeled by merging the nodes of

the two parts. Connections between blockout and rail were modeled using the "Spotweld cards" in LS-DYNA. 820c passenger car and 2000P pickup model, developed by NCAC, were used to perform impact simulations. The simulation results indicated that the guardrail model was performing properly and as expected.

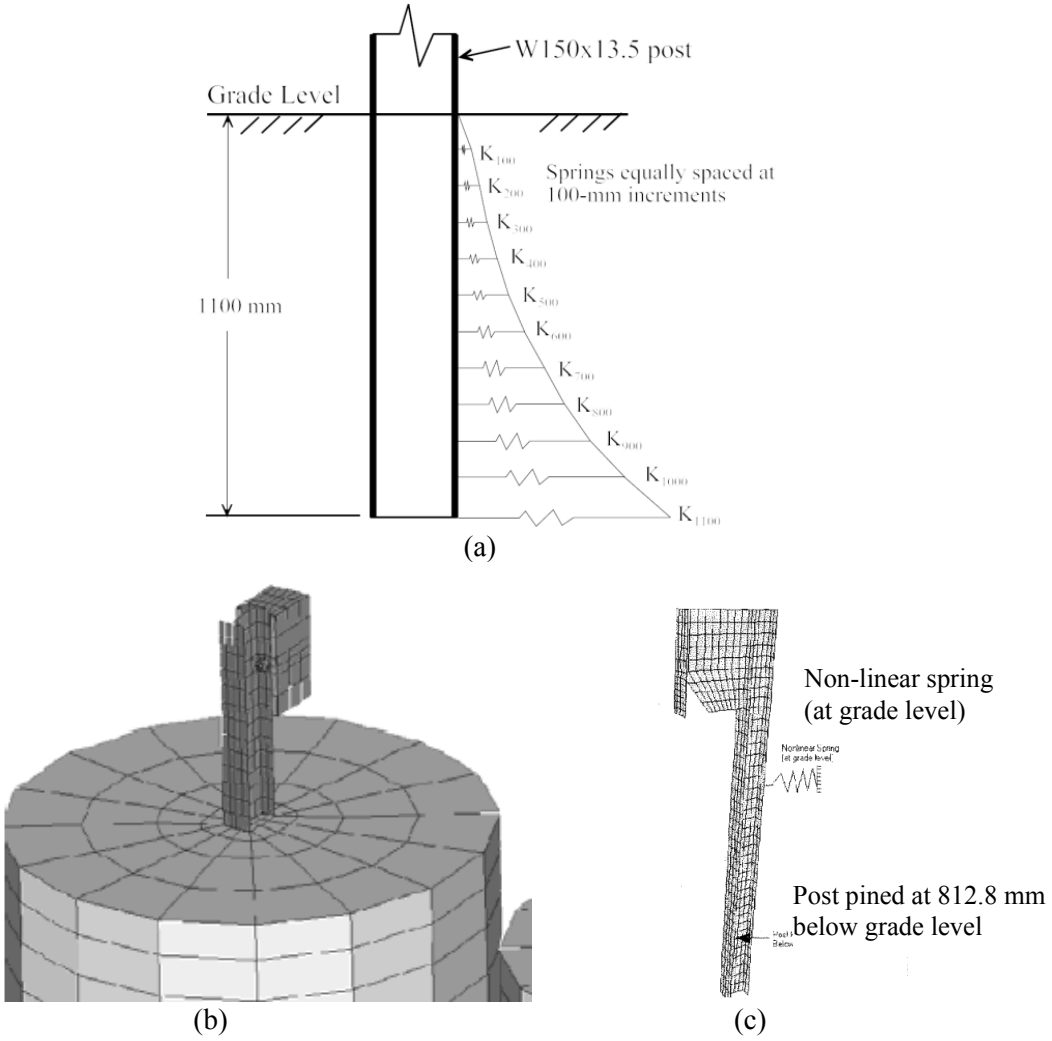

Figure 2.9 Different techniques used to model post-soil interaction: (a) Sub grade reaction approach(*27*) (b) Soil modeled as cylindrical block of solid elements with shape of the post incorporated into the mesh (*22*), (c) Nonlinear springs used to simulate soil response(*30*).

2.7.1.1. Model Validation

In this study, FE simulation results were compared with crash test results identified earlier in this section to validate and improve each of five FE guardrail models. The vehicle response and attitude signals, photographic documentations, occupant risk factors, and maximum dynamic deflection of the barrier during and after the impact obtained from simulation and crash test were compared. Methodologies for making quality assessments on a FE model by comparison with physical test data taken as the object have recently been presented by Ray et al. (*31*) and Schwer (*32*).

Ray et al. (*31*) recently developed the Roadside Safety Verification and Validation (RSVVP) program that can calculate comparison metrics between simulation and crash test signals that are helpful in quantitatively validating a roadside hardware model. The program compares the vehicle response and attitude signals obtained from simulation and crash tests to calculate two comparison metrics: (a) Sprague and Geers metrics and (b) Analysis of variance (ANOVA) of the signals. Sprague and Geers metrics represent integral comparison where time integrals of the response wave forms are combined in the metrics (*32*). The magnitude (M_{SG}) and phase (P_{SG}) components of the metrics are calculated using Equations (2.5) and (2.6):

$$M_{SG} = \sqrt{\frac{\sum c_i^2}{\sum m_i^2}} - 1 \tag{2.5}$$

$$P_{SG} = \frac{1}{\pi}\cos^{-1}\frac{\sum c_i m_i}{\sqrt{\sum c_i^2 \sum m_i^2}} \tag{2.6}$$

The ANOVA metrics are based on the residual between the measured and computed curves. Ray (*33*) proposed a method shown in Equation (2.7) and (2.8) to determine the average residual error and its standard deviation:

$$\bar{e}^r = \frac{\sum (c_i - m_i)/m_{\max}}{n} < 0.05 \cdot m_{\max} \tag{2.7}$$

$$\sigma^r = \sqrt{\frac{\sum\left(e^r - \bar{e}^r\right)^2}{n-1}} < 0.35 \cdot m_{\max} \tag{2.8}$$

Here, m_i and c_i are the measured and computed values, respectively. The average residual error ($\bar{e}^r$) and its standard deviation (σ^r) for the ANOVA metrics are normalized with respect to the peak value of the measured curve (m_{max}). The acceptance criteria for both metrics, suggested by Mongiardin and Ray (*34*), are shown in Table 2.4. Ray et. al (*31*) also recommended developing a phenomena importance ranking table (PIRT) in order to verify and validate roadside hardware model. Occupant risk factors, maximum dynamic deflection of the barrier, and data obtained from photographic documentations are compared in PIRT. The relative difference between the simulation and test results presented in PIRT should not exceed 20%. Both the RSVVP and PIRT were used in this research to improve and validate the numerical model of five guardrail systems.

Table 2.4 Acceptance criteria used in RSVVP program (*34*).

Sprague and Geers Metrics		**ANOVA metrics**	
M_{SG}	≤ 40	Mean	≤ 0.05
P_{SG}	≤ 40	Standard deviation	≤ 0.35

2.7.2. Vehicle Trajectory Analysis

Vehicle dynamic (VD) simulation packages are widely used to simulate vehicle handling and encroachments over roadside geometric features such as slopes, ditches, and driveways. There are several simulation codes available that can be used depending on the nature of the analyses being performed and the available computing resources. In early 1980s, Ross and Sicking (*1*) used Highway Vehicle Object Simulation Model (HVOSM) to determine bumper trajectory of the vehicle encroaching onto various terrain configurations. In HVOSM, several input parameters required to define the behavior of the vehicle suspension and tire models are relatively difficult to determine.

Marzougui et al. (*17*) used Human Vehicle Environment (HVE) to investigate the vehicle dynamics on sloped terrain. The HVE does not have the ability to automate parametric simulations. Another popular multi-rigid-body dynamics code being used by the automotive and other industries is MSC-ADAMS. This VD simulation package requires building specific vehicle models by customizing and integrating generic vehicle sub-system templates provided with the software. This process usually takes significant time and resources in measuring and inputting geometric and property data of the vehicles.

During subsequent evaluation of available codes, it was found that while ADAMS had most of the features required for this research, using another vehicle handling code named CARSIM (*35*) offered advantages. Commercial multi-rigid-body dynamic analysis code, CARSIM, has about 30 pre-built vehicle models in different vehicle classes. The list of these pre-built vehicles includes small passenger car and full-size pick-up truck models that can be minimally modified to represent NCHRP Report 350 specified 820c and 2000P test vehicles. Figure 2.10 shows the main setup window of CARSIM which is used to specify vehicle type and other input parameters such as driving input, initial conditions, analysis time, required output parameters, etc.

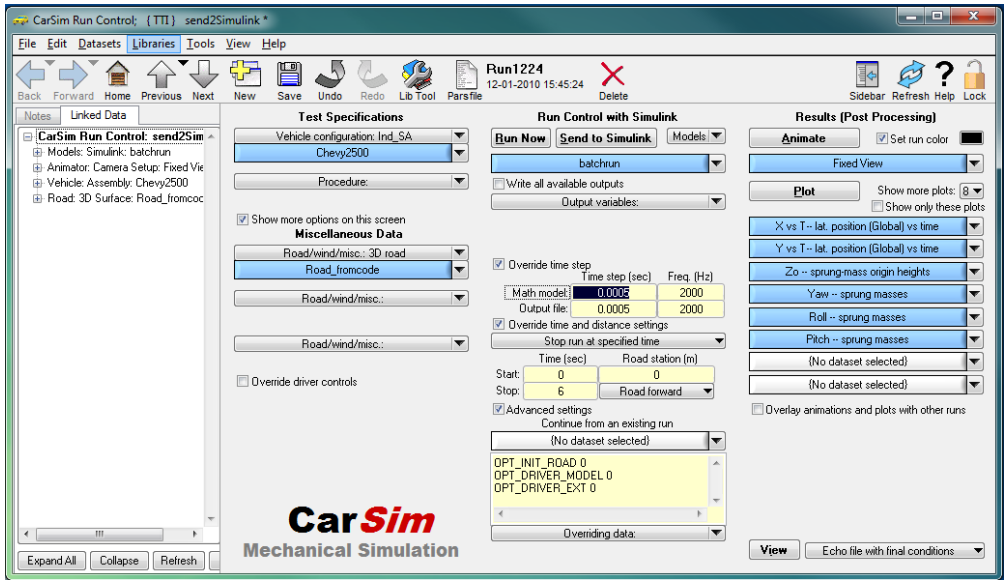

Figure 2.10 CARSIM Run window(*35*).

In CARSIM, vehicle subsystem properties such as suspension, vehicle body type, steering, etc. can be modified. Different three-dimensional terrain profiles for both on-road and off-road conditions can be defined. CARSIM can generate output plots of various entities including accelerations, velocities, angular rates, and angular displacements at the center of gravity (*36*). CARSIM also provides the feature to perform simulations in a batch mode. In addition, the CARSIM data and Vehicle SIM (VS) solver can be linked with the SIMULINK. This allows users to pre- and post-process the CARSIM inputs and outputs using external MATLAB codes during a batch run. This process allows a large number of simulations to run at a single command thus significantly reducing the computation time and user interventions.

3. RESEARCH APPROACH

3.1. INTRODUCTION

The purpose of this study was to evaluate the performance of five widely used barriers when placed on sloped terrains and develop comprehensive recommendations for their placement on roadside and median slopes. Representative combinations of slope configurations and vehicle encroachment conditions, investigated in this study, were identified from existing guidelines. Nonlinear finite element analysis was used to evaluate performance of the barrier during a crash event. Multi-rigid body vehicle dynamic analyses techniques were used to determine trajectories of the vehicles on roadside and median slopes. Parameters selected, methodologies used to perform the analyses, and how their results were used to develop guidelines are discussed in this section.

3.2. PARAMETER SELECTION

Several factors are known to affect the performance of a guardrail on sloping terrain. In what follows, these factors are identified and are ultimately used to construct a matrix of simulations needed to obtain data required to develop guardrail placement recommendations. The final simulation matrix is presented in a table at the end of this sub-section.

3.2.1. Barrier Types

Five guardrail and median barrier systems that successfully passed the evaluation criteria set forth in NCHRP report 350 were selected for this study. These are presented in Table 3.1. Single-sided guardrails, as shown in Figure 3.1(a), are generally placed on a roadside or on both sides of a median ditch. However, for V-shaped median

configurations with a single median barrier placed in the ditch, dual-sided barriers, shown in Figure 3.1(b), are used. In this study, LS-DYNA simulations were performed on single-sided guardrail systems to determine barrier performance limits in terms of acceptable vehicle impacts heights. It is expected that performance limits obtained for a single-sided guardrail system can be conservatively applied to a similar type dual-sided median barrier. Although for W-beam and Thrie-beam guardrail systems, the stiffness of the double-sided barrier is slightly higher than the single-sided guardrails due to the presence of an extra rail element, the flexural strength of the W-beam or Thrie beam is relatively small. Further, due to the 558 mm (22 in.) to 610 mm (24 in.) separation of the rail elements, they will behave somewhat independently. Thus, if a single-sided W-beam guardrail exhibits a tendency to lean over and permit vehicle override when impacted at a certain height, the impact side rail in a double-sided W-beam median barrier is expected to behave in a similar fashion. However, to verify and validate the preliminary guidelines prepared using performance limits of single-sided guardrail systems, a dual-sided barrier model was developed and studied by adding extra rail and blockout elements to the single-sided guardrail model.

Table 3.1 Barrier types selected for the currrent study.

Category	Guardrail/Barrier Type	AASHTO Designation
Strong-post Systems	Modified Strong Post W-beam System	Modified G4(1S)
	Midwest Guardrail System	MGS
	Modified Thrie-beam System	Modified G9-S
Weak-post Systems	Modified Weak Post W-beam System	Modified G2
	Box-Beam System	G3

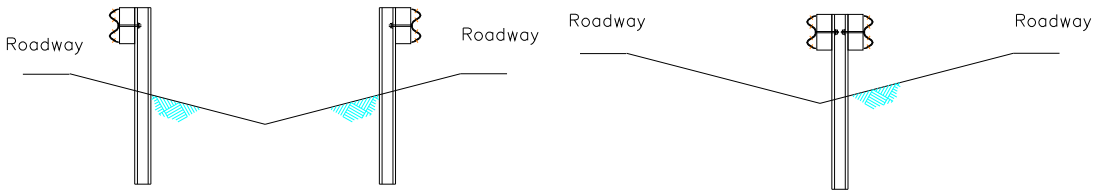

(a) (b)

Figure 3.1 (a) Single-sided modified G4(1S) guardrail used to protect vehicle traveling from one side, (b) Double-sided modified G4(1S) median barrier used to protect vehicle traveling from either side.

3.2.2. Vehicle Selection

NCHRP Report 350 test vehicles were used in this study to perform CARSIM and LS-DYNA simulations. CARSIM has several pre-built multi-rigid body dynamic vehicle models including small passenger car and pickup truck models that can be minimally modified to represent Report 350 test vehicles. Also, the LS-DYNA models of a Chevrolet C2500 pickup truck and an 820-kg Geo Metro passenger car that were originally developed by the NCAC comply with the *NCHRP Report 350* design vehicles for Test Level 3 conditions. These two vehicle models have been used extensively by the roadside safety community in a variety of roadside hardware analyses. Illustrative lists of CARSIM and LS-DYNA vehicle models that were used in this study are shown in Table 3.2. These existing vehicle models were assigned appropriate mass, inertia, suspension spring and damper properties, and other basic geometric properties to match those of the actual test vehicles.

3.2.3. Encroachment Condition

Encroachment angles of 15 degrees and 25 degrees were used along with encroachment speeds of 100 km/h (62 mph) and 80 km/h (50 mph). Speeds lower than 80 km/h (50 mph) are not expected to influence the barrier performance envelopes. The critical

encroachment condition for vehicle override is expected to be the highest speed (i.e., 100 km/h) and the highest angle (i.e., 25 degrees).

Table 3.2 Vehicle models used in simulations.

Criteria	Design Vehicle	LS-DYNA Models (Developed by NCAC)	CARSIM Models
NCHRP Report 350	820-kg Geo Metro	 Approx. 16,000 elements	 A-Class Hatchback
	2000-kg, ¾-ton, standard cab, Chevy C2500	 Approx. 55,800 elements	 Full-size Pickup

3.2.4. Median and Roadside Configuration

The classifications of median and roadside configurations used by the highway safety community are shown in Figure 3.2. A close examination reveals that several of these configurations can be analyzed as a subset of another, thus reducing the number of simulations required to develop placement guidelines. An evaluation of these median and roadside configurations with the objective of identifying typical scenarios, and thus developing a simulation matrix for median and roadside configuration is presented below.

As indicated in Figure 3.2(a), the roadside cross-slope can be either positive (cut) or negative (fill). For the case of a vehicle encroaching onto the roadside, simulations were performed for the positive (cut) cross-slopes. The scenario where the cross-slope is negative (fill) is a subset of the case when the vehicle encroaches onto a depressed median (Figure 3.2b). Thus no additional simulation was needed for the roadside case beyond this scenario.

For the case of a vehicle encroaching onto a depressed median (Figure 3.2b), the simulations were performed for all variations of design parameters (slopes, velocities, vehicle types, encroachment angles, etc.). The depressed medians were modeled as a V-shaped ditch having symmetric cross section with equal foreslope and backslope ratios. This is considered to be a critical subset of a more general trapezoidal-shaped ditch, where wider ditch bottom allows less severe interaction with the backslope which reduces the compression of the suspension and decreases the likelihood of vehicle underride. Similarly, performance of barrier on a higher cross-slope can be considered more critical. Thus, for placement of barrier on the backslope of a non-symmetric depressed median, the guideline for the symmetric median with highest cross-slope can be used. For example, if an 8:1 foreslope leads into a 6:1 back-slope, the guidelines for the 6:1 can be conservatively used. This greatly reduces the complexity of the final design guidelines and makes them easier to use and implement.

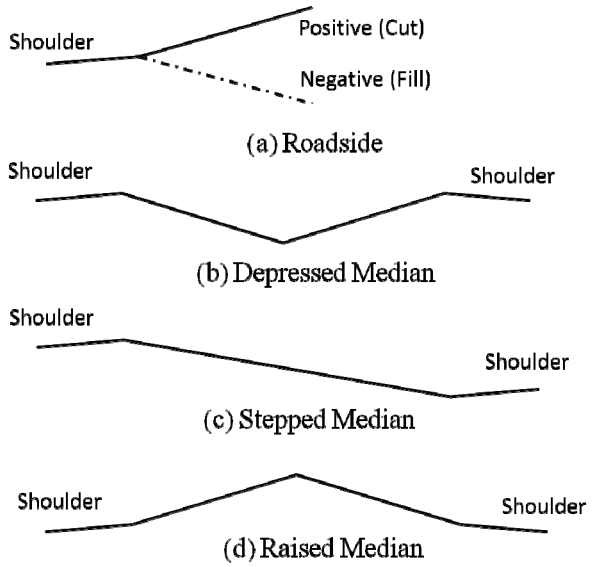

Figure 3.2 Typical roadside and median configurations(*37*).

The stepped median shown in Figure 3.2 (c) can be analyzed using trajectory data derived from the analyses of the roadside cut and fill (which is a subset of the

depressed median configurations) slopes. For a stepped median configuration, a median barrier will generally be placed at or near the edge of the slope break on the higher elevation travel lanes. If the vehicle encroaches from the lower travel lanes, it will impact the median barrier in a manner similar to when it encroaches onto a roadside with a positive (cut) cross-slope. If the median barrier is laterally offset onto the median cross slope, the trajectory of a vehicle traveling down the slope from the upper travel lanes is analogous to encroaching onto a roadside negative (fill) slope. Hence no additional simulation was needed to explore this median configuration.

The raised median (Figure 3.2d) can generally be analyzed using trajectory data from the analyses of roadside positive (cut) slopes. If a median barrier is needed in a raised median, it is generally recommended that the barrier be placed at the break point between the two median cut slopes. Thus, the trajectory of a vehicle off either side of the roadway will be analogous to a roadside cut slope. Hence no additional simulation was needed for this median configuration.

As defined in AASHTO *Roadside Design Guide* (*12*), (see Figure 3.3) the median width is the distance from edge of travel-way to edge of opposite travel-way, which includes shoulders if present. The width of the ditch section is, therefore, simply the overall median width minus the combined shoulder width. Typical median widths and shoulder widths used by the states on their divided highway range from 11.6 m (38 ft) to 23.2 m (76 ft) and 1.22 m (4 ft) to 1.89 m (6 ft), respectively (*12*). In this study, simulations were performed using 12.2 m (40ft), 18.3 m (60 ft), and 23.2 m (76 ft) wide medians with shoulder widths of 1.22 m (4 ft) and 1.83 m (6 ft). 6:1 is the most common median slope used in United States. There is little concern regarding the performance of barriers placed on slopes that are 10:1 or flatter. Hence, median cross-slopes of 8:1 and 6:1 were included in the analyses conducted under this study.

Depending on the type of facility, the width of roadside shoulders can range from zero to 3 m (10 ft). However, for the roadside cases, the shoulder width does not play a significant role in influencing the vehicle interaction with a barrier placed on the

foreslope. Therefore, a constant 1.22 m (4 ft) wide shoulder was used during the simulation analysis.

Based on the above discussions, a final matrix for the vehicle trajectory analysis is presented in Table 3.3. Simulation analyses were performed to evaluate all roadside and median configurations listed in this table.

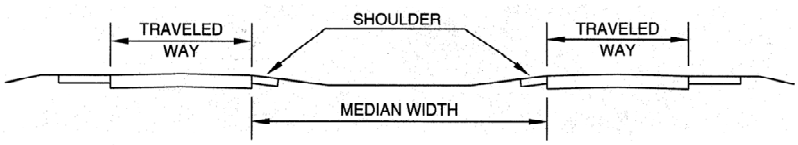

Figure 3.3 Typical depressed median configuration (*12*).

Table 3.3 Simulation matrix for vehicle trajectory analysis.

Vehicle Types	
NCHRP Report 350 design vehicles	820-kg (1806 lb) Geo Metro 2000-kg (4406 lb), Chevrolet C2500
Encroachment Conditions	
Angles	15°and 25°
Speeds	100 km/h (62 mph) and 80 km/h (50 mph)
Roadside and Median Configurations	
Median Cases	
Shoulder Width (SW)	1.22 m (4 ft) and 1.83 m (6 ft)
Median Width (MW)	12.2 m (40ft); 18.3 m (60 ft); 23.2 m (76 ft)
Ditch Width (DW= MW-2×SW)	8.5 m (28 ft); 9.8 m (32 ft); 14.6 m (48 ft); 15.9 m (52 ft); 19.5 m (64 ft); 20.7 m (68 ft).
Cross-slope	6:1 and 8:1
Shape	V
Roadside Cases	
Shoulder width	1.22 m (4 ft)
Cross-slope	6:1 and 8:1
Shape	Positive slope (cut)

3.3. RESEARCH METHODOLOGY

The current study investigated the performance of five commonly used barrier systems placed on sloped median and roadside terrain. Ideally, a single finite element code would

simulate the vehicle traversing the slope and impacting the barrier. However, the total encroachment event is relatively long in duration and large computational times are required to capture both events. Thus, considering the large number of parametric runs needed to address the variables of interest, exclusive use of a single-code two-event simulation scenario was not the most suitable approach for this research. Initial simulation analysis was therefore divided into two parallel parts. One part used a multi-rigid-body dynamics code to quantify the trajectory of the vehicles across selected roadside and median configurations for different encroachment conditions. Short run times for the multi-rigid-body code allowed an extensive parametric study of the influence of terrain on vehicle trajectory. The other part of the simulation focused on developing performance envelopes in terms of vehicle containment heights for selected guardrail and median barrier systems installed on flat and level terrain. This part was executed using a non-linear finite element code capable of modeling vehicle to barrier contact. Figure 3.4 shows flow chart of the tasks performed in this study. Details of these tasks are discussed below.

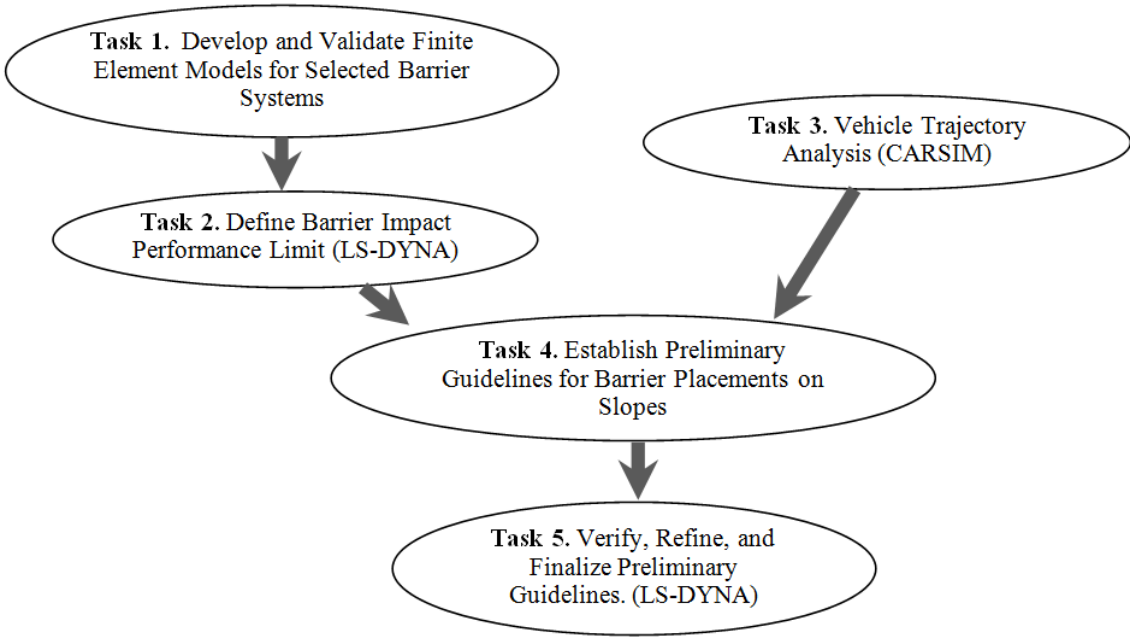

Figure 3.4 Flow chart of the research approach.

3.3.1. Develop and Validate Finite Element Model

To properly evaluate the selected guardrail systems, suitable FE representations must first be developed in LS-DYNA. A significant component of the current study addressed preparing quality FE guardrail LS-DYNA models. While public domain FE models for the needed vehicles exist and are well documented, this is not the case for some of the selected guardrail systems. Although FE models for most of the components used in selected guardrail systems are readily available, preparing quality FE model for these systems required component assembly, defining contact algorithms, and modifications to attain satisfactory simulation results. To ensure reliable results, model fidelity was assessed through comparison of simulated and measured responses reported in full scale crash test studies conducted on flat terrain. Finite element impact simulations were performed, using the public domain vehicle models and the guardrail models developed in this study, to mimic the conditions used in previously performed crash tests. An event time-sequence comparison approach and approaches proposed by Ray et al. (*31*) were followed to verify and validate the simulation results. Roadside Safety Verification and Validation program (RSVVP) developed by Mongiardin and Ray (*38*) were used to compare the acceleration and angular response data obtained from crash tests and simulations.

3.3.2. Define Barrier Impact Performance Limit

LS-DYNA simulations were used to construct a vehicle containment limit for each roadside guardrail and median barrier system. Crash simulations were performed on the guardrails placed on flat and level terrain. The height of the impact were parametrically varied to determine the performance limits of the barrier as defined by initiation of override or rollover for the pickup truck and underride for the small passenger car. The impact conditions used to establish the barrier performance limits conformed to *NCHRP Report 350* testing guidelines. As shown in Table 3.4, on average, a total of three

simulations were required to identify the override or underride limits for each guardrail system.

Table 3.4 LS-DYNA simulation matrix for barrier performance analysis.

Rail Type	Impact Analyses		Total Simulation
	Pickup Truck (Override Limit Analysis)	Small Car (Underride Limit Analysis)	
Modified G4(1S) W-beam System	3	3	6
Midwest Guardrail System	3	3	6
Modified Thrie-beam System	3	3	6
Modified Weak Post W-beam System	3	4	7
Box-Beam System	3	3	6
Totals	15	15	31

3.3.3. Vehicle Trajectory Analysis

The multi-rigid-body dynamics analysis software package CARSIM was used to quantify trajectories of vehicles traversing across selected roadside and median configurations for different encroachment conditions. The outputs taken from these simulations included graphical plots of vehicle bumper height with respect to local terrain along the ditch cross-section. Other related vehicle dynamic parameters such as vehicle orientation, speed, and angular velocities were also recorded during the encroachment event and at the time of barrier impact.

Accurate trajectory simulation requires accurate suspension properties in the vehicle model. While the overall suspension response is affected by the properties of several suspension components including bushings, tie-rods, stabilizer bars, suspension to body attachments, etc., the most critical components are the suspension springs and dampers (*39*). CARSIM vehicle models have default values for the spring and damper properties. However, these properties generally do not completely capture the loading range or rates typical of off-road encroachments. Consequently, coil-springs and dampers of actual test vehicles were sent to an independent test lab to obtain their actual response properties.

While extracting vehicle dynamics parameters such as trajectory of sprung mass origin, yaw, pitch, and roll angles is readily obtained in CARSIM, extracting the vehicle's bumper trajectory is slightly more involved. A computer code was developed to determine the bumper height with respect to its local terrain along the ditch cross-section based on other output data available from the CARSIM simulations. As a first step, the geometric location of the bumper corner in a free-standing condition, were determined for both vehicles. Orientation data from CARSIM output (i.e. yaw, pitch, and roll angles) were used to extrapolate and trace the path of the vehicle bumper corner. As illustrated in Figure 3.5, traces of the bumper top traveling across the median were then projected on a plane perpendicular to the ditch. The thick solid curve in the figure represents the trace of the bumper top projected on ditch section, and the dotted curve indicates the relative height of the bumper top assuming a reference line along the horizontal axis. When integrated with the barrier performance limits, this curve allows the user to identify acceptable and unacceptable lateral barrier placement ranges along the ditch section. The vehicle dynamics (VD) analysis results obtained using CARSIM were validated against the results obtained from a full scale crash test conducted at TTI. In the test, a C2500 pickup impacted a barrier placed on a sloping terrain. The test condition prior to the point of impact was simulated using CARSIM. The trajectory and angular orientation of the vehicle obtained from the simulation was then compared against those observed in crash test. Next, relative bumper trajectories for two different design vehicles encroaching at various encroachment speeds and angles combinations were calculated to develop trajectory envelop onto a selected ditch configuration. These envelopes as shown in Figure 3.6, trace the upper and lower projections of the individual bumper plots across the ditch profile. A total of 112 CARSIM simulations were performed to determine the vehicle trajectory envelopes for the 14 roadside and median ditch configurations used in this study.

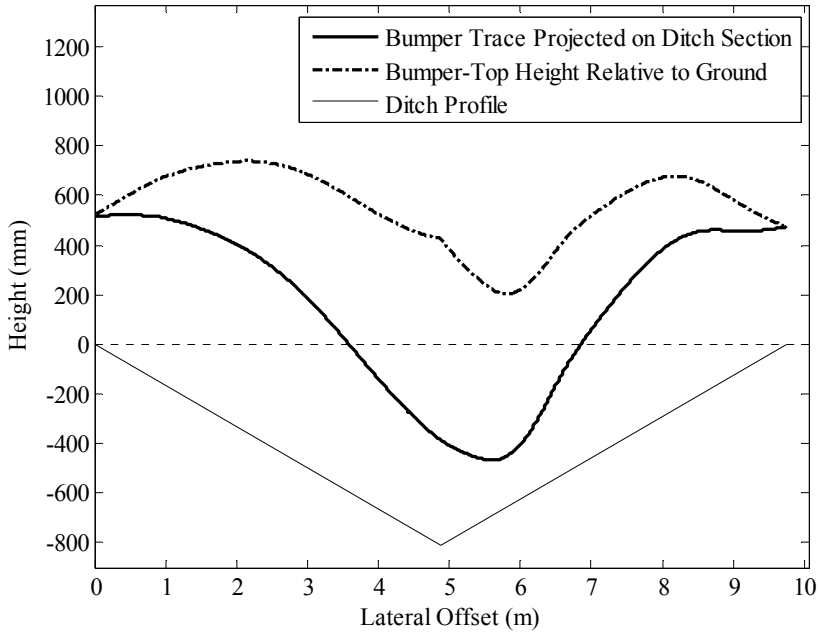

Figure 3.5 Vehicle bumper profile along the ditch cross section.

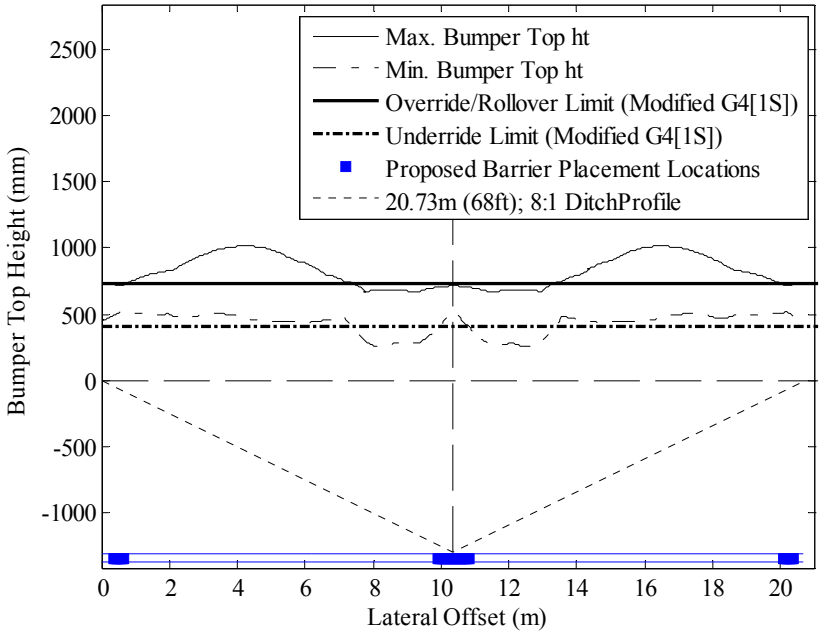

Figure 3.6 Barrier performance limits superimposed onto vehicle trajectory envelope to obtain acceptable barrier offset locations.

3.3.4. Develop Preliminary Guideline

Once the barrier performance limit and vehicle trajectory analyses were concluded, the derived barrier containment ranges were superimposed on the vehicle trajectory data to quantify the performance of a given barrier on a given slope as a function of barrier offset. Horizontal lines superimposed on the trajectory envelopes shown in Figure 3.6 are the performance limits (i.e., override/rollover limit and underride limit) for a given barrier. If, at a given lateral offset, the thin solid line (maximum bumper height) exceeds the barrier override/rollover limit, it is highly probable that a pickup truck will rollover or override the barrier placed at that location. Similarly, if the thin dotted line (minimum bumper height) extends below the underride limit line, it is likely that a small car can underride the barrier placed at that location, resulting in severe vehicle snagging and excessive decelerations. The solid bars plotted at the bottom of the figure indicate locations for which barrier performance is predicted to be acceptable (i.e., neither override/rollover nor underride is expected). Using these graphical representations, preliminary guidelines for the placement of each barrier type on roadside and median slope were developed.

3.3.5. Validate and Refine Performance Guideline

Once the preliminary guidelines were developed, additional simulations of selected configurations of vehicle type, barrier type, barrier offset, and slope/ditch configuration were conducted using LS-DYNA simulations. These simulations captured the full encroachment event from departure of the vehicle off the traveled way through impact with the barrier. These runs were conducted to verify, validate, and refine the guidelines developed from the superposition of the independent impact and trajectory analyses. Configurations selected for simulation included both the scenarios for which failure was expected and those for which successful containment was predicted. It is important for these validation analyses to include failure scenarios in order to establish confidence

in the simulation results. The terrain configurations simulated included vehicle encountering the barrier on a foreslope and on a backslope of the depressed median. For the simulations on V-shaped median configurations with a single median barrier placed in the ditch, dual-sided barrier model was developed by adding extra rail and blockout elements to the single-sided guardrail model.

4. DEVELOPMENT AND VALIDATION OF FINITE ELEMENT MODELS

4.1. INTRODUCTION

Detailed finite element models for the modified G4(1S) W-beam guardrail, Midwest guardrail, modified Thrie-beam guardrail, modified weak post W-beam guardrail, and box-beam guardrail systems were developed in this study to evaluate their performances on non-level terrain. Public domain FE models of 2000P and 820c test vehicles were used to conduct crash simulations. In the past, crash tests were performed on each of the selected guardrail systems installed on flat terrain as per NCHRP report 350 test conditions. Finite element simulations were performed on each guardrail model to mimic these crash tests. Results from the physical tests and simulations were compared to validate the FE guardrail models. A brief description of the vehicle models used for the simulations is provided in this section. Material properties used for various guardrail components and procedures used to develop and validate each of the five guardrail systems are discussed in subsequent sections.

4.2. VEHICLE MODEL

The test matrix for longitudinal barriers in NCHRP report 350 includes tests with an 820 kg (1800 lb) passenger car and a 2000 kg (4409 lb), $^{3}/_{4}$ ton, standard cab pickup truck. The FE models of the two vehicles used in this study are shown in Figure 4.1. These vehicle models were originally developed by the National Crash Analysis Center (NCAC) and were modified by the researchers at Texas Transportation Institute (TTI) over a period of time. The FE models of the passenger car and the pickup truck consist of 16,100 elements and 58,313 elements, respectively. In this study, pickup truck model was used to simulate the existing crash tests in order to validate the FE models developed for five guardrail systems. For the performance limit analyses both the pickup

and passenger car models were used to determine override and underride limits for the guardrails. Several modifications were made to the pickup model before using it for the simulations.

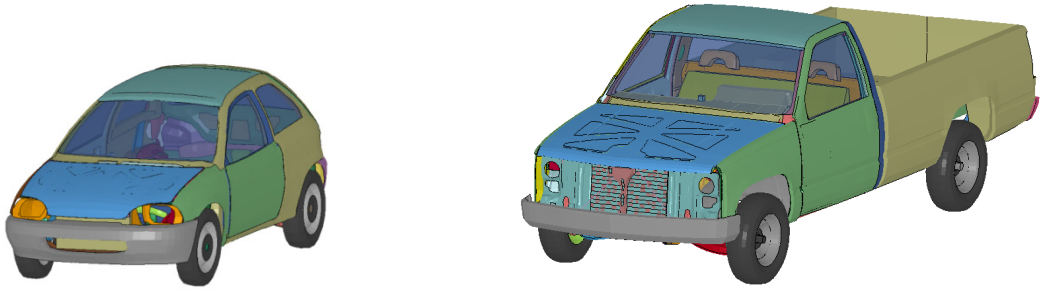

(a) (b)

Figure 4.1 (a) 16,100 elements Geo Metro passenger car model (Release date: Oct 2000) and (b) 58,313 elements detailed C2500 Pickup model (Release date: Nov 2008) (*40*).

Some vehicle characteristics of the 2000P truck model were modified based on measured values of crash test vehicles representative of those used at TTI. Constrained nodal rigid body inertia was used to adjust the inertia properties of the pickup model to measured values. Location and inertia of this nodal rigid body were adjusted to obtain the measured vehicle center-of-gravity (C.G.) height of 675 mm (26.5 inches). Table 4.1 shows the measured and adjusted values of mass inertia properties for the pickup model.

The mass of the pickup model was reduced from 2029 kg to 2000 kg by reducing mass from different vehicle parts such that the C.G. height of the vehicle remains the same. The overall mass distribution of the modified pickup model was verified by performing a zero-velocity simulation in which the truck reaches an equilibrium condition under gravity load. The reaction forces between the truck tires and the ground surface obtained from the simulation were compared to the measured weight distribution from a representative test vehicle. Figure 4.2 shows the comparison between the simulation and test vehicle reaction forces for all four tires. The oscillation in the

simulation forces results from sudden application of gravity, which causes the vehicle suspension to oscillate as it approaches a steady state response.

Table 4.1 Measured and adjusted values of mass inertia properties for the pickup model.

Mass Moment of Inertia	Measured Value ($kg\text{-}m^2$)	Raw Vehicle Model ($kg\text{-}m^2$)	Inertia for the Nodal rigid Body ($kg\text{-}m^2$)	Modified Vehicle Model ($kg\text{-}m^2$)
Ixx	961.4	788.2	173.2	960
Iyy	5621.98	4368	1254	5621
Izz	5596.22	4728	863	5591

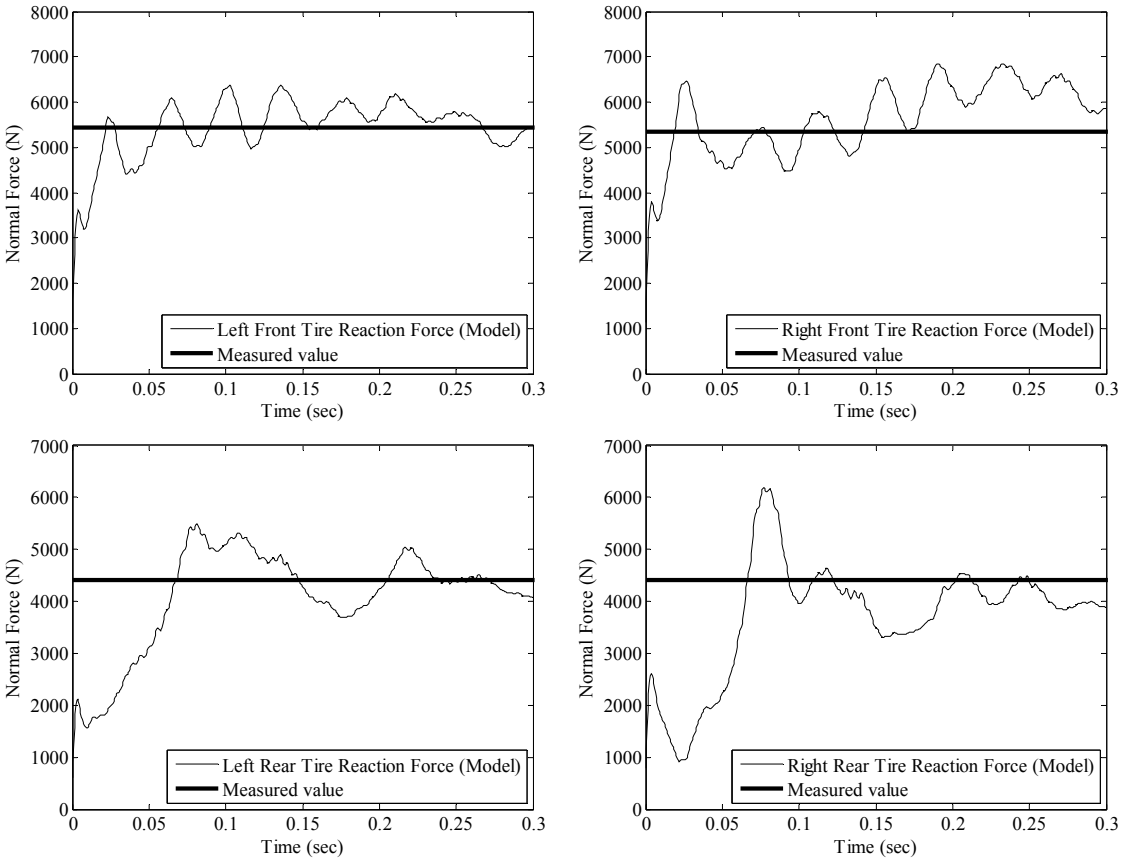

Figure 4.2 Comparisons of overall weight distribution of pickup model and test vehicle.

To obtain better contact behavior between the truck fender and guardrail during impact analyses, impact side (front left) fender of the truck model was re-meshed to have finer elements as shown in Figure 4.3(a). Some of the simulations performed in the beginning of this study failed due to high hourglass energy created by under integrated quadrilateral Belytschko-Tsay (*29,41*) shell elements used in impact side door stiffener as shown in Figure 4.3(b). These quadrilateral shell elements were replaced by much stiffer triangular shell elements as shown in Figure 4.3(c).

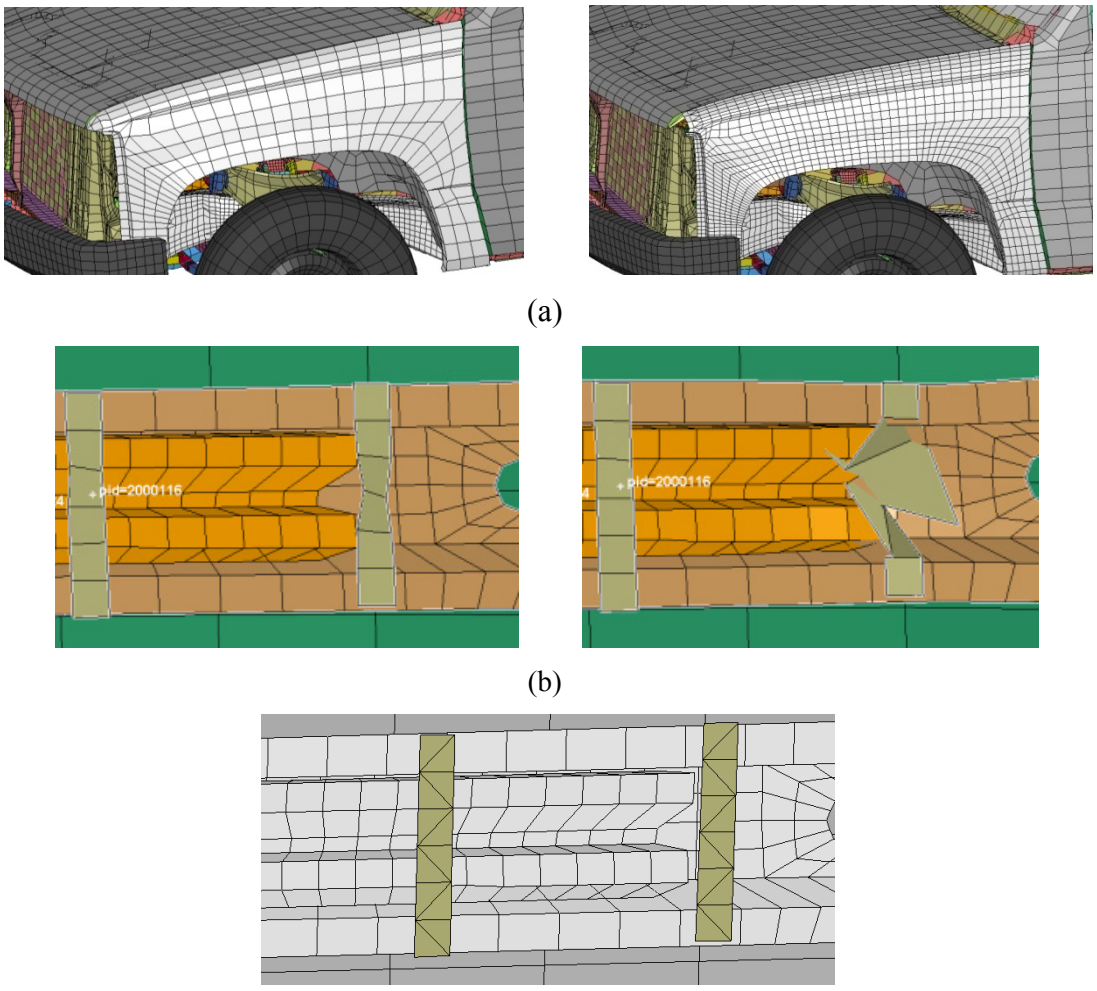

(a)

(b)

(c)

Figure 4.3 (a) Vehicle fender before and after the re-mesh (b) hourglass problem on quadrilateral shell elements used in impact side door stiffener (c) Triangular shell elements in modified door stiffener.

4.3. MATERIAL MODEL

Guardrails selected for this study consists of several components with different shapes and material properties. Geometries and material properties of these components are specified in AASHTO/ARTBA/AGC *Barrier Hardware Guide* (*13*). Table 4.2 lists the types of materials specified for some key components of the five guardrail systems. LS-DYNA material models that closely represent these material types are also shown in the table.

Table 4.2 Material types used for key components of selected guardrail systems.

Key Components	Material Type Specified (*13*)	LS-DYNA Material model	
		Type	Material Name
Rail:			
W-beam Rail (RWM02) (*13*) Thrie-beam Rail (RTM01)	AASHTO M180 Class A Type II Steel	Type 24	Piecewise Linearly Plastic
Box-Beam Rail (RBM01)	ASTM A500 Grade B Cold-rolled tubing		
Post:			
W150×13.5 Strong Post (PWE01-04); S75×8.5 Weak Post (PSE 08)	AASHTO M270M (ASTM A709M) Grade 250 Steel	Type 24	Piecewise Linearly Plastic
Blockout:			
W-beam Blockout (PDB01)	Timber	Type 1	Elastic
Modified Thrie-beam Blockout (PWB03)	AASHTO M270M Grade 250 Steel	Type 24	Piecewise Linearly Plastic
Others:			
Soil Plate (PLS01); Splice plate (RBS01); Support Bracket (FPP01) Square Washers	AASHTO M270M Grade 250 Steel	Type 24	Piecewise Linearly Plastic
Soil	--	Type 198	Jointed Rock

The metal components of the guardrail such as rails, posts, Thrie-beam blockout, square washers, and soil plate were modeled using piecewise linearly plastic material (Type 24) representation. This material model has been extensively used to represent structural metals, such as steel and aluminum, and it has been fully validated and optimized. The material properties of the W-beam and Thrie-beam rail used in the simulation correspond to AASHTO M180 Class A Type II Steel. Material with higher density was used for the finer elements around the bolt slot cuts within the guardrail. Reid and Bielenberg (*42*) presented the effective true stress vs. strain curves for these materials as shown in Figure 4.4. Material properties shown for the elements surrounding the slot cut were determined from coupon tearing test and properties for remaining elements were determined from tensile coupon test (*42*). The material around the slot was found weaker due to the stress concentration produced around the slots during fabrication (*42*). The material properties of the guardrail posts, modified Thrie-beam blockout, and other steel components used in the model corresponds to AASHTO M270M grade 250 steel (*13*). Code specified yield stress and tensile stress capacities for this steel grade are 250 MPa (36 ksi) and 400 MPa (58 ksi), respectively(*43*). However, these specifications are barely minimum. To obtain more accurate material behavior, uniaxial tests of steel coupons from W150×13.5 (W6×9) guardrail posts were performed at TTI (*44*). The average of the properties obtained from these tests, as shown in Figure 4.4, were closer to the yield stress and tensile stress capacities specified for grade 345 (grade 50) steel (*44*). Piecewise linearly plastic material with the properties obtained from these tests were used to model the AASHTO M270 grade 250 steel. Tensile ($\sigma_{ult|eng.}$) and yield (σ_y) stress capacity of ASTM A500 Grade B steel used for box-beam rail are specified as 400 MPa (58 ksi) and 317 MPa (46 ksi), respectively(*43*). 50 mm (2 inch) elongation ($\varepsilon_{ult|eng.}$) specified for this material is 23%(*43*). Using these values in Equations (4.1) to (4.3), true tangent modulus ($E_{Tan|true}$) for this material can be calculated as 851.9 MPa (123.5 ksi). The effective true stress vs. strain curve for the material is shown in Figure 4.4.

$$\varepsilon_{ult|true} = \ln(1 + \varepsilon_{ult|eng.}) \tag{4.1}$$

$$\sigma_{ult|true} = \sigma_{ult|eng.}(1 + \varepsilon_{ult|eng.}) \tag{4.2}$$

$$E_{Tan|true} = \frac{\sigma_{ult|true} - \sigma_y}{\varepsilon_{ult|true} - \frac{\sigma_y}{E}} \tag{4.3}$$

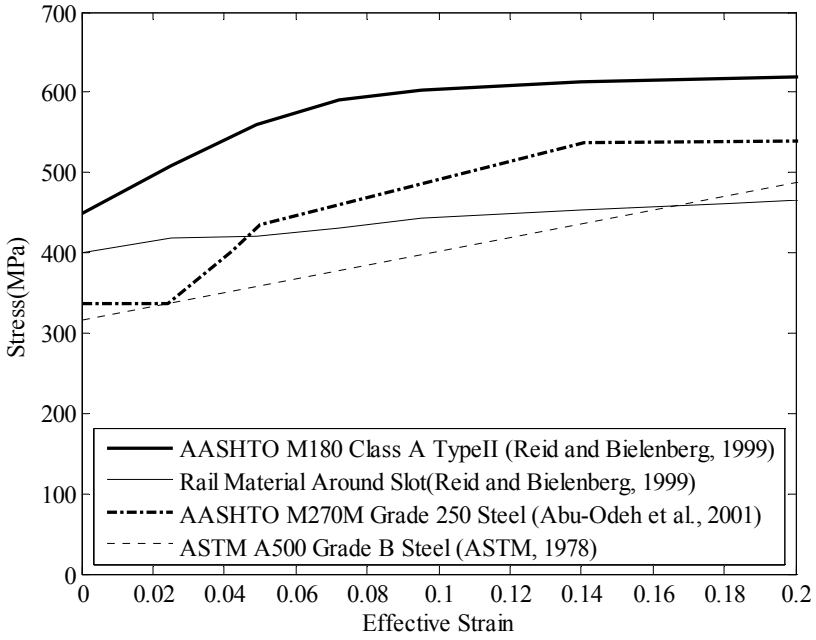

Figure 4.4 Stress-strain curves for steel components used in guardrail models.

The timber blockout used in strong post W-beam guardrail was modeled using elastic material (Type 1). The soil was modeled using jointed rock (Type 198) where joints are assumed to exist throughout the material at spacing small enough to be considered ubiquitous (*41*). This material type contains most of the soil parameters to accurately represent the soil behavior. The properties used for the soil material, as shown in Table 4.3, were obtained from previous studies performed at TTI.

Table 4.3 Soil properties used for Type 198 material card.

Mass Density tonne/mm^3	Elastic Shear Modulus, Gmod	Poisson's Ratio	Failure Surface Shape Parameter, rkf	Angle of friction, phi (rad)	Cohesion Value, cval	Dilation Angle psi, (rad)	Minimum shear Strength of Material, str_lim
2.09E-9	18.51MPa (2.7 ksi)	0.35	1.0	0.698 (40 deg.)	0.015	0.0	0.05×cval

4.4. MODIFIED STRONG POST G4(1S) W-BEAM GUARDRAIL

The modified strong-steel post, G4(1S) W-beam guardrail system is one of the most commonly used guardrail systems on the nation's highways. The system is designated as SGR04a by the AASHTO *Roadside Design Guide* (*12*). This designation follows that used in the AASHTO/ARTBA/AGC *Barrier Hardware Guide* (*13*). The modified G4(1S) W-beam guardrail is the result of improvements to the original G4(1S) W-beam guardrail system which failed to comply with *NCHRP Report 350*(*2*). The key difference between the modified and standard G4(1S) w-beam guardrail system is the use of a 150 mm×200 mm (6 in×7.88 in) timber blockout in place of the W150×13.5 (W6×9) steel blockout.

4.4.1. System Description

The modified G4(1S) W-beam guardrail system consists of 3.8 m (12.46 ft) long, 12-gauge W-beam rail elements mounted on 1.83 m (6 ft) long W150×13.5 (W6×9) steel posts spaced 1.9 m (6.2 ft) on center (*7*). Splice connections are placed at alternate post locations. 150 mm× 200 mm × 360 mm-long (6 in×7.88 in×14 in) timber blockouts are used to offset the W-beam rail from the support posts. The W-beam rail elements and the timber blockouts are attached to the posts with 16 mm (5/8 in) diameter button bolts without washers. The bolt hole on the blockout is offset to match one of the two bolt holes in the flange of the steel post. The height of the guardrail to the top of the W-beam

rail element is 710 mm (27.9 in). A photograph of a modified G4(1S) guardrail is shown Figure 4.5. Figure 4.6 presents details of the guardrail and its key components.

Figure 4.5 Typical modified G4(1S) W-beam guardrail system(*7*).

4.4.2. Model Development

Finite element model of a modified G4(1S) W-beam guardrail, as shown in Figure 4.7(a), was developed by the researchers at Texas Transportation Institute (TTI). This model was used and modified in this study to evaluate the performance limits of modified G4(1S) system in terms of acceptable vehicle impact heights. Geometry of different components of this system were modeled based on the latest specifications provided in the AASHTO Barrier Hardware Guide (*13*). The 30.5 m (100 ft) long section of modified G4(1S) W-beam guardrail model consisted of 427,913 elements.

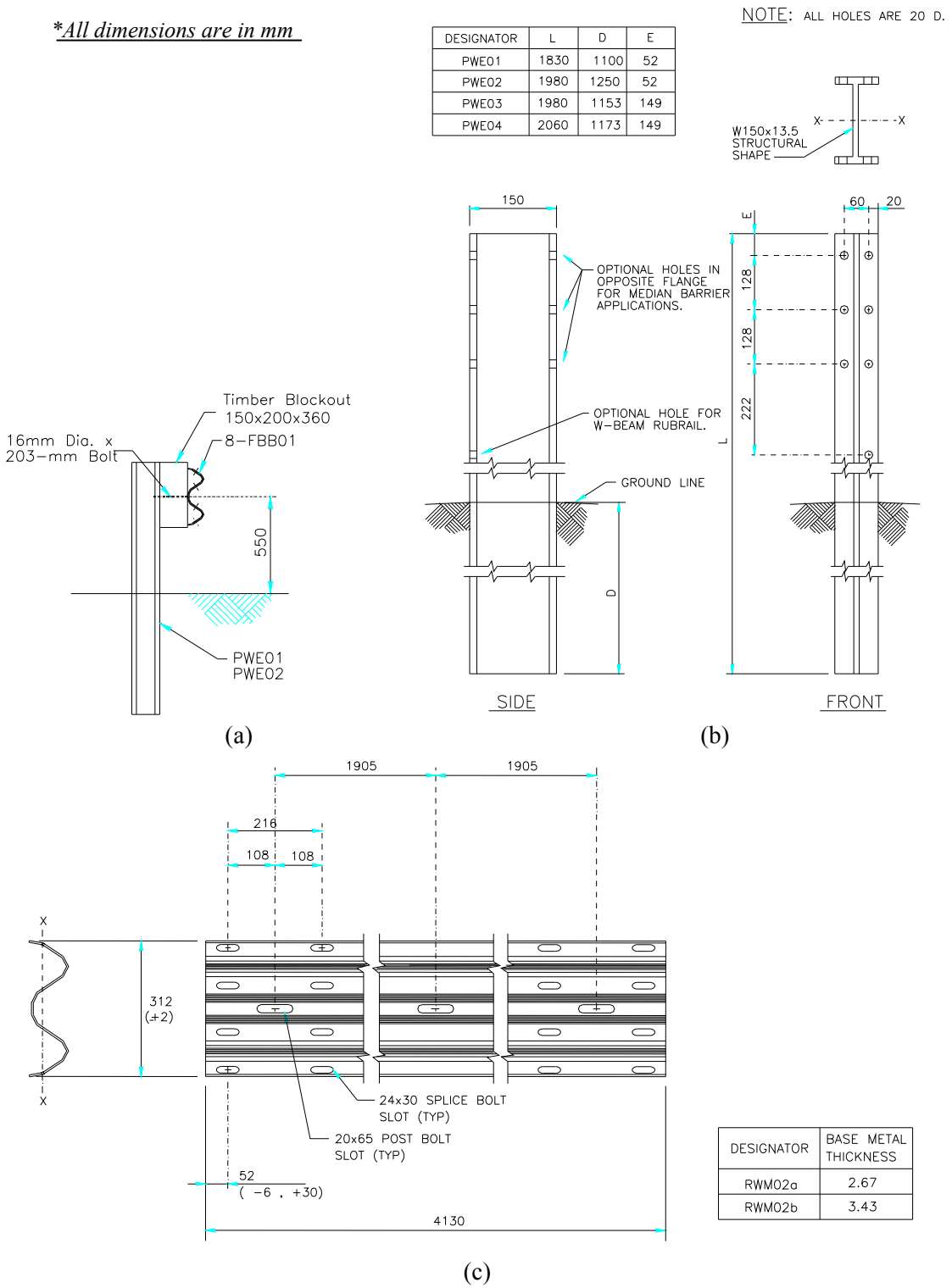

Figure 4.6 Details of (a) Modified G4(1S) strong post W-beam guardrail, (b) Wide-flange guardrail post (PWE01-04), and (c) 2-space W-beam guardrail (RWM 02a-b) (*7,13*).

The 4.13 m (13.5 ft) long W-beam guardrail segments were modeled using Belytschko-Tsay(*41*) shell elements with an average element size of 20 mm (0.78 in). Splice connections, as shown in Figure 4.7(b), between two adjacent rails segments were modeled at every alternate post location. The bolts in the model were incorporated using beam elements for bolt-shaft, and shell elements for bolt heads and nuts. The bolt heads and nuts were constrained to the ends of the bolt shaft so that they could only move and rotate with the shaft. A cylindrical cover of shell elements surrounded the bolt shaft to incorporate the contact between the shaft and the edges of the rail slots. The idealized bolt and nut assembly is shown in Figure 4.7(c). The timber blockout was modeled using constant stress solid elements(*29,41*) as shown in Figure 4.7(b).

The W150×13.5 (W6×9) posts were modeled using Belytschko-Tsay(*29,41*) shell elements. The posts were embedded 1100 mm (43 in) into the soil. To reduce the size of the model and save computational time and cost, the soil was modeled as rectangular buckets of constant stress solid elements(*29,41*) at each post location instead of one large, continuous volume. Larger soil buckets were incorporated in the impact region to accurately capture the post-soil interaction as the post deflected in soil. The rectangular soil buckets around these critical locations were 1.76 m wide × 3.14 m long (laterally) × 1.63 m deep (5.8 ft× 10.3 ft× 5.3 ft). The soil was modeled using the Type 198(*29,41*) material model. Embedment of the post shell elements into the soil solid elements is shown in Figure 4.7(d). Automatic Surface to Surface contact was used to model the contacts between post and soil.

To reduce the model size and hence computation time and cost, the end terminals of the guardrail system were modeled using non-linear axial springs. The force-deflection response of these springs was determined by performing a separate simulation on the guardrail end terminal model shown in Figure 4.6(e). The end-terminal model was 11.45 m (37.5 ft) long. The rail at the end of the terminal where it is attached to the standard guardrail system was pulled in a quasi-static manner by applying a linear longitudinal displacement. The resulting resistance force was measured to determine the overall force-deflection response, as shown in Figure 4.6(f), of the end terminal system.

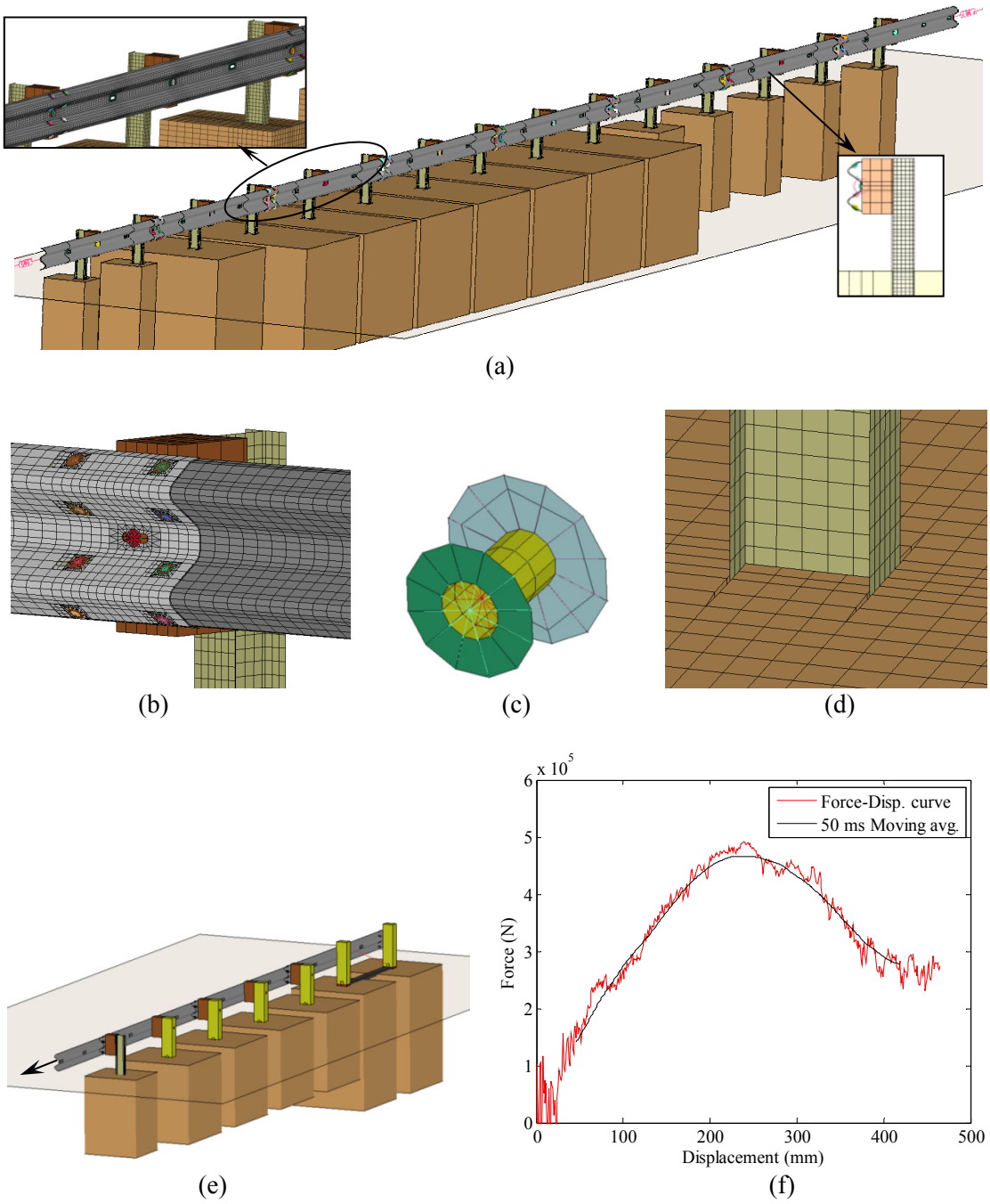

Figure 4.7 (a) FE model for modified G4(1S) W-beam guardrail system. (b) Splice plate and post-blockout-rail connection, (c) Bolt model using NRB; (d)Post to soil embedment (e) FE model of the ET terminal system and (f) Force-displacement curve obtained for the terminal.

4.4.3. Model Validation

The modified G4(1S) W-beam guardrail model was validated by performing a full-scale vehicle impact simulation and comparing the results to a previously conducted crash test of the system. The crash test used for the validation exercise was conducted at TTI (*7*) under *NCHRP Report 350* Test Level 3 (TL-3) impact conditions. A 1989 Chevrolet C2500 pickup truck with a gross static weight of 2076 kg (4573 lb) impacted the Modified G4(1S) W-beam guardrail on flat terrain at a speed of 101.5 km/h (62.9 mph) and at an angle of 25.5 degrees. the pickup impacted the guardrail 4.5 m (14.8 ft) upstream of the rail splice at post 13. The height to the upper and lower edges of the vehicle bumper was 615 mm (14.2 in) and 395 mm (15.6 in), respectively. The vehicle was successfully contained and redirected by the guardrail system. The vehicle became parallel with the installation at 0.278 sec and lost contact with the guardrail at 0.691 sec. The maximum dynamic deformation of the guardrail was 1.0 m (3.28 ft).

To validate the FE guardrail model developed for modified G4(1S) system, an impact simulation was performed similar to the full-scale crash test described above. The NCAC developed finite element model of the C2500 pickup truck model was used to impact the modified G4(1S) W-beam guardrail model. The vehicle in the simulation was successfully redirected and the overall results matched closely with the crash test results. A detailed comparison of the simulation and test results is presented below.

4.4.3.1. Event Time-sequence Comparison

A descriptive time-sequence comparison is presented in Table 4.4. Sequential photographs of simulation and test results are compared in Figure 4.8. As can be seen, the vehicle in the simulation closely followed the trend observed in the crash test. Comparisons of longitudinal accelerations and lateral accelerations obtained at vehicle C.G. during crash tests and simulations are presented in Figure 4.9. Vehicle's yaw, roll, and pitch angles are also compared in Figure 4.10. A reasonable overall correlation

between the test and simulation results was observed from these figures. As can be seen from Figure 4.10, the vehicle's yaw angle obtained from the simulation closely followed the test results. A comparison of roll angle versus time shows that the magnitude was reasonably captured, but there was a phase shift of approximately 0.15 sec. Although the pitch angle varied slightly between test and simulation, the overall pitch angle value was small (less than 5 degrees) for most of the impact duration and the variation is not believed to be significant.

4.4.3.2. Quantitative Validation

Energy balance curves produced by LS-DYNA were analyzed as a measure of numerical stability of the simulation. As shown in Figure 4.11, the total energy curve did not vary more than 0.5% throughout the simulation and the hourglass energy at the end of the run were less than 1% of the initial total energy.

Table 4.4 Event time-sequence comparison of modified G4(1S) W-beam simulation and test.

Incident	Crash test	Model Simulation
Left front tire passed the front face of post 12	0.037s	0.04s
Left front tire made contact with the front flange of post 13	0.107s	0.12s
Left front tire made contact with the front flange of post 14	0.178s	0.2s
Rear bumper of the vehicle made contact with the W-beam rail element	0.225s	0.23s
Left front tire made contact with the front flange of post 15	0.278s	0.305s
Vehicle became parallel with the guardrail	0.278s (68.9km/h)	0.325s (53.8km/h)
Left front tire made contact with the front flange of post 16	0.364s	0.425s
Vehicle lost contact with the rail element	0.691s	0.56s

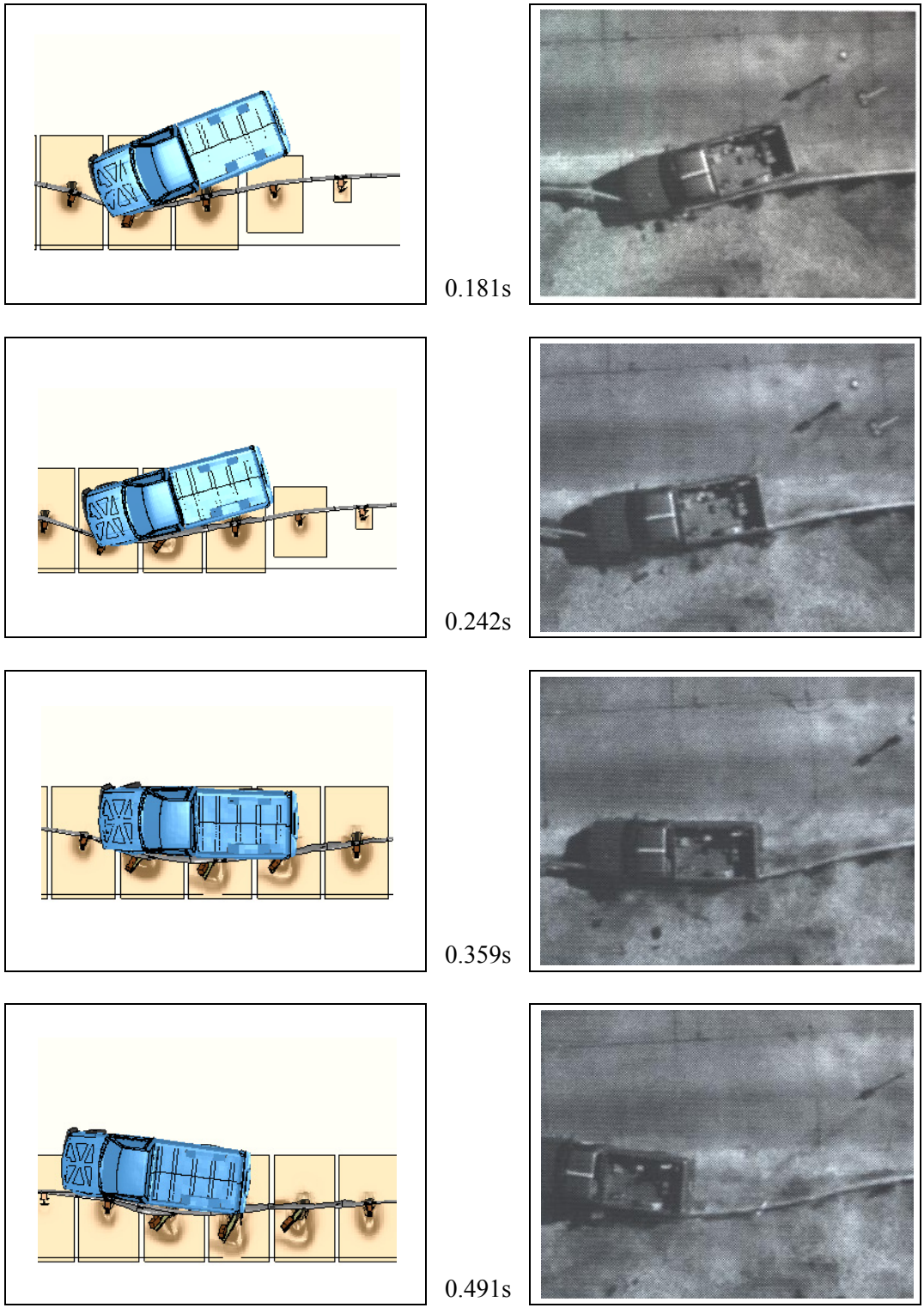

Figure 4.8 Sequential photographs of modified G4(1S) W-beam system model simulation and TTI Test 405421-1(*7*).

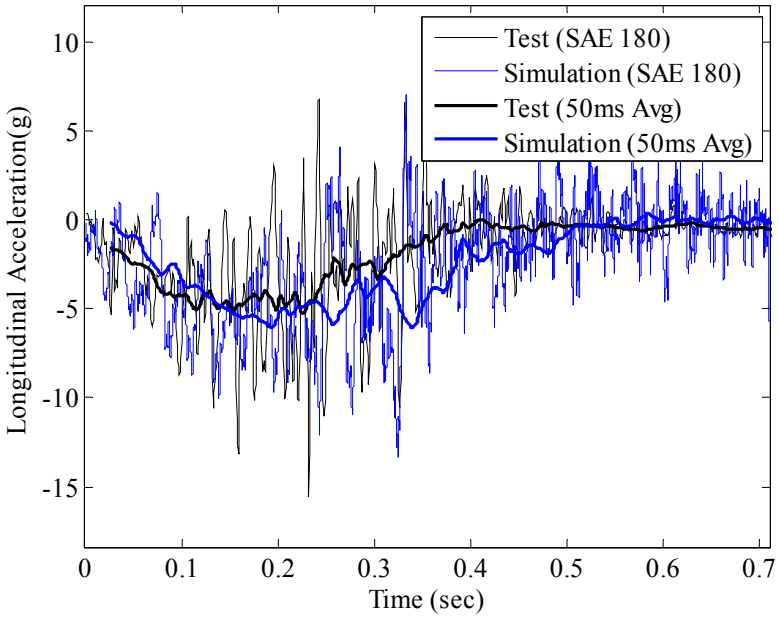

(a)

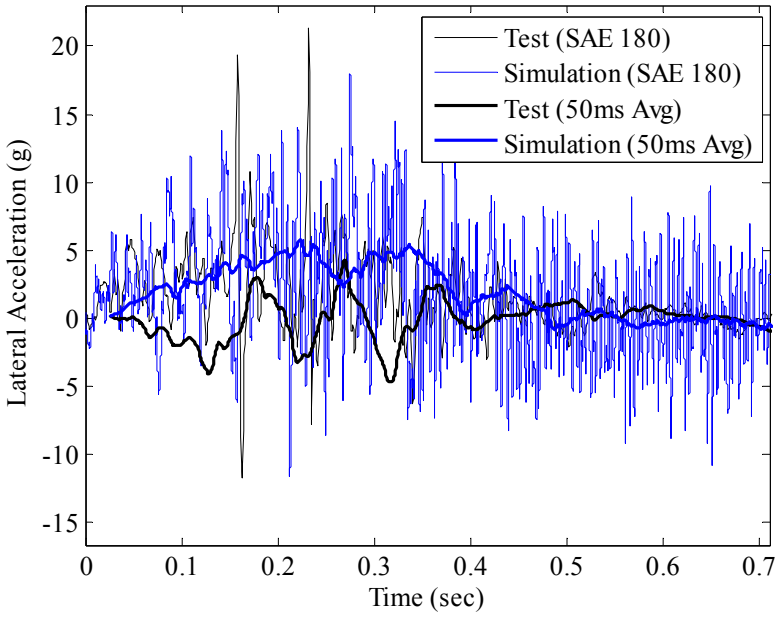

(b)

Figure 4.9 Comparisons of (a) longitudinal accelerations, (b) lateral accelerations obtained at vehicle C.G. during crash tests and simulations for modified G4(1S) guardrail system.

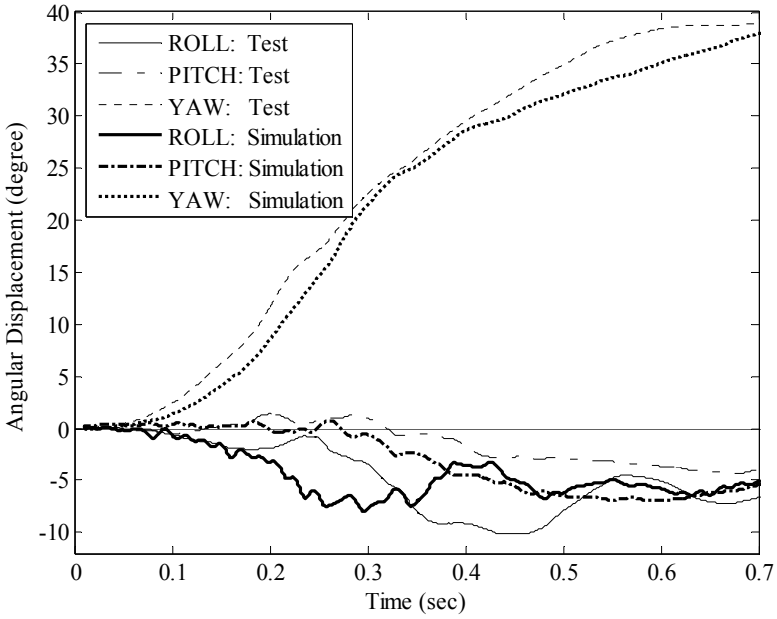

Figure 4.10 Comparisons of roll, pitch and yaw angles obtained at vehicle C.G. during crash tests and simulations for modified G4(1S) guardrail system.

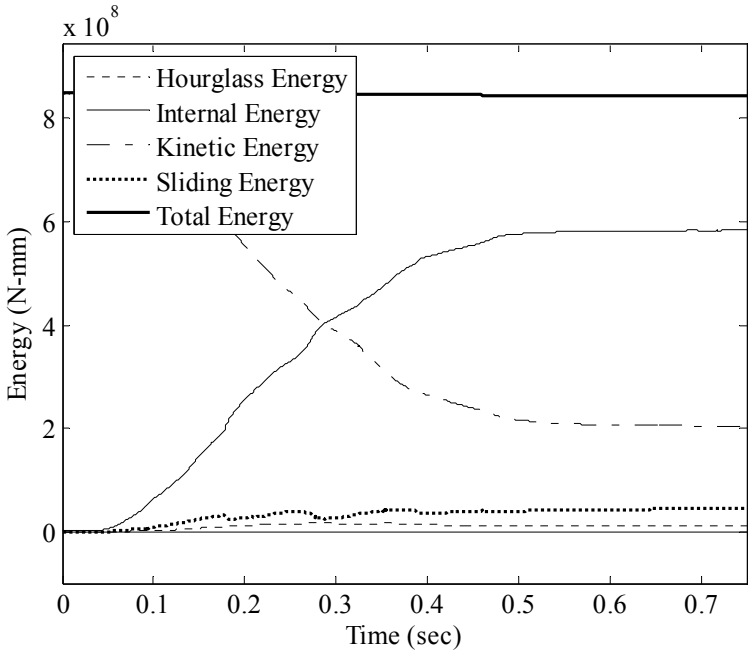

Figure 4.11 Energy balance curve obtained from the simulation on modified G4(1S) guardrail model.

Mongiardin and Ray (*38*) recently developed the Roadside Safety Verification and Validation (RSVVP) program that can calculate comparison metrics between simulation and crash test signals that are helpful in quantitatively validating a roadside hardware model. These metrics are mathematical measures of the agreement between two curves. The Sprague and Geers metrics and Analysis-of-Variance (ANOVA) metrics were computed for the three acceleration channels and three angular rate channels obtained from the LS-DYNA simulation and TTI crash test (*7*) using the RSVVP computer program. According to the procedure, if one or more channels do not directly satisfy the criteria, a multi-channel weighting option may be used. For vehicle to barrier impact tests, barrier redirects the vehicle by keeping its asset horizontal during all the crash events (*45*). Hence for these cases, acceleration collected along the vehicle vertical axis and roll and pitch motions of the vehicle can be considered insignificant compared to other two vehicle acceleration components and vehicle yaw motion. The default multi-channel weighting option in RSVVP calculates weighting factors based on area under the curve with equal distribution of weights between acceleration and rotational rate group. As shown in Table 4.5, the distribution of weights calculated following this approach reflects the actual importance of the channels. Therefore, in the acceleration group, X- and Y-acceleration channels received the higher weights and Z-acceleration channel received the lowest. Similarly, in rotational rate group, yaw rate channel received the highest weight compared to roll and pitch motions. Time history comparison metrics between the crash test and simulation performed on modified G4(1S) system, as shown in Table 4.5, satisfied the criteria for the multiple channel weighting option.

Ray et al. (*31*) recommended developing a phenomena importance ranking table (PIRT) as another means of comparing the test and simulation. The relative difference between the simulation and test results presented in PIRT should not be greater than 20%. As shown in Table 4.6, simulation results satisfied all but one of these PIRT evaluation criteria. While the variation in maximum pitch angle of the vehicle was greater than 20%, the overall pitch magnitude was relatively small for both the test and

the simulation and the difference is not believed to substantially affect the vehicle response.

Table 4.5 Time History Evaluation Table for modified G4(1S) system model.

Compare Test 405421-1(*7*) (Filter Type: C180) and Simulation (Filter Type: SAE180, source: TRAP (*10*))						
Channel Type	Weighting factor: (Area II) (*45*)	Sprague-Geers Metrics		ANOVA Metrics		Pass ?
		M ≤ 40	P ≤ 40	Mean Residual ≤ 0.05	Std. Deviation ≤ 0.35	
X acceleration	0.31	13.6	33.5	-0.03	0.24	Y
Y acceleration	0.26	47.1	42	0.01	0.24	N
Z acceleration	0.02	123	49	0.02	0.57	N
Roll rate	0.05	191	50	0	0.96	N
Pitch rate	0.05	175	43.8	0.01	0.79	N
Yaw rate	0.30	4.3	18.7	0	0.24	Y
Multiple Channel	1.0	37.6	32.7	-0.01	0.3	Y

Table 4.6 Phenomena Importance Ranking Table for modified G4(1S) system model.

Evaluation Criteria	TTI Test	Simulation	Relative Difference ≤ 20%	Pass?
Maximum Dynamic Deflection (m)	1.0m (3.28 ft)	1.19m (3.9 ft)	< 20%	Y
Number of broken or significantly bent posts	9(10~18)	8(10~17)	< 20%	Y
Maximum Roll (deg.)	-10	-8.2	< 20%	Y
Maximum Pitch (deg.)	-4	-7.1	> 20%	N
Maximum Yaw (deg.)	38.9	38	< 20%	Y
Longitudinal direction: Occupant Impact Velocity < 12m/s (30ft/s); Ridedown Acceleration <20g's	7.1m/s (23.3ft/s); -7.9g's	6.3m/s (20.66 ft/s); -10g's	 < 20% < 20%	Y
The rail did not rapture or fail	Yes	Yes	--	Y

4.4.3.3. Vehicle Damage

The vehicle sustained moderate damage in both the crash test and simulation. In both cases, the vehicle's left tie rod, stabilizer bar, and upper and lower A-arms were bent,

and the bumper, fan, radiator, left front tire and rim, and left door were damaged. A comparison of the damage profile of the vehicle in the simulation and the crash test is shown in Figure 4.12.

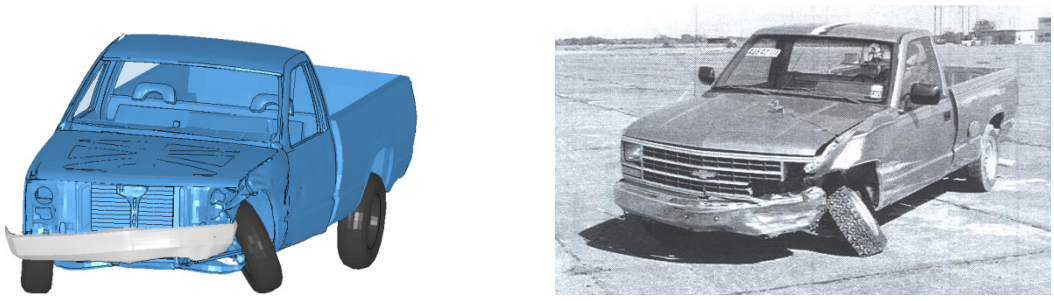

(a) (b)

Figure 4.12 Vehicle after (a) Simulation, and (b) Crash test 405421-1(*7*).

4.4.4. Summary

Results of the simulation performed with the modified G4(1S) W-beam guardrail model showed good correlation with the crash test data. Reasonable correlation was achieved in regard to post and rail damage characteristics, vehicle damage, and key vehicle kinematics parameters. The maximum dynamic deflection of the rail showed good agreement. Vehicle's yaw angles obtained in simulation closely matched those obtained in crash test. Although roll angles showed slight phase difference and there were some differences in pitch angles between simulation and test results, the values were relatively small and the variation is not considered to be significant enough to influence the validity of the model. The occupant impact velocity and ridedown acceleration data obtained from the simulation closely matched the crash test data. Based on these comparative analyses, the model was considered sufficiently valid to proceed with the evaluation of the performance limits of the modified G4(1S) guardrail system.

4.5. MIDWEST GUARDRAIL SYSTEM

In 2000, the Midwest Roadside Safety Facility (MwRSF) developed a new strong-post W-beam guardrail system to improve barrier performance for higher center-of-gravity light truck vehicles, provide reasonable barrier height tolerance, and reduce the potential for W-beam rupture(*5*). The system, as shown in Figure 4.13, is referred to as the Midwest Guardrail System (MGS). The system successfully passed Test level 3 impact conditions for NCHRP Report 350(*2*). In this study, full scale finite element model of the Midwest Guardrail System with standard post spacing was developed and validated to determine its performance limit at different vehicle impact height. Presented below is a brief description of the Midwest Guardrail System, followed by the details of the development and validation of the finite element model of this system.

4.5.1. System Description

As shown in Figure 4.14, the Midwest Guardrail System is comprised of 12-gauge W-beam rail elements mounted on 1.8 m (6 ft) long W150×13.5 (W6×9) steel posts spaced at 1.9 m (6.25 in). The rail splices are placed at the center between posts. The nominal mounting height of the W-beam is 787 mm (31 in) to the top of the rail element. Timber blockouts are used to offset the W-beam rail from the posts. The offset blocks are 150 mm wide × 305 mm deep × 356 mm long (6 in×12 in×14 in) . The W-beam rail elements and the offset blocks are attached to the posts with 16 mm (5/8 in) diameter button head bolts. The bolt hole on the blockout is offset to match one of the two bolt holes on the steel post.

4.5.2. Model Development

A finite element model was developed to conduct crashworthiness analyses of the Midwest Guardrail System (MGS) based on the latest specifications provided in a report

prepared by Midwest Roadside Safety Facility (*14*). The system model, as shown in Figure 4.15, was developed using techniques similar to those employed in developing modified G4(1S) W-beam guardrail model. Major differences between two systems include rail splice location, mounting height of the W-beam rail, and size of the offset blockouts.

Figure 4.13 Midwest Guardrail System –standard post spacing(*14*).

4.5.3. Model Validation

The crash test selected for the validation exercise was conducted at Midwest Roadside Safety Facility (MwRSF)(*14*). The test article consisted of a 53.3 m (175 ft) length of MGS with 11.4 m (37.5 ft) long terminal at each end. A 1995 Chevrolet C2500 pickup truck, with a gross static weight of 1986 kg (4374 lb), impacted the MGS with standard post spacing at a speed of 98.1 km/h (60.8 mph) and at an angle of 25.6 degrees. The vehicle was successfully contained and redirected by the guardrail system. The vehicle became parallel with the installation at 0.396 sec while traveling at a velocity of 61.2 km/h (37.9 mph), and left the guardrail at 0.597 sec at an exit angle of 19.3 degrees and an exit velocity of 55.1 km/h (34.2 mph). The maximum dynamic deflection of the guardrail was 1.094 m (3.34 ft).

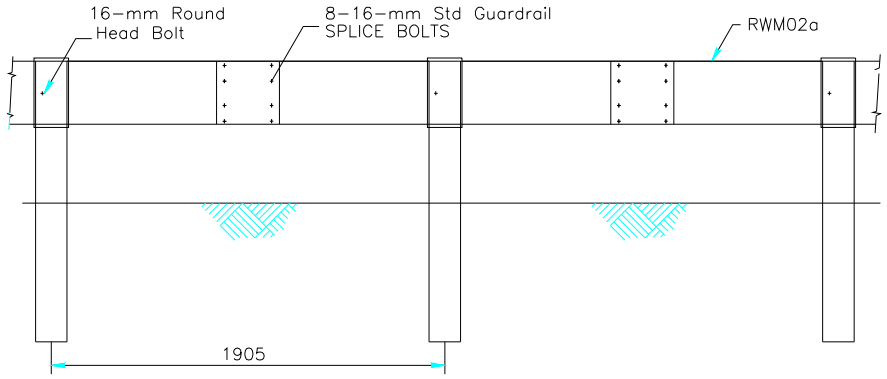

Elevation

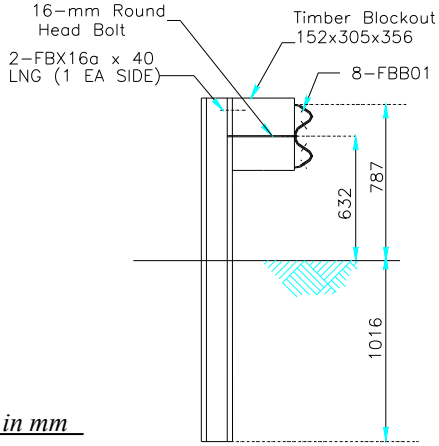

*All dimensions are in mm

Section

Figure 4.14 Detailed drawing of Midwest Guardrail System –standard post spacing(*14*).

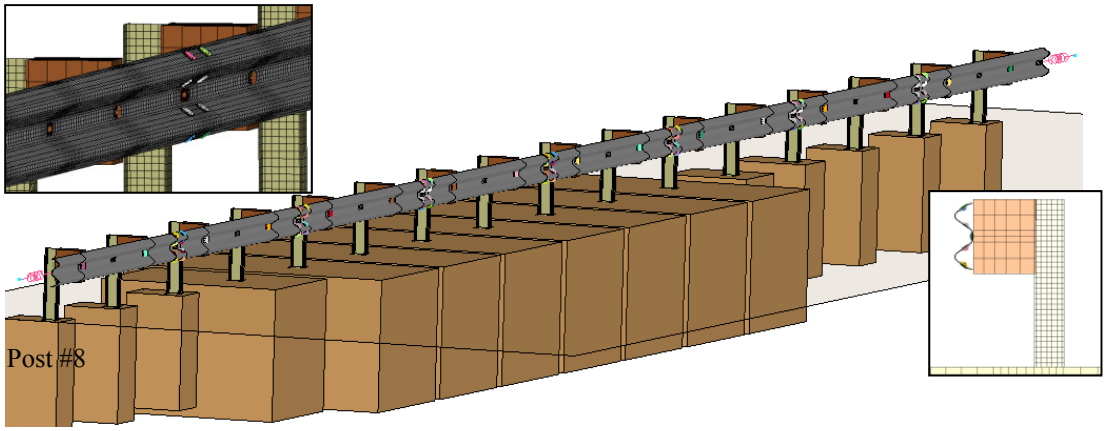

Figure 4.15 Finite Element Model developed for the Midwest Guardrail System.

To validate the Midwest guardrail system model, an impact simulation was performed similar to the full-scale crash test described above. The NCAC developed pickup model impacted the guardrail model at a speed and angle similar to those observed in crash test. The vehicle in the simulation was successfully redirected and the overall results matched closely with the crash test results. A detailed comparison of the simulation and test results is presented below.

4.5.3.1. Event Time-sequence Comparison

A descriptive event time-sequence comparison between simulation and test results is presented in Table 4.7. A comparison of sequential photographs obtained from the two is also shown in Figure 4.16. As can be seen from the table and figure, there is a reasonable overall correlation between the test and simulation results. However, the exit speed of the vehicle in the crash test was slightly higher than that obtained in the simulation. Longitudinal accelerations and lateral accelerations obtained at vehicle C.G. during crash tests and simulations are compared in Figure 4.17. The comparisons of vehicle yaw and roll angles as a function of time are also presented in Figure 4.18. The pitch angle data for the crash test were not available. Both the yaw and roll angles obtained in simulation closely matched those obtained in crash test.

Table 4.7 Event time-sequence comparison between simulation and test for MGS.

Incident	Crash test	Model Simulation
Right front tire snagged on post 13	0.101s	0.095s
Front of the vehicle was located at post 14	0.157s	0.16s
Front of the vehicle was located at post 15	0.232s	0.255s
Right rear corner contacted the rail	0.252s	0.225s
Front of the vehicle was located at post 16	0.323s	0.365s
Vehicle became parallel to the installation	0.397s (61.2km/h)	0.370s (56.8km/h)
Front of the vehicle was located at post 17	0.446s	0.495s
Right rear corner lost contact with the rail	0.521s	0.540s
Vehicle exited the guardrail	0.597s	0.580s
Exit speed and Angle	55.1 km/h; 19.3 deg.	51.5km/h; 17.3 deg.

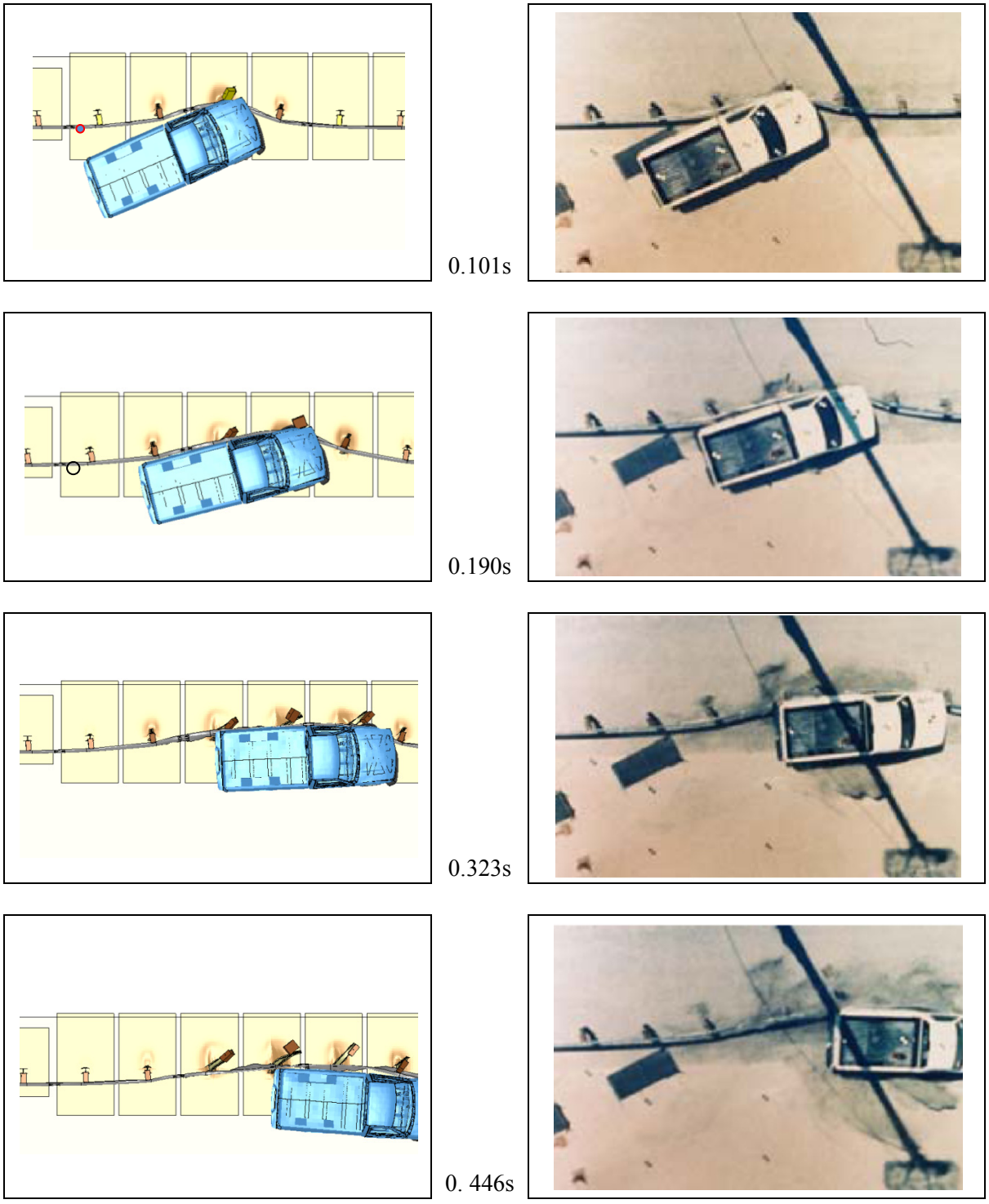

Figure 4.16 Sequential photographs for Midwest Guardrail System model simulation and MwRSF test NPG-4 (*14*).

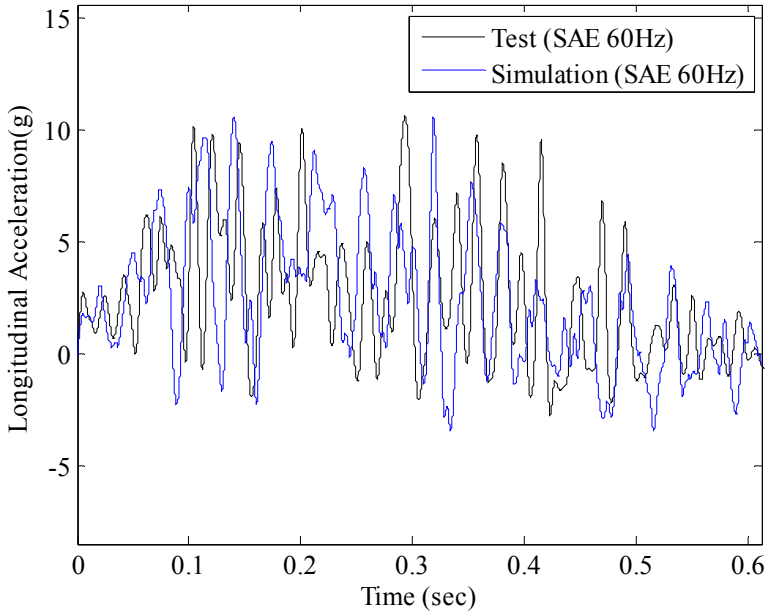

(a)

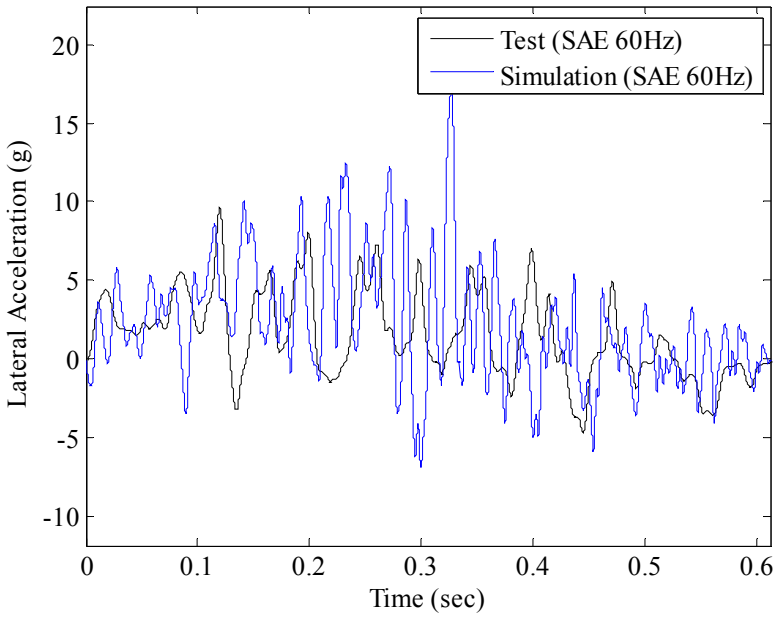

(b)

Figure 4.17 Comparisons of (a) longitudinal accelerations and (b) lateral accelerations obtained at vehicle C.G. during crash tests and simulations for MGS.

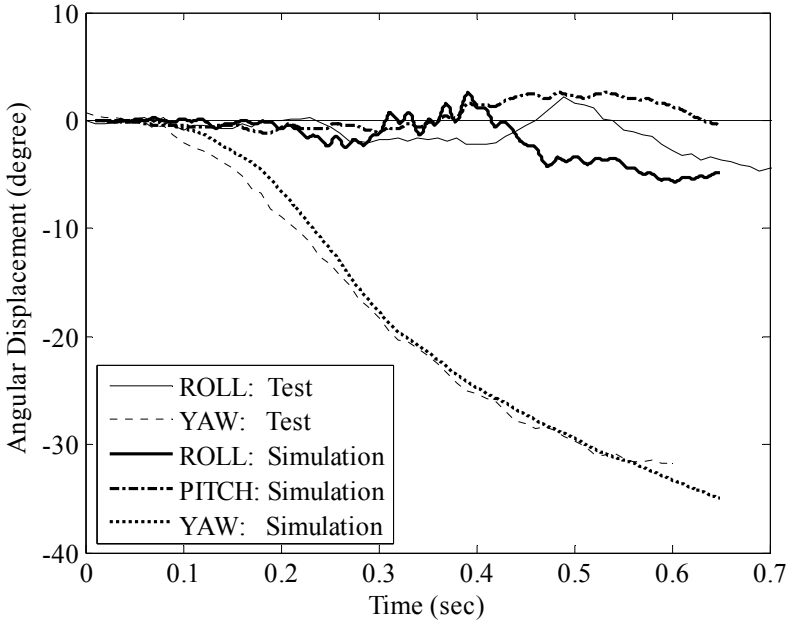

Figure 4.18 Comparisons of roll and yaw angles obtained at vehicle C.G. during crash tests and simulations for MGS.

4.5.3.2. Quantitative Validation

Energy balance curves obtained from LS-DYNA, shown in Figure 4.19, verifies the numerical stability of the analytical solution.

The Roadside Safety Verification and Validation (RSVVP) program developed by Ray, et al. (*31*) was used to help validate the Midwest Guardrail System model. Signal analysis metrics (e.g., Sprague-Geers MPC metrics and ANOVA metrics) were computed to compare vehicle accelerations and rotational displacement channels. Simulation results were filtered at CFC 60 using the Test Risk Assessment Program (TRAP) (*10*) to match the filtering of the crash test data. As shown in Table 4.8, all channels except the lateral and vertical acceleration channels passed the acceptance criteria. However, due to the negligible importance of vertical acceleration channel the signal comparison metrics with multiple channel weighting option satisfied the acceptance criteria. A Phenomena Importance Ranking Table (PIRT), as recommended by Ray, et al. (*31*), was also prepared for the comparison of test and analytical solution.

As shown in Table 4.9, the simulation results satisfied all of the evaluation criteria. Maximum dynamic deflection, number of severely twisted posts, important occupant risk factors, and maximum yaw and roll angles obtained from the simulation closely matched the test results.

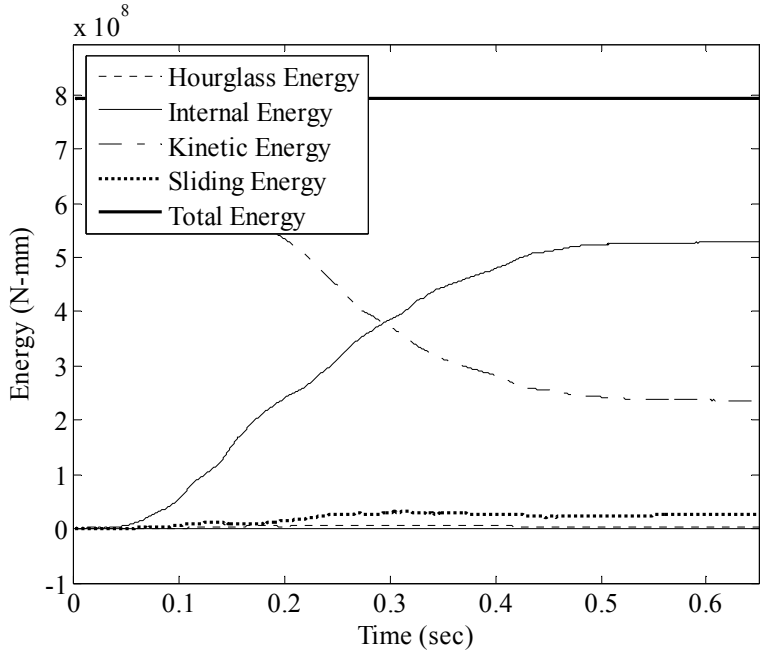

Figure 4.19 Energy balance curve obtained from the simulation on MGS model.

Table 4.8 Time History Evaluation Table for MGS model.

Compare Test NPG-4 (Filter Type: C60) and Simulation (Filter Type: SAE60, source: TRAP)						
Channel Type	Weighting factor: (Area II)	Sprague-Geers Metrics		ANOVA Metrics		Pass?
		M ≤ 40	P ≤ 40	Mean Residual ≤ 0.05	Std. Deviation ≤ 0.35	
X acceleration	0.59	3	26.8	0	0.32	Y
Y acceleration	0.41	44	35.1	0.07	0.45	N
Z acceleration	0.00	162	45	0.01	0.77	N
Roll angle	-	1	18	0.06	0.26	Y
Yaw angle	-	0.4	1	0	0.02	Y
Multiple Channel	1.0	19.8	30.2	0.03	0.35	Y

Table 4.9 Phenomena Importance Ranking Table for MGS model.

Evaluation Criteria	TTI Test	Simulation	Relative Difference ≤ 20%	Pass ?
Maximum Dynamic Deflection (m)	1.094m (3.59ft)	1.08m (3.54ft)	<20%	Y
Number of broken or significantly bent posts	4 (13~16)	4 (13~16)	<20%	Y
Maximum Roll (deg.)	-4.95	-5.9	<20%	Y
Maximum Yaw (deg.)	-31.8	-35.2	<20%	Y
Longitudinal direction: Occupant Impact Velocity ≤ 12m/s (30ft/s); Ridedown Acceleration ≤20g's	5.58m/s (18.3ft/s); 9.5g's	5.5m/s (18.0ft/s); 8.4g's	<20% <20%	Y
The rail did not rapture or fail	Yes	Yes	--	Y

4.5.3.3. Vehicle Damage

In both the crash test and simulation, exterior vehicle damage was moderate. Damage was observed on the right front corner of the vehicle. Minor damage was observed in the occupant compartment. The damaged profiles of the vehicles in the simulation and the crash test are shown in Figure 4.20.

(a) (b)

Figure 4.20 Vehicle after (a) Simulation and (b) MwRSF test NPG-4(*14*) for MGS.

4.5.4. Summary

Results of the simulation performed with the Midwest guardrail model showed good correlation with the crash test data. The maximum dynamic deflections of the rail in the simulation and test matched reasonably. The yaw and roll angles of the vehicle also matched between the simulation and test results. Since a reasonable overall correlation was achieved in the maximum dynamic deflection, occupant risk criteria, post and rail damage characteristics, and key vehicle kinematics parameters, the model was considered sufficiently validated to use in defining impact performance limits of the Midwest Guardrail System.

4.6. MODIFIED THRIE-BEAM GUARDRAIL

Thrie-beam guardrails were developed to extend the performance of strong post guardrail systems. The potential for vehicle rollover is reduced with the use of these guardrails. There are two basic types of Thrie-beams guardrails: (a) standard strong steel or wood post Thrie-beam and, (b) modified Thrie-beam. The modified Thrie-beam guardrail, as shown in Figure 4.21, is the result of improvements to the standard Thrie-beam and was specifically designed to reduce the rollover incidences for heavy vehicle impacts. Changes that increase the capacity of modified Thrie-beam guardrail include raising the rail height and incorporating different blockout. This high containment level system is designated as SGR09b by the AASHTO B*arrier Hardware Guide* (*13*).

4.6.1. System Description

Details of the modified Thrie-beam guardrail and its components are shown in Figure 4.22. As shown in the figure, the modified Thrie-beam guardrail system consists of 2.1 m (6.9 ft) long W150×13.5 (W6×9) steel posts, W360×32.9 (W14×22) blockouts, and 3.8 m (12.5 ft) long sections of standard Thrie-beam rail. As shown in Figure

4.22(d), the webbing of the blockout has a cutout measuring 152 mm (6 in) at the bottom and angled upward at 40 degrees to the flange on which the Thrie-beam is attached. This offset block design allows the lower portion of the Thrie-beam and the flange of the steel offset block to bend inward during a crash, thus keeping the rail face nearly vertical in the impact zone as the posts are pushed backwards. This feature also maintains the height of the rail during the impact, which minimizes the likelihood of a vehicle rollover. The blockout is attached to the post with four 16 mm (5/8 in) diameter bolts and to the Thrie-beam rail element with a single 16 mm (5/8 in) diameter button head bolt without a washer. The mounting height of the Thrie-beam should be 610 mm (24 in) to the center and 866 mm (34 in) to the top of the rail element.

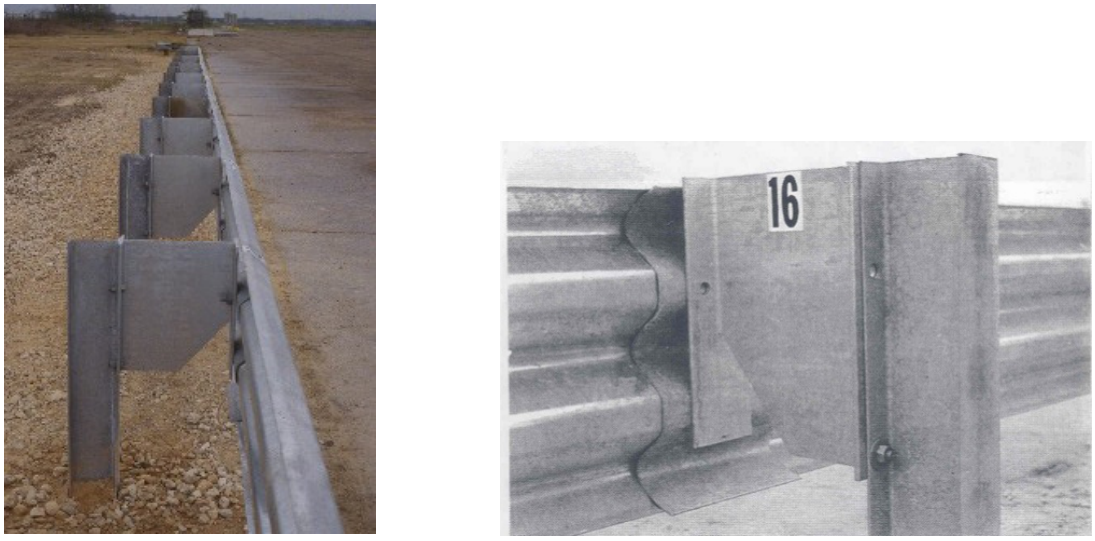

Figure 4.21 Typical modified Thrie-beam guardrail system (SGR09b)(*6*).

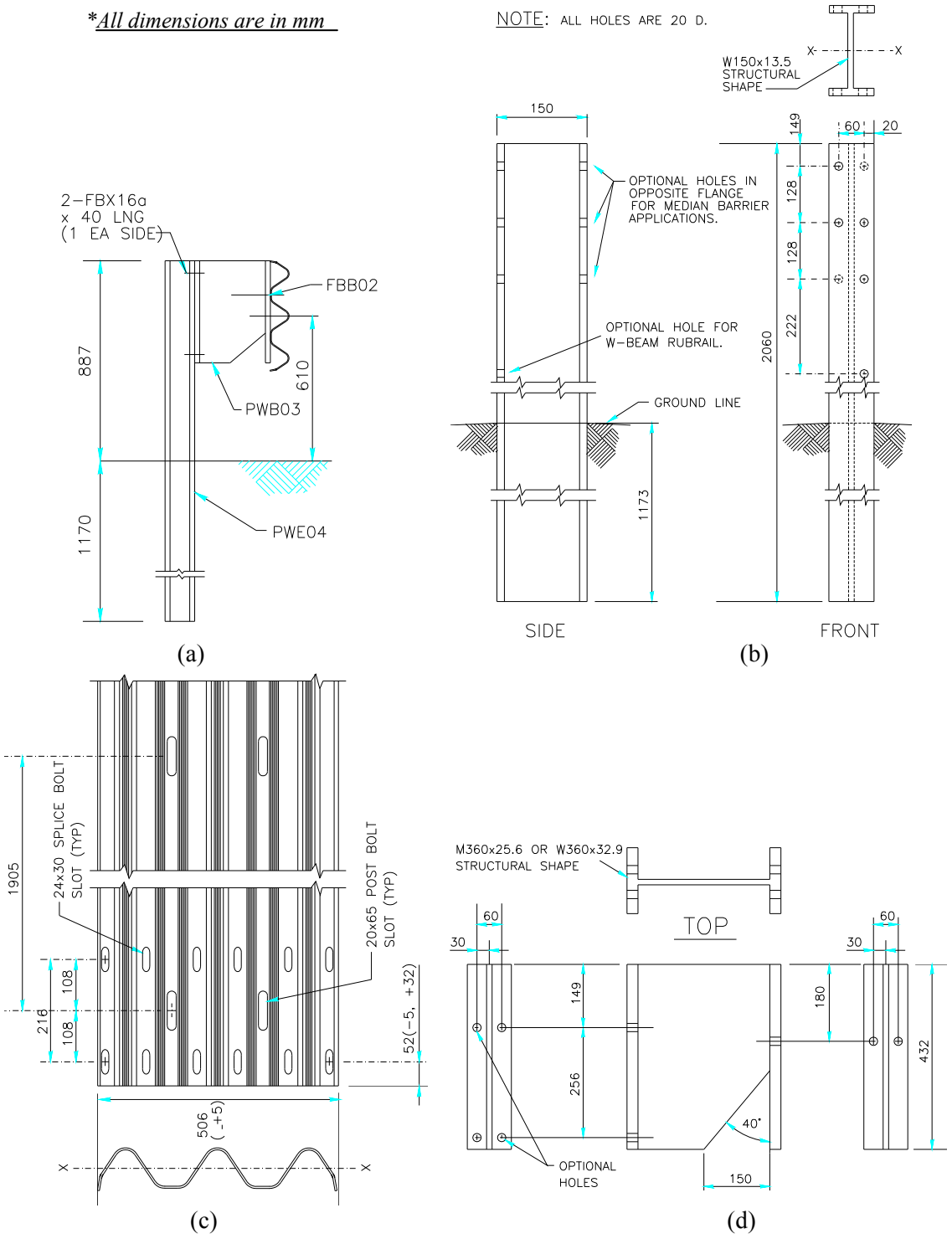

Figure 4.22 Detailed drawing of (a) Modified Thrie-beam guardrail, (b) Wide-flange guardrail post (PWE 04), and (b) 2-space Thrie-beam guardrail (RTM 01a) (c) modified Thrie-beam blockout (PWB03) (*6,13*).

4.6.2. Model Development

Finite element model developed for the modified Thrie-beam system is shown in Figure 4.23. The total length of the guardrail model was 30.48 m (100 ft). 2.67 mm (0.1 in) thick and 4.13 m (13.5 ft) long Thrie-beam rail segments were modeled using shell elements. Splice connections between two adjacent rail segments, as shown in Figure 4.23(b), were modeled at every 3.81 m (12.5 ft) along the longitudinal direction. Each alternate posts spacing had a back plate placed behind the guardrail. W360×32.9 (W14×22) blockouts were modeled using shell elements. The end terminals used in Modified Thrie-beam Guardrail are the same as those used in modified G4(1S) guardrail system and MGS. Hence, as shown in Figure 4.23(c), the end terminals of the modified Thrie-beam system were modeled using nonlinear spring elements with properties similar to those used in previous guardrail models. Other components like post, soil, and bolts were also modeled following the same approaches used in developing previous models. The posts were embedded 1173 mm (46 inches) in the soil. The final modified Thrie-beam guardrail model consisted of 171,720 elements.

4.6.3. Model Validation

In a crash test performed at TTI, a C2500 pickup truck impacted the Modified Thrie-beam guardrail at post 15 at a speed of 100.2 km/h (62.2 mi/h) and at an angle of 25.1 degrees (*6*). The height to the upper and lower edges of the vehicle bumper was 670 mm (26.4 in) and 470 mm (18.5 in), respectively. The entire left wheel assembly of the vehicle was torn from the axle at 0.189 sec. However, the vehicle was successfully contained and redirected by the guardrail system. To validate the Modified Thrie-beam guardrail model, an impact simulation was performed similar to the full-scale crash test described above. Even though the failure of the wheel assembly was not captured, the vehicle in the simulation was successfully redirected.

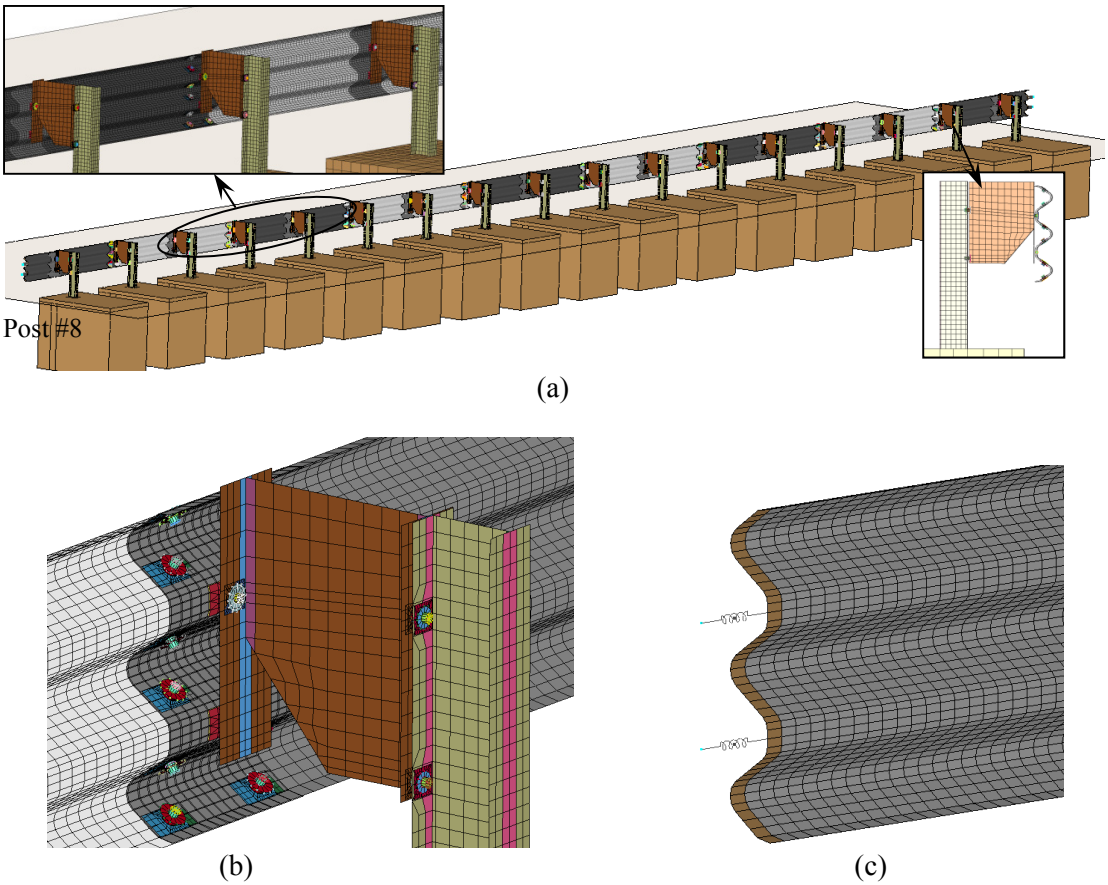

Figure 4.23 (a) FE model developed for modified Thrie-beam guardrail system. (b) Splice plate and post-blockout-rail connection, (c) Nonlinear spring elements used as end terminal.

4.6.3.1. Event Time-sequence Comparison

A descriptive time-sequence comparison is presented in Table 4.10. Sequential photographs of simulation and test results are compared in Figure 4.24. As can be seen from the table and the figure, there is a reasonable overall correlation between the test and simulation results. However, at 0.189 sec, in the crash test, the left front wheel assembly of the vehicle failed and detached from the axle after impacting the flange at post 17. In the simulation on the other hand, due to the limitation of lacking ball-joint failure, the wheel did not detach from the axle. Thus in simulation results, the impact of

the wheel with post 17 resulted in taking out greater kinetic energy from the vehicle and slowing it down faster than the crash test vehicle. This also created higher occupant impact velocities and ride down accelerations during the simulation. State of the left wheel assembly near post 17 during simulation and crash test is shown in Figure 4.25(a) and (b), respectively. In both crash test and simulation post 17 was the only significantly bent post. Maximum dynamic deformation observed in crash test and simulation was 1.02 m (3.34 ft) and 0.81 m (2.66 ft), respectively.

Table 4.10 Event time-sequence comparison of simulation and test for modified Thrie-beam guardrail.

Incident	Crash test	Model Simulation
Left front tire made contact with flange and face of post 16	0.077s	0.080
Post 17 started to rotate about vertical axis	0.125s	0.115s
Post 18 started to rotate about vertical axis	0.161s	0.155s
Left front assembly caught flange at post 17	0.189s (Impact wheel detached)	0.190s (Wheel did not detach)
Front of vehicle reached post 18	0.232s	0.250s
Rear of the vehicle made contact with rail	0.232s	0.260s
vehicle became parallel with the installation	.264s 74.5 km/h (46.2 mi/h)	0.32s 57.2 km/h (35.5 mi/h)
Vehicle lost contact with the test installation	0.560s 67.5 km/h (41.9 mi/h)	0.58s 52.7km/h (32.7 mi/h)

The comparisons of vehicle yaw, pitch, and roll angles as a function of time are also presented in Figure 4.26. It can be seen that the vehicle's pitch and yaw angles obtained from the simulation closely followed the test results till 0.189sec. After 0.189s, due to the presence of left front wheel assembly attached to the axle, the vehicle kinematics in the simulation deviated largely from that observed in the crash test. Hence, it is not logical to compare the crash test and simulation data beyond 0.189 sec. Since this model will be used to evaluate the performance of the modified Thrie-beam when impacted by airborne pickup trucks, ball-joint failure is not expected to occur during the future simulations.

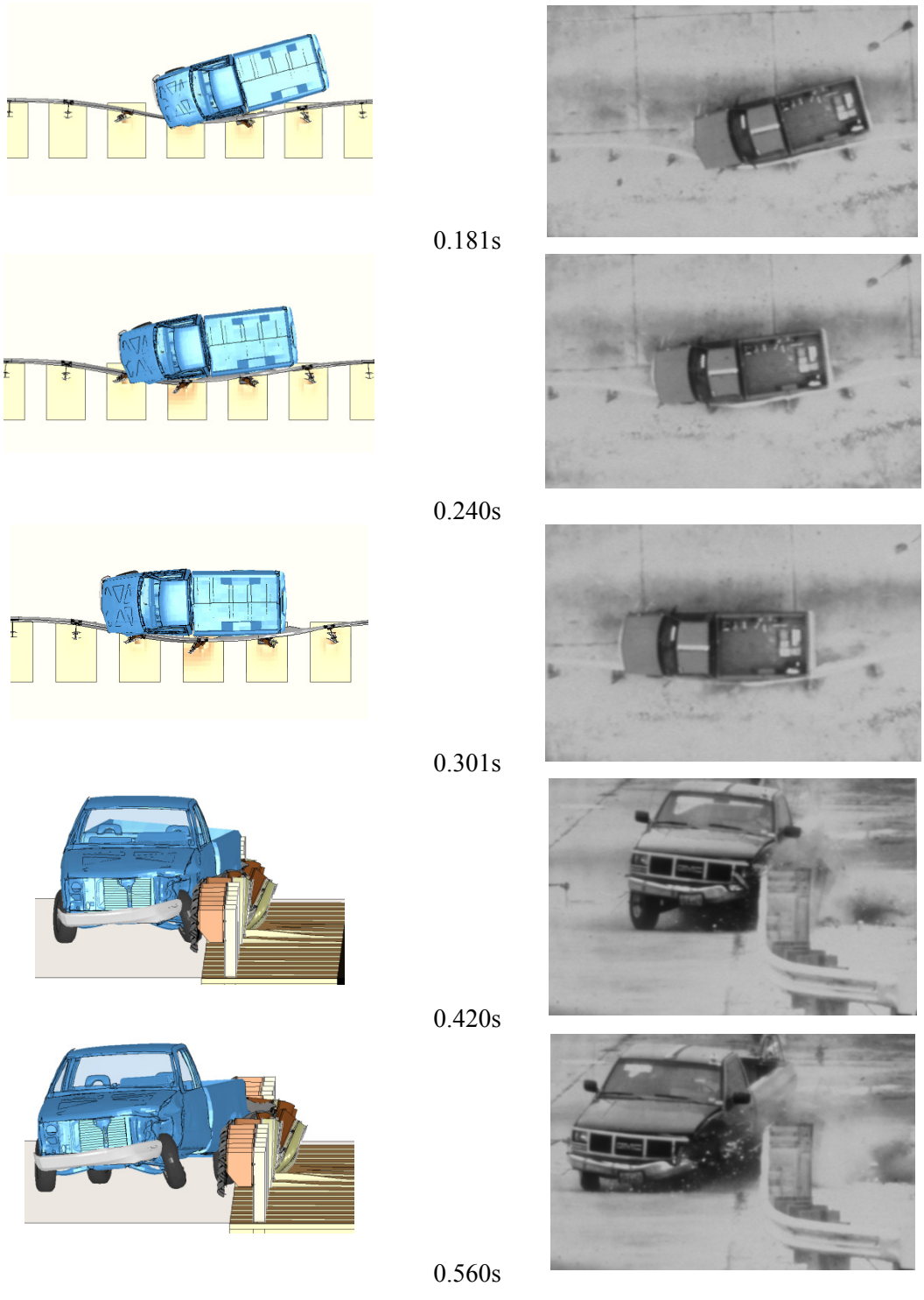

Figure 4.24 Sequential photographs of simulation and TTI Test 471470-30(*6*) performed on modified Thrie-beam guardrail system model.

(a) (b)

Figure 4.25 (a) Simulation: Left wheel exits post 17 without the failure at 0.189 sec. (b) Crash test: Left front wheel assembly detached from vehicle near post 17(*6*).

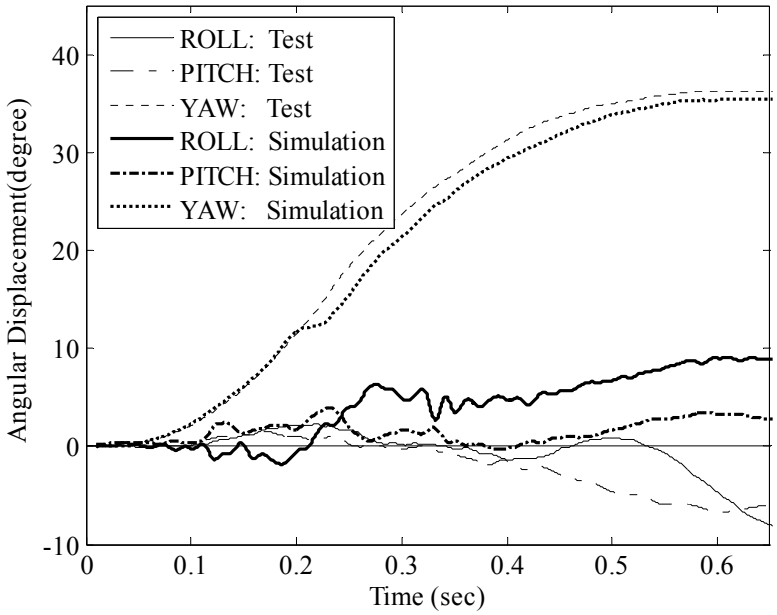

Figure 4.26 Comparisons of roll, pitch and yaw angles obtained at vehicle C.G. during crash tests and simulations for modified Thrie-beam guardrail system.

LS-DYNA generated energy balance curves, as shown in Figure 4.27, verify the numerical stability of the analytical solution. A sudden rise in sliding interface energy is observed at 0.189s due to the excessive contact force developed between the post and impact wheel assembly.

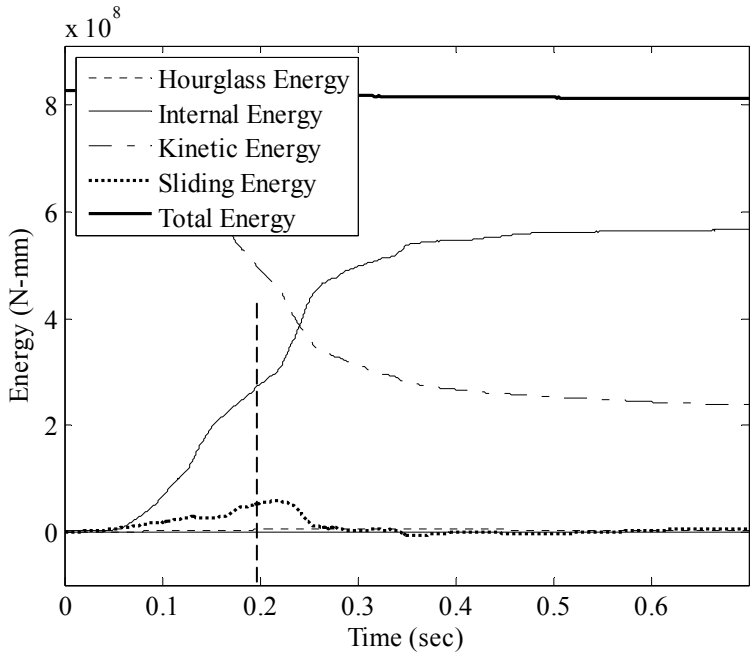

Figure 4.27 Energy balance curve obtained from the simulation on modified Thrie-beam guardrail model.

4.6.3.2. Vehicle Damage

Both in crash test and simulation, vehicle sustained moderate damage. In crash test, the left front wheel assembly detached from the vehicle's axle. In the simulation however, the wheel assembly remained attached to the axle due to the lack of suspension ball-joint failure as discussed previously. The damaged profile of the vehicle in the simulation and the crash test is shown in Figure 4.28.

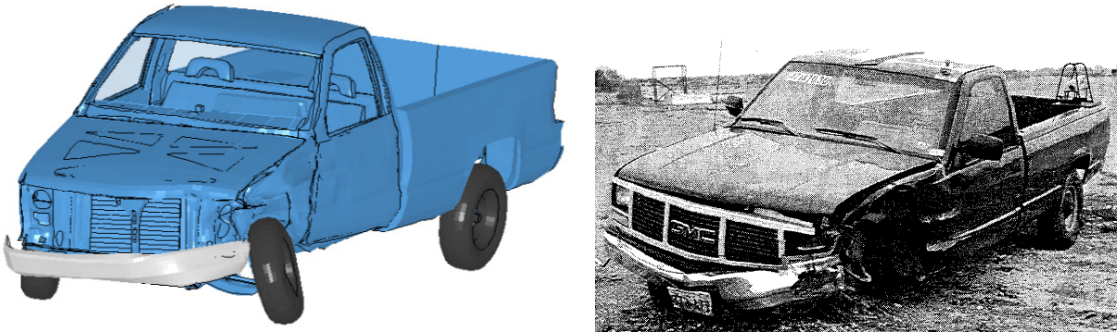

(a) (b)

Figure 4.28 Vehicle after (a) simulation, and (b) crash test 471470-30(*6*).

4.6.4. Summary

Simulation performed using modified Thrie-beam guardrail model closely followed the trend observed in crash test. The pickup truck was successfully contained and redirected in both the simulation and crash test. The maximum dynamic deflection of the rail and number of severely detached posts observed in the simulation was within 20% of those observed in crash test. The yaw and pitch angles of the vehicle obtained from the simulation closely followed the test results till 0.189sec. The front left wheel assembly failed and detached from the vehicle in the crash test. The failure of suspension components was not included in the vehicle model used in the simulation and, thus, the detachment of the wheel assembly was not observed in the simulation. Consequently, the simulated vehicle experienced more snagging between the tire and the guardrail system. This caused some differences in vehicle kinematics after the time at which the snagging contact occurred. However, since this model will be used to evaluate the performance of the Modified Thrie-beam guardrail when impacted by airborne pickup trucks suspension failure due to severe post to wheel snagging is not expected to occur during the future simulations. Hence, the model was considered sufficiently validated to continue with the evaluation of the modified Thrie-beam guardrail performance when placed on slope.

4.7. MODIFIED WEAK POST W-BEAM GUARDRAIL

The weak post W-beam guardrail system, as shown in Figure 4.29, is a flexible guardrail system that is widely used in some states. The standard G2 weak post W-beam guardrail failed to demonstrate acceptable performance in crash tests performed in accordance to *NCHRP report 350* guidelines under test level 3 (TL-3) impact conditions. Pennsylvania Department of Transportation and researchers from Bucknell University and Worcester Polytechnic Institute (WPI) modified the system to improve its impact performance and comply with *NCHRP Report 350*. The key modifications to the standard weak post W-beam guardrail included increasing the guardrail height to prevent 2000 kg (4405 lb) pickup truck from riding over the rail element, improving post-rail connection to provide more consistent and reliable release of the rail from the posts, and relocating the rail splice mid-span between posts to effectively increase rail strength and reduce chances for rail rapture(*23*). This system is herein referred to as the modified weak post W-beam guardrail and is designated as SGR02 by AASHTO (*12-13*).

Figure 4.29 Modified weak-post W-beam guardrail system(*3*).

4.7.1. System Description

As shown in Figure 4.30, the modified weak post W-beam guardrail system consists of 12-gauge W-beam rail elements mounted at a rail top height of 820 mm (32 in.) on 1.6 m (5.3 ft) long S75×8.5 (S3×5.7) steel posts spaced 3.81 m (12.5 ft) apart(*3*). The posts are attached to 200 mm ×600mm ×6.25 mm (8.0 in.× 24.0 in.× 0.25 in.) soil plates 74 mm (3 in.) below the ground surface. The rail splices are located mid-span between posts and 12 gauge W-beam backup plates are installed behind the W-beam guardrail at each post location. The W-beam rail elements are attached to the post with 8 mm (5/16 in.) diameter bolts, a round flat washer, two 44 mm (1.75 in.) square plate washers, and two nuts. A shelf bolt is placed in the traffic side flange of each post to help support the W-beam at each post location.

4.7.2. Model Development

The finite element model, as shown in Figure 4.31, was developed to conduct crashworthiness analyses of the modified weak post W-beam guardrail system using LS-DYNA. A 68.6 m (225 ft) length of the system was modeled. Spring elements were used at the upstream and downstream ends of the W-beam to represent the axial stiffness of turned down terminals. The final modified weak post W-beam model consisted of 377,286 elements.

Components like W-beam rail, post, bolts in rail splice connections, and soil were modeled following the same approaches used in developing previous guardrail models. Steel soil plates, modeled using shell elements, were attached to the posts using constrained spot-weld option available in LS-DYNA. As shown in Figure 4.32, the post and soil plates were embedded in the rectangular soil bucket, modeled using solid elements. Larger soil buckets were chosen near the impact and possible vehicle-rail contact locations to accurately capture the post-soil interaction as the post deflected in

soil. The rectangular soil buckets around these critical locations were 2.34 m (7.7 ft) wide × 2.34 m (7.7 ft) long (laterally) × 1.26 m (4.1 ft) deep.

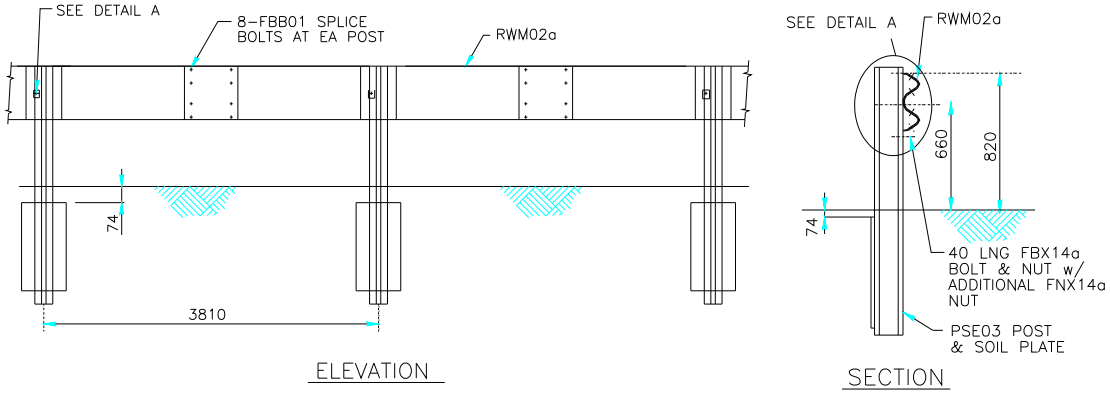

(a)

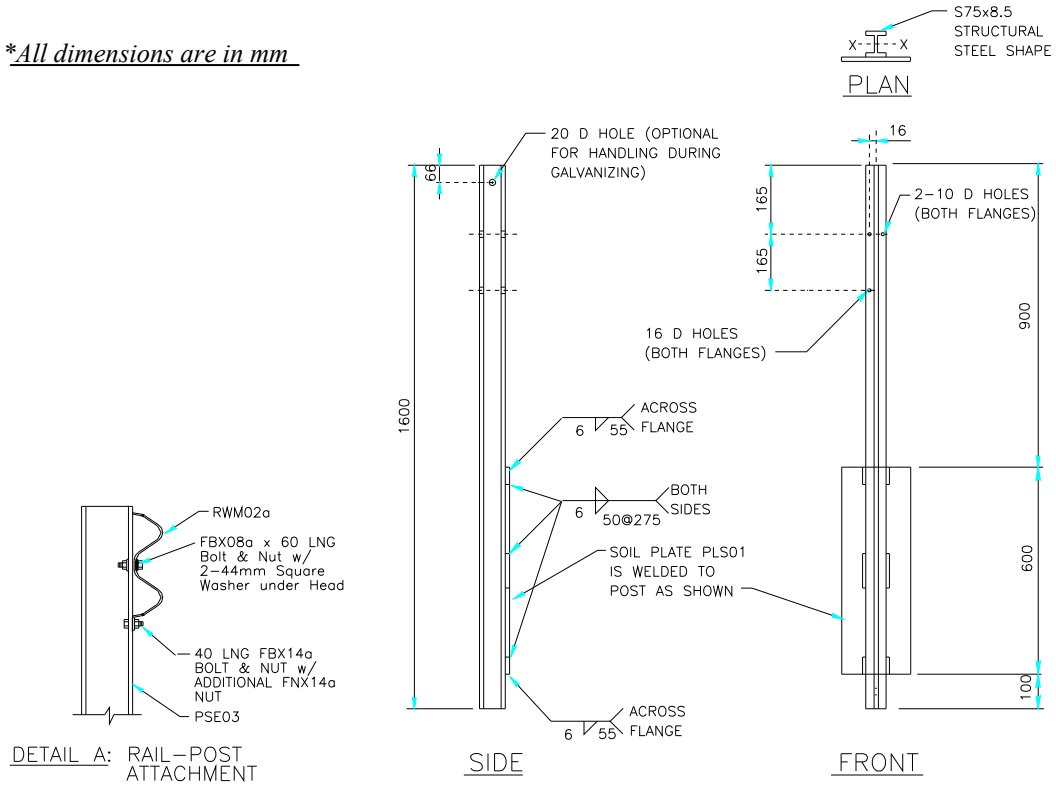

(b) (c)

Figure 4.30 (a) Details of modified weak post W-beam guardrail system, (b) Rail-post connection, and (d) Weak post (PSE 03) with soil plate (*3,13*).

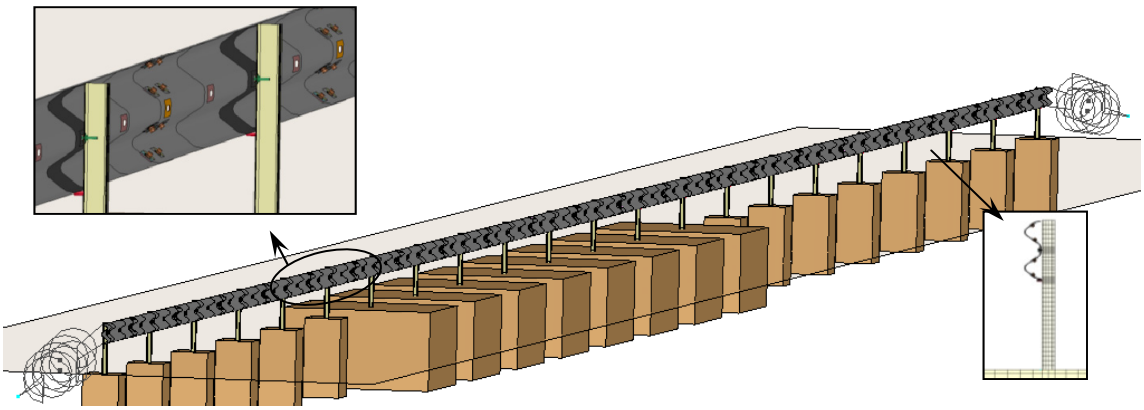

Figure 4.31 Finite Element Model developed for the modified weak-post W-beam system.

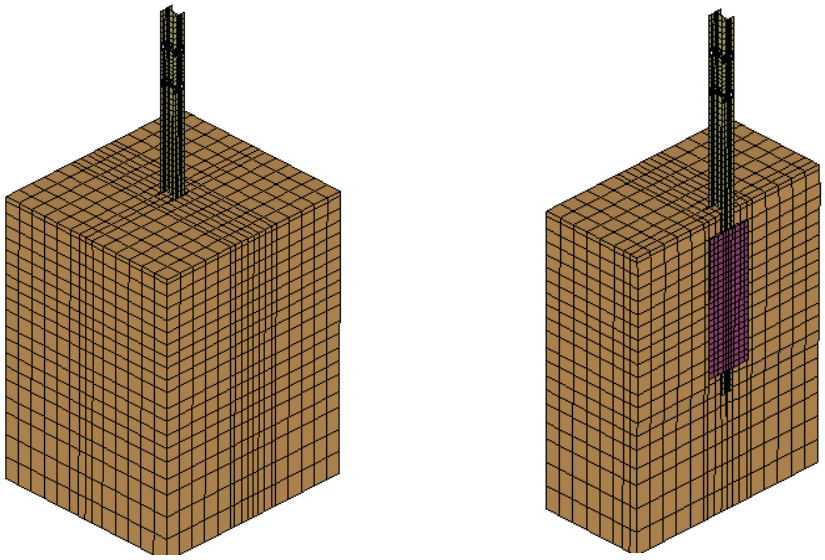

Figure 4.32 Post-soil interaction model.

The bolts in rail splice connection were modeled using beam elements for bolt-shaft and shell elements for bolt heads and nuts. The shell-element heads and nuts were constrained to the ends of the bolt shaft. Since these bolts do not fail during impact, no failure criterion was implemented. The small post-to-rail connection bolts in weak post system, on the other hand, do fail in tension to permit the W-beam to readily and reliably detach from the posts prior to the vehicle impacting the posts (*23*). Too strong a

connection will delay the rail release and permit the rail to be pulled down by the deflecting posts. If the connection is too weak, the rail can detach from too many posts and drop in elevation in advance of the vehicle. Both scenarios can lead to the vehicle overriding the barrier.

A post-to-rail connection can fail through one of the following modes: (a) bolt pullout through the rail slot, (b) the nut stripping off the bolt threads, or (b) bolt fracture. Ray et. al. (*23*) developed a connection that consistently induces bolt fracture rather than a mixed mode of failure. The post-to-rail connection in the modified weak post W-beam system consists of a 8 mm (5/16 inch) diameter A307 bolt with two 44 mm (1.75 inch) square plate washers under the head and a round washer and double nuts on the end. The double square washer prevents the bolt from pulling through the rail slot, and the double nuts prevent stripping of the bolt threads.

Hence, a damage/failure mechanism had to be incorporated into the system model to account for the bolt fracture. The FE model of the post-to-rail connection is shown in Figure 4.33. The bolt shaft was modeled using solid elements. Constrained nodal rigid bodies were still used between the bolt shaft and the nuts since there is no need to model the stripping of the nuts off the bolt threads. Material type 100 (*29*) was used for the bolt shaft to incorporate the desired damage mechanics. A bilinear elastic-plastic material formulation was used based on Von-Mises criteria as shown in Figure 4.34(a). Figure 4.34(b) shows the material card used for the bolts in post-rail connections. The OPT flag in the card determines how failure is computed from the force resultants. The condition OPT=0 evokes a failure criteria in which the element fails when the force resultant falls outside the failure surface defined in Equation (4.4) (*29,41*).

$$\left(\frac{\max\left(N_{rr},0\right)}{N_{rr_F}}\right)^2+\left(\frac{N_{rs}}{N_{rs_F}}\right)^2+\left(\frac{N_{rt}}{N_{rt_F}}\right)^2+\left(\frac{M_{rr}}{M_{rr_F}}\right)^2+\left(\frac{M_{ss}}{M_{ss_F}}\right)^2+\left(\frac{M_{tt}}{M_{tt_F}}\right)^2-1=0 \qquad (4.4)$$

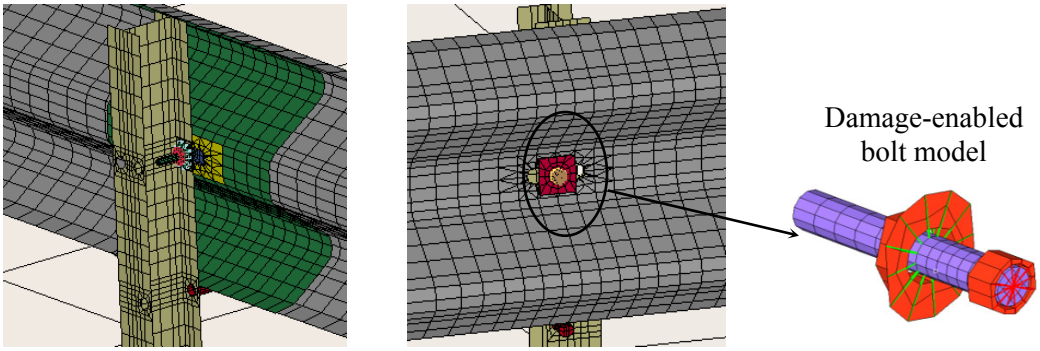

Figure 4.33 Model for the W-beam rail and post connection.

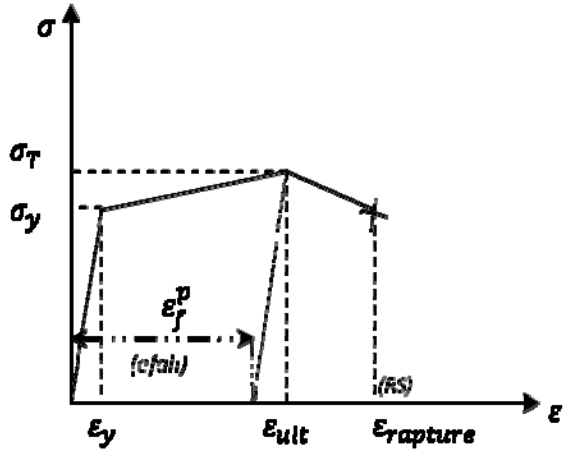

(a)

*MAT_SPOTWELD_DAMAGE_FAILURE_(TITLE) (1)

TITLE							
bolt_Shaft							
MID	RO	E	PR	SIGY	ET	DT	TFAIL
8000015	7.890e-009	2.000e+005	0.2900000	240.00000	6200.0000	0.0	0.0
EFAIL	NRR	NRS	NRT	MRR	MSS	MTT	NF
0.1650000	1.657e+004	9940.0000	9940.0000	1.066e+004	1.131e+004	1.131e+004	25.000000
RS	OPT	FVAL	TRUE_T	_	BETA		
0.1850000	0.0	0.0	0.0	0	0.0		

(b)

Figure 4.34 (a) Stress-strain relationship for bolt material used in post-rail connection(*25*) (b) Material card for the bolts used in rail to post connection.

where, numerators are the resultants calculated in the local coordinate of the cross section at a given time step, and the denominators are the resultants at failure specified in the input. Nrr_F is the maximum axial force, and Nrs_F and Nrt_F are the maximum shear forces at failure. Mrr_F is the torsional moment, and Mss_F and Mtt_F are the bending moments at failure.

The amount of damage evolved is represented by the damage constant, ω, which varies from zero for no damage to unity for complete failure. Damage in this model is defined in terms of plastic strain as shown in Equation (4.5). Damage begins when the effective plastic strain exceeds the failure strain ($\varepsilon_{failure}^{p}$). After exceeding the failure strain softening begins and continues until the rupture strain ($\varepsilon_{rupture}^{p}$) is reached(*29*).

$$\omega = \frac{\varepsilon_{eff}^{p} - \varepsilon_{failure}^{p}}{\varepsilon_{rupture}^{p} - \varepsilon_{failure}^{p}} \quad \text{if} \quad \varepsilon_{failure}^{p} \le \varepsilon_{eff}^{p} \le \varepsilon_{rupture}^{p} \tag{4.5}$$

Ultimate strength and yield strength for ASTM F568/A307 bolt are 415 MPa (60 ksi) and 240 MPa (35 ksi), respectively(*43*). The 50 mm (2 in) elongation for the material is 18%(*43*). These ASTM specified engineering stress and strain values were converted to the corresponding true stress and strain values required in the LS-DYNA material model. Ultimate axial force capacity (Nrr_F) for the bolt was obtained by multiplying the true ultimate strength with the net cross sectional area of the bolt thread. Shear force capacity was taken as 65% of the axial force capacity. Ultimate torsional and bending moment capacities of the bolt were calculated considering compact section using Equations (4.6) and (4.7).

$$M_{Tor_{p|ult}} = M_{rr_F} = \frac{4\tau_y J}{3C} \tag{4.6}$$

$$M_{Bend_{p|ult}} = M_{SS_F} = M_{tt_F} = \frac{2AD\sigma_y}{3\pi} \tag{4.7}$$

Slope of the stress-strain curve from yield stress to ultimate tensile stress indicates the hardening modulus. Use of a bilinear representation, as shown in Figure 4.34(a), limits the description of the material in plastic region and does not fully capture the nonlinear behavior of the actual material in hardening and softening regions. Hence,

the value of the hardening modulus was calibrated during the full-scale simulations such that number of post-to-rail connection detachments (i.e., bolt failures) in the simulation equaled the number observed in full-scale crash tests.

Ray, et al.(*23*) performed a series of tensile tests on the 8 mm (5/16 in) diameter A307 post-to-rail connection bolts. The results of these tests are shown in Table 4.11. The bolts failed at a load of 20 kN or greater in all but one case. A tensile test simulation, depicted in Figure 4.35, was performed on the damage-enabled bolt model. Figure 4.35(c) shows the force displacement curve obtained from the simulation. The force required to create fracture of the bolt was 28.65 kN, which was near the upper range of the test results.

Table 4.11 Results of tensile tests on 8 mm (5/16 in.) diameter A307 bolts (*23*).

Test No.	Orientation	Ultimate Strength (kN)	Failure Mode
99092001	Axial	27.3	Fractured through the Thread
99092002	Axial	27.0	Fractured through the Thread
99092003	Axial	26.1	Fractured through the Thread
99092004	Axial	22.4	Fractured through the Thread
99092005	Axial	15.4	Fractured through the Thread
99092006	Axial	19.9	Fractured through the Thread

The 7.62 m (25 ft) long inclined portion of the turned down end terminal on each side of the tested system was modeled using spring elements as shown in Figure 4.36. The equivalent axial stiffness of the terminal was calculated using the Equation (4.8).

$$K_{rail} = \frac{AE}{L} \tag{4.8}$$

where, A and E are the cross sectional area and elastic modulus of the W-beam rail. L is the length of the inclined portion.

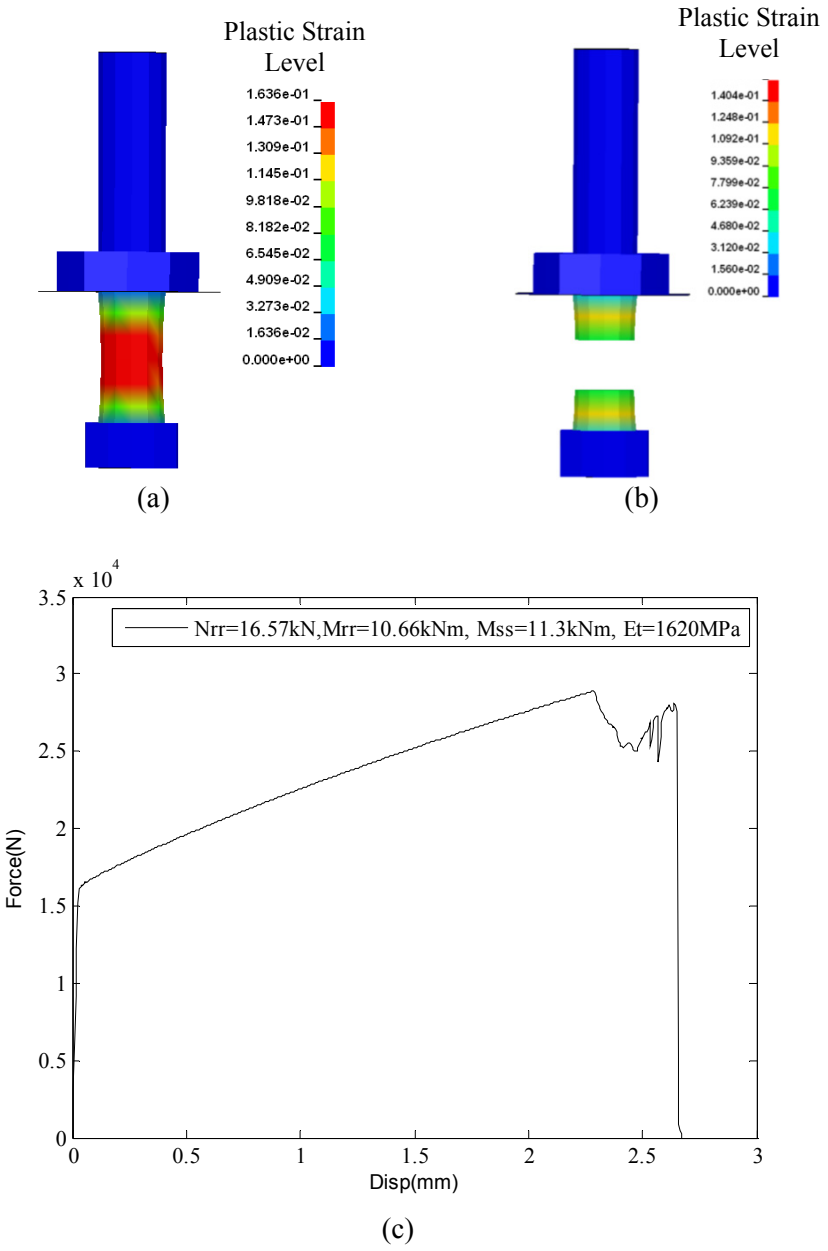

Figure 4.35 Damage-enabled bolt under tension test simulation: (a) Immediately before the failure. (b) After the failure where the solid elements achieving the failure criteria was deleted (c) Force-displacement curve for the bolt model during tension test simulation.

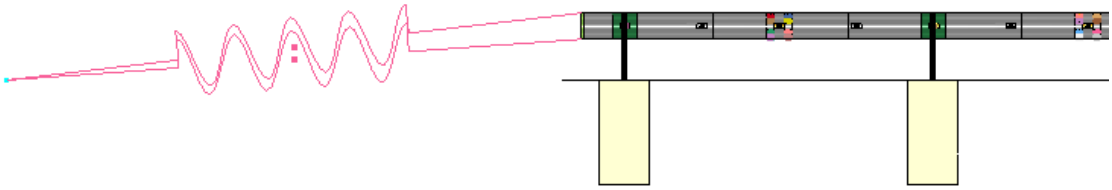

Figure 4.36 Spring elements used to model the turned down end terminal.

4.7.3. Model Validation

FE model of the modified weak post W-beam guardrail was validated by performing a full-scale vehicle impact simulation similar to the full-scale crash test performed at TTI (*3*). The guardrail in both crash test and simulation successfully contained and redirected the vehicle.

The 99 m (325 ft) long test installation consisted of 68.6 m (225 ft) of modified weak post W-beam guardrail with 15.2 m (50 ft) long turned down terminals attached on each end. A 1995 Chevrolet C2500 pickup truck with a gross static weight of 2000 kg (4409 lb) was used for the test. The height to the upper and lower edges of the vehicle bumper was 655.3 mm (25.8 in.) and 449.6 mm (17.1 in.), respectively.

The vehicle impacted the modified weak post W-beam guardrail 1.72 m (5.6 ft) upstream of post 7 at a speed of 102.4 km/h (63.6 mi/h) and an angle of 26.5 degrees. The vehicle was successfully contained and redirected by the guardrail system. The vehicle became parallel with the installation at 0.371 sec and lost contact with the guardrail at 1.418 sec. The maximum dynamic deflection of the guardrail was 2.12 m (6.95 ft).

4.7.3.1. Sensitivity Analysis for Post-Rail Connection

The post-rail connection for the weak post w-beam guardrail model was highly sensitive to the hardening modulus (ET) value assigned in the material card for bolt shown in Figure 4.34(b). Use of a bilinear elastic-plastic material formulation limits the

description of the material in the plastic region and does not fully capture the nonlinear behavior of the actual material in the hardening and softening regions. Also, because of the presence of clamping force, post-rail connections in practice tend to become stiffer. Since the preloading on the bolt shank was not present in the simulation, using the ET value calculated from the slope of the linear hardening curve was found too small to cause a softer connection. The performance of the connection also depended on the soil property used. Softer soil allowed posts to translate with little bending and twisting during the impact, thus delaying the connection failure. Hence, several full scale simulations were performed with different combinations of bolt hardening modulus (ET) and soil elastic modulus (Es) to capture identical post-rail detachment behavior observed during the crash test. Table 4.12 shows the results obtained from these sensitivity analyses. Maximum dynamic deflection, number of posts detached, and detachment time at each post location during crash test and simulations are compared in the table. As can be seen, simulation performed considering the ET value (1613 MPa) obtained from the slope of the linear curve in the hardening region showed larger number of post detachments. The 6th simulation with 7300 MPa (1058 ksi) of hardening modulus for bolt and 25 MPa (3.63 ksi) of elastic modulus for soil showed best correlation with the crash test results. The failure sequence of the post-rail connection model at post 10 is shown in Figure 4.37.

Table 4.12 Sensitivity analysis for post to rail connection.

	Bolt ET, (MPa)	Soil Es, (MPa)	Time at which post to rail connection failed (sec)							Max Dyn. Def (mm)	# of posts detached (Detached Post #)
			Post #5	Post #6	Post #7	Post #8	Post #9	Post #10	Post #11		
Crash Test	--	--	--	--	0.05	0.126	0.398	0.592	0.824	2.12	6(7~12)
Sim.1	1613	50	0.23	0.07	0.05	0.095	0.154	0.175	0.198	3.14	11(5~15)
Sim.2	8000	50	--	--	0.05	0.133	0.208	0.244	0.50	2.41	5(7~11)
Sim.3	6000	50		0.45	0.05	0.130	0.180	0.270	0.30	2.49	7(6~12)
Sim.4	6000	35		--	0.05	0.130	0.2	0.25	0.3	2.49	6(7~12)
Sim.5	6200	25	--	--	0.05	0.135	0.22	0.515	0.68	2.41	6(7~12)
Sim.6	7300	25	--	--	0.05	0.135	0.356	0.60	0.840	2.32	5(7~11)

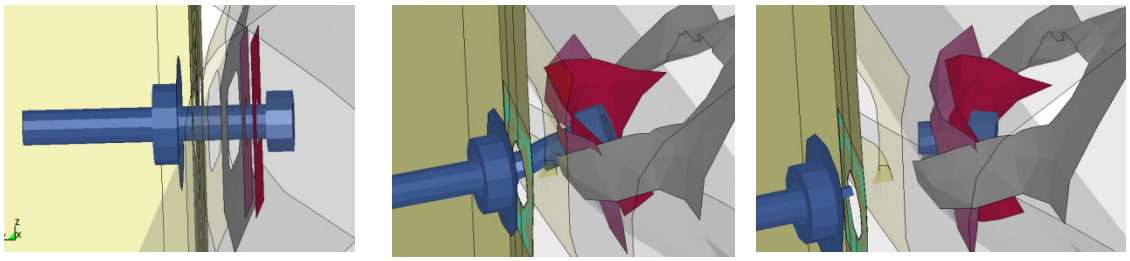

0 sec *0.55 sec* *0.60sec*

Figure 4.37 Failure of the post to W-beam rail connection at post #10.

4.7.3.2. Event Time-sequence Comparison

A descriptive time-sequence comparison between the test and simulation with 7300 MPa of ET and 25 MPa of Es is shown in Table 4.13. A comparison of sequential photographs obtained from the test and simulation is also presented in Figure 4.38. As can be seen from these table and figure, there is a reasonable overall correlation between the test and simulation results. Longitudinal accelerations and lateral accelerations obtained at vehicle C.G. during crash tests and simulations are compared in Figure 4.39. The comparisons of vehicle yaw, pitch, and roll angles as a function of time are also presented in Figure 4.40. As can be seen, the roll and pitch angles obtained from simulation reasonably matched the crash test values. The simulation yaw angle closely followed the crash test value until 0.65 sec.

Table 4.13 Event time-sequence comparison between simulation and test for modified weak post W-beam guardrail.

Incident	Crash test	Model Simulation
Left front tire contacted post 7	0.082s	0.080s
Top of post 7 touched the ground	0.102s	0.10s
Front bumper of the vehicle contacted post 8	0.192s	0.195s
The vehicle became parallel with the system	0.371s (77.8km/h)	0.395s (77.2 km/h)
Left front tire reached post 9	0.383s	0.40s
Left front tire contacted post 10	0.589s	0.585s
Left front tire contacted post 11	0.822s	0.820s

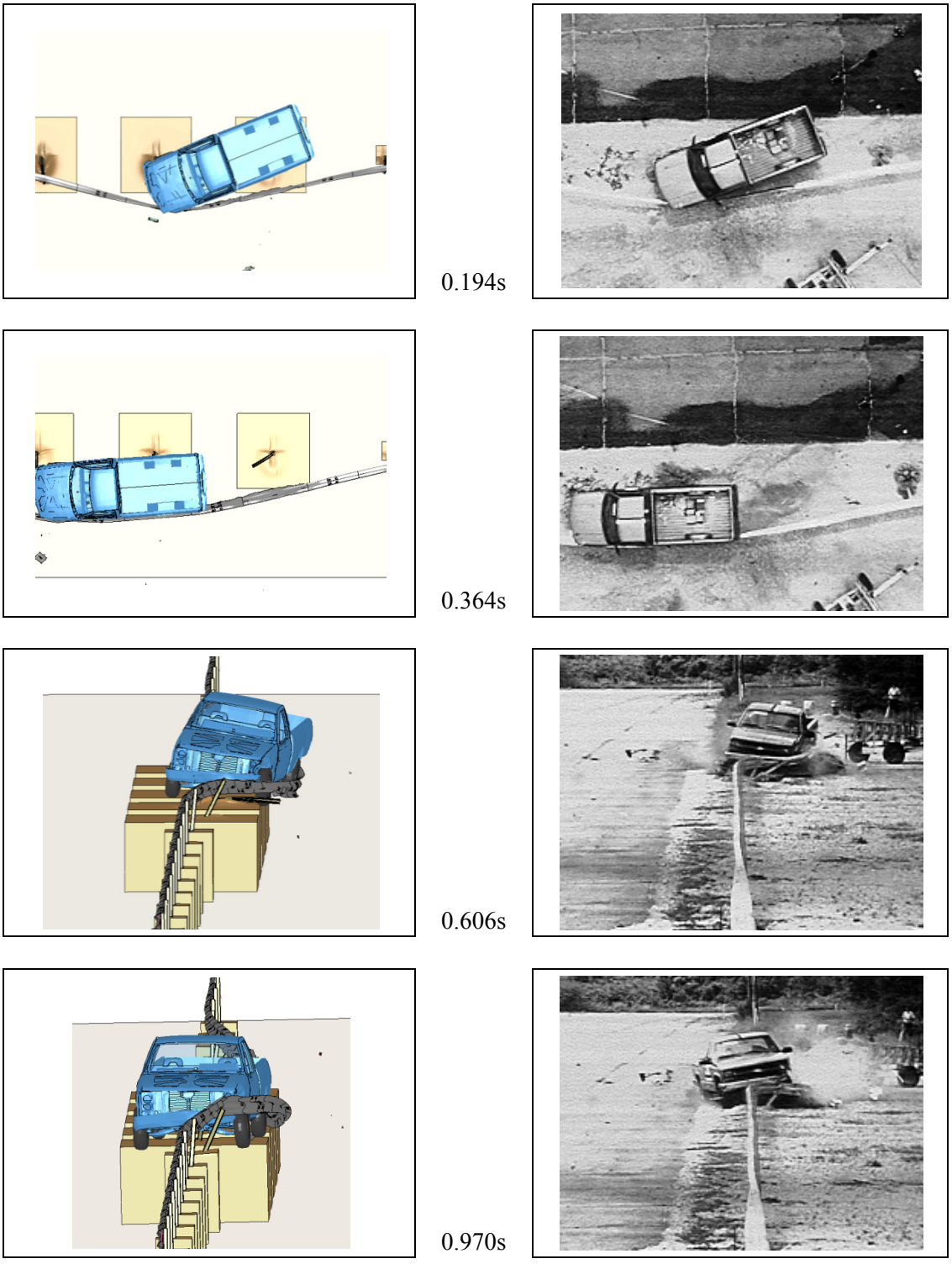

Figure 4.38 Sequential photographs of modified weak post W-beam guardrail model simulation and TTI Test 473750-3(*3*).

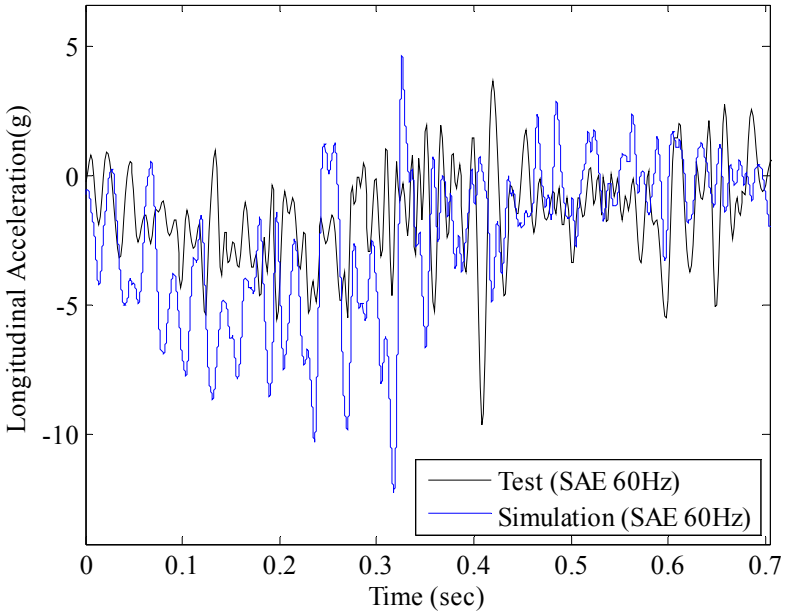

(a)

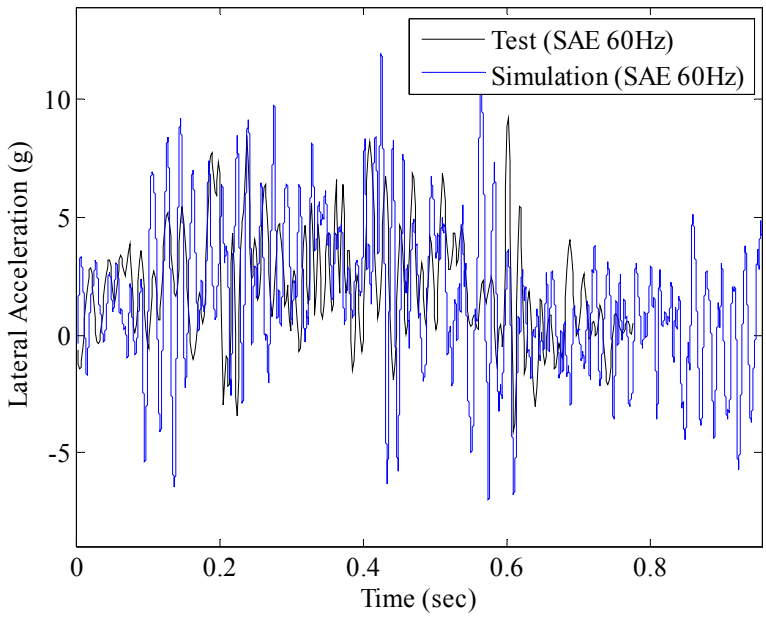

(b)

Figure 4.39 Comparisons of (a) longitudinal and (b) lateral accelerations obtained at vehicle C.G. during crash tests and simulations for modified weak post w-beam guardrail.

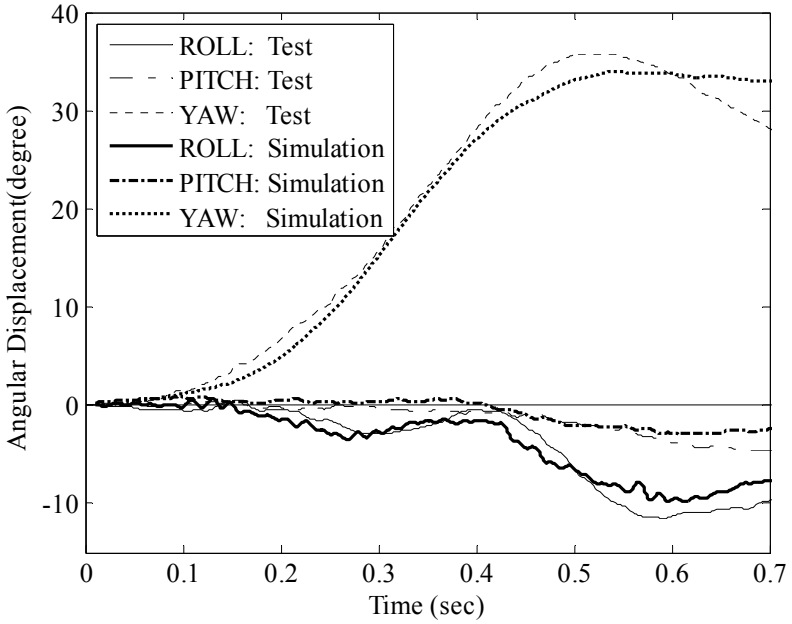

Figure 4.40 Comparisons of roll, pitch, and yaw angles obtained at vehicle C.G. during crash tests and simulations for modified weak post W-beam guardrail.

4.7.3.3. Quantitative Validation

LS-DYNA generated energy balance curves, shown in Figure 4.41, verify the numerical stability of the analytical solution. The Sprague and Geers metrics and Analysis-of-Variance (ANOVA) metrics were computed for the three acceleration channels and three angular rate channels obtained from the LS-DYNA simulation and TTI crash test using the RSVVP computer program(*31*). Simulation results were filtered at CFC 60 using TRAP(*10*) to match the filtering of the crash test data. As shown in Table 4.14, the signal comparison metrics with multiple channel weighting option satisfied the recommended acceptance criteria(*31*).

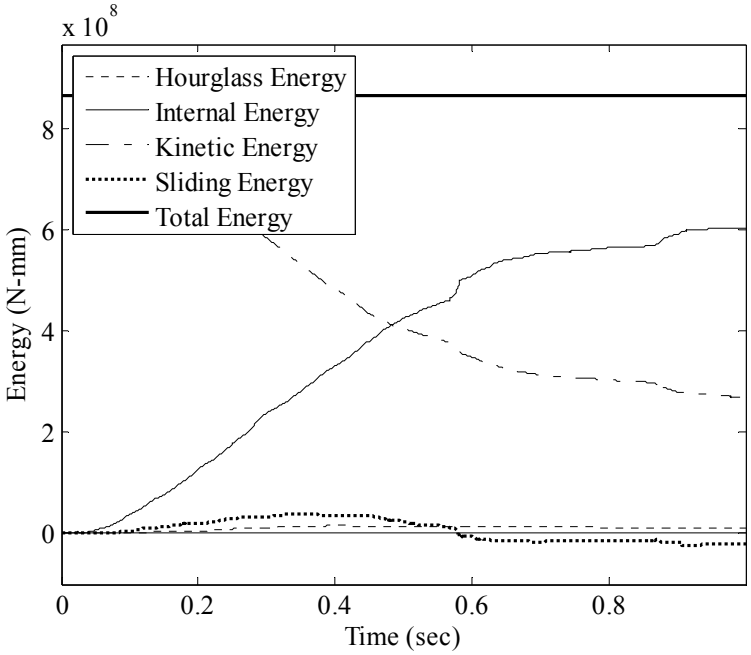

Figure 4.41 Energy balance curve obtained from the simulation on modified weak post W-beam guardrail.

Table 4.14 Time History Evaluation Table for modified weak post W-beam guardrail model.

Compare Test 473750-3 (Filter Type: C60) and Simulation (Filter Type: SAE60, source: TRAP)						
Channel Type	Weighting factor (Area II)(*45*)	Sprague-Geers Metrics		ANOVA Metrics		Pass ?
		M ≤ 40	P ≤ 40	Mean Residual ≤ 0.05	Std. Deviation ≤ 0.35	
X acceleration	0.19	61	30	0.09	0.31	N
Y acceleration	0.29	17	33	-0.01	0.35	Y
Z acceleration	0.01	270	48	-0.01	1.38	N
Roll rate	0.07	11.6	7	0.01	0.11	Y
Pitch rate	0.02	25	12.8	0.13	0.12	Y
Yaw rate	0.40	1.3	2	-0.01	0.04	Y
Multiple Channel	1.0	22	18	0.02	0.22	Y

A Phenomena Importance Ranking Table (PIRT), as recommended by Ray, et al. (*46*), was also prepared for the comparison of test and analytical solution. As shown in Table 4.15, the simulation results satisfied all of the evaluation criteria. Maximum

dynamic deflection, number of severely twisted posts, important occupant risk factors and, maximum roll, pitch and yaw angles obtained from the simulation within a period of 0.7 sec after impact closely matched the test results.

Table 4.15 Roadside safety Phenomena Importance Ranking Table (PIRT).

Evaluation Criteria	TTI Test	Simulation	Relative Difference ≤ 20%	Pass ?
Maximum Dynamic Deflection (m)	2.12m (6.95ft)	2.32m (7.60ft)	<20%	Y
Number of broken or significantly bent posts	6 (7~12)	5(7~11)	<20%	Y
Maximum Roll (deg.)	-12	-11	<20%	Y
Maximum Pitch (deg.)	-5	-3.9	<20%	
Maximum Yaw (deg.)	36	35.5	<20%	Y
Longitudinal direction: Occupant Impact Velocity ≤ 12m/s (30ft/s); Ridedown Acceleration ≤20g's	3.9m/s (12.8ft/s); -5.9g's	4.3m/s (14.1ft/s); -7.4g's	<20% <20%	Y
The rail did not rapture or fail	Yes	Yes	--	Y

4.7.3.4. Vehicle Damage

The vehicle sustained relatively minor damage in both the simulation and crash test as shown in Figure 4.42. The bumper, grill, left front and rear quarter panels, left door and left rear tire of the vehicle were damaged in both cases. The maximum exterior crush to the vehicle at the left front corner was 230 mm (9 in) and 254 mm (10 in) in the test and simulation, respectively.

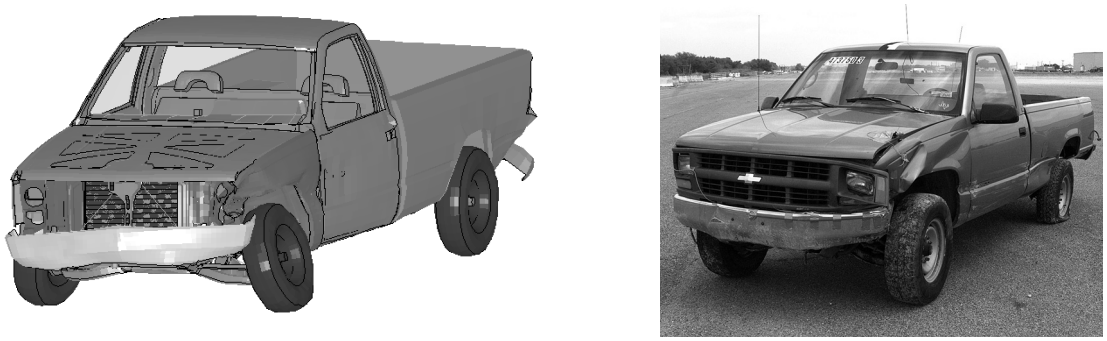

(a) (b)

Figure 4.42 Vehicle after (a) Simulation, and (b) Crash test 473750-3(*3*).

4.7.4. Summary

Results of the simulation performed with the modified weak post W-beam guardrail model showed good correlation compared to the crash test data. The number of post-to-rail detachments observed in the simulation matched the crash test results. Note that a calibration exercise was performed to achieve this result. The maximum dynamic deflection of the rail in the simulation and test matched reasonably. The roll and pitch angles closely matched the crash test results. Yaw angle showed good correlation until 0.62 seconds. The Occupant impact velocity and ride down acceleration data obtained from the simulation closely matched the crash test data. Since a reasonable overall correlation was achieved in terms of maximum dynamic rail deflection, post and rail damage characteristics, and key vehicle kinematics parameters, the model was considered sufficiently validated to use in defining impact performance limits of the modified weak post W-beam guardrail system.

4.8. BOX BEAM GUARDRAIL SYSTEM

The box beam guardrail system, as shown in Figure 4.43, can be classified as a weak post system. Weak post systems are generally very flexible and have the largest dynamic deflections(*4*). The “weak” posts of the box beam guardrail serve primarily to support

the rail elements at their proper elevation for contact with an impacting vehicle. The posts are readily detached from the rail and dissipate little energy as they yield to the impacting vehicle and are pushed to the ground. Provided there is adequate space to accommodate the large lateral deflection, the box beam system imposes lower deceleration on the impacting vehicle and is more tolerant and less likely to cause occupant injury.

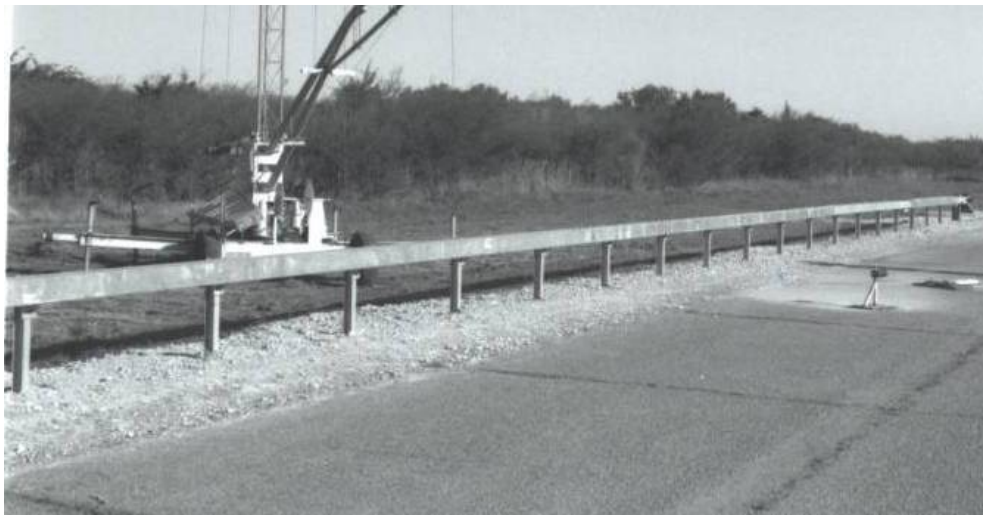

Figure 4.43 Typical box-beam guardrail system(*6*).

4.8.1. System Description

Detailed drawing of box beam guardrail and its key components are shown in Figure 4.44. As can be seen from the figure, the box beam guardrail system consists of 1.6 m (5.25 ft) long S75×8.5 (S3×5.7) steel posts spaced 1.83 m (5.9 ft) apart. A 114 mm (4.49 inch) long L127×89×10 shelf angle is attached to the post using a 12.5 mm (0.5 inch) diameter and 38 mm (1.5 inch) long hex bolt with washer and nut. A TS152×152×4.8 tubular steel box-beam rail element is attached to the support angle with a 10 mm (0.39 inch) diameter long hex bolt as shown in Figure 4.44(a). The box-beam rail is mounted at 610 mm (24 inches) from the ground level. As shown in Figure

4.44(b), the post is connected to a 600 mm×200 mm×6 mm (24 inch×8 inch×0.25 inch) soil-plate below the ground level. Two 680 mm×136 mm×68 mm (26.77 inch× 5.35 inch ×0.63 inch) splice plates are used to connect 10.98 m (36 ft) long box beam sections. The details of the splice connection are shown in Figure 4.44(c).

4.8.2. Model Development

The finite element model, as shown in Figure 4.45, was developed to conduct crashworthiness analyses of box beam guardrail system using LS-DYNA. Dimensions of different components of the box beam guardrail system were based on the latest specifications provided in the guideline prepared by AASHTO-AGG-ARTBA joint committee (*13*). The total length of the guardrail was 45.7 m (150 ft) along with WYBET (Wyoming Box-beam end terminal) end terminal on upstream end and turned-down end-terminal on downstream end (*6*). The final box-beam system model comprised of 430,657 elements.

The 10.98 m (36 ft) long box beam rail segments were modeled using shell elements that had a thickness of 4.76 mm (0.188 inch). Splice connections between two rails were modeled at every 10.98 m (36 feet). The bolts in the connection between the splice plates and the rail elements were modeled explicitly as shown in Figure 4.45(b). Automatic node to surface contact was defined between the bolts, splice plates, and stamps. Tied node to surface contact was used to attach the stamps to the box beam rail. The L127×89×9.5 support bracket and S7.5×8.5 posts were modeled using shell elements as shown in Figure 4.45(c). Both the bolts connecting the rail splices and the bolts connecting the support bracket to the post were modeled using a combination of beam and shell elements following the same approach described in Section 4.4.2. Since these bolts do not fail during impact, no failure criterion was implemented.

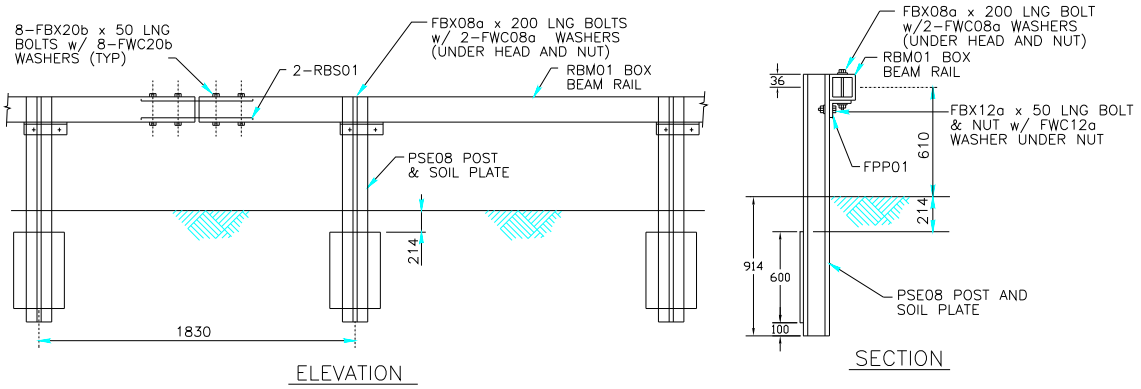

(a)

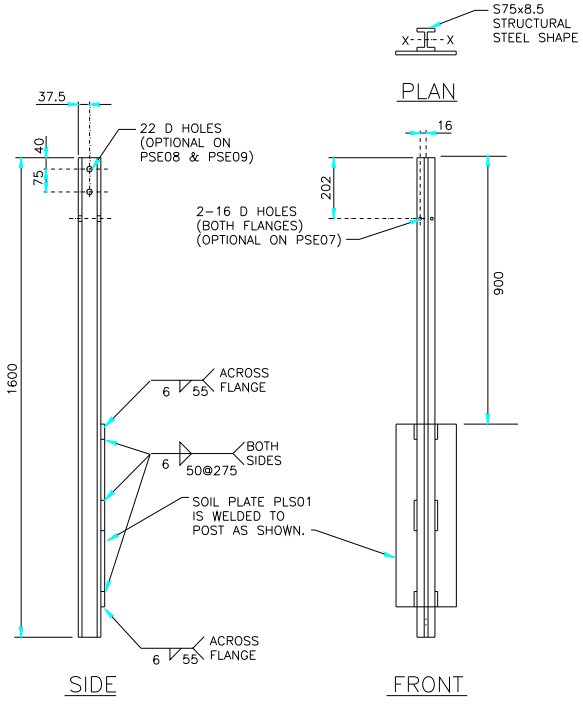

(b)

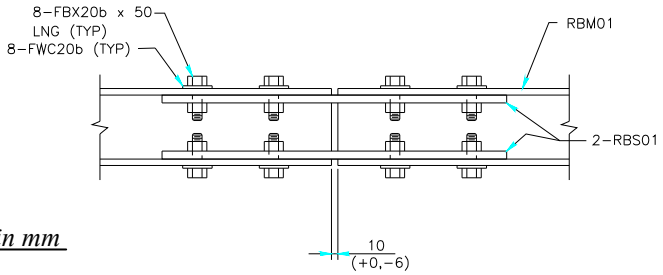

*All dimensions are in mm

(c)

Figure 4.44 Detailed drawings of (a) box-beam guardrail System, (b) weak post (PSE08), and (c) splice connections (*13*).

In weak posts system the post to rail connection is designed such that the bolt fails in combined action of shear and tension to permit the rail to readily and reliably detach from the posts prior to vehicle impacting the posts(*23*). In the weak post box-beam guardrail system, the support bracket and the box beam rail are connected using an 8 mm (0.315 inch) diameter (FB×08a) bolt as shown in Figure 4.44(a). To capture the bolt failure through fracture, damage enabled bolt model were used in this study. The methodology used was similar to that used in developing post-to-rail connections for modified weak post W-beam system model. As shown in Figure 4.45(c), the 8 mm (0.315 inch) diameter bolt shaft was modeled using solid elements with Material type 100. Constrained nodal rigid bodies were still used between the bolt shaft and the nuts since there is no need to model the stripping of the nuts off the bolt threads.

S75×8.5 steel posts with 200 mm×600 mm×6 mm (8.0 in x 24.0 in x 0.25 in) soil plates were modeled using shell elements. Post and soil plates were embedded into the soil. Soil was modeled as 1.34-m wide ×1.46-m long ×1.34-m deep (4.4-ft ×4.8-ft ×4.4-ft) rectangular buckets of solid elements. The WYBET end terminal, used in upstream end of the guardrail system was modeled using non-linear axial spring. The spring properties were calculated following the similar approach used in developing previous guardrail models. Finite element model of the turned-down end-terminal, used in downstream end of the box-beam guardrail system, is shown in Figure 4.45(c). End of the turned down rail near the ground was fully constrained to provide anchorage.

4.8.3. Model Validation

The box-beam system model was validated by performing a full-scale vehicle impact simulation and comparing the results to a previously conducted crash test of the system. The crash test used for the validation exercise was conducted at TTI (Test No. 471470-33(*6*)) under *NCHRP Report 350* test level 3 impact conditions.

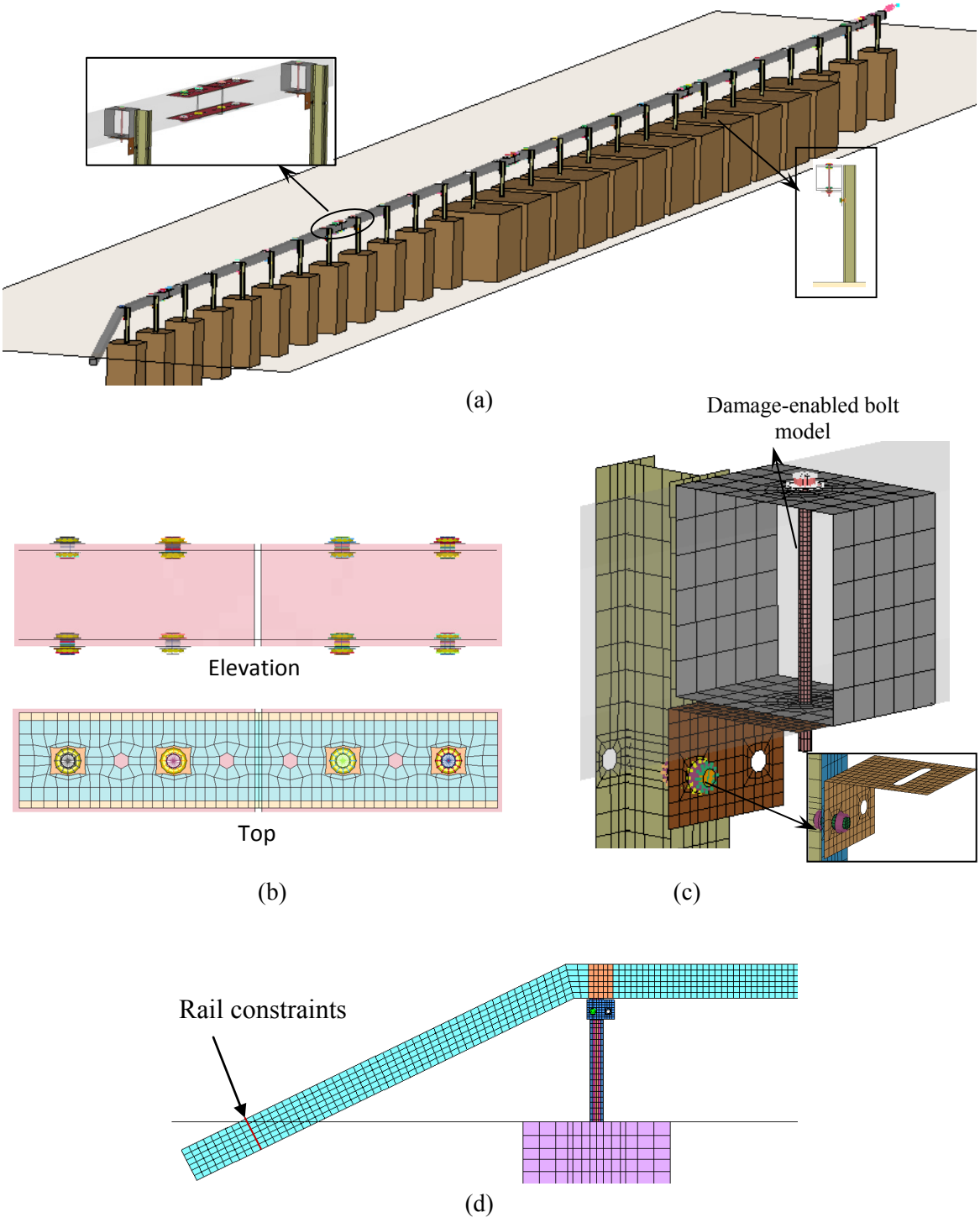

Figure 4.45 (a) Finite element model developed for the box-beam guardrail system. (b) Model for connection between rail, supporting bracket, and post (c) splice plate connection (d) Turned-down end-terminal.

The test article consisted of a 45.4 m (150 ft) long section of box beam guardrail with 15 m (49.21 ft) long telescoping tube terminal on the impact end and a turned-down terminal on the downstream end. A 1989 Chevrolet C2500 pickup truck with a test inertia weight of 2000 kg (4,409 lb) and a gross static weight of 2078 kg (4,577 lb) was used for the test. The height of the upper and lower edge of the vehicle bumper was 640 mm (25.2 inches) and 414 mm (16.3 inches), respectively.

The vehicle impacted the guardrail section 0.9 m (2.95 ft) upstream of post 15 at a speed of 95.2 km/h (59.15 mph) and an angle of 25.5 degrees. The vehicle was successfully contained and redirected by the guardrail system. After impact, the vehicle became parallel with the installation at 0.287s while travelling at a speed of 73 km/h (45.36 mph). The vehicle lost contact with the installation at 0.798s, travelling at a speed of 44.82 km/h (27.84 mph) and at an exit angle of approximately 0.7 degrees towards the guardrail. The maximum deflection of the guardrail was 0.74 m (29.1 inches).

To validate the box beam guardrail model, an impact simulation was performed similar to the full-scale crash test described above. A finite element model of the C2500 pickup truck model, with a mass of 2052 kg (4519 lb) was used to impact the box beam system model. The simulation was conducted using the same impact conditions as in the crash test (i.e. 95.2 km/h impact speed and 25.5 degree angle).

4.8.3.1. Splice Plate Connection and Post-to-Rail Connection

Performance of splice plate connection and post-to-rail connection during the simulation is shown in Figure 4.46. As can be seen, the FE model used for the splice plate connection was strong enough to withhold the rail splices during the impact simulation. The damage enabled bolts used in connections between rails and supporting brackets at post 15 to 19, on the other hand, failed through fracture to enable post detachments. Number of posts detached during the simulation matched the number observed during the crash test.

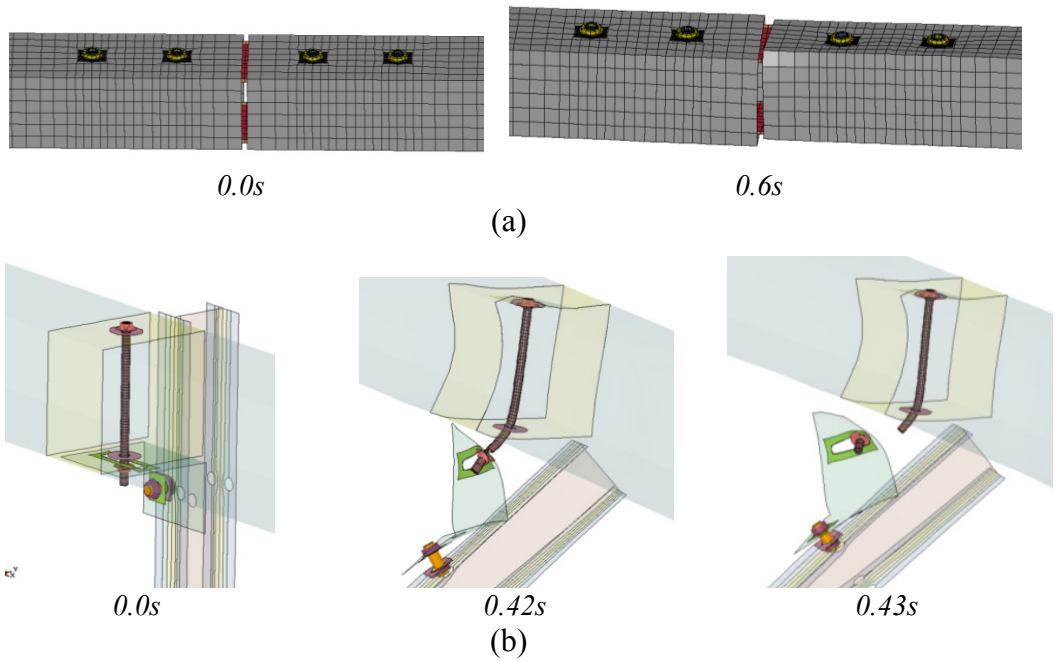

Figure 4.46 Performance of (a) Splice plate connection model and (b) Post to rail connection model at post #19 during impact simulation.

4.8.3.2. Event Time-sequence Comparison

Time-sequence comparison between the simulation and test results is shown in Figure 4.47. As can be seen from the figure, there is a reasonable overall correlation between the test and simulation results. In the simulation however, the vehicle lost contact with the rail slightly earlier than the crash test vehicle. A descriptive time-sequence comparison is also presented in Table 4.16.

Comparisons of yaw, pitch, roll angles and longitudinal and lateral accelerations obtained at vehicle C.G. during crash tests and simulations are presented in Figure 4.48 and Figure 4.49, respectively. It can be seen that the vehicle's yaw and pitch angles obtained from the simulation closely follow the trend observed in the crash test. Vehicle's roll angle obtained from the simulation continues to increase after 0.18 sec where the roll in test decreases. In the crash test, front right fender of the vehicle starts to

ramp on the rail at 0.18 sec creating larger negative roll compared to that observed during simulation.

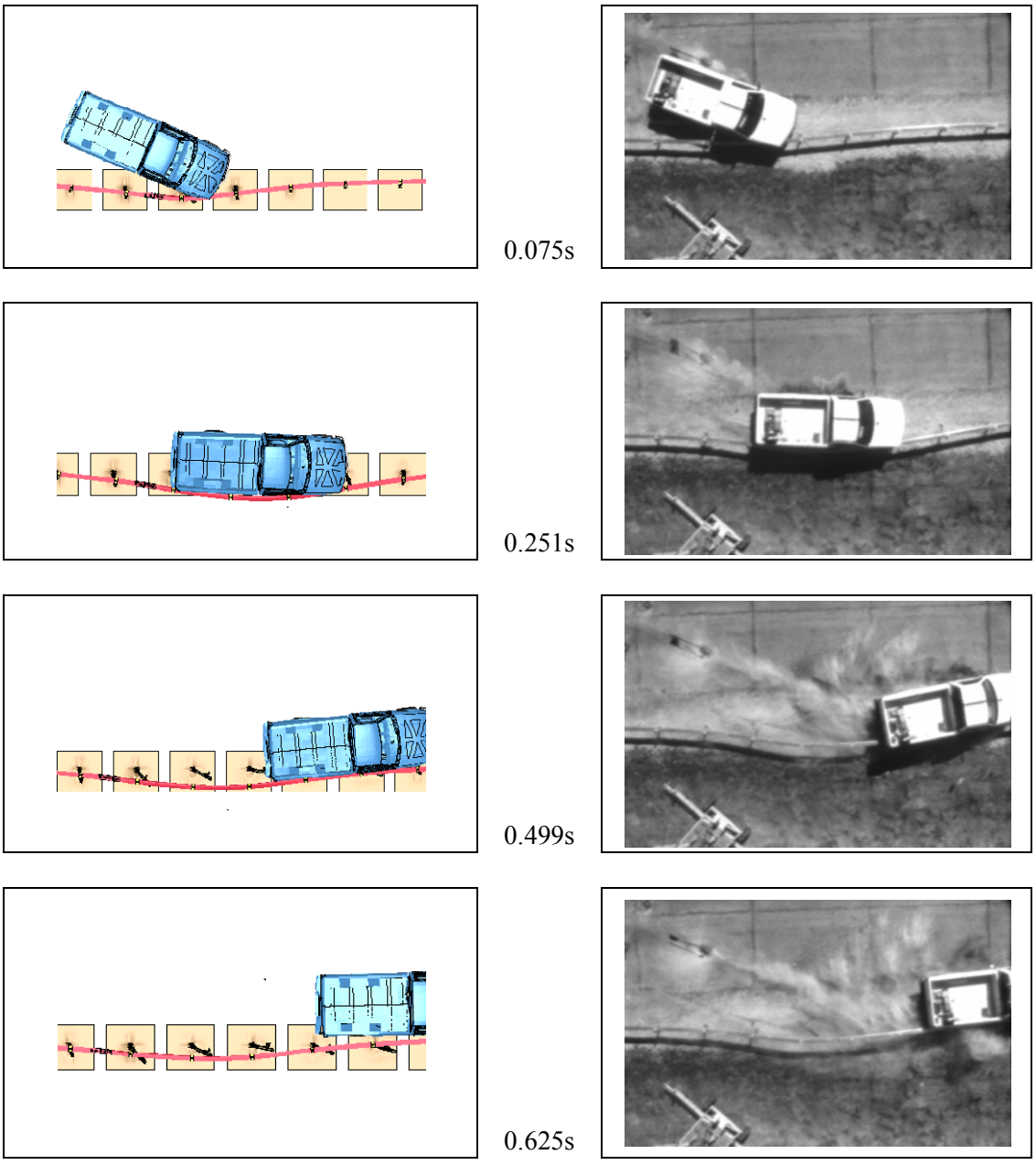

Figure 4.47 Sequential photographs for box-beam guardrail model simulation and TTI test 471470-33(*6*).

Table 4.16 Event time-sequence comparison of box-beam guardrail simulation and test.

Incident	Crash test	Model Simulation
Right front tire made contact with flange and face of post 15	.056s	0.05s
Right front tire made contact with post 16	.118s	0.135s
Right front tire made contact with post 17	.188s	0.215s
Right front tire made contact with post 18	.265s	0.30s
vehicle became parallel with the installation	.287s (73 km/h)	0.315s(64.1km/h)
The vehicle contacted post 19	.364s	0.405s
Maximum dynamic deflection occurred at	.364s (1.15m)	0.35s (0.873m)
vehicle lost contact with the installation	0.798s (44.8km/h)	0.63s (54.4km/h)
exit speed	44.8 km/h	54.4 km/h

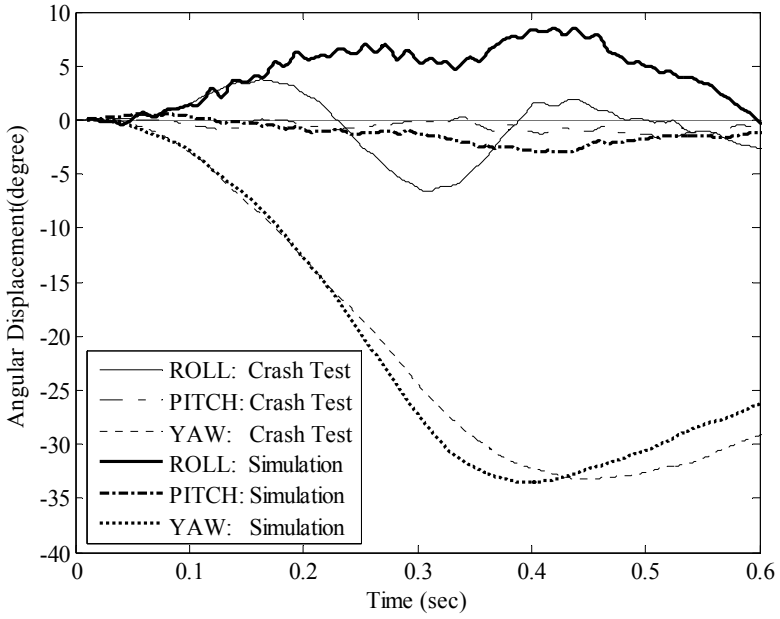

Figure 4.48 Comparisons of roll, pitch, and yaw angles obtained at vehicle C.G. during crash test and simulation of box-beam guardrail system.

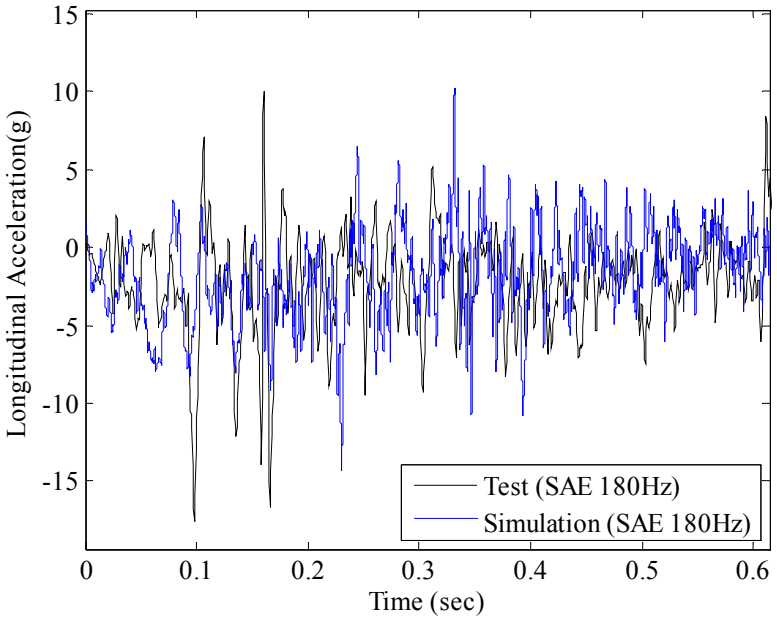

Figure 4.49 Comparisons of (a) longitudinal and (b) lateral accelerations obtained at vehicle C.G. during crash tests and simulations for box-beam guardrail system.

4.8.3.3. Quantitative Validation

Energy balance curve produced by LS-DYNA as shown in Figure 4.50 verifies the numerical stability of the simulation. The Sprague and Geers metrics and Analysis-of-Variance (ANOVA) metrics were computed for the three acceleration channels and three angular rate channels obtained from the LS-DYNA simulation and TTI crash test (*7*) using the RSVVP computer program(*38*). As shown in Table 4.17, time history comparison metrics between the crash test and computer simulation satisfied the criteria for the multiple channel weighting option.

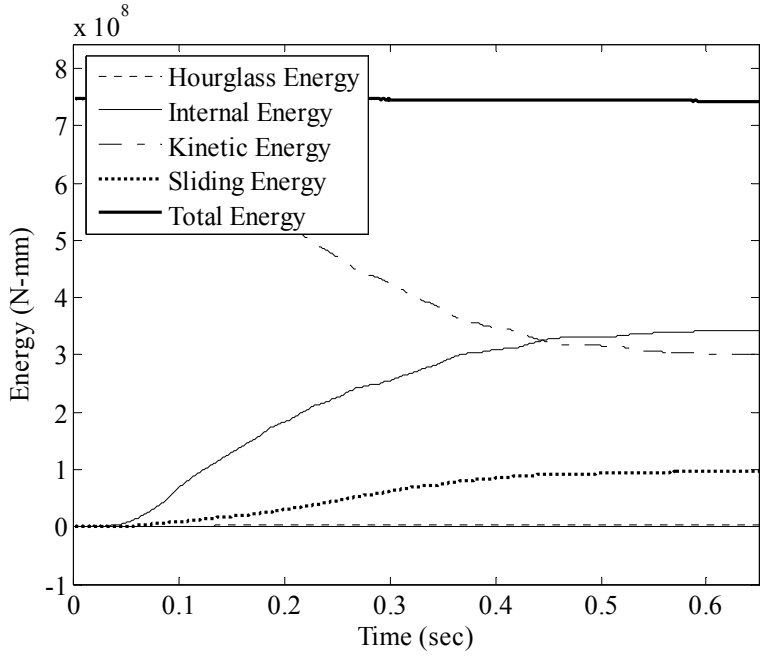

Figure 4.50 Energy balance curve obtained from the simulation using box-beam guardrail model.

Phenomena importance ranking table (PIRT), as recommended by Ray et. al (*31*), was also prepared as shown in Table 4.18. As can be seen, the simulation results satisfied all but one of these PIRT evaluation criteria. While the variation in maximum roll angle of the vehicle was greater than 20%, the overall roll magnitude was relatively

small for both the test and the simulation and the difference is not believed to substantially affect the vehicle response. Maximum dynamic deflection, number of severely twisted posts, important occupant risk factors, and maximum yaw and pitch angles obtained from the simulation closely matched the test results.

Table 4.17 Time History Evaluation Table for box-beam system model.

Compare Test 471470-33 (Filter Type: C180) and Simulation (Filter Type: SAE180, source: TRAP)						
Channel Type	Weighting factor (Area II)(*45*)	Sprague-Geers Metrics		ANOVA Metrics		Pass ?
		M ≤ 40	P ≤ 40	Mean Residual ≤ 0.05	Std. Deviation ≤ 0.35	
X acceleration	0.28	10.2	38.2	0.03	0.23	Y
Y acceleration	0.21	67	41	0.04	0.45	N
Z acceleration	0.003	159	51	0.01	0.77	N
Roll rate	0.048	172	46	0.01	1.16	N
Pitch rate	0.0007	176	48	0.01	0.30	N
Yaw rate	0.45	19	15	0.04	0.31	Y
Multiple Channel	1.0	34.9	29.1	0.019	0.35	Y

Table 4.18 Phenomena Importance Ranking Table for box-beam system model.

Evaluation Criteria	TTI Test	Simulation	Relative Difference ≤ 20%	Pass?
Maximum Dynamic Deflection (m)	1.15m (3.77 ft)	1.11m (3.64 ft)	<20%	Y
Number of broken or significantly bent posts	5 (16~20)	5 (15~19)	<20%	Y
Maximum Roll (deg.)	-7	8	>20%	N
Maximum Pitch (deg.)	-2	-3	<20%	Y
Maximum Yaw (deg.)	-33	-33	<20%	Y
Longitudinal direction: Occupant Impact Velocity < 12m/s (30ft/s); Ridedown Acceleration <20g's	 6.3m/s (20.6ft/s); -5.8g's	 4.5m/s (14.8ft/s); -7.8g's	 <20% <20%	Y
The rail did not rapture or fail	Yes	Yes	--	Y

4.8.3.4. Vehicle Damage

As shown in Figure 4.51, the vehicle sustained moderate damage in both the crash test and the simulation. The lower A-arm, stabilizer bar, tie rod ends, front and rear quarter panel, door, and front bumper on the impact side were damaged in both cases.

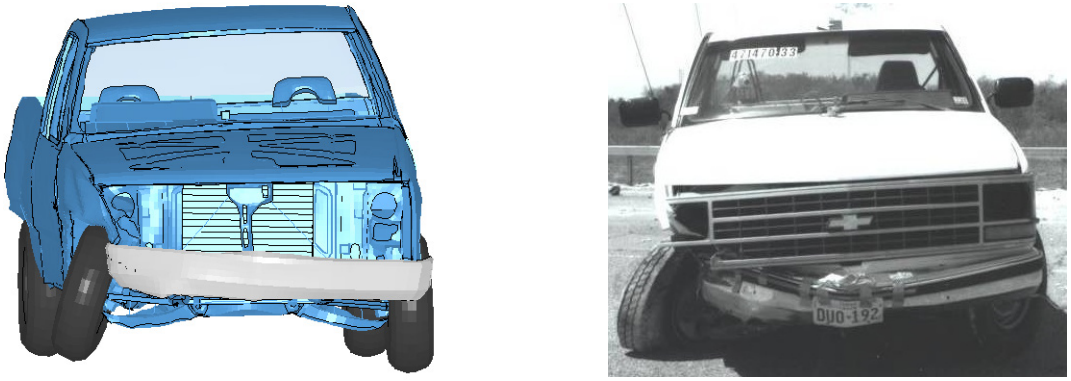

(a) (b)

Figure 4.51 Vehicle after (a) simulation and (b) crash test 471470-33(*6*).

4.8.4. Summary

Results of the simulation performed using the box beam guardrail model showed reasonable overall correlation with the crash test data. The maximum dynamic deflection of the rail showed good agreement. The vehicle yaw and pitch angles matched reasonably well with the test results. Differences in roll angle were not considered significant to the validity of the model as overall roll magnitude was relatively small. Damage characteristics of the test article and the test vehicle were very similar in the test and simulation. Based on this assessment, the model was considered sufficiently valid to proceed with the evaluation of the performance limits of the box beam guardrail system.

5. PERFORMANCE LIMIT ANALYSES

5.1. INTRODUCTION

LS-DYNA simulations were used in this study to define vehicle containment limits for five guardrail systems. Simulations were performed with guardrail models placed on flat and level terrain. The height of vehicle impact was parametrically varied to determine performance limits of the barrier as defined by initiation of override or rollover for the pickup truck and underride for the small passenger car. *NCHRP Report 350* specified design vehicles, a 2000-kg, ¾-ton, standard cab pickup truck (Chevrolet C2500) and an 820-kg passenger car (Geo Metro), were used in the analysis. Vehicle models used for the simulations were originally developed by the National Crash Analysis Center (NCAC) and were modified by the researchers at Texas Transportation Institute (TTI) over a period of time. Performance limits were determined in terms of acceptable heights of bumper-top with respect to local terrain at the point of impact. In equilibrium position on a flat terrain, heights of the bumper top of NCAC developed 2000-kg pickup and 820 kg passenger car models are 635 mm (25") and 535 mm (21"), respectively. The bumper height at the point of impact to a guardrail on slope varies depending on the trajectory of the vehicle and lateral offset of the guardrail. The impact conditions used to establish the barrier performance limits conformed to NCHRP Report 350(*2*) testing guidelines. The impact conditions for test designation 3-11 consist of the pickup truck impacting the barrier at a speed of 100 km/h (62 mph) and an angle of 25 degrees. The corresponding impact conditions for test designation 3-10 consist of the small passenger car impacting the barrier at 100 km/h (62 mph) and 20 degrees. Vehicle to barrier impact points in longitudinal direction were selected based on the guidelines provided to determine critical impact points (CIP)(*2*) for crash tests.

This section discusses the methodology used to analyze performance limits for five guardrail systems. Results obtained from these analyses are also presented and compared with the values suggested in the past.

5.2. PREVIOUS ASSUMPTIONS

In the early 1980s, Ross and Sicking(*1*) suggested the barrier containment criteria for standard strong post G4(1S) W-beam, standard thrie-beam, and box-beam guardrail systems based on a limited number of crash tests and engineering judgments. The barrier containment criteria assumed for W-beam guardrail and boxbeam guardrail system placed on a median barrier are shown in Figure 5.1. For W-beam and Thrie-beam guardrail systems, Ross and Sicking(*1*) assumed that acceptable barrier behavior is expected when mid-height of the bumper impacts between the upper and lower corrugation centers of the "W-beam" or "Thrie-beam" rail. For box-beam guardrail system, the acceptable barrier behavior is expected when mid height of the bumper impacts below the top of the box beam rail and upper front corner of the vehicle fender impacts above the rail base. Effectiveness of these assumptions, however, has not been verified. Performance limits of three similar guardrail systems, in terms of bumper top height during an impact, can be calculated following these assumptions. Table 5.1 presents the override and underride limits calculated for modified G4(1S) W-beam, modified Thrie-beam, and Box-beam guardrail systems based on Ross and Sicking (*1*) suggested criteria.

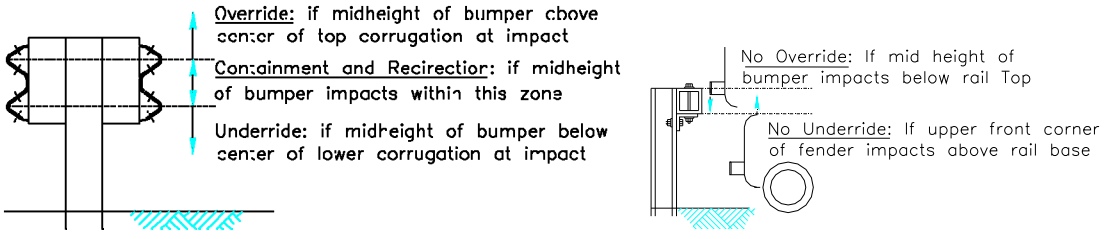

Figure 5.1 Containment criteria for (a) W-beam barrier (b) Box-beam barrier(*1*).

Table 5.1 Performance limits calculated using Ross and Sicking (*1*) suggested criteria.

Guardrail Type	Rail Top Height	Bumper Top Height	
		Override Limit	Underride Limit
Modified G4(1S) W-beam	710 mm (27.9″)	758 mm (29.8″)	564 mm (22.2″)
Modified Thrie-beam	866 mm (34″)	914 mm (35″)	526 mm (20.7″)
Box Beam Guardrail	686 mm (27″)	793 mm (31.2″)	374 mm (14.7″)

5.3. CRITICAL IMPACT POINT (CIP)

For the performance limit analyses, vehicle to guardrail impact points in longitudinal direction were selected based on the critical impact point (CIP) guideline provided in NCHRP report 350(*2*). In general there are two CIPs for a longitudinal barrier: (a) one that produces the greatest potential for wheel snagging and (b) one that produces the greatest loading on a critical part of the guardrail, such as rail splice. For the guardrails with splice located at a post the two CIP's coincides. For guardrails with splice in between two posts, post spacing are generally small and all failure mode of concern can be evaluated with one test by placing the rail splice just upstream from the reference post(*2*).

The critical impact distance "x" from the reference post, as shown in Figure 5.2, is measured following the guidelines specified in Section 3.4.2 of Report 350(*2*). According to the guideline, the CIPs are controlled by effective plastic moment (M_p) of the barrier rail elements and dynamic yield force per unit length (F_p) of the barrier posts. Effective plastic moments (M_p) for common guardrail rail elements are presented in Table A3.1(*2*) in report 350. The dynamic yield force (F_p') for the post embedded in soil is controlled by the smaller of two forces: (a) force (F_y) necessary to yield a rigidly anchored post and (b) force (F_s') necessary to yield the soil in which the post is embedded. These two forces are calculated using Equations (5.1) and (5.2), respectively:

$$F_y = D\left(\frac{\sigma_y Z_p}{H_r}\right) \tag{5.1}$$

$$F_s' = F_s \times \left(\frac{D_e'}{D_e} \right)^2 \tag{5.2}$$

where, D is the dynamic magnification factor. Typical value for D is 1.5 for steel posts(*2*). σ_y and Z_p are the yield stress and plastic section modulus for the post, respectively. H_r is the height of the highest rail above the post base. The dynamic forces required to yield the soil (F_s) for some common post types with given embedment depths, D_e, are presented in Table A3.3(*2*) in report 350. D_e' is the post embedment depth for the candidate guardrail. Post dynamic yield force per unit length (F_p) of the barrier is obtained by dividing the post dynamic yield force (F_p') by the barrier post spacing. For Test level 3-10 and 3-11, the critical impact distance "x" from the reference post is determined using Figures 3.8 and 3.10 presented in Report 350(*2*), respectively. These figures present the post dynamic yield force per unit length (F_p) vs. effective rail plastic moment (M_p) curves for the barriers at different x values. Using these curves, critical impact point locations for the five guardrail systems are calculated as shown in Table 5.2. Effective rail plastic moment (M_p) and dynamic yield force per unit length for the posts (F_p) are calculated following the procedures discussed above.

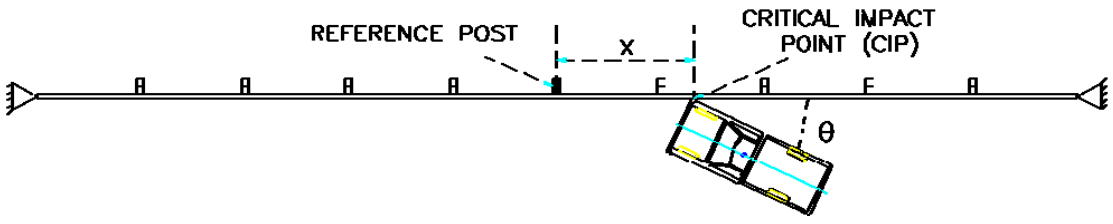

Figure 5.2 Impact condition for longitudinal barrier test.

Table 5.2 Calculation of Critical Impact Point (CIP) in longitudinal direction.

Guardrail Type	Post Spacing (m)	Post Type	σy (MPa)	Zx (m3) × 10^{-5}	Hr , m	D_e', m	Fs', kN	Fy, kN	Fp', kN	Fp, kN/m	Mp, kN-m	Critical Impact Distance "x" (m)	
												TL 3-10	TL 3-11
Modified G4(1S)	1.905	W150×13.5	336 (*44*)	10.2	0.55	1.10	53.3	94	53.3	27.9	10.9	2.3	4.3
MGS	1.905	W150×13.5	336 (*44*)	10.2	0.63	1.02	45.4	81	45.4	23.8	10.9	2.3	4.4
Modified Thrie-beam	1.905	W150×13.5	336 (*44*)	10.2	0.61	1.17	60.6	84	60.6	31.8	17.2	2.1	4.0
Modified Weak post W-beam	3.81	S75 ×8.5	336 (*44*)	3.18	0.66	0.77	26.4	24	24.1	6.33	10.9	3.1	5.5
Box-beam	1.83	S75 ×8.5	336 (*44*)	3.18	0.61	0.91	36.8	26	26.3	14.4	49.5	2.5	5.4

5.4. OVERRIDE LIMIT ANALYSES

Override limit for a given barrier can be defined as the maximum acceptable vehicle impact height for a pickup truck beyond which the truck is expected to override or rollover after impacting the barrier. In order to determine the override limit for a given barrier, three LS-DYNA simulations were performed where an airborne pickup truck impacted the guardrail placed on flat terrain at three different impact heights. Thus, fifteen LS-DYNA simulations were performed to determine override limits for five guardrail systems. For all the cases, pickup truck impacted the barrier at a nominal speed and angle of 100 km/h (62 mph) and 25 degrees, respectively. The results of the simulations are presented below.

Three full-scale LS-DYNA simulations, as presented in Table 5.3 and Figure 5.3, were performed with a Chevrolet C2500 pickup impacting the modified G4(1S) W-beam guardrail model on flat and level terrain to obtain the override/rollover limit for the guardrail system. For all three cases vehicle impacted the guardrail system 4.3 m (14 ft)

upstream of the rail splice located at post 13. Note that the post numbering in the FE guardrail model starts from 8 as the first 7 posts are included in the end terminal modeled using nonlinear spring elements. The bumper top height at time of impact and the corresponding containment results are shown in Table 5.3. Figure 5.3 shows sequential images for the three simulations. As can be seen from the table and figure, modified G4(1S) guardrail system successfully contained and redirected the airborne pickup when 1/3rd of its bumper was above the rail upper corrugation center at the time of impact. When mid height or 5/12th of the bumper was above rail upper corrugation center during an impact, vehicle overrode the guardrail model. Hence, vehicle override or rollover should be expected if a pickup impacts the modified G4(1S) guardrail system with the upper edge of its bumper at a height greater than 726 mm (28.58") above the system base.

Table 5.4 and Figure 5.4 present the results obtained from the three impact simulations performed on Midwest guardrail model placed on flat terrain using airborne C2500 pickup model. For all three cases, initial impact occurred 3.45 m (11.3 ft) upstream from the centerline of splice between post nos. 13 and 14 at different impact heights. The bumper top heights at time of impact and the corresponding containment results are shown in Table 5.4. Figure 5.4 shows sequential images for the three simulations. It can be seen that the vehicle overrode the guardrail model when mid-height of its bumper impacted above the rail upper corrugation center. The guardrail, however, successfully contained and redirected the vehicle when the airborne pickup impacted the MGS with 5/12th of its bumper above rail upper corrugation center. Height of the bumper top during this impact was 818 mm (32.2") above the guardrail base.

Table 5.3 Override limit analysis results for modified G4(1S) W-beam guardrail.

Vehicle Type	Rail upper corrugation center height	Impact point description	Height of bumper top above ground level	Containment Result	Override/ Rollover Limit
2000-kg Chevy 2500	651 mm (25.6″)	½ of bumper above rail upper corrugation center	761 mm (29.96")	Override	726 mm (28.58")
		5/12th of bumper above rail upper corrugation center	743 mm (29.25")	Override	
		1/3rd of the bumper above rail upper corrugation center	726 mm (28.58")	Contained	

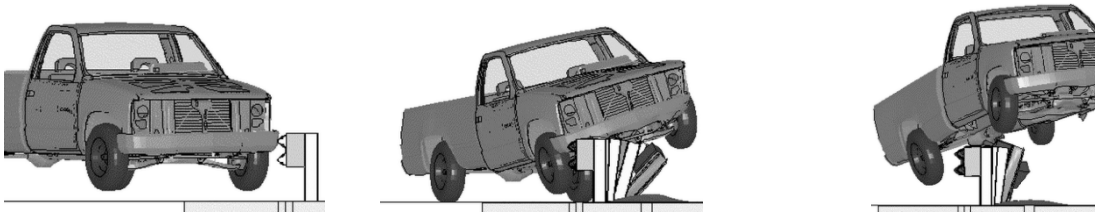

0s 0.18s 0.48s

(a) ½ of the bumper above rail upper corrugation center; Bumper top height=761 mm (29.96")

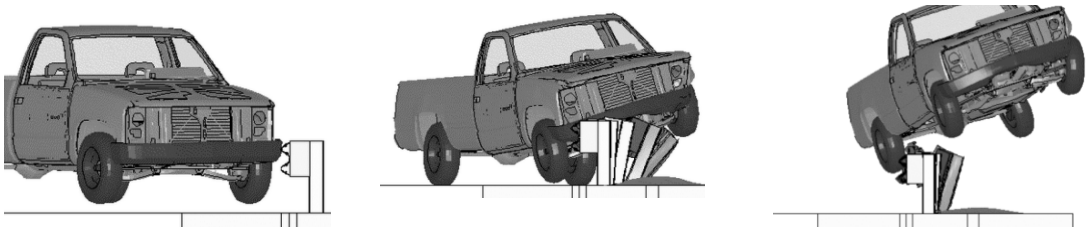

0s 0.18s 0.48s

(b) 5/12th of the bumper above rail upper corrugation center; Bumper top height=743 mm (29.25")

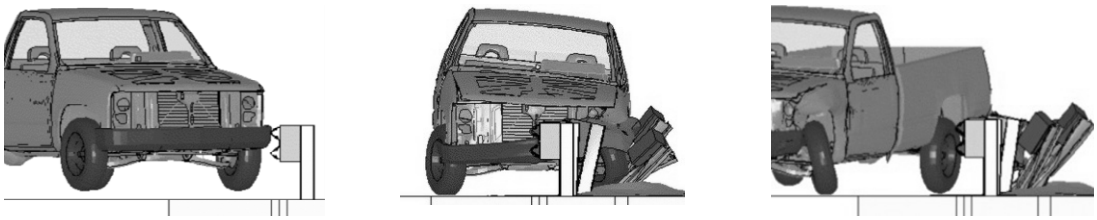

0s 0.35s 0.75s

(c) 1/3rd of the bumper above rail upper corrugation center; Bumper top height=726 mm (28.58")

Figure 5.3 Sequential photographs of override limit analysis for modified G4(1S) W-beam guardrail.

Table 5.4 Override limit analysis results for Midwest Guardrail System.

Vehicle Type	Rail upper corrugation center height	Impact point description	Height of bumper top above ground level	Containment Result	Override/ Rollover Limit
2000-kg Chevy 2500	728 mm (28.7″)	½ of bumper above rail upper corrugation center	836 mm (32.9")	Override	818 mm (32.2")
		1/3rd of bumper above rail upper corrugation center	800 mm (31.9")	Contained	
		5/12th of the bumper above rail upper corrugation center	818 mm (32.2")	Contained	

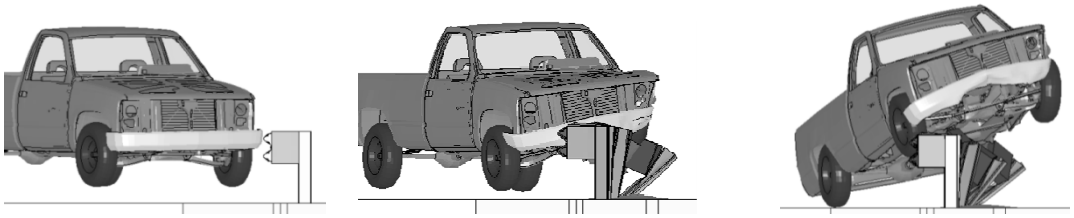

0s 0.16s 0.28s

(a) ½ of the bumper above rail upper corrugation center; Bumper top height=836 mm (32.9")

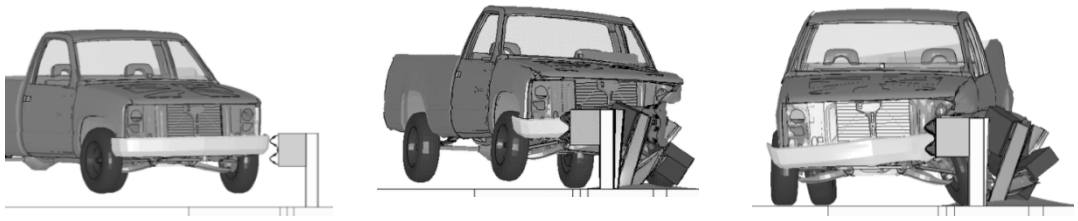

0s 0.20s 0.41s

(b) 1/3rd of the bumper above rail upper corrugation center; Bumper top height=800 mm (31.9")

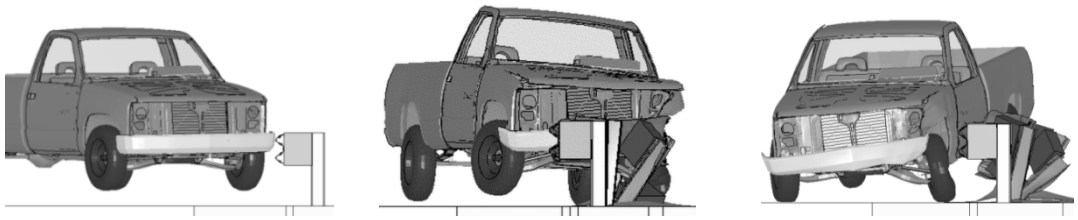

0s 0.25s 0.51s

(c) 5/12th of the bumper above rail upper corrugation center; Bumper top height=818 mm (32.2")

Figure 5.4 Sequential photographs of override limit analyses for Midwest Guardrail System.

In LS-DYNA simulations performed to evaluate the override limit for modified Thrie-beam guardrail system, the airborne pickup model impacted the guardrail model 4.0 m (13.1 ft) upstream of the rail splice located at post 15. The bumper top heights at time of impact and the corresponding containment results are shown in Table 5.5. Figure 5.5 shows sequential images for the three simulations. As can be seen from the table and the figure, the vehicle overrode the guardrail when it impacted the system with ½ or 1/6th of its bumper above rail upper corrugation center. The only containment was observed when 1/10th of the bumper was above rail upper corrugation center with its top edge 830 mm (32.7") above the system base during impact. Hence, bumper top height of 830 mm (32.7") at the time of impact is selected as override limit for modified Thrie-beam guardrail.

For modified weak post W-beam guardrail, the airborne pickup impacted the guardrail model 5.5 m (18 ft) upstream of post 8 at a speed of 100 km/h (62 mph) and 25 degrees. The bumper top heights at the time of impact and the corresponding containment results are shown in Table 5.6. Figure 5.6 shows sequential images for the three simulations. It can be seen that the guardrail successfully contained and redirected the vehicle when it impacted the system with top edge of its bumper at upper corrugation center of the rail, i.e. 757 mm (29.8") above the guardrail base. The vehicle impacting above this height overrode the system.

The airborne pickup model impacted the box-beam guardrail model 5.4 m (17.7 ft) upstream of post 17. As shown in Table 5.7 and Figure 5.7, the vehicle overrode the system when it impacted the guardrail with 5/8th of its bumper above rail top. According to Ross and Sicking(*1*) assumptions, the acceptable barrier behavior is expected when mid height of the bumper impacts below the top of the box beam rail. However, in the second impact simulation, as shown in Figure 5.7(b), the vehicle impacting the guardrail at this impact height overrode the system. In the next simulation vehicle impact height was lowered by 1/8th of its bumper. As shown in Figure 5.7(c), the guardrail successfully contained and redirected the pickup as it impacted the guardrail with 3/8th of its bumper above rail top. Upper edge of the bumper was 764 mm (30")

above ground at this impact height. Hence, bumper top height exceeding this value during an impact on a box-beam guardrail should be considered unacceptable.

Table 5.5 Override limit analysis results for modified Thrie-beam guardrail.

Vehicle Type	Rail upper corrugation center height	Impact point description	Height of bumper top above ground level	Containment Result	Override/ Rollover Limit
2000-kg Chevy 2500	807 mm (31.8″)	½ of bumper above rail upper corrugation center	973 mm (35.3")	Override	830 mm (32.7")
		1/6th of bumper above rail upper corrugation center	840 mm (33")	Override	
		1/10th of the bumper above rail upper corrugation center	830 mm (32.7")	Contained	

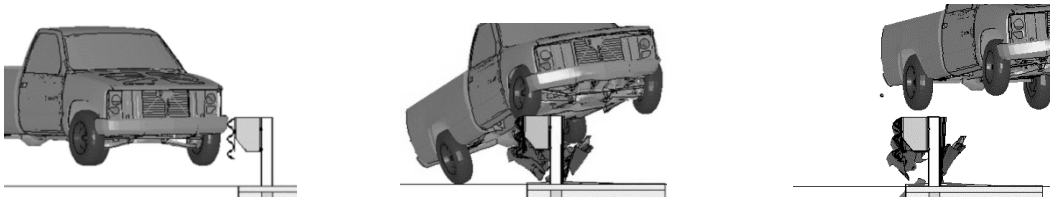

0s 0.18s 0.48s

(a) ½ of the bumper above rail upper corrugation center; Bumper top height=973 mm (35.3")

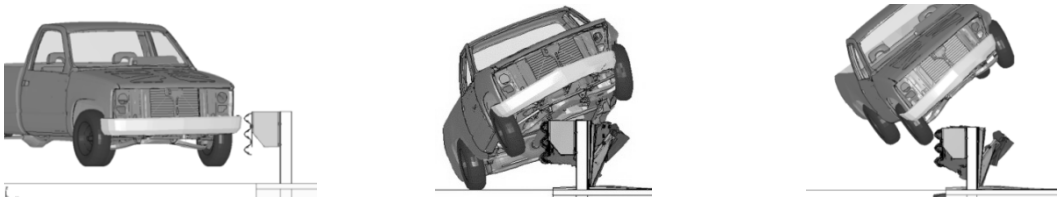

0s 0.18s 0.65s

(b) 1/6th of the bumper above rail upper corrugation center; Bumper top height=840 mm (33")

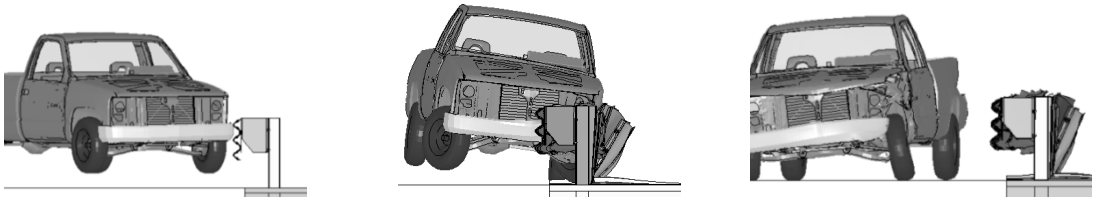

0s 0.24s 0.65s

(c) 1/10th of the bumper above rail upper corrugation center; Bumper top height=830 mm (32.7")

Figure 5.5 Sequential photographs of override limit analyses for modified Thrie-beam guardrail.

Table 5.6 Override limit analysis results for modified weak post W-beam guardrail.

Vehicle Type	Rail upper corrugation center Height	Impact point description	Height of bumper top above ground level	Containment Result	Override/ Rollover Limit
2000-kg Chevy 2500	757 mm (29.8″)	1/3rd of bumper above rail upper corrugation center	828 mm (32.6")	Override	757 mm (29.8")
		Top of the bumper at rail upper corrugation center	757 mm (29.8")	Contained	
		1/10th of the bumper above upper corrugation center	778 mm (30.6")	Override	

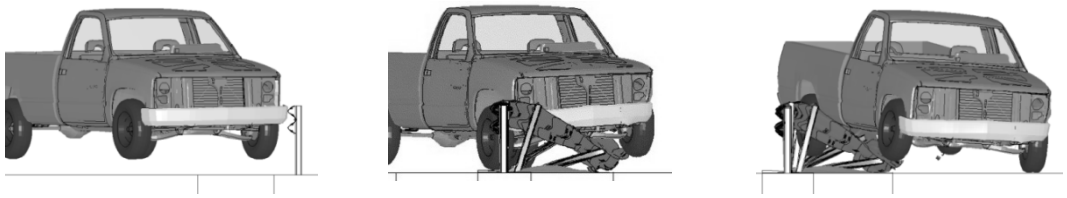

0s 0.19s 0.38s

(a) 1/3rd of the bumper above rail upper corrugation center; Bumper top height=828 mm (32.6")

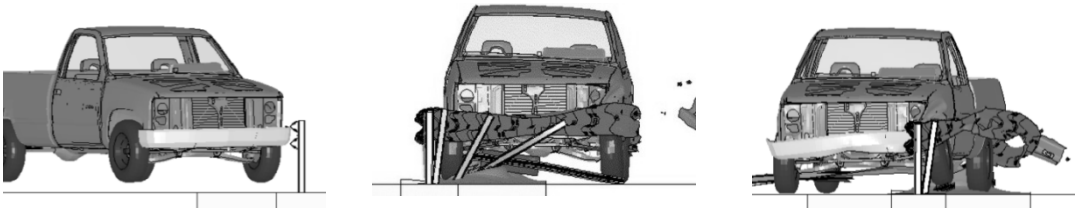

0s 0.44s 0.87s

(b) Top of the bumper at rail upper corrugation center; Bumper top height=757 mm (29.8")

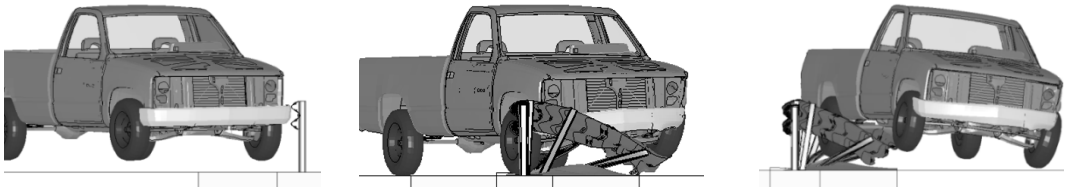

0s 0.20s 0.40s

(c) 1/10th of the bumper above upper corrugation center; Bumper top height=778 mm (30.6")

Figure 5.6 Sequential photographs of override limit analyses for modified weak post W-beam guardrail.

Table 5.7 Override limit analysis results for box-beam guardrail system.

Vehicle Type	Rail top height	Impact point description	Height of bumper top above ground level	Containment Result	Override/ Rollover Limit
2000-kg Chevy 2500	686 mm (27″)	5/8th of the bumper above rail top	818 mm (32.2")	Override	764 mm (30″)
		½ of bumper above rail upper corrugation center	790 mm (31.1")	Override	
		3/8th of the bumper above rail top	764 mm (30″)	Contained	

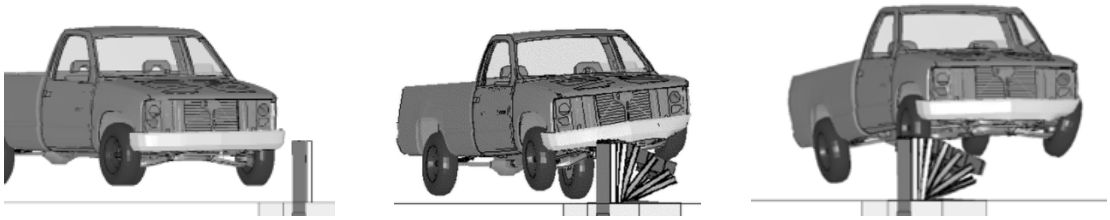

0s 0.15s 0.3s

(a) 5/8th of the bumper above box beam rail top; Bumper top height=818 mm (32.2")

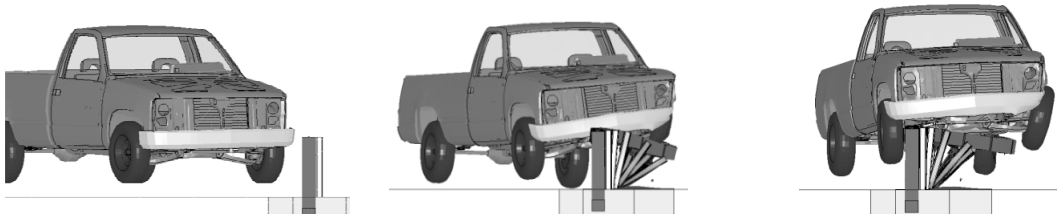

0s 0.145s 0.32s

(b) ½ of the bumper above rail upper corrugation center; Bumper top height=790 mm (31.1")

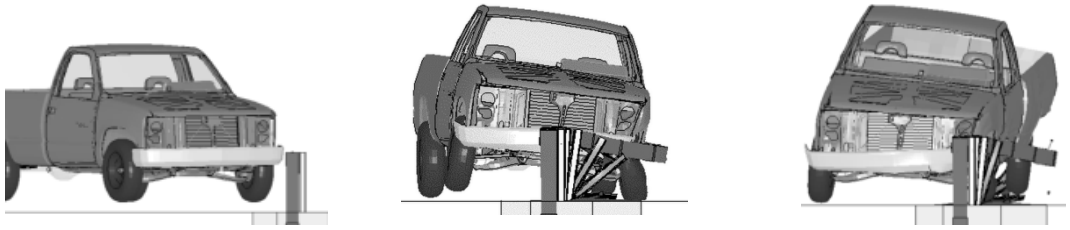

0s 0.235s 0.41s

(c) 3/8th of the bumper above box beam rail top; Bumper top height=764 mm (30″)

Figure 5.7 Sequential photographs of override limit analyses for box-beam guardrail system.

5.5. UNDERRIDE LIMIT ANALYSES

Underride limit for a given barrier can be defined as the lowest acceptable vehicle impact height for a passenger car below which the impacting car is expected to severely snag or underride the guardrail to cause serious occupant injury. Underride limit can be obtained through LS-DYNA simulations of small car model impacting the guardrail at reduced impact heights that correspond to different levels of suspension compression. However, rather than achieve actual compression of the vehicle suspension, the bumper top of the 820C car model was lowered with respect to its normal equilibrium position by lowering the ground surface for the vehicle as shown in Figure 5.8. The guardrail remains at its original height with respect to the soil it is embedded in, and the contact between the soil bucket and vehicle is ignored.

Several LS-DYNA simulations were performed with a Geo Metro impacting the guardrail model at reduced impact heights to obtain the underride limit for each guardrail system. For all the cases 820C model impacted the barrier at a nominal speed and angle of 100 km/h (62 mph) and 20 degrees, respectively. A simulation was considered acceptable if the occupant risk factors obtained from the analysis remained within the acceptable NCHRP Report 350 thresholds. Therefore, the occupant impact velocity and ride down acceleration along the longitudinal or lateral direction should not exceed 12 m/s (40 ft/s) and 20g's, respectively. Exceeding these values is an indication that the vehicle snagging due to underriding the guardrail is too severe and serious occupant injury is probable.

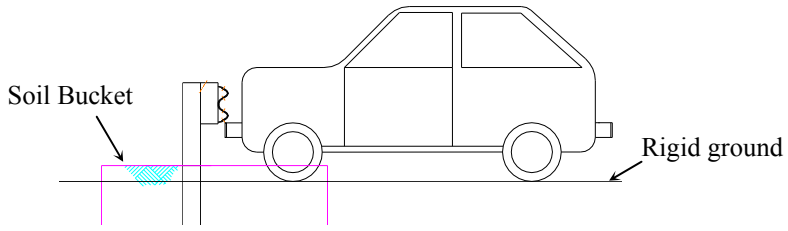

Figure 5.8 Vehicle is traveling on a lower ground compared to the guardrail-soil model.

Three impact simulations were performed to determine the underride limit for modified G4(1S) W-beam system. Small car model in these simulations impacted the modified G4(1S) guardrail model on flat terrain 2.3 m (7.5 ft) upstream of the rail splice located at post 13 at three different impact heights. The bumper heights at time of impact and the corresponding occupant risk factors are shown in Table 5.8. Figure 5.9 shows the sequential images obtained from the three simulations. It can be seen that the guardrail successfully contained and redirected the vehicle when its bumper top impacted at rail lower corrugation center. Height of the W-beam lower corrugation center for modified G4(1S) system is 453 mm (17.86") above guardrail base. In the next simulation, the bumper top impacted the guardrail at a height 50 mm (2") below the rail lower corrugation center and 403 mm (15.86") above the guardrail base. Although the vehicle snagged into the system, the occupant risk factors obtained from this simulation were within acceptable limit. Thus the crash simulation passed the safety evaluation criteria set forth in report 350. In the third simulation, the small car model impacted the guardrail model with its bumper top 75 mm (3") below the rail lower corrugation center. The car, during this simulation, severely snagged into the system producing an occupant ride down acceleration larger than that accepted. Thus it was concluded that serious occupant injury is probable when upper edge of the small car bumper impacts the modified G4(1S) system at a height lower than 403 mm (15.86") above guardrail base.

Table 5.8 Underride limit analysis results for modified G4(1S) W-beam guardrail system.

Vehicle Type	Rail lower corrugation center height	Impact point description	Height of bumper top above G.L.	Acceptance Criteria: Occupant Risk Factors		Simulation result	Under-ride Limit
				OIV ≤ 12 m/s (40 ft/s)	RDA ≤20 g's		
820-kg Geo Metro	453 mm (17.86")	Bumper top at rail lower corrugation center	453 mm (17.86")	6.7 m/s (21.6 ft/s)	12.0 g's	Pass	403 mm (15.86")
		Bumper top 50 mm (2") below rail lower corrugation center	403 mm (15.86")	9.7 m/s (22 ft/s)	15.5 g's	Pass	
		Bumper top 75 mm (3") below rail lower corrugation center	378 mm (14.8")	8.5 m/s (27.9 ft/s)	20.2 g's	Fail	

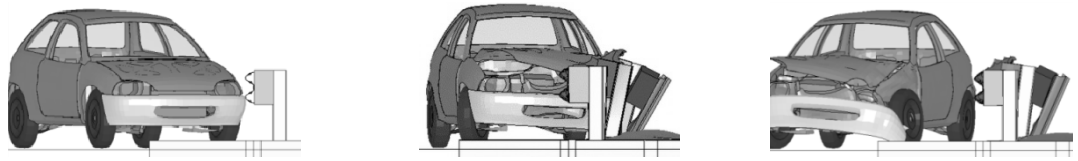

0s 0.18s 0.50s

(a) Bumper top at rail lower corrugation center; Bumper top height=453 mm (17.8")

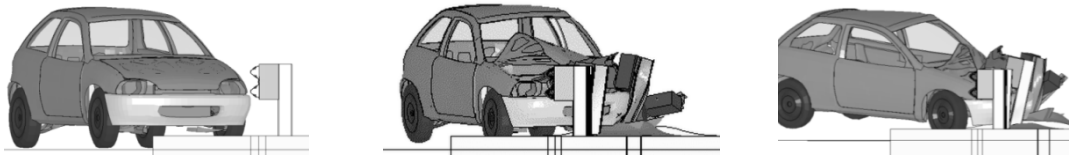

0s 0.20s 0.40s

(b) Bumper top 50 mm (2") below rail lower corrugation center; Bumper top height=403 mm (15.8")

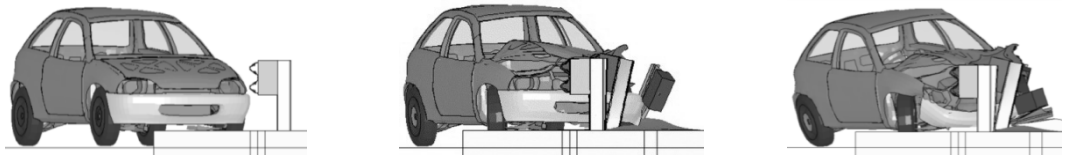

0s 0.35s 0.28s

(c) Bumper top 75 mm (3") below rail lower corrugation center; Bumper top height=378 mm (14.8")

Figure 5.9 Sequential photographs of underride limit analyses for modified G4(1S) W-beam guardrail system.

Three small car impact simulations were performed to determine the underride limit for Midwest guardrail system (MGS). For all three cases, initial impact occurred 1.3 m (4.3 ft) upstream from the centerline of splice between post nos. 13 and 14. The bumper heights at time of impact and the corresponding occupant risk factors are shown in Table 5.9. Figure 5.10 shows the sequential images obtained from the three simulations. In the first simulation, the small car was successfully contained and redirected by the MGS as the car impacted the system with its bumper top 100 mm (4") below the rail lower corrugation center. Lower corrugation center of the W-beam for MGS is 453 mm (17.86") above the guardrail base. In the second simulation, top of the small car bumper impacted the guardrail 125 mm (5") below the rail lower corrugation center. Bumper top during this impact was 410 mm (16.1") above guardrail base. Although the car slightly snagged into the system, the MGS successfully contained the vehicle. Occupant risk factors obtained from the simulation were within acceptable values. Small car in the final simulation severely snagged into the system producing an occupant ride down acceleration larger than the 20g's threshold. The bumper top during this impact was 150 mm (6") below the rail lower corrugation center. Hence, bumper top height of 410 mm (16.1") during impact was selected as underride limit for MGS system.

In the LS-DYNA simulations performed to determine underride limit for modified thrie-beam guardrail, the small car impacted the guardrail model 2.1 m (6.9 ft) upstream of rail splice located at post 15. The bumper heights at time of impact and the corresponding occupant risk factors are shown in Table 5.10. Figure 5.11 shows the sequential images obtained from the three simulations. It can be seen that the vehicle was successfully contained and redirected when it impacted the guardrail with its bumper top 50 mm (2") and 100 mm (4") below the rail lowest corrugation center. Lowest corrugation center of the Thrie-beam for modified Thrie-beam system is 415 mm (16.4") above the guardrail base. Small car in the third simulation severely snagged into the system as it impacted the system with its bumper top 150 mm (5") below the lowest corrugation center of the Thrie-beam. Maximum occupant ride down accelerations

obtained from this simulation exceeded the report 350 specified 20g's threshold. Hence, the minimum acceptable bumper top height during an impact for the modified Thrie-beam guardrail was selected as 100 mm (4") below the rail lowest corrugation center and 315 mm (12.4") above the guardrail base.

Table 5.9 Underride limit analysis results for Midwest Guardrail System (MGS).

Vehicle Type	Rail lower corrugation center height	Impact point: Bumper top below rail lower corru-gation center by	Height of bumper top above G.L.	Acceptance Criteria: Occupant Risk Factors		Simulation result	Under-ride Limit
				OIV <12 m/s (40 ft/s)	RDA <20 g's		
820-kg Geo Metro	535 mm (21")	100 mm (4")	435 mm (17")	5.1 m/s (16.7 ft/s)	10.3 g's	Pass	410mm (16")
		125 mm (5")	410 mm (16")	6.5 m/s (21.3 ft/s)	14.2 g's	Pass	
		150 mm (6")	385 mm (15")	5.5 m/s (18 ft/s)	22.5 g's	Fail	

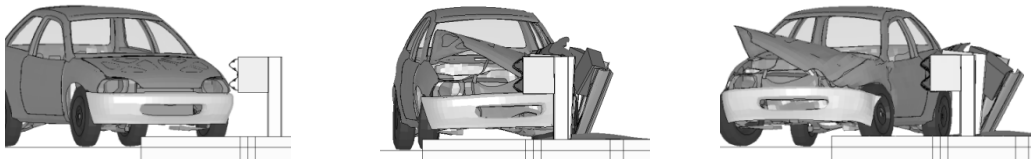

0s 0.20s 0.40s

(b) Bumper top 100 mm (4") below rail lower corrugation center; Bumper top height=435 mm (17")

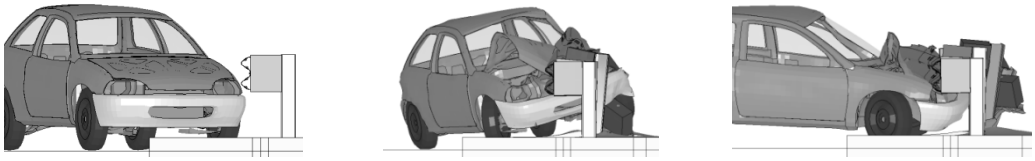

0s 0.30s 0.60s

(c) Bumper top 125 mm (5") below rail lower corrugation center; Bumper top height=410 mm (16")

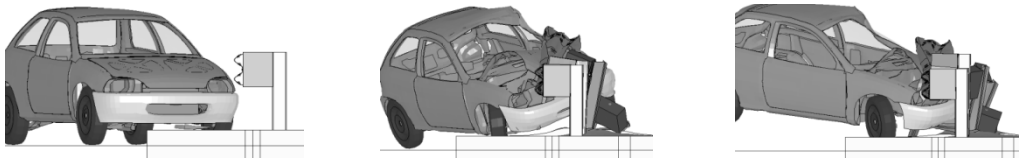

0s 0.35s 0.60s

(c) Bumper top 150 mm (6") below rail lower corrugation center; Bumper top height=385 mm (15")

Figure 5.10 Sequential photographs of underride limit analyses for Midwest Guardrail System.

Table 5.10 Underride limit analysis results for modified Thrie-beam guardrail system.

Vehicle Type	Rail lower corrugation center height	Impact point: Bumper top below rail lower corrugation center by	Height of bumper top above G.L.	Acceptance Criteria: Occupant Risk Factors		Simulation result	Under-ride Limit
				OIV < 12 m/s (40 ft/s)	RDA <20 g's		
820-kg Geo Metro	415 mm (16.4″)	50 mm (2")	365 mm (14.4")	7.3 m/s (24 ft/s)	9.0 g's	Pass	315 mm (12.4")
		100 mm (4")	315 mm (12.4")	5.2 m/s (17 ft/s)	9.4 g's	Pass	
		125 mm (5")	290 mm (11.4")	5.5 m/s (18 ft/s)	20.8 g's	Fail	

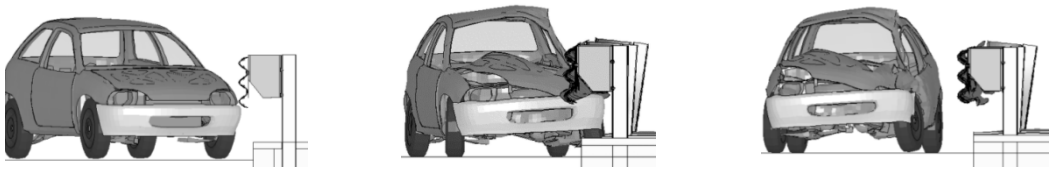

0s 0.20s 0.40s

(a) Bumper top 50 mm (2") below rail lower corrugation center; Bumper top height=365 mm (14.4")

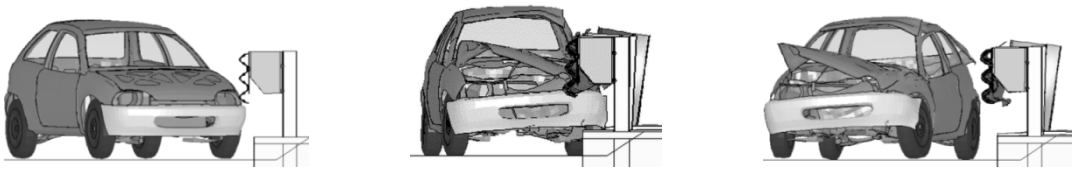

0s 0.18s 0.38s

(b) Bumper top 100 mm (4") below rail lower corrugation center; Bumper top height=315 mm (12.4")

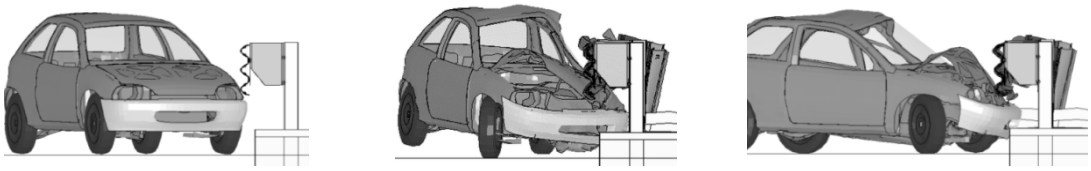

0s 0.35s 0.65s

(c) Bumper top 150 mm (5") below rail lower corrugation center; Bumper top height=290 mm (11.4")

Figure 5.11 Sequential photographs of underride limit analyses for modified Thrie-beam guardrail system.

Four impact simulations were performed to determine underride limit for modified weak post W-beam guardrail. In all four cases, the small car impacted the guardrail model 3.1 m (10.2 ft) upstream of post 8 at impact heights lower than its normal equilibrium position. The bumper heights at time of impact and the corresponding occupant risk factors are shown in Table 5.11. Figure 5.12 shows the sequential images obtained from the four simulations. In the first simulation, 820c model impacted the guardrail with its bumper top 100 mm (4") below the rail lower corrugation center. Guardrail successfully contained and redirected the vehicle at this impact height. As shown in Figure 5.12(b), the small car under-rode the W-beam rail as it impacted the guardrail model with its bumper top 200 mm (8") below the rail lower corrugation center. In the third simulation, vehicle was contained by the guardrail as its bumper top impacted the system 150 mm (6") below the rail lower corrugation center. However, although the occupant risk factors were within acceptable limits top of edge of the driver side windshield contacted the W-beam rail at 0.325 sec (see Figure 5.12(c)). Compression and drag forces created by the rail elements on windshield during this contact can potentially shutter the windshield causing severe occupant injury. The report 350 safety evaluation criteria do not permit any deformation of, or intrusion into, the occupant compartment that could cause serious occupant injury. The vehicle model used in this study does not have the capability to capture windshield damage and therefore it was uncertain whether the rail to windshield contact observed from 0.325 sec to 0.65 sec would cause occupant compartment intrusion. To remain on the safer side performance of the guardrail in the simulation was considered unacceptable. In the final simulation, small car impacted the guardrail with its bumper top at a height 137.5 mm (5.5") below the rail lower corrugation center and 421 mm (16.5") above the guardrail base. As shown in Figure 5.12(d), vehicle, during this simulation, was successfully contained and redirected by the guardrail. There was no contact between the windshield and W-beam rail. Occupant risk factors, as shown in Table 5.11, were within acceptable limits. Hence, bumper top height of 421 mm (16.5") during impact was selected as underride limit for modified weak post W-beam guardrail.

Table 5.11 Underride limit analysis results for modified weak post W-beam system.

Vehicle Type	Rail lower corrugation center height	Impact point: Bumper top below rail lower corrugation center by	Height of bumper top above G.L.	Acceptance Criteria: Occupant Risk Factors		Simulation result	Under-ride Limit
				OIV<12 m/s (40 ft/s)	RDA <20 g's		
820-kg Geo Metro	557 mm (22″)	100 mm (4")	457 mm (18")	4.3 m/s (14.1ft/s)	7.6 g's	Pass	421 mm (16.5")
		200 mm (8")	357 mm (14")	--	--	Underride	
		150 mm (6")	407 mm (16")	3.8 m/s (12.5 ft/s)	13.9 g's	Fail	
		137.5 mm (5.5")	421 mm (16.5")	4.0 m/s (13.1 ft/s)	12.9 g's	Pass	

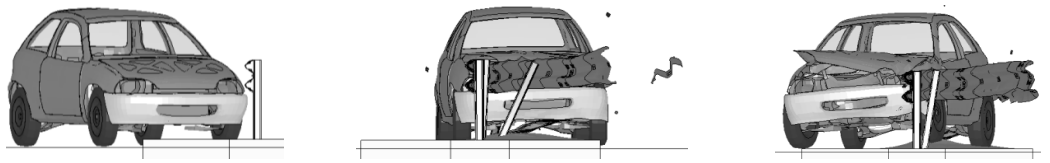

0s 0.325s 0.65s

(a) Bumper top 100 mm (4") below rail lower corrugation center; Bumper top height=457 mm (18")

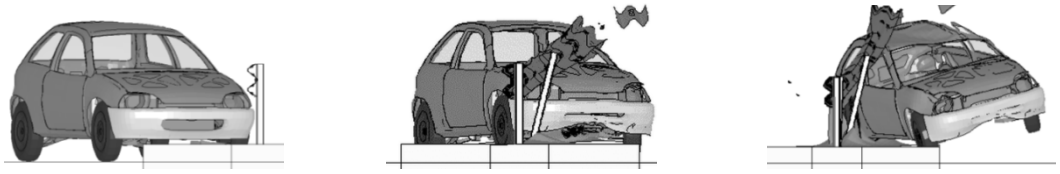

0s 0.20s 0.40s

(b) Bumper top 200 mm (8") below rail lower corrugation center; Bumper top height=357 mm (14")

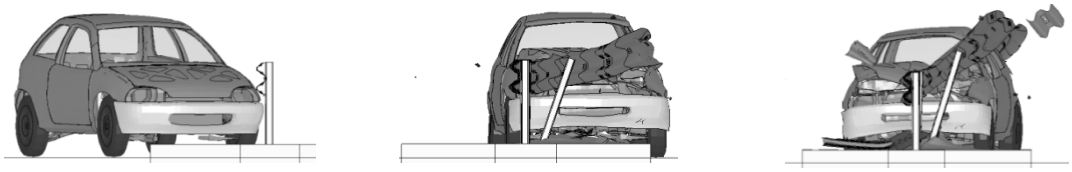

0s 0.325s 0.65s

(c) Bumper top 150 mm (6") below rail lower corrugation center; Bumper top height=407 mm (16")

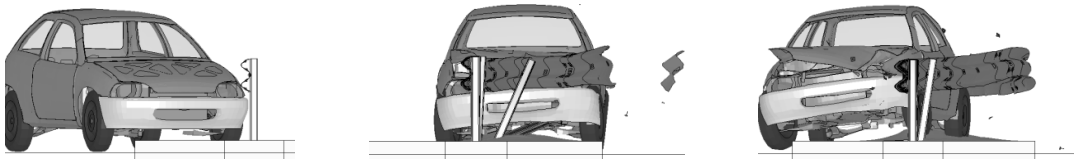

0s 0.325s 0.65s

(d) Bumper top 127.5 mm (5.5") below rail lower corrugation center; Bumper top height=421 mm (15.5")

Figure 5.12 Sequential photographs of underride limit analyses for modified weak post W-beam system.

Three LS-DYNA simulations were performed, where small car impacted the box-beam guardrail model 2.5 m (8.2 ft) upstream of post 17 at a speed and angle of 100 km/h (62 mph) and 20 degrees, respectively. The bumper heights at time of impact and the corresponding occupant risk factors are shown in Table 5.12. Figure 5.13 shows the sequential images obtained from these simulations. In the first simulation, vehicle was successfully contained and redirected as it impacted the system with its bumper top 100 mm (4") below the rail base. The vehicle, however, severely snagged the guardrail model as it impacted the system with its bumper top 200 mm (8") below the rail base. The maximum occupant ride down acceleration obtained from this simulation exceeded the report 350 specified 20g's threshold. In the final simulation, small car impacted the box-beam guardrail with its bumper top at a height 150 mm (6") below the rail base and 384 mm (15") above the guardrail base. As shown in and Figure 5.12(c), the guardrail during this simulation successfully passed the safety evaluation criteria set forth in report 350. Hence, bumper top height of 384 mm (15") during impact was selected as underride limit for box-beam system.

Table 5.12 Underride limit analysis results for box-beam guardrail system.

Vehicle Type	Box-beam Rail base height	Impact point: Bumper top below box-beam rail base by	Height of bumper top above G.L.	Acceptance Criteria: Occupant Risk Factors		Simulation result	Under-ride Limit
				OIV < 12 m/s (40 ft/s)	RDA <20 g's		
20-kg Geo Metro	534 mm (21″)	100 mm (4")	436 mm (17″)	3.9 m/s (13 ft/s)	7.9 g's	Pass	384 mm (15″)
		200 mm (8")	336 mm (13″)	9.8 m/s (32 ft/s)	25.5 g's	Fail	
		150 mm (6")	384 mm (15″)	6.1 m/s (20 ft/s)	16.1 g's	Pass	

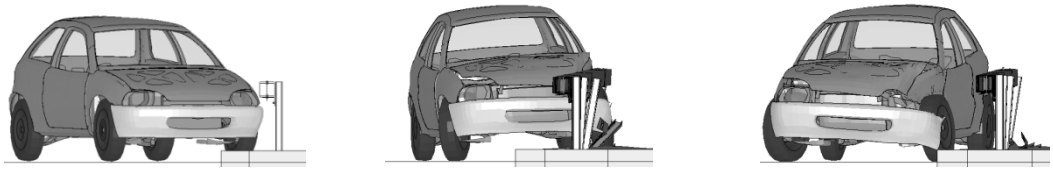

0s 0.18s 0.34s

(a) Bumper top 100 mm (4") below the rail base; Bumper top height=436 mm (17")

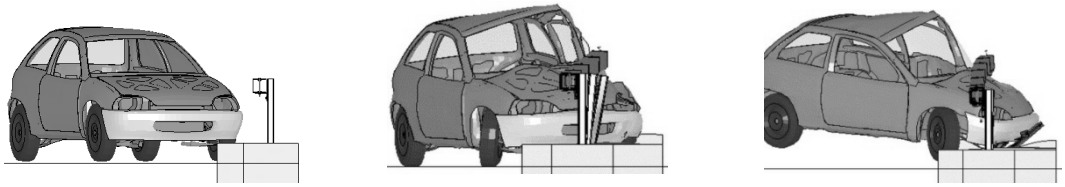

0s 0.s 0.3s

(b) Bumper top 200 mm (8") below the rail base; Bumper top height=336 mm (13")

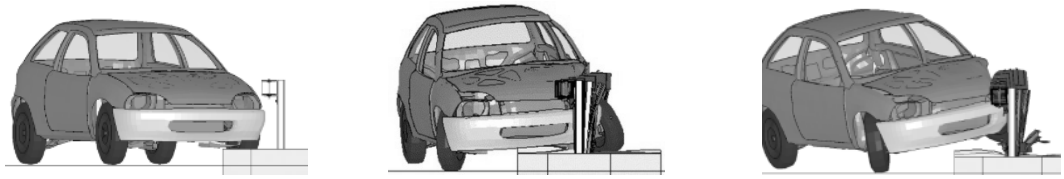

0s 0.23s 0.45s

(c) Bumper top 150 mm (6") below the rail base; Bumper top height=384 mm (15")

Figure 5.13 Sequential photographs of underride limit analyses for box-beam guardrail system.

5.6. RESULTS AND DISCUSSIONS

For the barriers placed on sloped terrain, vehicle impact heights vary based on vehicle trajectories along the slope and barrier offset locations. Hence, performance limits of each barrier in terms of acceptable vehicle impact heights were established using the simulations performed on flat terrains. Limits obtained from these simulations are summarized in Table 5.13 and Figure 5.14. As can be seen from the table and figure, modified Thrie-beam guardrail system has the highest performance limit band making it most suitable for the placements on sloped terrain. Modified G4(1S) W-beam, on the other hand, can be judged ineffective for the placements on wide ranges of sloped

terrain. Due to the higher rail mounting heights, the modified thrie beam and midwest guardrail systems have higher override limits compared to the modified G4(1S) guardrails. Due to the presence of narrower blockouts, modified G4(1S) W-beam guardrail is more susceptible to the vehicle to post snagging during the impacts with passenger car. Although the system has relatively high rail mounting height, absence of blockout makes modified weak post W-beam guardrail system less effective for an airborne pickup. Similarly, the high rail mounting height and readily detachable post-rail connections allow the small passenger car underride the weak post W-beam system with minimum effort. The relatively low rail mounting height and substantial flexural and tensile strength of the tubular rail make the box-beam system more effective in containing the small car with compressed suspension.

Table 5.13 Performance limits obtained for different guardrail systems.

Guardrail Type	Rail Top Height	Override Limit		Under-ride Limit		Performance limit band
		Impact point description	Bumper top above GL	Impact point description	Bumper top above GL	
Modified G4(1S) W-beam	710 mm (27.9″)	1/3rd of the bumper above rail upper corrugation center	726 mm (28.6″)	Bumper top 50 mm (2″) below rail lower corrugation center	403mm (15.86″)	323 mm (12.7″)
Midwest Guardrail System	787 mm (31″)	5/12th of the bumper above rail upper corrugation center	818 mm (32.2″)	Bumper top 125 mm (5″) below rail lower corrugation center	410 mm (16″)	408 mm (16″)
Modified Thrie-beam	866 mm (34″)	1/10th of the bumper above rail upper corrugation center	830 mm (32.7″)	Bumper top 100mm (4″) below rail lower corrugation center	315mm (12.38″)	515 mm (20.3″)
Modified Weak-post W-beam	816 mm (32″)	Top of the bumper at rail upper corrugation center	757 mm (29.8″)	Bumper top 137.5mm (5.5″) below rail lower corrugation center	421mm (16.5″)	336 mm (13.2″)
Box Beam Guardrail	686 mm (27″)	3/8th of the bumper above rail top	764 mm (30″)	Bumper top 150 mm (6″) below rail base	384 mm (15″)	380 mm (15″)

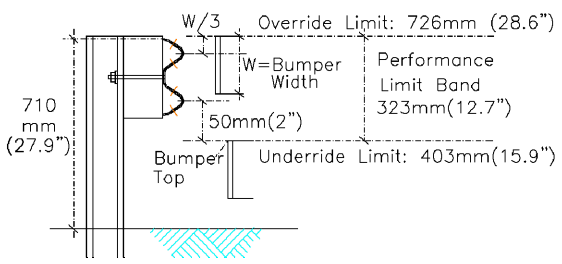

(a) Modified G4(1S) W-beam Guardrail

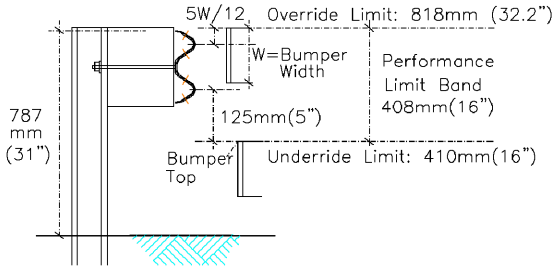

(b) Midwest Guardrail System (MGS)

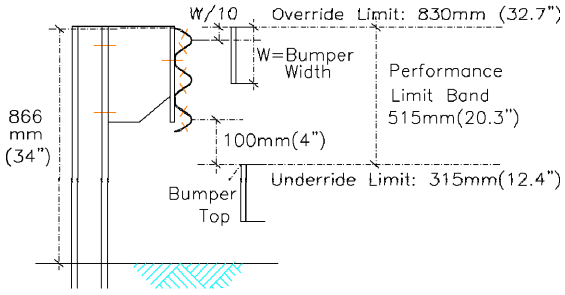

(c) Modified Thrie-beam Guardrail

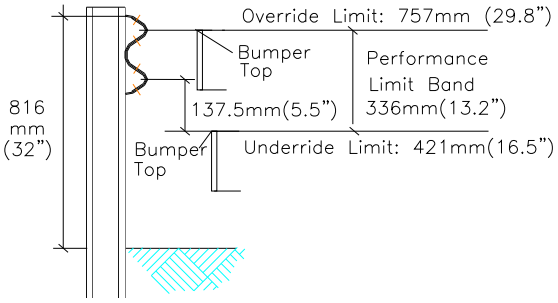

(d) Modified weak post W-beam Guardrail

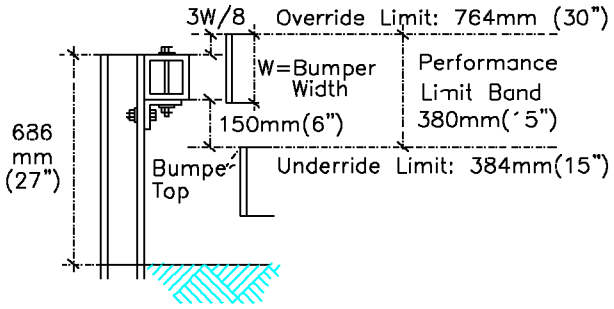

(e) Box-beam Guardrail System

Figure 5.14 Performance limits for the guardrails obtained using numerical simulations.

Table 5.14 compares the performance limits of modified G4(1S) W-beam, modified Thrie-beam, and Box-beam guardrail systems obtained using LS-DYNA simulations with those calculated using Ross and Sicking(*1*) assumptions. It can be seen that for all three guardrails, override limits calculated using previous assumptions are higher compared to those obtained using numerical analyses. Similarly, underride limit

of box-beam guardrail calculated using previous assumptions are smaller compared to that obtained using numerical analyses. These differences indicate that some of the vehicle impact heights allowed in previous assumptions may produce unacceptable barrier behavior. It can also be seen that underride limits of modified G4(1S) W-beam and modified Thrie-beam guardrail systems obtained using numerical analyses are smaller compared to those calculated using Ross and Sicking(*1*) assumptions. Thus the Ross and Sikcing(*1*) suggested criteria allow a very conservative underride limit for these two systems. Hence, to determine acceptable lateral offset locations for guardrails on roadside and median slopes, performance limits obtained using numerical simulations and as shown in Figure 5.14 should be used in future studies.

Table 5.14 Comparisons of performance limits obtained using numerical analysis with those obtained using Ross and Sicking (*1*) suggestions.

Guardrail Type	Override limit		Underride limit		Performance Limit Band	
	This Study	Ross and Sicking (*1*)	This Study	Ross and Sicking (*1*)	This Study	Ross and Sicking (*1*)
Modified G4(1S) W-beam	726 mm (28.6″)	758 mm (29.8″)	403mm (15.86″)	564 mm (22.2″)	323 mm (12.7″)	194 mm (7.64″)
Modified Thrie-beam	830 mm (32.7″)	914 mm (35″)	315mm (12.38″)	526 mm (20.7″)	515 mm (20.3″)	388 mm (15.3″)
Box Beam Guardrail	764 mm (30″)	793 mm (31.2″)	384 mm (15″)	374 mm (14.7″)	380 mm (15″)	419 mm (16.5″)

5.7. CONCLUSIONS

Several LS-DYNA simulations were performed in this study to determine performance limits in terms of acceptable vehicle impact heights for five guardrail systems. Impact simulations were performed using NCAC developed FE models for 2000P truck and 820c small car, and FE guardrail models developed and validated for this study as discussed in the Section 4. The procedures and impact parameters used for these simulations are discussed in this section. Results obtained from these simulations, and performance limits selected for each guardrail systems are also presented and discussed.

6. VEHICLE TRAJECTORY ANALYSES

6.1. INTRODUCTION

Vehicle dynamic simulations were performed in this study to evaluate trajectory of a vehicle as it traversed a median ditch at a prescribed speed and angle. A commercially available multi-rigid body dynamic analysis package from Mechanical Simulation Corporation (MSC) called CARSIM(*35*) was used for the analyses. CARSIM has about 30 pre-built vehicle models in different vehicle classes. The list of these pre-built vehicles includes a small passenger car and pickup truck model that were modified to represent *NCHRP Report 350* design test vehicles. CARSIM can be easily interfaced with MATLAB and SIMULINK code and has features to easily customize different vehicle and road geometry parameters. This section presents the methodology and parameters used to determine trajectories of two design vehicles traversing various ditch configurations using CARSIM.

6.2. SIMULATION MATRIX FOR VEHICLE TRAJECTORY ANALYSES

6.2.1. Vehicle Class

NCHRP Report 350 design vehicles were selected for the trajectory analysis. Vehicles that comply with the *NCHRP Report 350* specifications are an 820-kg Geo Metro and a 2000-kg, Chevrolet C2500 pickup truck. Appropriate mass, moments of inertia, suspension spring and damper properties, and other basic geometric properties were assigned to the existing generic vehicle models in CARSIM to match those of the actual design vehicles.

6.2.2. Roadside and Median Configurations

The simulations consisted of two design vehicles encroaching into different configurations of a depressed median at different speed and angle combinations. The depressed median was assumed to have a symmetric cross section with equal foreslope and backslope ratios. The median width is defined as the distance between the traveled-way edges, which includes shoulders. The depth of the ditch was dictated by the median width, shoulder width, and ditch cross slope.

For the case of a vehicle encroaching onto the roadside, simulations were performed for selected positive (cut) cross-slopes. The scenario in which the cross-slope is negative (fill) is a subset of the case when the vehicle encroaches into a depressed median. Thus no additional simulations were needed for the roadside case beyond this scenario.

6.2.3. Encroachment Angle and Vehicle Speed

Encroachment angles of 15 degrees and 25 degrees were used along with encroachment speeds of 100 km/h (62 mph) and 80 km/h (50 mph). The critical encroachment condition for vehicle override was the combination of the highest speed (i.e., 100 km/h) and the highest angle (i.e., 25 degrees).

The simulation matrix for the vehicle trajectory analyses is shown in Table 6.1. Based on the number of parameters selected, a simple permutation calculation shows that a total of 112 simulations were performed to complete the analysis.

6.3. METHODOLOGY USED FOR VEHICLE TRAJECTORY ANALYSES

The methodology used to obtain the vehicle bumper profiles along a ditch cross section included the following four steps:

Table 6.1 Simulation matrix for vehicle trajectory analysis.

Vehicle Types	
NCHRP Report 350 design vehicles	820-kg (1806 lb) Geo Metro 2000-kg (4406 lb), Chevrolet C2500
Roadside and Median Configurations	
Median Cases	
Shoulder Width (SW)	1.22 m (4 ft) and 1.83 m (6 ft)
Median Width (MW)	12.2 m (40ft); 18.3 m (60 ft); 23.2 m (76 ft)
Ditch Width (DW= MW-2×SW)	8.5 m (28 ft); 9.8 m (32 ft); 14.6 m (48 ft); 15.9 m (52 ft); 19.5 m (64 ft); 20.7 m (68 ft).
Cross-slope	6:1 and 8:1
Shape	V
Roadside Cases	
Shoulder width	1.22 m (4 ft)
Cross-slope	6:1 and 8:1
Shape	positive slope (cut)
Encroachment Conditions	
Angles	15°and 25°
Speeds	100 km/h (62 mph) and 80 km/h (50 mph)

- Define ditch profile
- Vehicle model selections and parameter modifications
- Run the CARSIM simulation
- Analyze CARSIM output to obtain bumper trajectory

An external code in MATLAB was developed to facilitate execution of these four steps. The code can iteratively modify the ditch profile, incorporate CARSIM into the SIMULINK, and analyze the CARSIM output for a given encroachment simulation. Each of these steps is explained in the following sections.

6.3.1. Define Ditch Profile

In CARSIM, a roadway profile can be customized to define a desired roadside or median geometry. The following three features were used to define a roadway profile:

(a) X-Y Coordinates of Centerline: This screen is used to define the horizontal geometry of the road, as shown in Figure 6.1, using a table of X-Y coordinates. Station

(S), defined as a function of X and Y by connecting the points with straight lines, is calculated automatically. The axis L is perpendicular to the longitudinal axis S. The S-L coordinate defines the centerline for the roadway.

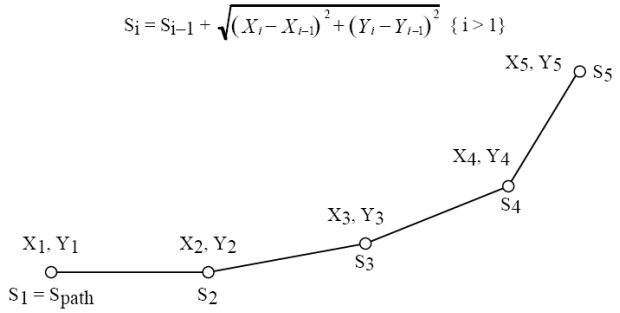

Figure 6.1 X-Y coordinates and station (S-L coordinates) of road centerline(*36*).

(b) Off-Center Elevation Map: "This screen is used to specify the off-center elevation changes as a function of S-L coordinates for roads whose widths vary or have elevation changes that run neither parallel nor perpendicular to the design line of the road"(*36*).

(c) Friction: "This screen is used to specify the tire/road friction as a function of S-L coordinates for roads that have frictional changes that run neither parallel nor perpendicular to the design line of the road"(*36*).

External Parsfiles, an example of which is shown in Figure 6.2(b), can be used to define the X-Y centerline geometry (top view), off-center elevation (vertical profile of the road), and friction. The vehicle was initialized to travel along the global X direction. To account for different encroachment angles, the ditch profiles were rotated about the Z axis as shown in Figure 6.3. The friction between the tires and the ground surface was also defined at this stage. The pavement was assumed to be dry asphalt, and thus received a friction value of 0.85, and the grass inside ditch received a value of 0.3. A MATLAB subroutine was created to write three external parsfiles based on the three input parameters: encroachment/approach angle, ditch width, and slope. These parsfiles were than input into the CARSIM to run the simulation.

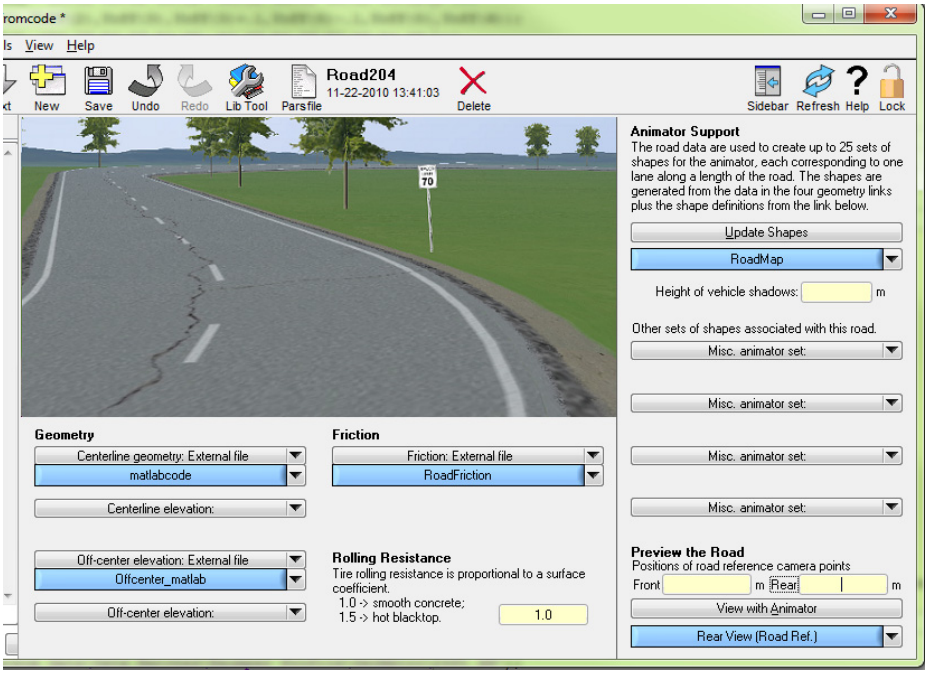

(a)

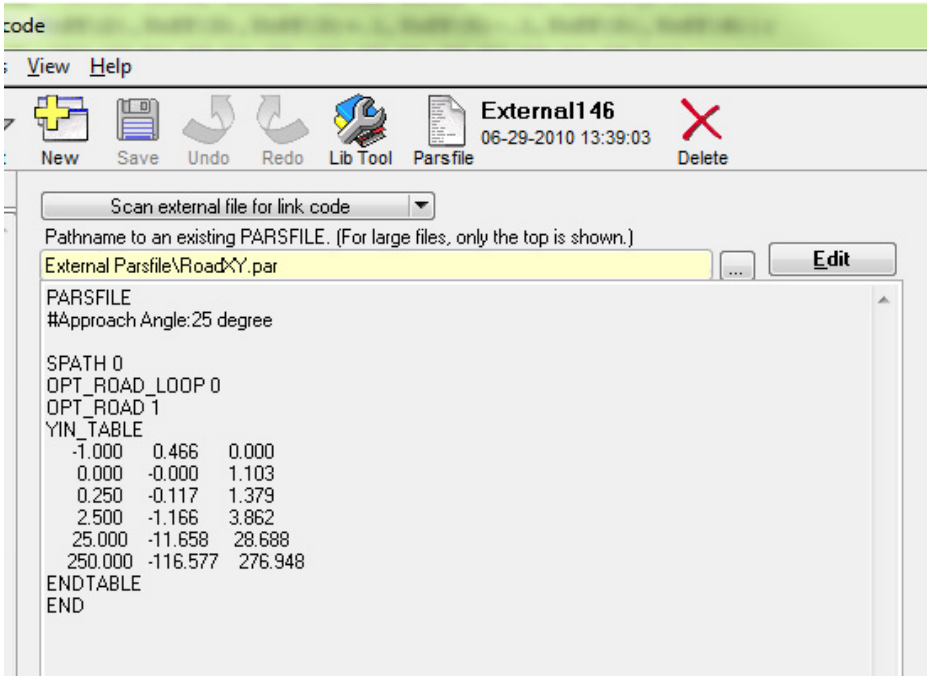

(b)

Figure 6.2 (a) Road Geometry and (b) External Parsfile screens used in CARSIM.

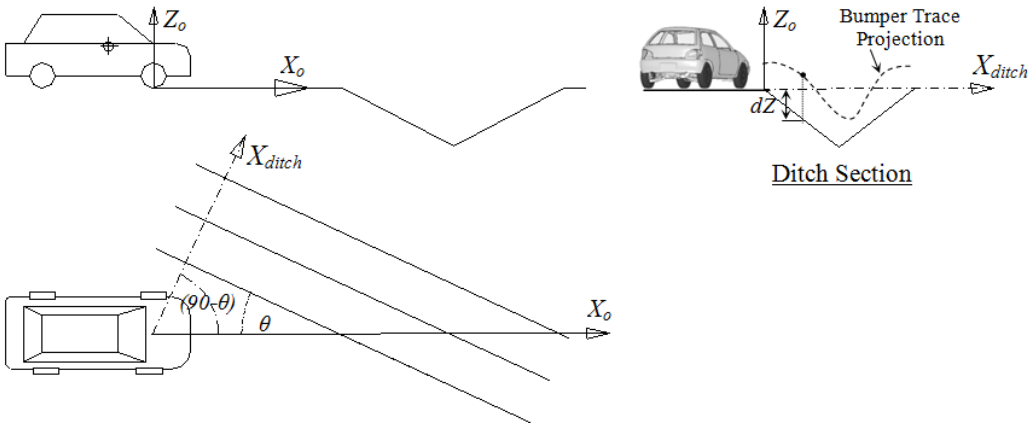

Figure 6.3 Rotating the ditch profile to account for different vehicle approach angles.

6.3.2. Vehicle Selection and Parameter Modification

The Vehicle Assembly screen for a typical vehicle model is shown in Figure 6.4. CARSIM allows nearly every parameter of the vehicle, from its geometric configuration to its inertial properties, to be user-defined. The pre-built A-Class hatchback and Full-size Pickup models available in the CARSIM vehicle library were modified to represent the 820C and 2000P design test vehicles of *NCHRP Report 350*, respectively. A description of some of the modifications made on these two pre-built CARSIM vehicle models is presented below.

6.3.2.1. Rigid Sprung Mass

Key geometric dimensions and inertia properties of the 820C and 2000P test vehicles are shown in Figure 6.5 and Figure 6.6, respectively. The geometric dimensions were selected based on actual measurements of test vehicles at the TTI Proving Ground. The vehicle measurement sheets for Chevrolet C2500 and Geo Metro vehicles are presented in Appendix B. The inertia properties for the sprung mass were obtained from the

National Highway Traffic Safety Administration's (NHTSA) database for measured vehicle inertia parameters(*47*).

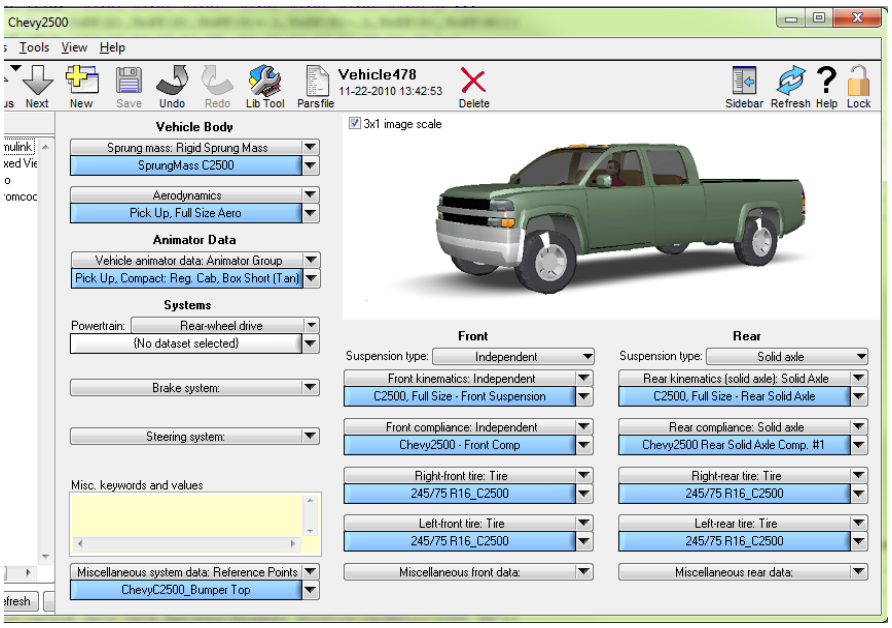

Figure 6.4 Vehicle properties window in CARSIM.

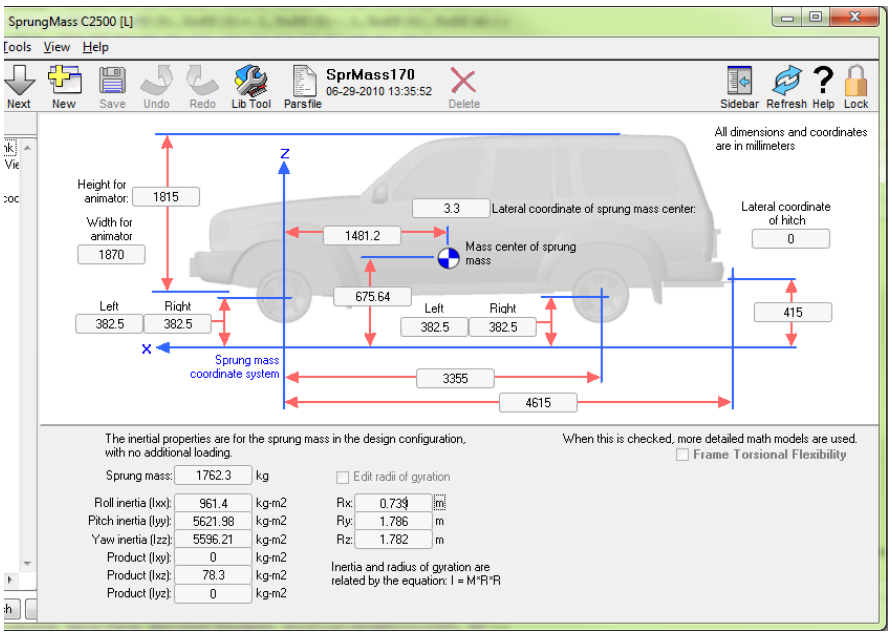

Figure 6.5 Sprung mass screen used for Chevy2500 vehicle.

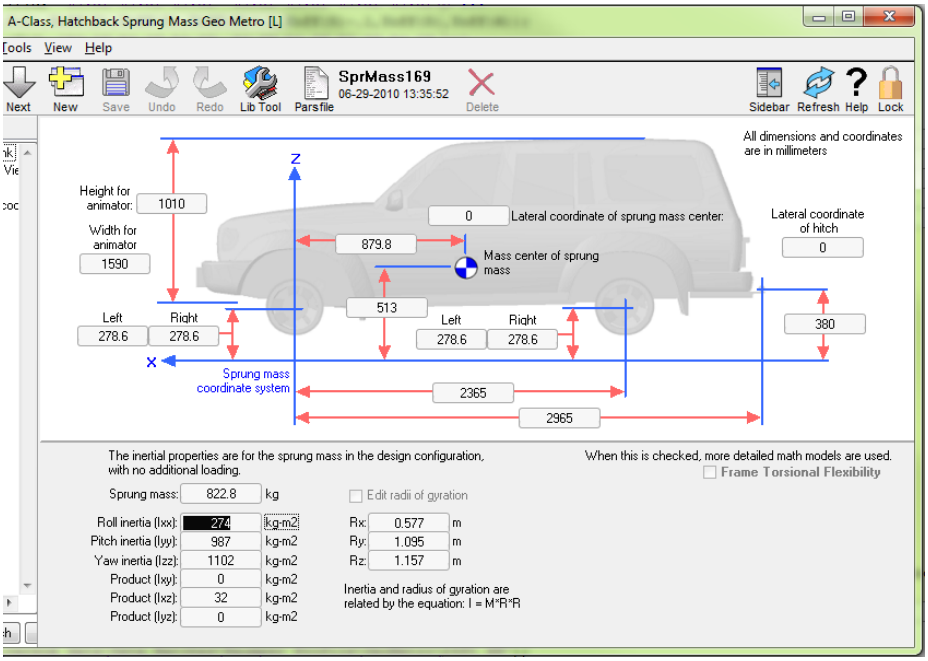

Figure 6.6 Sprung mass screen used for Geo Metro 820c vehicle.

6.3.2.2. Suspension Testing and Modeling

Since the focus of the simulation analysis is the trajectory of a vehicle through a median ditch, it is critical to incorporate accurate suspension properties in the vehicle models. Depending on the slope configuration of the median, the vehicle may become airborne upon entering the ditch, thus causing its suspension to extend (i.e. rebound). The vehicle will subsequently re-contact the ground resulting in a sudden compression (i.e. jounce) of the suspension springs and dampers. While the overall suspension response is affected by the properties of several suspension components such as bushings, tie-rods, stabilizer bars, suspension to body attachments, etc., the most critical components are the suspension springs and dampers(*39*). Table 6.2 shows the suspension types used in the selected vehicle models. CARSIM models have default values for the spring and damper properties. However, these properties generally do not completely capture the loading range or rates typical of off-road encroachments. To obtain more accurate suspension

response, coil-springs and dampers from actual test vehicles were sent to a third-party test lab (*48*) to obtain the desired properties.

Table 6.2 Suspension types used in selected vehicle models.

Geo Metro	
Front Suspension:	MacPherson strut with coil-spring
Rear Suspension:	MacPherson strut with coil-spring
Chevy C2500	
Front Suspension:	Wishbone front suspension with stabilizer bar and coil springs
Rear Suspension:	Leaf-springs and stabilizer bar

Determining the coil spring properties is rather straightforward. The spring is fixed at one end of a compression machine while the other end compresses the spring. The force and deflection of the spring are measured as the spring is compressed. The force-displacement data is collected up to a displacement associated with the maximum suspension travel possible for each vehicle design.

Due to the weight of the sprung mass, compression force on the spring at normal equilibrium position (i.e. at zero displacement) is nonzero. In a typical Wishbone front suspension used in Chevy C2500, the coil spring is located at the middle of the lower A-arm as shown in Figure 6.7(a). Using the free body diagram of the wheel assembly shown in Figure 6.7(a), the weight on the spring at zero displacement can be approximated as two times the total weight on the adjacent tire (W_T). For the Macpherson strut suspension used in Geo Metro, on the other hand, lower end of the coil spring is located by the linkage between the tire and steering as shown in Figure 6.7(b). Hence, at normal equilibrium position the spring for a Geo Metro suspension transfers a weight approximately equal to the total weight on the adjacent tire (W_T). The average weight on a single front tire for a 2000-kg C2500 pickup was measured to be 5.45 kN (1225 lb). The average weight measured on a single front and rear tire for an 820 kg Geo Metro were 2.45 kN (550.8 lb) and 1.45 kN (325.9 lb), respectively.

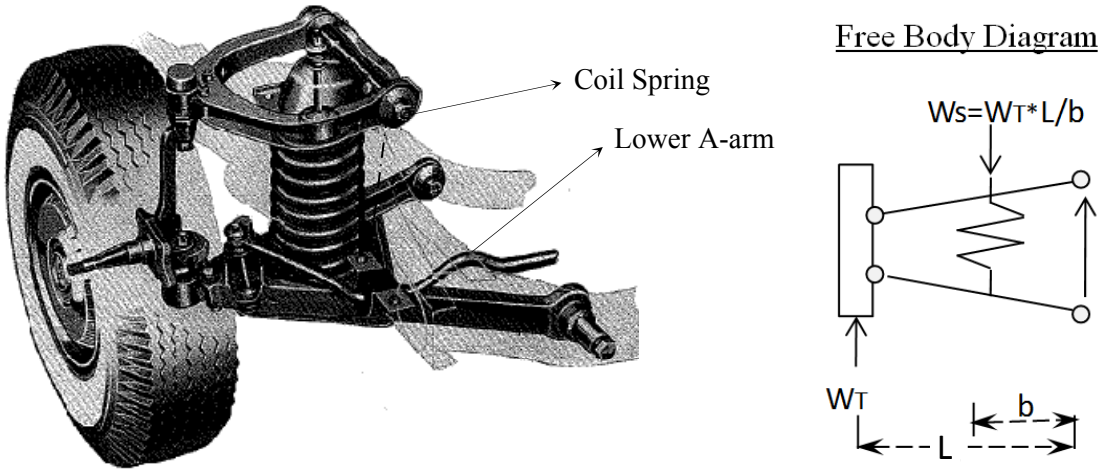

(a)

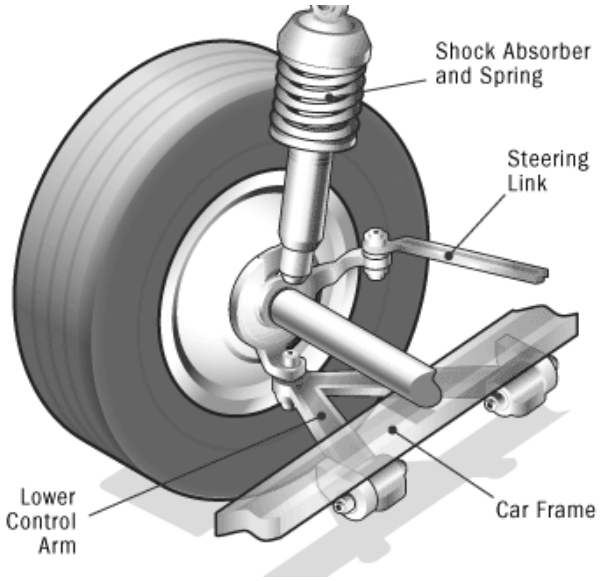

(b)

Figure 6.7 Coil spring location on wheal assembly for (a) Wishbone front suspension(*39*) (b) MacPherson strut suspension(*49*).

The test results for the coil springs used in Chevrolet C2500 and Geo Metro suspensions, obtained from RE Suspension Inc.(*48*), are shown in Figure 6.8 and Figure

6.9, respectively. These results include the jounce (compression) part of the force-displacement curve. The rebound (tension) part can be obtained from the mirror image of the jounce response. In the C2500 pickup and Geo Metro suspension assemblies, the coil springs have approximately 100 mm (4") and 50 mm (2") clearances, respectively, to the rebound or jounce limits of travel. Beyond those limits, infinite stiffness properties were assigned. As shown in Figure 6.10 and Figure 6.11, the force-compression properties for the coil springs prepared from test data closely match the default spring properties used in the CARSIM vehicle models. The spring properties obtained from the tests were used in the final vehicle models.

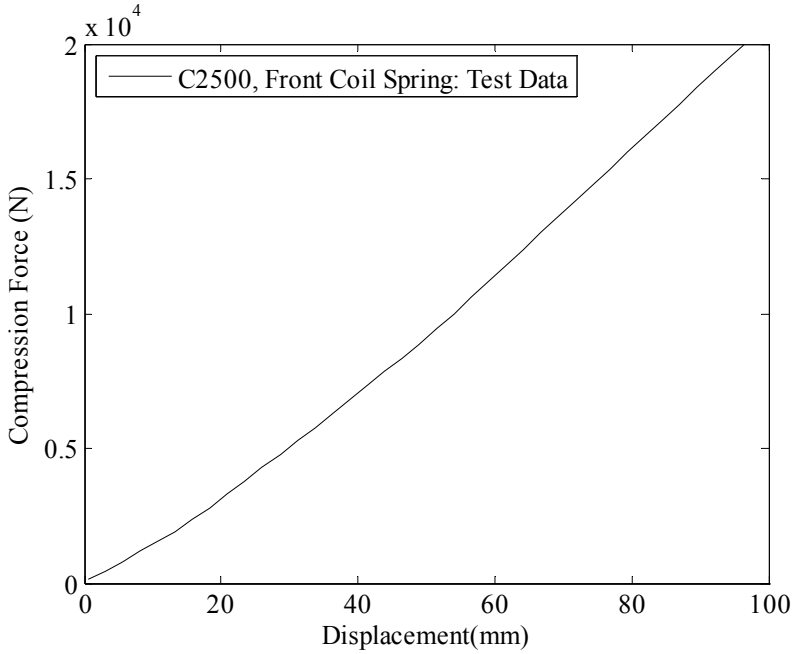

Figure 6.8 Test results for the coil spring used in the front suspension of C2500 Pickup.

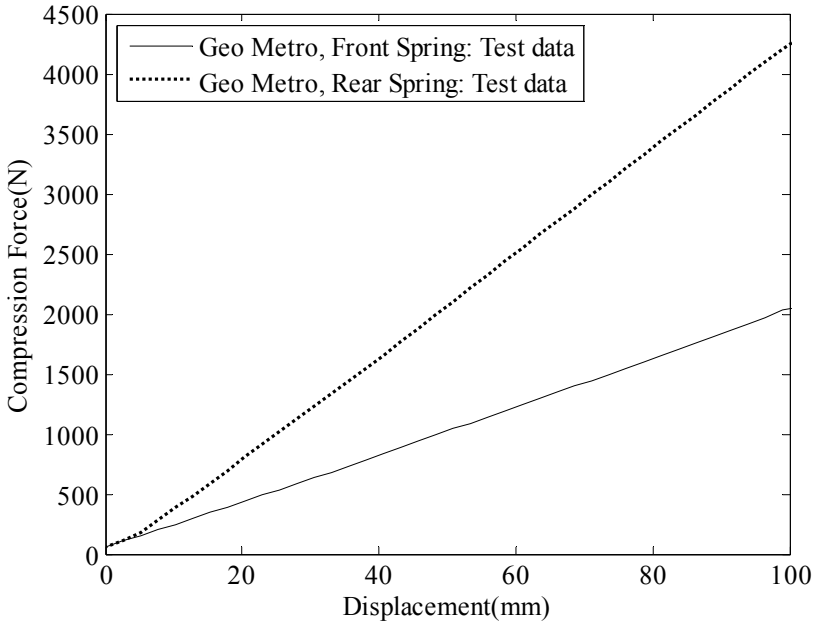

Figure 6.9 Test results for the coil springs used in front and rear suspensions of Geo Metro.

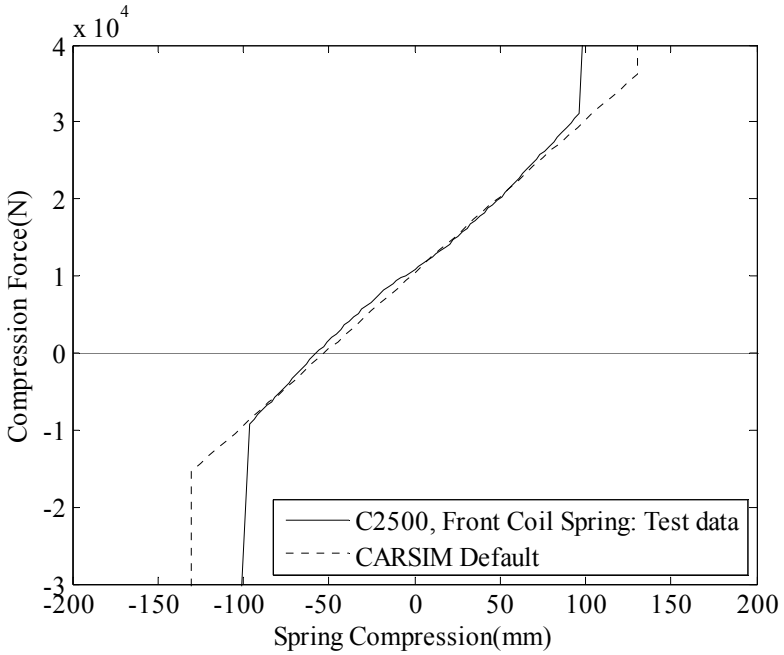

Figure 6.10 Chevrolet C2500 coil spring properties.

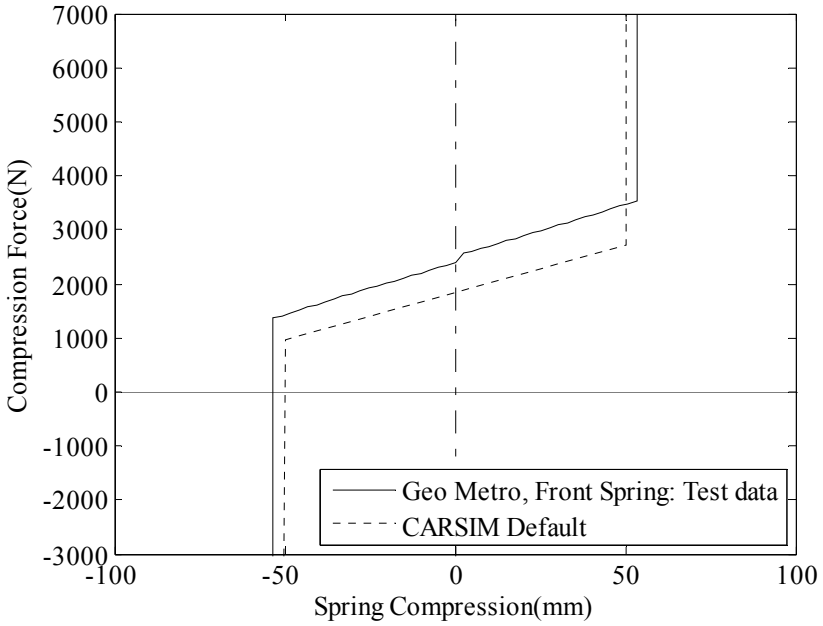

(a)

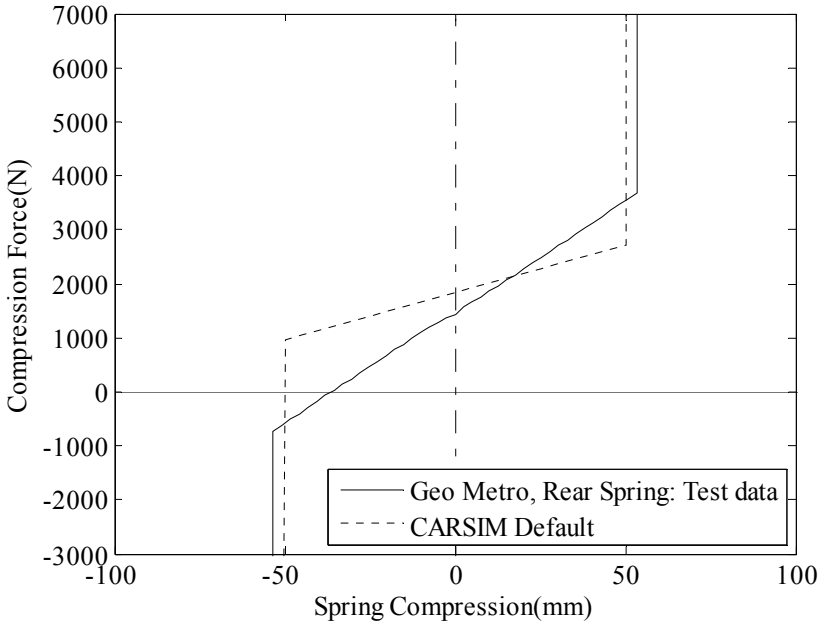

(b)

Figure 6.11 Geo Metro (a) Front and (b) Rear coil spring properties.

Measurement of damper properties is achieved through use of a dynamometer. As shown in Figure 6.12, the damper is fixed at its ends in an electro-magnetic dynamometer. One end of the dynamometer applies a variable sinusoidal velocity to compress and extend the damper at variable speeds for a specified damper stroke. The resistance force of the damper is measured by the dynamometer to obtain the desired force-velocity response. The force-velocity response curves for C2500 pickup and Geo Metro dampers, obtained from the third party test lab, are shown in Figure 6.13 and Figure 6.14, respectively. As shown in these figures, the response obtained from the test slightly differs from the default data built into CARSIM.

Figure 6.12 Setup for testing damper on a dynamometer(*48*).

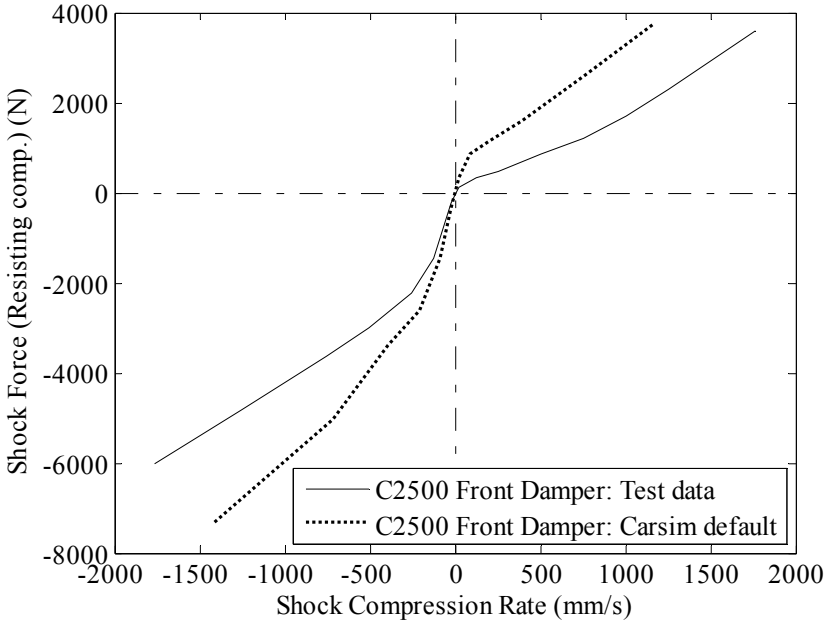

(a)

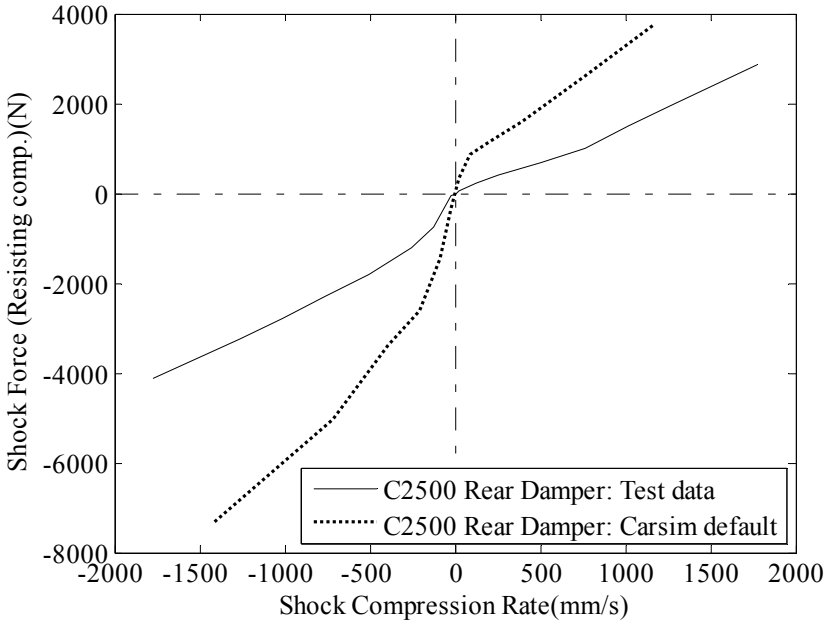

(b)

Figure 6.13 Force-velocity response curves from test and CARSIM default for Chevrolet C2500 (a) Front damper, and (b) Rear damper.

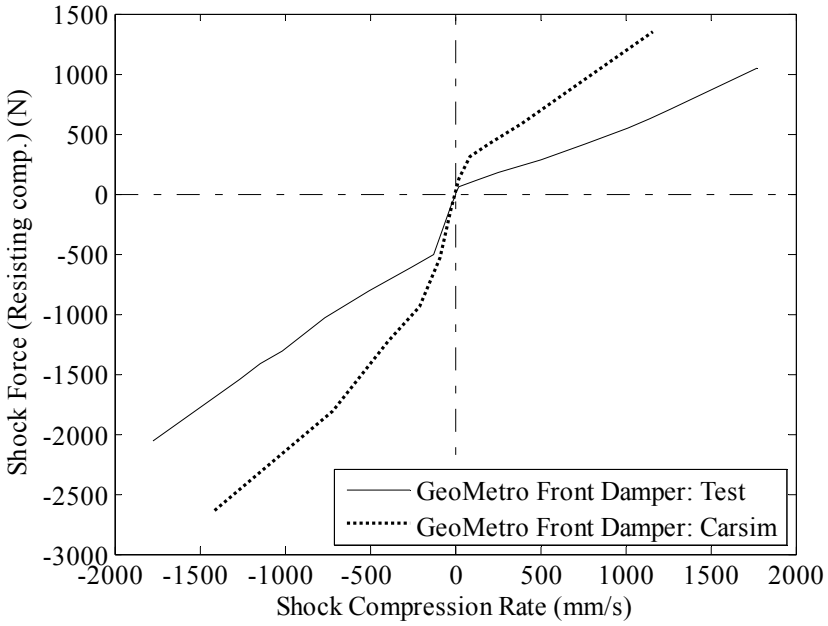

(a)

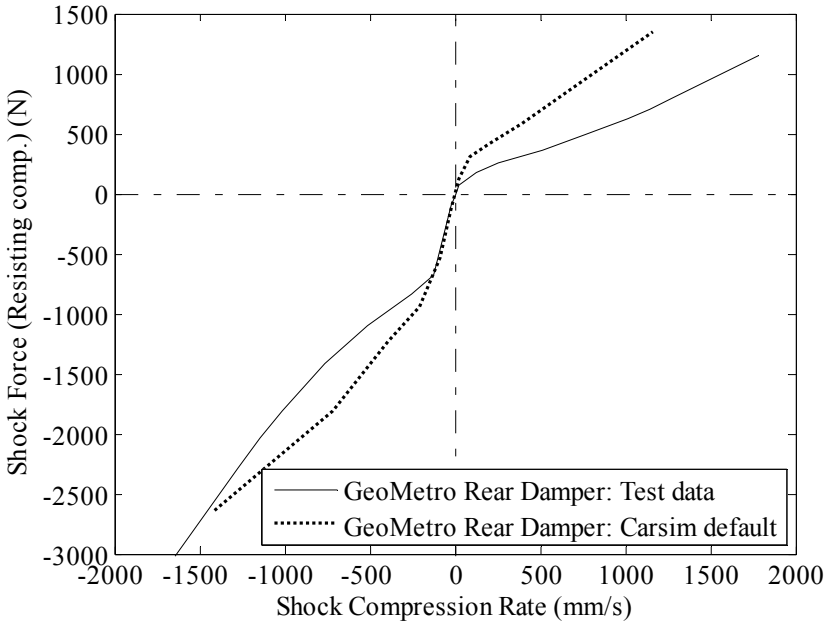

(b)

Figure 6.14 Force-velocity response curves from test and CARSIM default for Geo Metro (a) Front damper, and (b) Rear damper.

Figure 6.15(a) shows the bumper trajectory obtained from two CARSIM simulations of the modified Chevrolet C2500 pickup model traveling across a 9.75 m (32 ft) wide ditch with 6:1 slopes at an encroachment angle and speed of 25 degrees and 100 km/h (62 mph), respectively. The two curves indicate that the vehicle trajectories obtained using default values of suspension properties and the properties obtained from the lab test are almost identical.

Figure 6.15(b) compares the CARSIM trajectories obtained using test and default suspension properties for a Geo Metro car traveling across a 7.3 m (24 ft) wide ditch with 6:1 slopes at an encroachment angle and speed of 25 degrees and 100 km/h (62 mph), respectively. Also included for comparison are results reported by the National Crash Analysis Center (NCAC) for a similar simulation conducted using the Human Vehicle Environment (HVE) simulation code (*50*). In this case, the trajectory obtained using the default suspension properties deviated from those obtained using the test suspension data as the vehicle contacted the back slope. There was close agreement between the CARSIM simulation conducted using test suspension data and the HVE simulation conducted by NCAC.

6.3.2.3. Tire Model

Several tire models are available in CARSIM for the calculation of tire forces and moments. All these models are designed to produce the tire vertical force, shear forces at ground, and moments associated with the tire carcass (i.e., the tire body beneath the tread and sidewalls) deflection (*36*). The typical tire screen with the basic tire model selected for use in this project is shown in Figure 6.16. LT245/75R16 and L155/80R13 tires are typically used in the Chevrolet C2500 pickup and Geo Metro passenger car, respectively. These tire designations can be decoded as follows: 245 and 155 are the tire widths (mm), 75 and 80 are the sidewall height/width ratio (%), R is for a radial tire, and 16 and 13 are diameters (inches) of the rim. Hence, the unloaded radiuses for the two tires are 387 mm (15.2 in.) and 282 mm (11.1 in.), respectively.

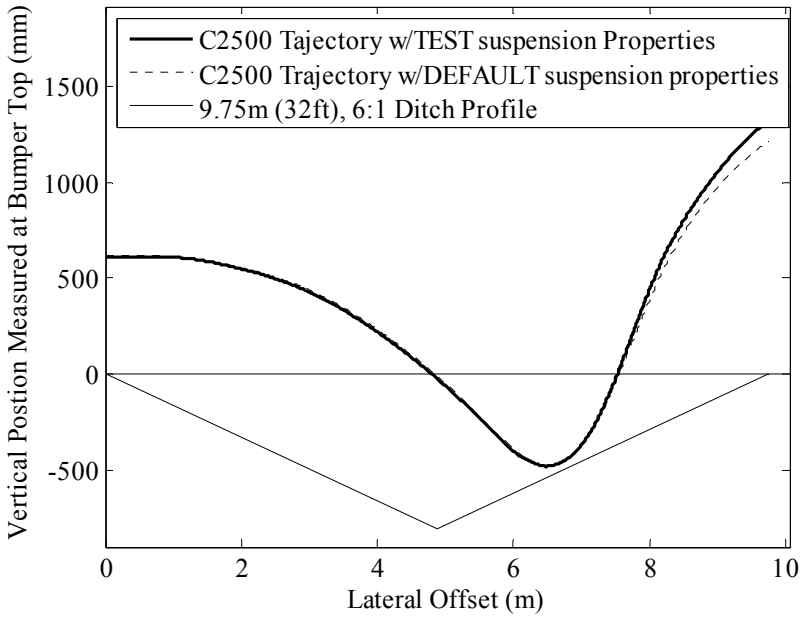

(a)

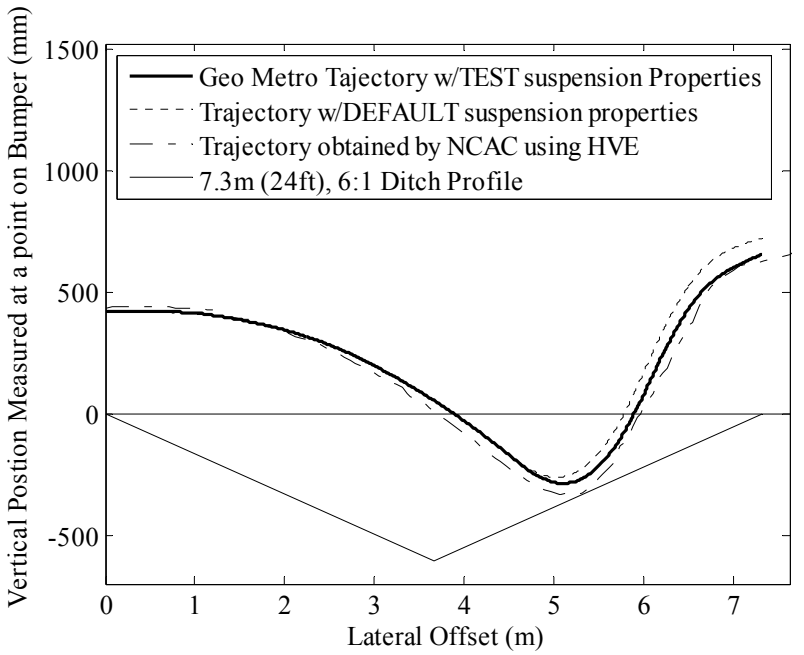

(b)

Figure 6.15 Effect of changes in suspension properties on bumper trajectory for (a) C2500 and (b) Geo Metro.

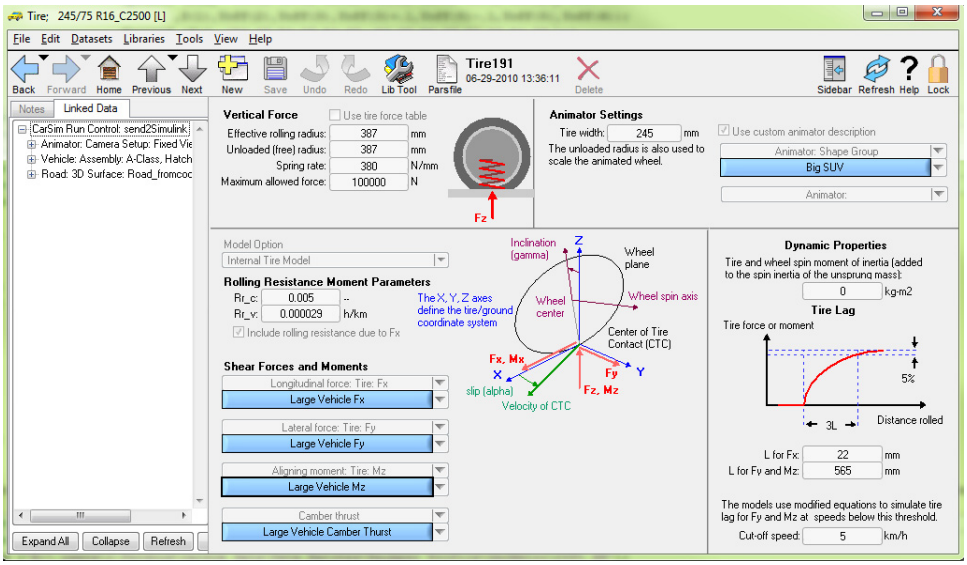

Figure 6.16 Tire screen with the basic tire model selected in CARSIM.

To calculate the vertical force on a tire, the tire is modeled as a spring with a constant vertical stiffness. The tire spring rate can be determined from a single sided compression test on the tire. The slope of the force-displacement curve obtained from this test is the tire spring rate. Vertical stiffness of the tire depends on the pressure inside the tire. Reid et. al. (*51*) conducted a single-sided compression test on the LT245/75R16 tire inflated at 0.48 MPa (70 psi) and obtained a tire spring rate of 430 N/mm (2.46 k/in). The same tire inflated at 0.24 MPa (35 psi) was tested by Orengo et. al. (*52*). The tire spring rate they obtained was 250 N/mm (1.43 k/in). In TTI crash tests, the LT245/75R16 tires used on the Chevrolet C2500 pickup trucks are inflated to 0.41 MPa (60 psi). The corresponding spring rate associated with this inflation pressure is 380 N/mm (2.17 k/in), as obtained from linear interpolation of the two test results. Figure 6.17 shows the effect of vertical tire spring rate on a C2500 pickup trajectory during a ditch traversal. A spring rate of 200 N/mm (1.14 k/in), the CARSIM default value, was used for the L155/80R13 tires used in Geo Metro. In TTI crash tests, these tires are inflated to 0.20 MPa (30 psi).

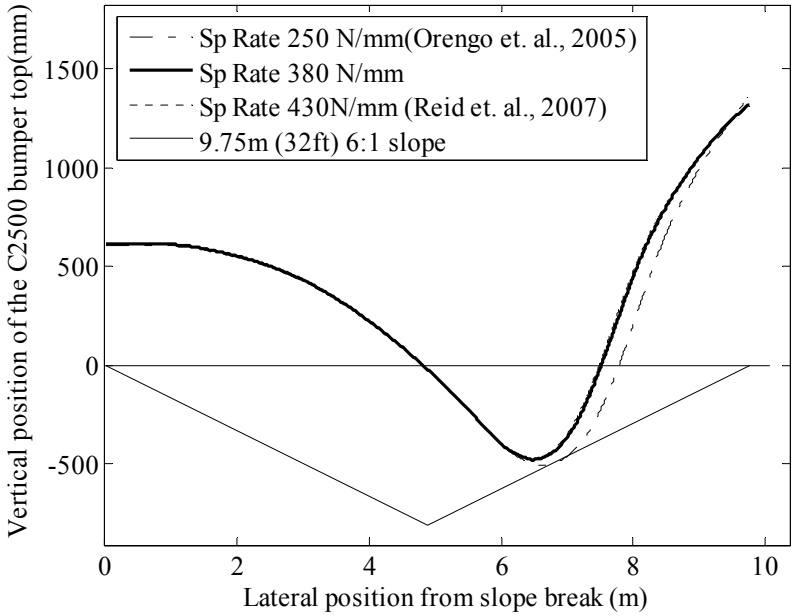

Figure 6.17 Effect of vertical tire stiffness on vehicle trajectory along ditch x-section.

6.3.3. Run CARSIM Simulation

Figure 6.18 shows the CARSIM run screen. The left-hand region of the screen has links to the vehicle datasets, test conditions, and optional inputs. As discussed earlier, a MATLAB subroutine was developed to create three external parsfiles that define the ditch profile. These three parsfiles were linked into the CARSIM road data. Vehicle speed can also be defined in another external parsfile. All the data linked into CARSIM and the CARSIM solver can be sent to the SIMULINK using a button located at the top middle region of the Run screen. This allows the users run a CARSIM simulation inside the SIMULINK. Thus the outputs obtained from CARSIM can be extracted and analyzed using MATLAB subroutines. Right-hand region of the screen includes controls for viewing simulation results with a 3D animator. Figure 6.19 shows the CARSIM generated sequential positions of a Chevrolet C2500 vehicle model traversing a V-shape ditch.

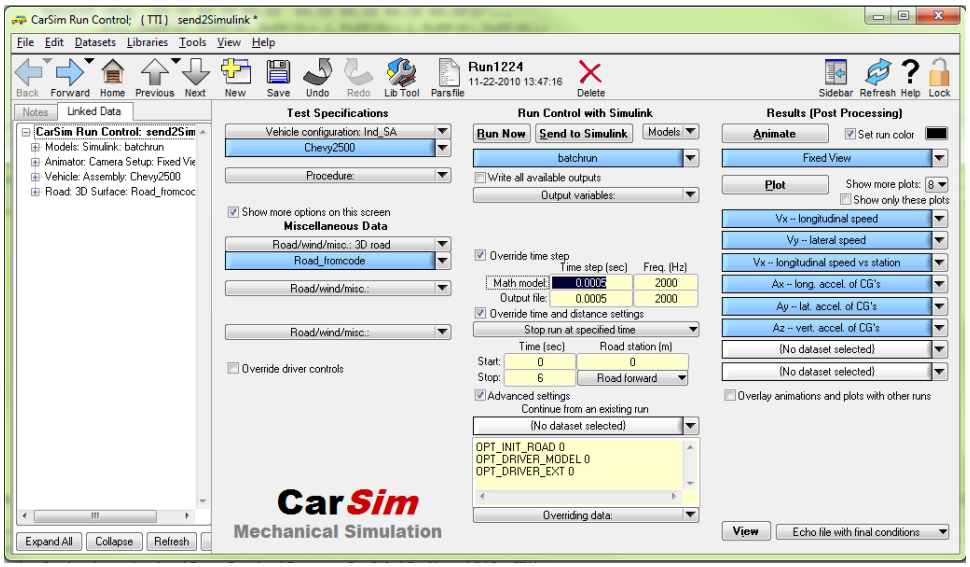

Figure 6.18 CARSIM run screen.

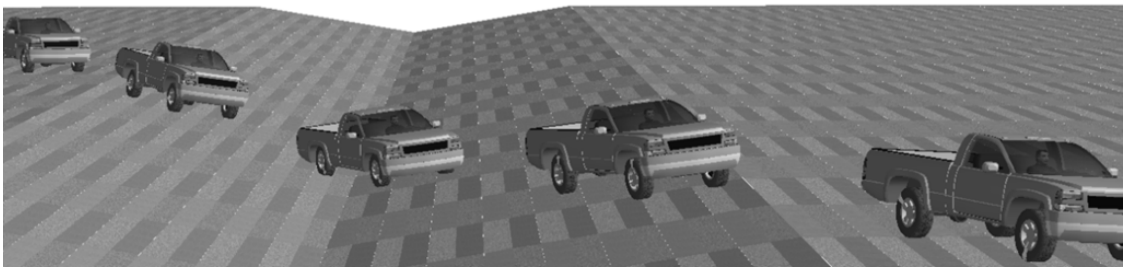

Figure 6.19 CARSIM generated sequential positions of a C2500 vehicle model traversing a 15.85 m (52 ft) wide 6:1 V-shape ditch.

6.3.4. Analyzing CARSIM Output to Extract Bumper Trajectory

Six CARSIM output vectors were used to analyze the vehicle bumper profile along the ditch cross section: three sprung mass origin vectors (X_o, Y_o, Z_o), and three angular displacement vectors *(**Yaw, Roll, Pitch**)* of the vehicle sprung mass. As shown in Figure 6.20, the origin of the sprung mass in CARSIM is defined by the center of the front axle (X_o, Y_o) and initial tire-ground contact level (Z_o). In order to obtain bumper top/tracking

point heights with respect to its local terrain along the ditch cross-section, following steps were performed:

Step 1: The initial tracking point vector, $\mathbf{V_{tr}}$, and vehicle C.G. vector, $\mathbf{V_{cg}}$, (shown in Figure 6.20) were rotated following a prescribed Yaw-Pitch-Roll sequence. These modified vectors were then added to the 3 sprung mass origin vectors (X_o, Y_o, Z_o), to obtain the coordinate vectors (X_{tr}, Y_{tr}, Z_{tr}) of the bumper top/tracking point along the direction of vehicle travel.

Step 2: The bumper top coordinate vectors (X_{tr}, Y_{tr}, Z_{tr}) were then projected on a plane perpendicular to the ditch as shown in Figure 6.3 to obtain a bumper trace projection along the ditch cross-section (X_{ditch}).

Step 3: The adjustment of Z_{tr} for ditch offset (dZ) as shown in Figure 6.3 was then calculated.

Step 4: Relative bumper heights were then calculated by adding the adjustment dZ to the bumper trace projection heights Z_{tr} to obtain bumper top heights relative to local terrain. This is represented by the dotted curve in Figure 6.21(b).

A MATLAB subroutine was created to perform these four steps, analyze the six CARSIM output vectors and extract the bumper point profile along ditch cross-section. Figure 6.21 shows graphical user interface (GUI) input screen and output plot of the MATLAB subroutine. The continuous curve in the output plot represents the bumper height with respect to the actual ditch profile, and the dotted curve indicates the bumper height assuming a reference line along the horizontal axis. When integrated with the barrier performance limits, this curve allows a user to identify acceptable and unacceptable lateral barrier placement ranges along the ditch section.

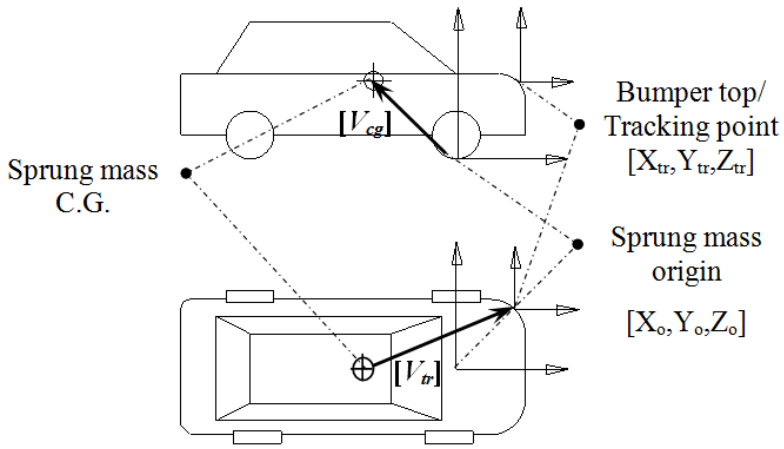

Figure 6.20 Sprung mass origin and bumper point locations on CARSIM vehicle.

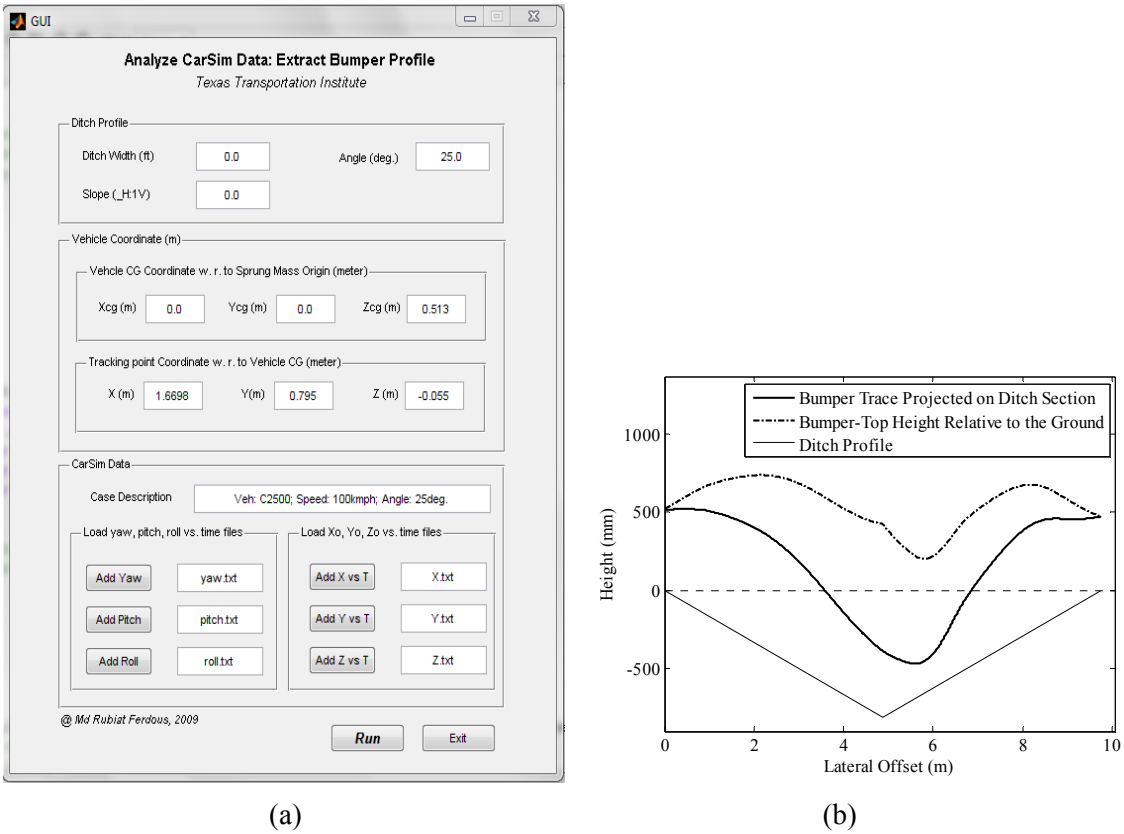

(a) (b)

Figure 6.21 (a) Input screen for analyzing CARSIM output (b) Bumper profile curves obtained from the MATLAB subroutine.

6.3.5. Incorporating CARSIM into MATLAB and SIMULINK

Trajectory analyses for each vehicle class require four input variables. An external MATLAB code was created to efficiently perform the preprocessing according to these variables, run the CARSIM simulation, and post process the CARSIM output in a single run. In the code, the CARSIM model is incorporated into SIMULINK so that it runs inside the SIMULINK and the outputs are stored in a MATLAB workspace. This allows the MATLAB code to analyze the outputs without the extra effort of manually storing and loading the data. Figure 6.22 presents an annotated description of this portion of the code and the steps used to perform a vehicle trajectory simulation. The complete code including the subroutines used to extract bumper trajectory along the ditch cross-section is presented in Appendix C.

6.3.6. Validation

The vehicle dynamics (VD) analysis results obtained using the described approaches were validated against the results obtained from a full scale crash test conducted at TTI(*16*). The test involved a 2000 kg (4406 lb) Chevrolet C2500 pickup impacting an F-shape barrier placed on a 6:1 slope at a speed and angle of 101.2 km/h (62.7 mph) and 24.7 degrees, respectively. The barrier was offset 4 m (13.25 ft) from the hinge of the slope as shown in Figure 6.23.

The acceleration and angular displacement data were recorded using onboard sensors at a rate of 10 kHz. Digitization of high-speed video footage provides vehicle trajectory during the slope encroachment. An identical vehicle dynamic simulation was conducted using CARSIM. The Chevrolet C2500 pickup truck model encroached onto a 6:1 slope at a speed of 101.2 km/h (62.7 mph) and an angle of 24.7 degrees. Results obtained from the crash test prior to barrier impact were compared to results from the VD simulation.

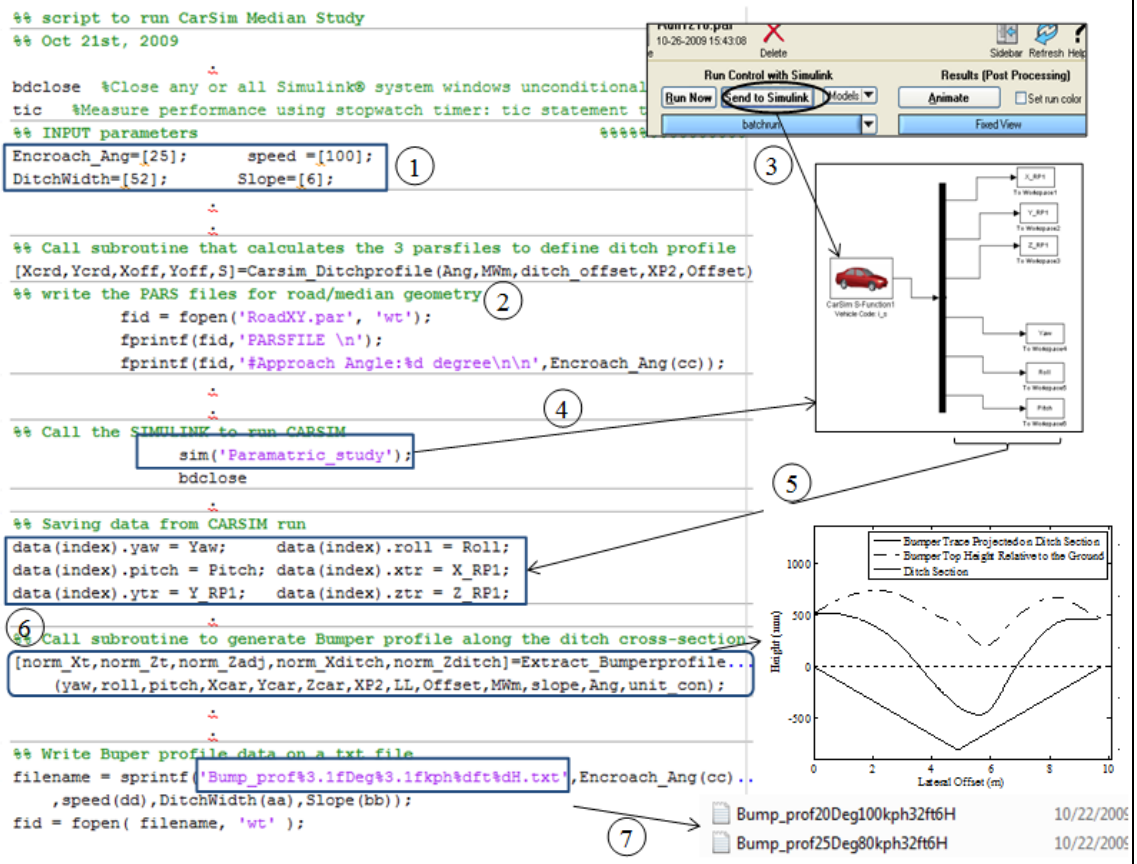

1. Four input parameters are defined for each vehicle class.
2. Ditch profile and vehicle speed are modified and written in external parsfiles.
3. CARSIM model is sent to the SIMULINK.
4. Simulation is performed inside the SIMULINK
5. The 6 output vectors are stored in MATLAB workspace
6. Calls the subroutine that post process the 6 output vectors and extract bumper profile along ditch cross-section
7. The bumper profile data is stored in a predefined folder.

Figure 6.22 Flow chart of the MATLAB and SIMULINK codes that extract and analyze CARSIM outputs to obtain bumper profile.

Figure 6.23 Ditch profile for full scale crash test (TTI test: 452106-3)(*16*).

Stine (*53*) digitized the high speed video footage of the crash test to obtain 52 data points for vertical positions of the vehicle C.G. along the ditch cross section prior to barrier impact. The vehicle position was defined to be at the edge of the shoulder at time t=0. As shown in Figure 6.24(a), vehicle trajectory obtained from the CARSIM simulation closely matched the results obtained from the crash test. The angular displacement data (roll, pitch, and yaw angle) for the crash test were obtained using the coupled integration of angular rate data recorded using onboard rate gyros. Comparisons of these data with results obtained from the CARSIM simulation are shown in Figure 6.24 and Figure 6.25. The correlation between test and simulation was considered reasonable.

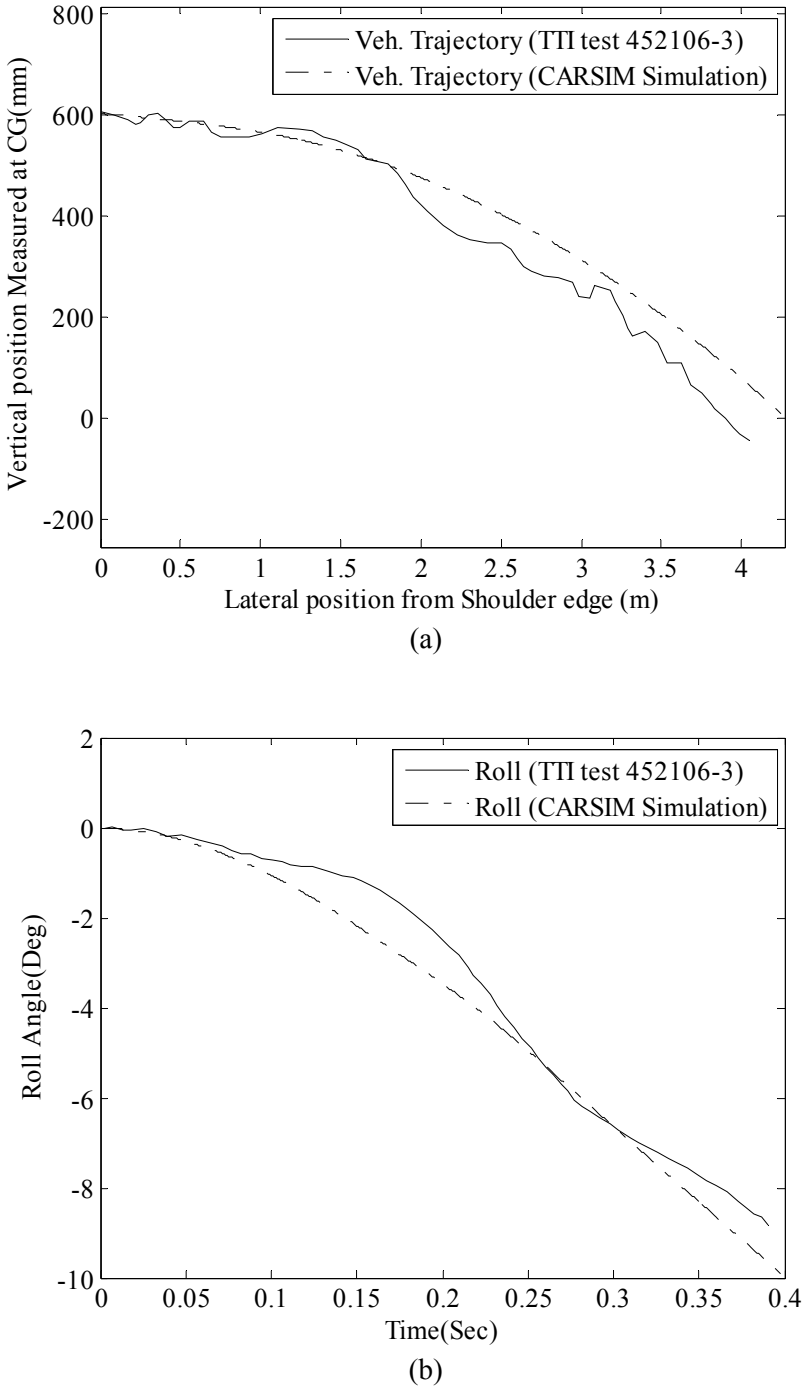

Figure 6.24 Crash test and CARSIM simulation results for vehicle (a) Trajectory and (b) Roll angle.

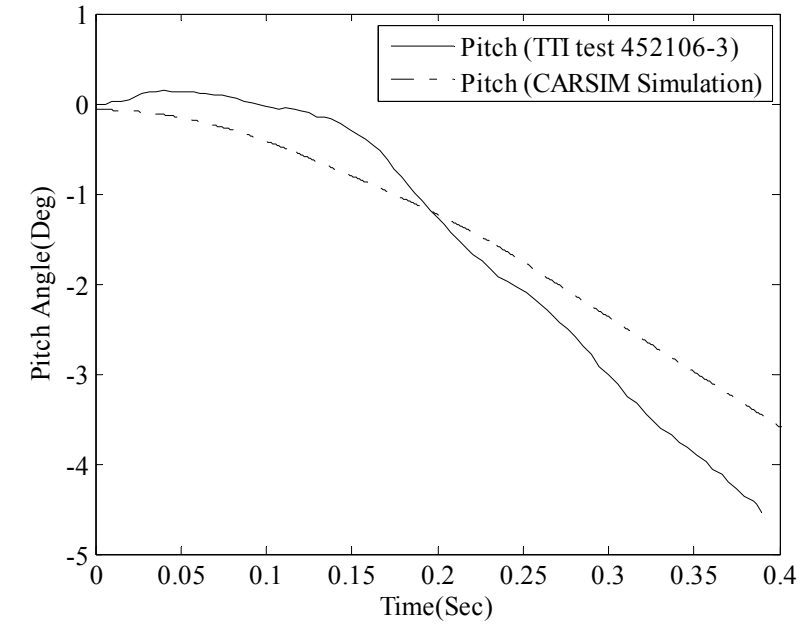

(a)

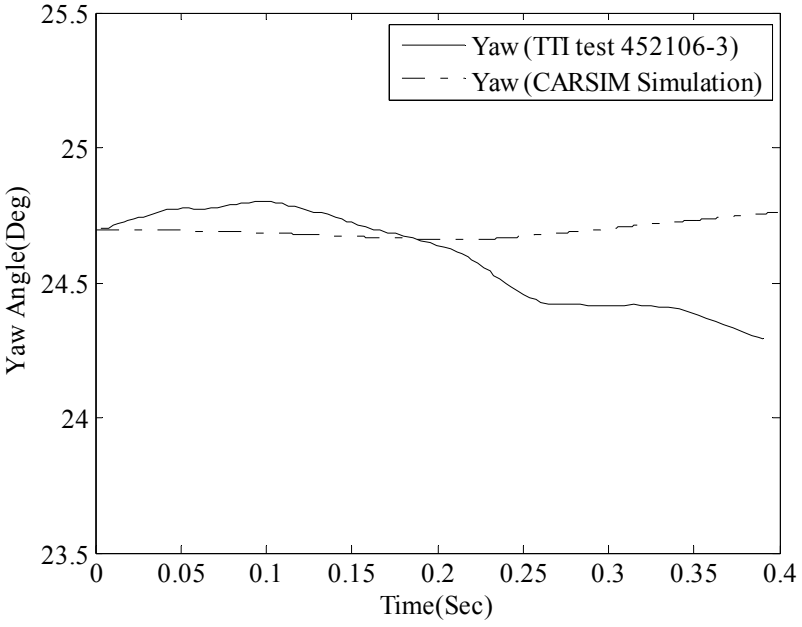

(b)

Figure 6.25 Crash test and CARSIM simulation results for vehicle (a) Pitch and (b) Yaw angles.

6.3.7. Vehicle Trajectory Envelope

The tracking point on the vehicle was taken as the top corner of the bumper closest to the shoulder edge as depicted in Figure 6.26. Using the results obtained from VD simulation of vehicle traversing the median ditch, bumper profiles relative to the terrain along the ditch cross-section were plotted as illustrated in Figure 6.21(b). Figure 6.27(a) shows a superposition of all the bumper profiles (relative) obtained for the two different design vehicles encroaching onto a selected ditch configuration at various encroachment speed and angle combinations. These plots are for the vehicles traversing across the median from the left side. This data is sufficient for evaluating a scenario in which a guardrail is placed on a roadside or on both sides of a median ditch.

(a) (b)

Figure 6.26 Tracking point located on the bumper top for (a) Chevy 2500 (b) GeoMetro.

However, for V-shaped median configurations with a single median barrier placed in the ditch, consideration needs to be given to vehicles encroaching into the median from either side of the divided roadway. This is accomplished by mirroring the traces plotted in Figure 6.27(a) on the same ditch cross-section. Figure 6.27(b) shows bumper profiles for the two vehicle classes encroaching from both sides of the selected ditch configuration. The dotted lines represent the vehicles traversing across the median from the right side.

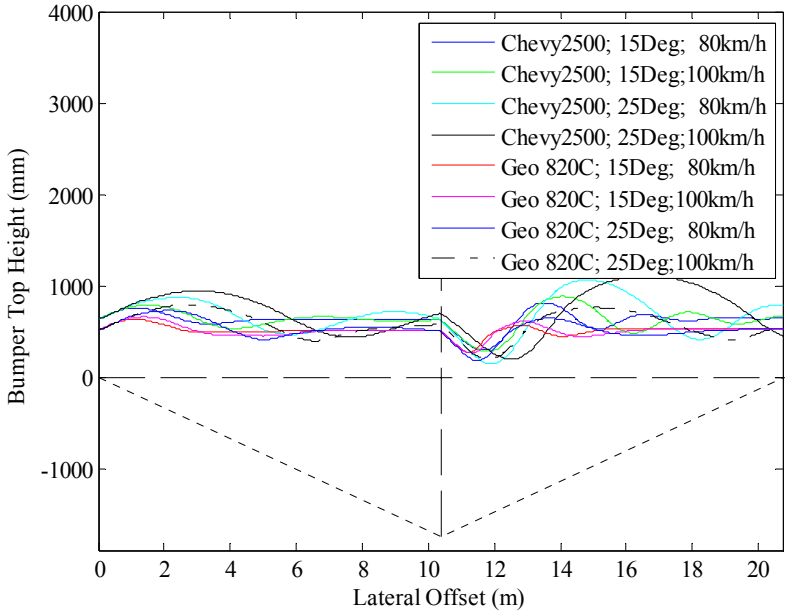

(a)

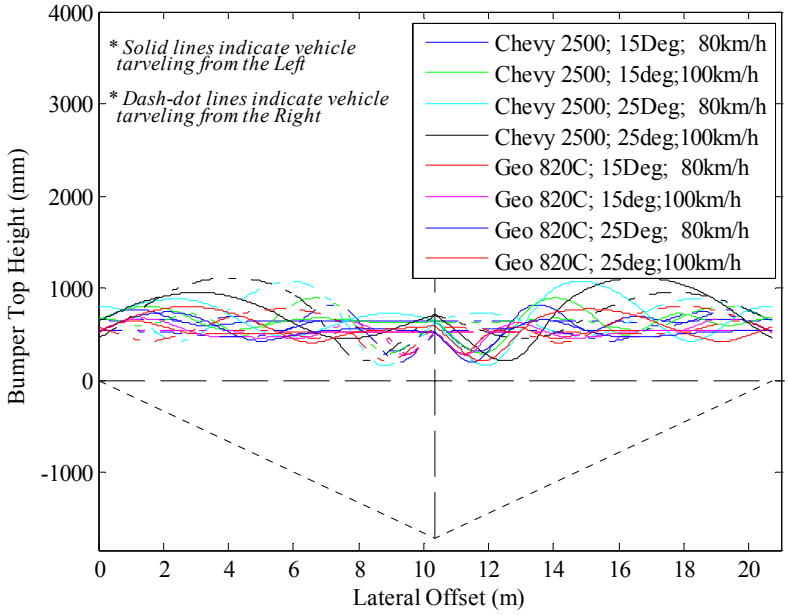

(b)

Figure 6.27 Bumper profile on a given ditch configuration for different vehicle class, speed and approach angle: Vehicle traversing from (a) Left, and (b) both directions.

Figure 6.28(a) and Figure 6.28(b) show the trajectory envelopes for vehicles traversing from one side and both sides of the median ditch, respectively. These envelopes trace the upper and lower projections of the individual bumper plots across the ditch profile. The upper continuous line represents the maximum bumper heights obtained at each location along the sloped terrain, and the lower dotted line of the envelope indicates the minimum values of bumper top height for any point along the slope/ditch.

Superimposed as horizontal lines on these trajectory envelopes are the barrier performance limits (i.e., override/rollover limit and underride limit). If, at a given lateral offset, the thin continuous line (maximum bumper top height) exceeds the barrier override/rollover limit, it is highly probable that a pickup truck will rollover or override a barrier placed at that location. Similarly, if the thin dotted line (minimum bumper top height) extends below the underride limit line, it is likely that a small car can underride the barrier placed at that location, resulting in severe vehicle snagging and excessive decelerations. The solid bars plotted at the bottom of the figures indicate locations for which barrier performance is predicted to be acceptable (i.e., no override/rollover or underride is expected).

6.4. CONCLUSIONS

Multi-rigid body vehicle dynamic analysis code “CARSIM” was used in this study to determine trajectories of the 2000 kg Chevrolet C2500 pickup truck and 820 kg Geo Metro passenger car traversing various ditch cross-sections. This section presents the vehicle properties and terrain configurations used in CARSIM deck and validation approach used for the CARSIM simulations. Procedures used to determine trajectory envelops for the tracking point on the vehicle along the ditch cross-sections and use of these envelops in determining lateral offset locations for the barriers on roadside and median slopes are also discussed.

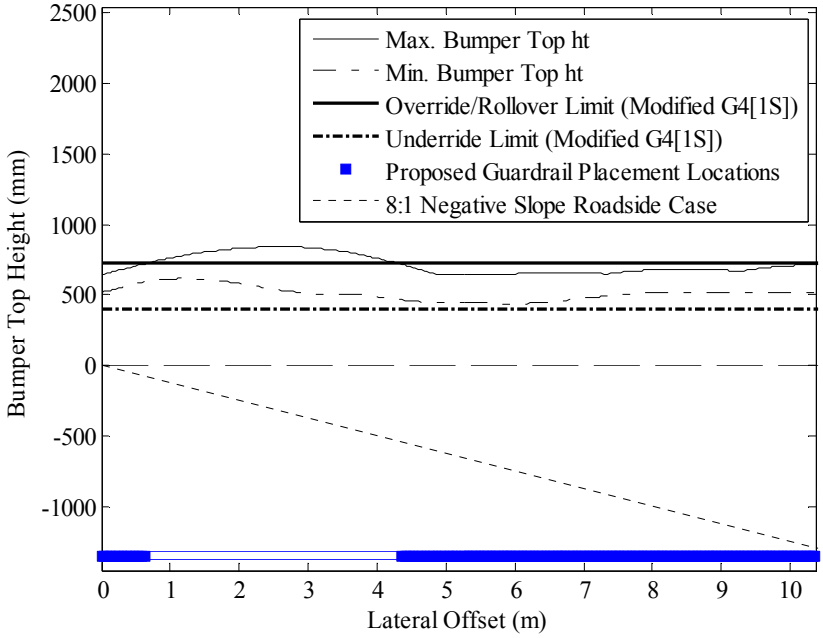

(a)

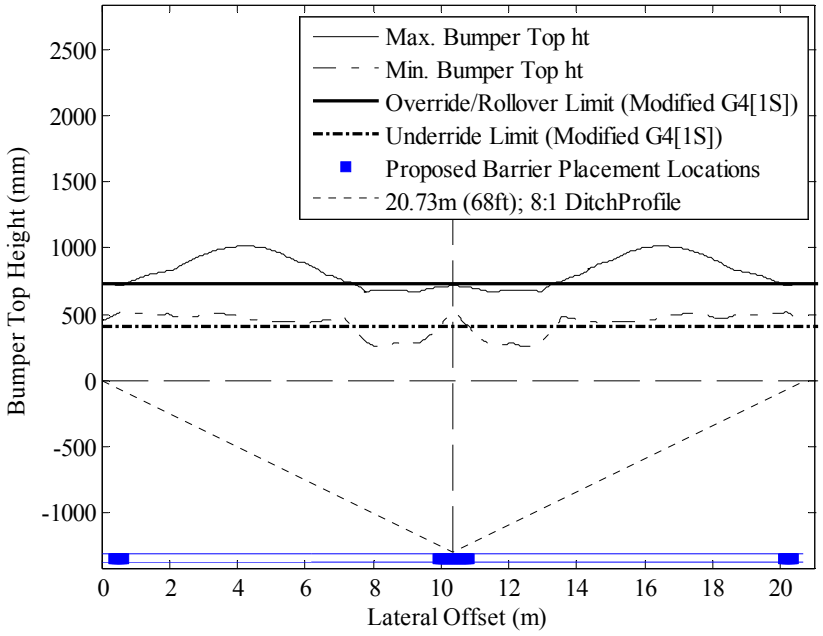

(b)

Figure 6.28 Vehicle Trajectory Envelope: vehicle encroaching from (a) left, and (b) both directions.

7. PRELIMINARY GUIDELINES

7.1. INTRODUCTION

This section presents the results obtained from vehicle trajectory analyses performed following the procedures discussed in Section 6. It also presents the preliminary guidelines prepared for the placement of five guardrail systems on roadside and median slopes. Barrier performance limits, derived as discussed in Section 5, were superimposed on the vehicle trajectory data to quantify performance of a given barrier on a given slope as a function of barrier offset. These graphical representations were used to develop preliminary guidelines for the placement of each guardrail/median barrier on slope configurations selected for the study.

7.2. PLACEMENT GUIDELINE FOR MODIFIED G4(1S) W-BEAM SYSTEM

7.2.1. Median Case

Figure D.1 to Figure D.8, presented in appendix D shows the CARSIM generated bumper top trajectories of the two design vehicles traversing various median and roadside configurations. For the placement of a single median barrier in a depressed median, consideration must be given to vehicles encroaching from both directions. Hence, trajectory data obtained for the vehicle traversing from one direction were mirrored to obtain the trajectory of the vehicle traveling from opposite direction. The vehicle trajectory envelopes comprising the bumper trajectory of different vehicle classes traversing the median ditch from both directions at various speeds and approach angles were also calculated for different median configurations. Figure 7.1 to Figure 7.6 show the vehicle trajectory envelopes and corresponding recommended placement locations along the ditch section for a modified G4(1S) W-beam barrier. The median configurations included in the analyses were 12.2 m (40ft), 18.3 m (60 ft), and 23.2 m

(76 ft) wide medians with 1.22 m (4 ft) and 1.83 m (6 ft) wide shoulders and 6:1 and 8:1 slopes. The combinations of different median and shoulder widths produced ditch widths ranging from 8.5 m (28 ft) to 20.7 m (68 ft).

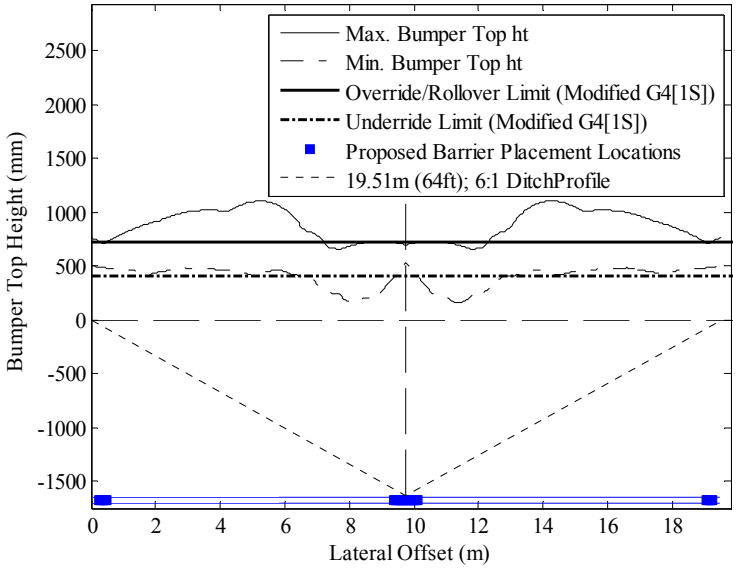

(a)

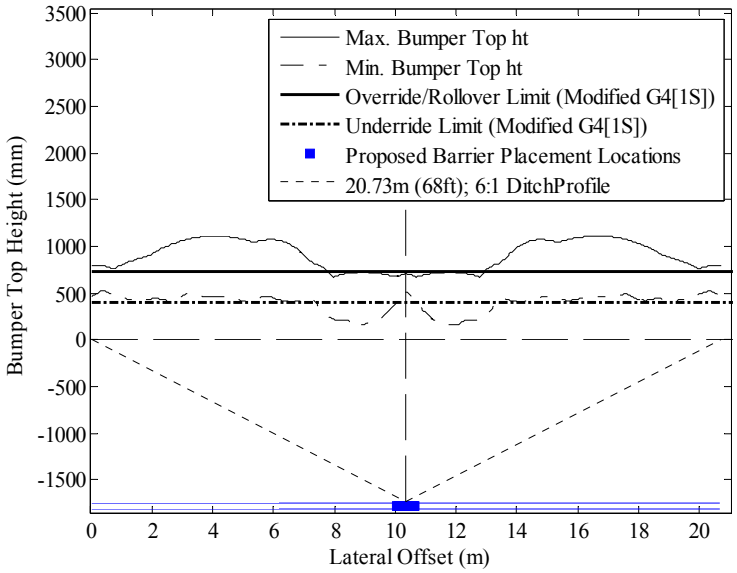

(b)

Figure 7.1 Determining placement locations: Modified G4(1S) system on a 6:1, 23.2 m (76') wide median with (a) 1.8 m (6') and (b) 1.2 m (4') wide shoulders.

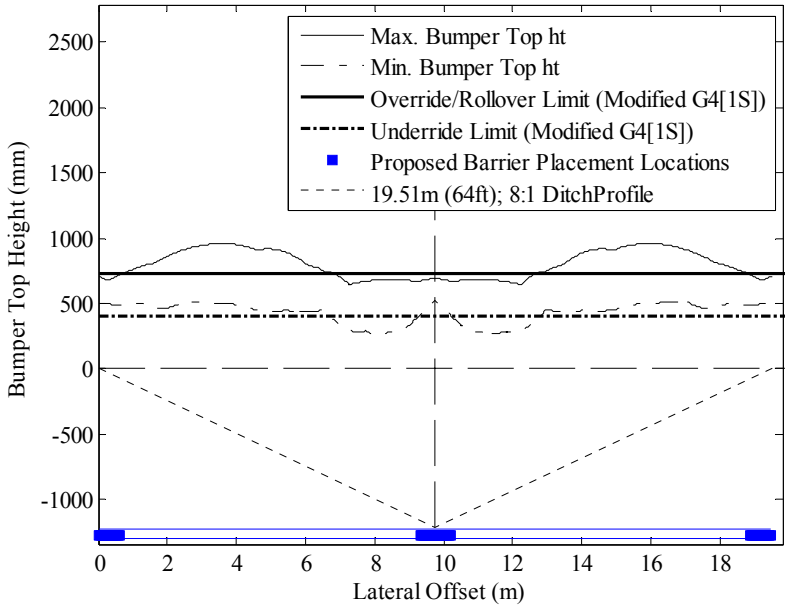

(a)

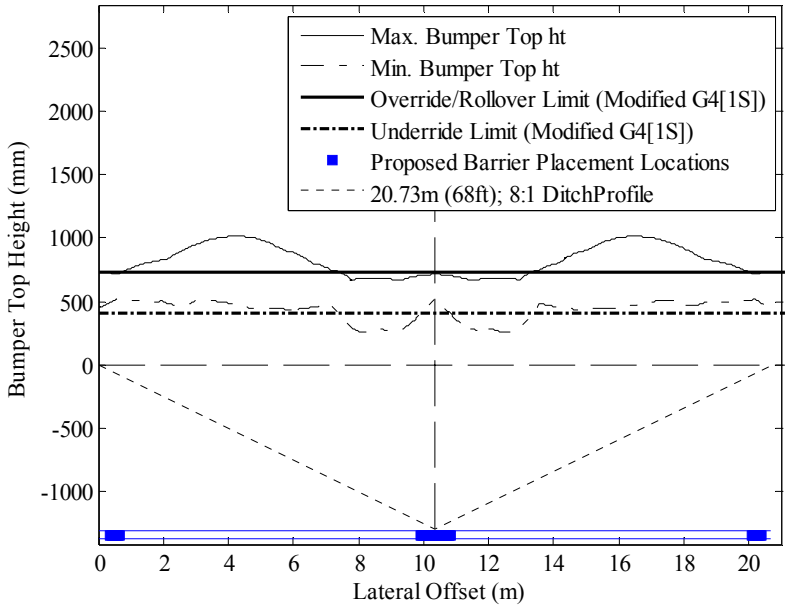

(b)

Figure 7.2 Determining placement locations: Modified G4(1S) system on an 8:1, 23.2 m (76') wide depressed median with (a) 1.8 m (6') and (b) 1.2 m (4') wide shoulders.

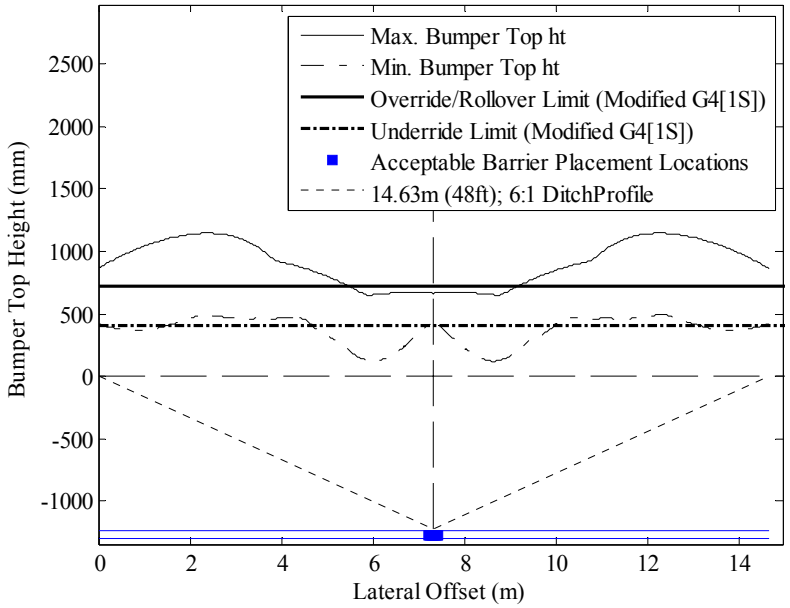

(a)

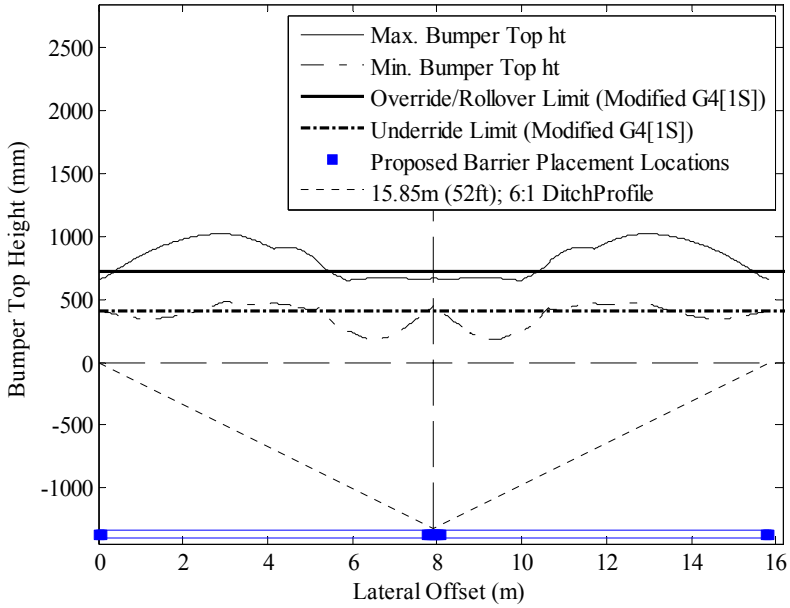

(b)

Figure 7.3 Determining placement locations: Modified G4(1S) system on a 6:1, 18.3 m (60') wide depressed median with (a) 1.8 m (6') and (b) 1.2 m (4') wide shoulders.

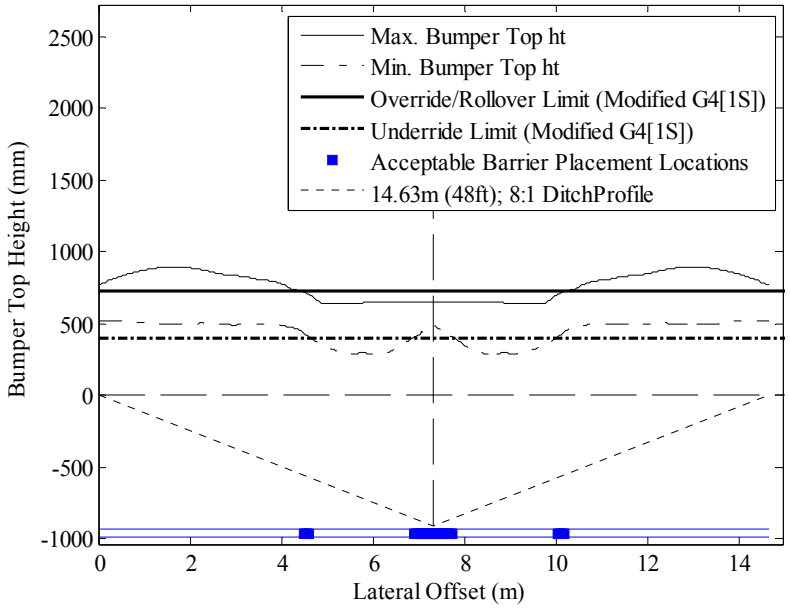

(a)

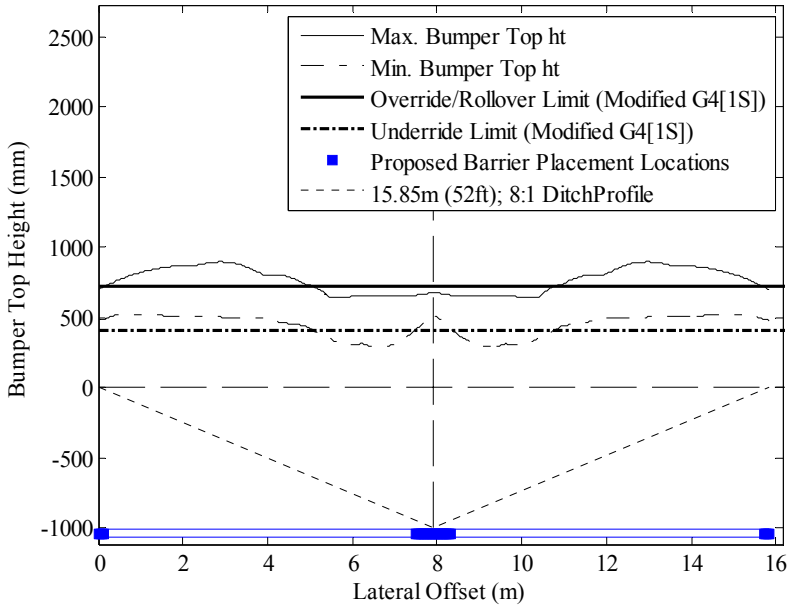

(b)

Figure 7.4 Determining placement locations: Modified G4(1S) system on an 8:1, 18.3 m (60') wide depressed median with (a) 1.8 m (6') and (b) 1.2 m (4') wide shoulders.

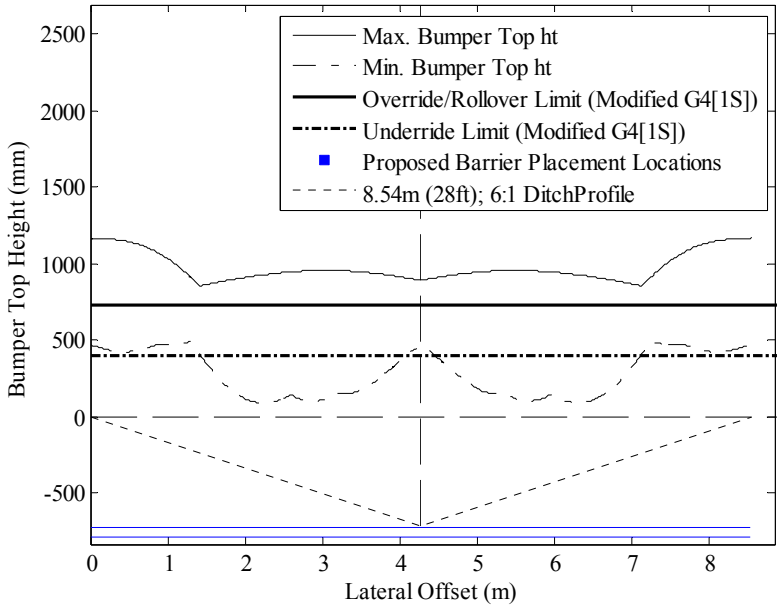

(a)

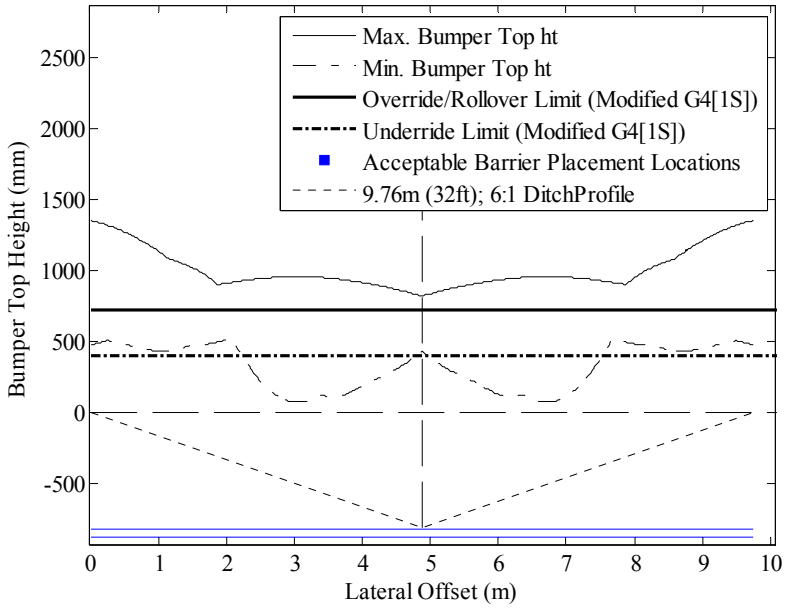

(b)

Figure 7.5 Determining placement locations: Modified G4(1S) system on a 6:1, 12.2 m (40') wide depressed median with (a) 1.8 m (6') and (b) 1.2 m (4') wide shoulders.

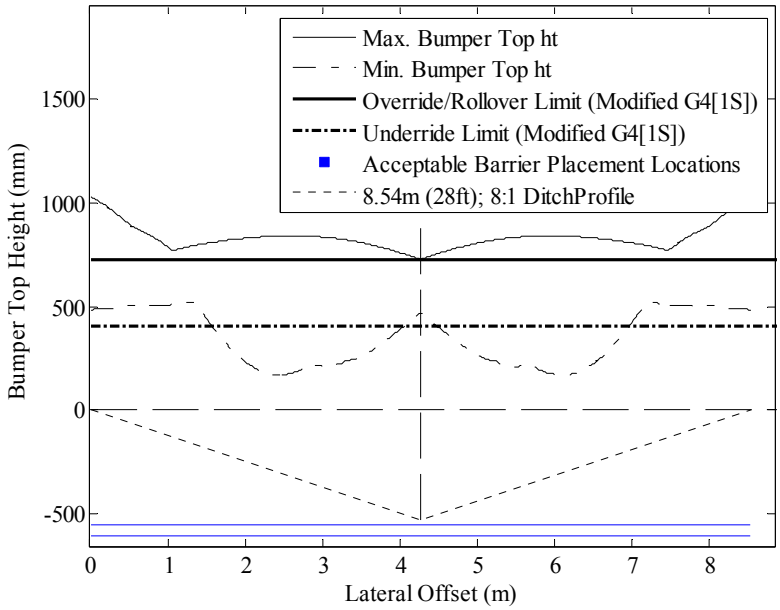

(a)

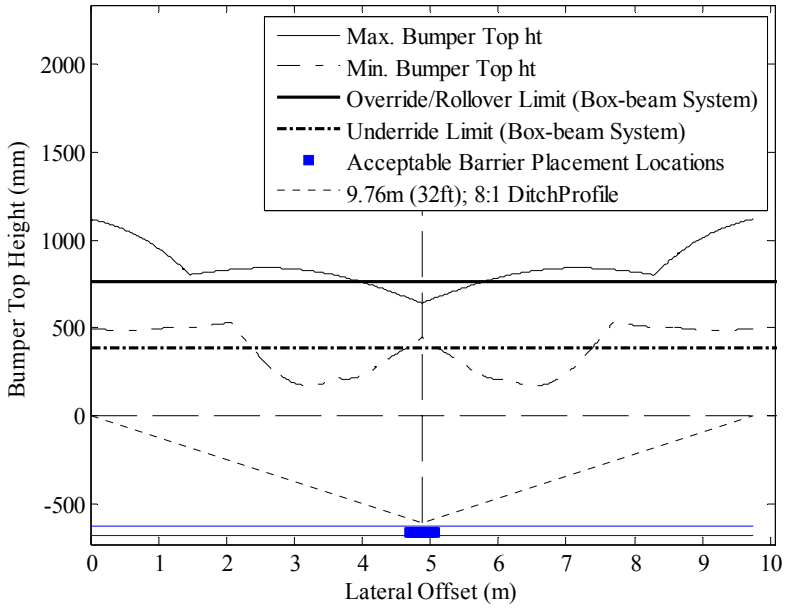

(b)

Figure 7.6 Determining placement locations: Modified G4(1S) system on an 8:1, 12.2 m (40') wide depressed median with (a) 1.8 m (6') and (b) 1.2 m (4') wide shoulders.

As discussed in Section 6, the solid bars shown in Figure 7.1 to Figure 7.6 define the effective lateral offset locations for the barriers. As shown in Figure 5.14(a) and Table 5.13, override and underride limits for a modified G4(1S) W-beam guardrail were obtained as 726 mm (28.6") and 403 mm (15.9"), respectively. If at a given lateral position, the maximum bumper height in the trajectory envelope falls below the barrier override limit and the minimum bumper height remains above the underride limit, the barrier can effectively be placed at that location. As can be seen in Figure 7.5 and Figure 7.6, the modified G4(1S) W-beam barrier is not recommended for use in a 12.2 m (40 ft) wide median with 1.83 m (6 ft) shoulders for either of the slopes analyzed. The barrier is also not suitable for placement in a 12.2 m (40 ft) wide median with 1.2 m (4 ft) shoulder and 6:1 slopes (see Figure 7.5a).

As shown in Figure 7.1(a), which corresponds to a 23.2 m (76 ft) wide median with 1.83 m (6 ft) shoulders and 6:1 ditch slopes, the maximum bumper height falls below the override limit in a range of 0 to 0.46 m (1.5 ft) and 7.6 m (25 ft) to 9.76 m (32 ft) from the slope break point. Note that the distance of 9.76 m (32 ft) constitutes the centerline or bottom of the 19.51 m (64 ft) wide V-ditch. However, the minimum bumper height is below the underride limit in a range of 6.0 m (19.67 ft) to 9.45 m (31 ft) from the shoulder edge. This limits acceptable placement of the barrier within 0.46 m (1.5 ft) of the slope break point or within 0.3 m (1 ft) from the center of the ditch.

Other configurations of the 18.3 m (60 ft) and 23.2 m (76 ft) wide medians follow this same general pattern. The 23.2 m (76 ft) wide medians with 8:1 slopes offers the most flexibility of barrier placement of the ditch configurations analyzed, but it is still very limited (see Figure 7.2). Acceptable barrier placement for these medians ranges from 0 to 0.62 m (2 ft) from the shoulder edge and within 0.46 m (1.5 ft) of the ditch centerline. This should not be a surprising revelation for the modified G4(1S) W-beam barrier given that testing has demonstrated that it is near its performance limits on flat, level terrain. Table 7.1 and Figure 7.7 summarizes the preliminary guideline for the placement of Modified G4(1S) W-beam barrier on median slopes. Hatched bars in Figure 7.7 indicates the acceptable lateral placement locations (i.e. no override or

underride) for a single dual-sided modified G4(1S) W-beam barrier. Two bars for each median at a given slope indicates placement locations for two ditches with 1.2 m (4ft) and 1.8 m (6ft) wide shoulders. The bar for each ditch width starts from the slope break point and ends at the centerline of the ditch.

Table 7.1 Preliminary guideline for the placement of modified G4(1S) W-beam on median slope.

Barrier Type	Median Width	Shoulder Width	Ditch Width	Slope	Acceptable barrier offset locations from slope break, X, "m" (ft)
Modified G4(1S) System	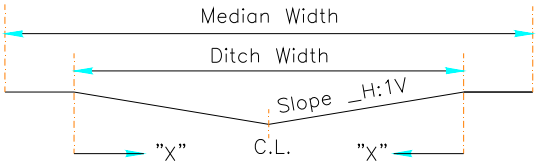				
	23.2 m (76 ft)	1.2 m (4')	20.7 m (68')	6:1	10.0 m (33') - C.L.
				8:1	0- 0.62 m (2.0'); 9.91m (32.5') - C.L.
		1.8 m (6')	19.5 m (64')	6:1	0-0.46 m (1.5'); 9.45 m (31')-C.L.
				8:1	0- 0.62 m (2.0′); 9.3 m (30.5′) -C.L.
	18.3 m (60 ft)	1.2 m (4')	15.9 m (52')	6:1	7.8 m (25.5′) -C.L.
				8:1	0-0.12 m (0.4'); 7.5 m (24.6')-C.L.
		1.8 m (6')	14.6 m (48')	6:1	7.2 m (23.6') - C.L.
				8:1	6.96 m (22.8') - C.L.
	12.2 m (40 ft)	1.2 m (4')	9.8 m (32')	6:1	Not Recommended
				8:1	4.8 m (15.7′) -C.L.
		1.8 m (6')	8.5 m (28')	6:1 & 8:1	Not Recommended

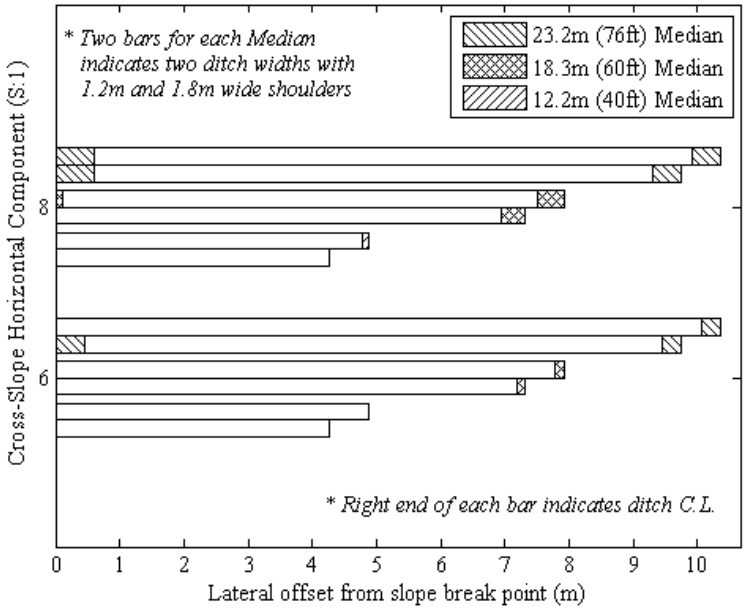

Figure 7.7 Preliminary guideline for the placement of modified G4(1S) system on V-shaped median slopes.

7.2.2. Roadside Case

A roadside cross-slope can be either positive (cut) or negative (fill). Additional vehicle dynamics simulations were conducted for the case of a vehicle encroaching onto a roadside with a positive (cut) slope. The scenario with a negative (fill) cross-slope is a subset of the case of the vehicle encroaching into a depressed median and, therefore, did not require further simulation runs.

7.2.2.1. Positive (Cut) Slope

Vehicle trajectory analyses were performed for the roadside encroachment cases with a positive 6:1 slope. Figure 7.8(a) shows the bumper profile for a roadside encroachment simulation involving a Chevrolet C2500 pickup truck traveling at a speed of 100 km/h (62 mph) and an angle of 25 degrees. The solid line indicates the trace of the bumper top

projected on positive slope section (which is represented by the dotted line). The dash-dot line represents the relative heights of the bumper-top assuming a reference line along the horizontal axis.

Figure 7.8 (b) shows the relative bumper height plots for different combinations of vehicle type, speed, and approach angle for encroachment on a positive 6:1 slope. Using these plots, a vehicle trajectory envelope was generated for the selected slope configuration. A similar process was followed for a positive 8:1 slope. Figure 7.9 shows the vehicle trajectory envelopes and corresponding guardrail placement locations obtained for these two cases.

For the positive 6:1 roadside slope (see Figure 7.9(a)), acceptable barrier placement locations are 0 to 0.6 m (1.95 ft), 2.6 m (8.5 ft) to 3.2 m (10.5 ft), and beyond 7.4 m (24.3 ft) from the slope break point. As shown in Figure 7.9(b), the barrier placement options for the positive 8:1 slope are slightly expanded and include ranges 0 - 0.9m (2.9 ft), 1.9 m (6.3 ft) - 4.3 m (14 ft), and greater than 6.65 m (21.8 ft) from the slope break point. Table 7.2 and Figure 7.10 summarize the preliminary guideline for the placement of modified G4(1S) W-beam guardrail on positive (cut) roadside slope.

7.2.2.2. Negative (Fill) Slope

For the roadside cases with negative cross-slope and the depressed median cases in which guardrails will be placed on both the foreslope and backslope, only one direction of vehicle travel onto the slope had to be considered. Figure 7.11 shows the vehicle trajectory envelopes and possible guardrail placement locations on the foreslope of a 23.2 m (76 ft) wide median with 1.2 m (4 ft) shoulder width (i.e., 20.7 m ditch width). The solid bar at the bottom of the figure indicates the effective lateral positions where the modified G4(1S) W-beam guardrail can be placed without creating a significant probability of vehicle override or underride.

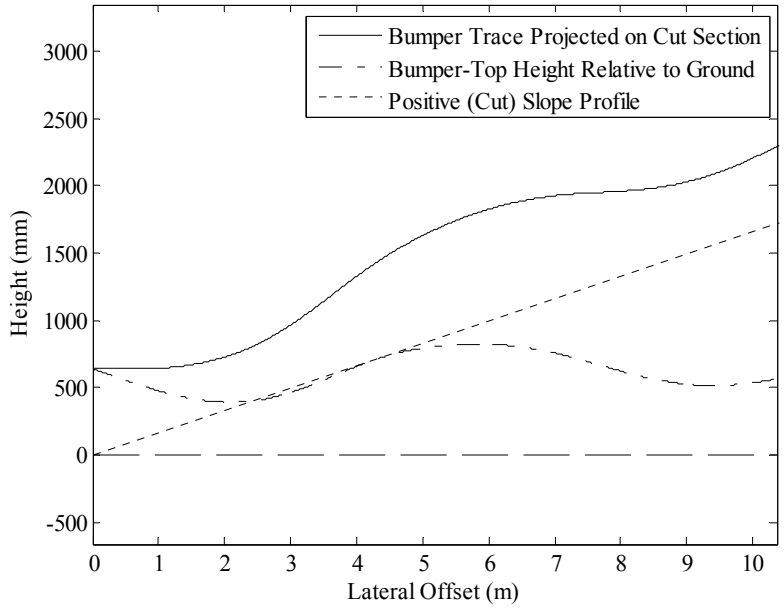

(a)

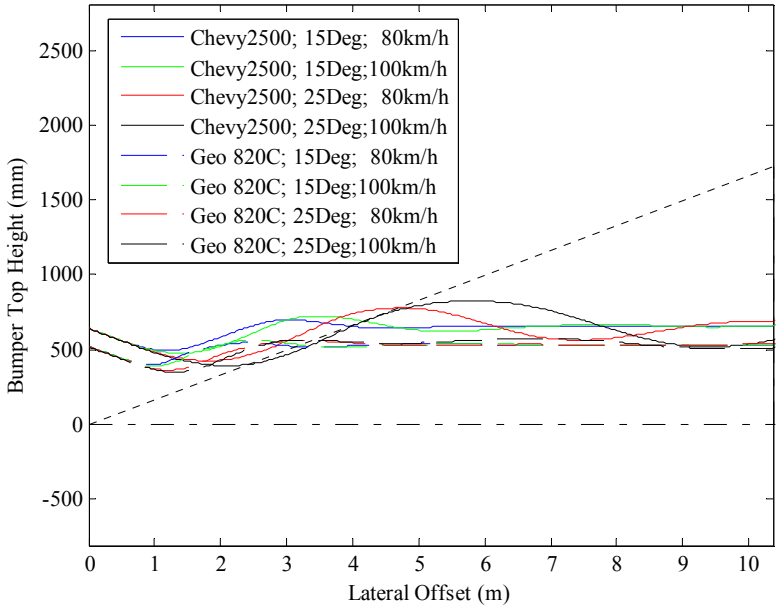

(b)

Figure 7.8 (a) Bumper profile for a pickup traversing a 6:1 positive roadside slope. (b) Bumper trajectory relative to local terrain on a 6:1 positive slope for various combinations of vehicle types, encroachment speeds and approach angles.

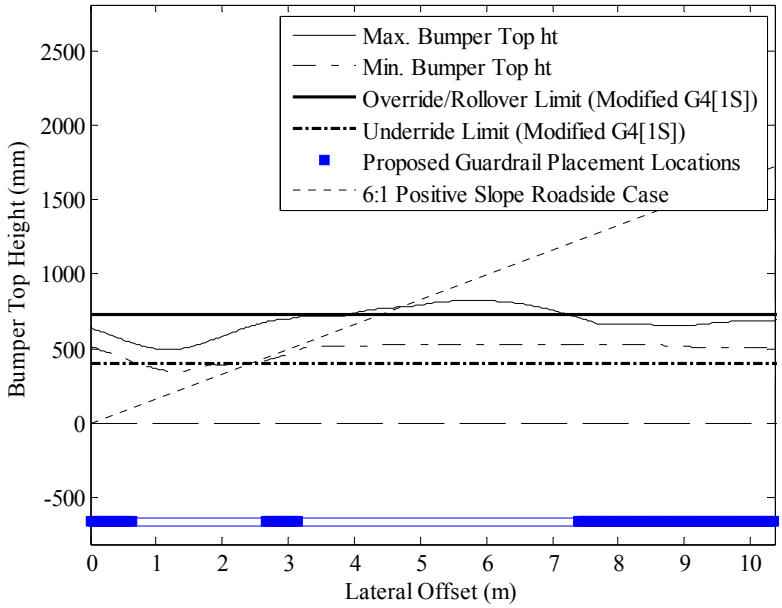

(a)

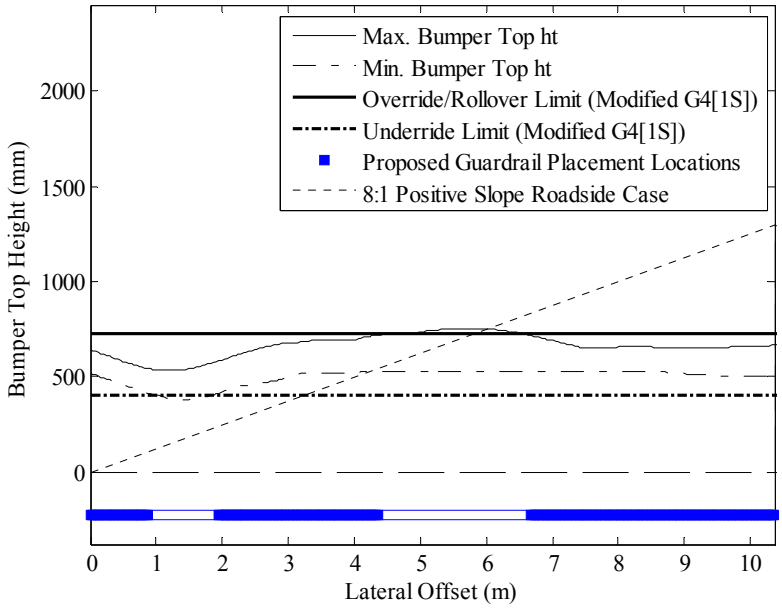

(b)

Figure 7.9 Determining placement locations: Modified G4(1S) system on positive (cut) (a) 6:1 and (b) 8:1 roadside slopes.

Table 7.2 Preliminary guideline for the placement of modified G4(1S) W-beam on roadside slopes.

Barrier Type	Case	Slope	Acceptable guardrail offset locations from slope break, X, "m" (ft)
Modified G4(1S) System	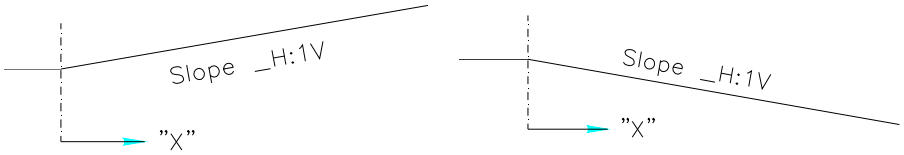 Roadside Positive Slope		Roadside Negative Slope
	Positive (cut) Roadside slope	6:1	0-0.6 m (1.95'); 2.6 m (8.5')-3.2 m (10.5'); >7.4 m (24.3')
		8:1	0-0.9 m (2.9'); 1.9 m (6.3')-4.3 m (14'); >6.65 m (21.8')
	Negative (fill) Roadside slope	6:1	0-0.45 m (1.5'); 5.5 m (18')-8.54 m (28'); >9.33 m (30.6')
		8:1	0-0.62 m (0-2.0'); >4.4 m (14.3')

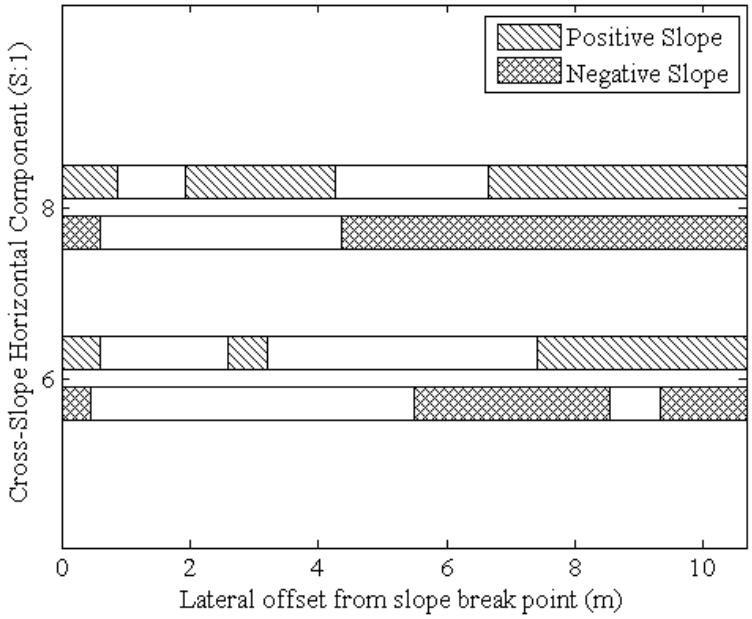

Figure 7.10 Preliminary guideline for the placement of modified G4(1S) W-beam on roadside slopes.

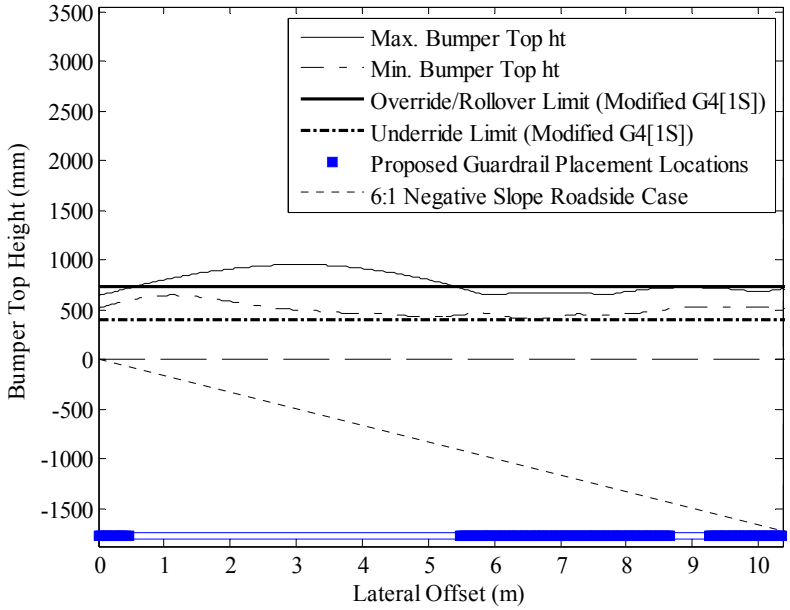

(a)

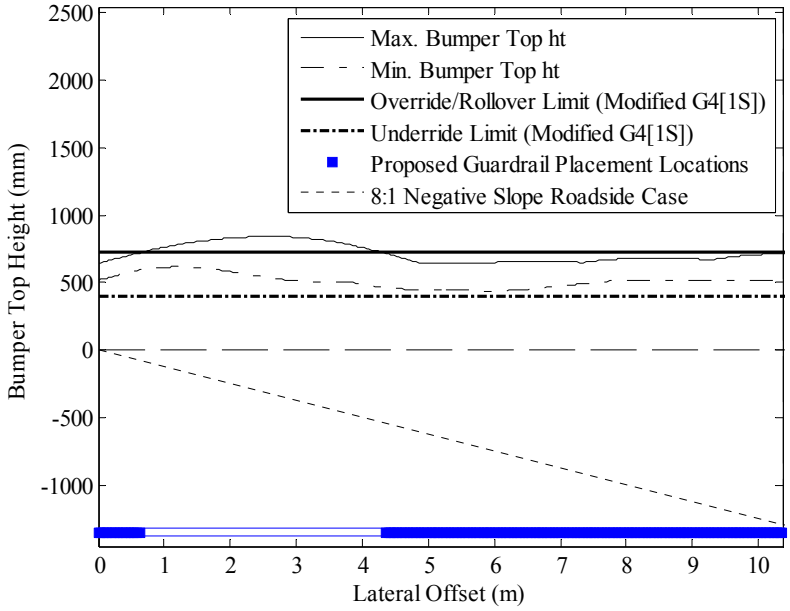

(b)

Figure 7.11 Determining placement locations: Modified G4(1S) system on negative (fill) (a) 6:1 and (b) 8:1 roadside slopes.

As can be seen in Figure 7.11 (a), the guardrail can be placed within the ranges 0-0.45 m (1.5 ft), 5.5 m (18 ft)-8.58 m (27.9 ft), and beyond 9.33 m (30 ft) from the break point of a 6:1 slope (provided that another guardrail is placed on the backslope of a depressed median to take care of the traffic from opposite direction). The analysis showed that the acceptable lateral offset locations for barrier placement do not change for the foreslope encroachment case with a change in ditch width. Therefore, for depressed medians with 6:1 slopes and a ditch width of 15.9 m (52 ft) or less, the modified G4(1S) guardrail can only be placed within 0.45 m (1.5 ft) and beyond 5.5 m (18 ft) from the slope break point. For a negative 8:1 slope, shown in Figure 7.11 (b), the acceptable barrier placement locations are slightly expanded and include ranges of 0-0.62 m (2 ft) and greater than 4.4 m (14.3 ft) from the slope break point. Table 7.2 and Figure 7.10 summarize the preliminary guideline for the placement of Modified G4(1S) W-beam barrier on negative roadside slopes.

7.3. PLACEMENT GUIDELINE FOR MIDWEST GUARDRAIL SYSTEM

As discussed in Section 5, override and underride limits obtained for the Midwest Guardrail System (MGS) are 818 mm (32.2") and 410 mm (16"), respectively. To determine the acceptable lateral offset locations for MGS, these limits were superimposed on the trajectory data for vehicles traversing various median and roadside slopes in Figure E.1 to Figure E.8 presented in appendix E. The override limit obtained for MGS were higher compared to that obtained for modified G4(1S) system due to the presence of wider blockouts and higher rail mounting heights. Hence, the acceptable lateral offset locations obtained for MGS were wider compared to those obtained for modified G4(1S) w-beam guardrail systems. However, as can be seen in Figure E.5, the MGS, like modified G4(1S) W-beam guardrail, was also found unfit for the placements on a 12.2 m (40 ft) wide median with 6:1 slope when used as a single barrier to protect vehicle from both directions. For these cases, two single-sided guardrails should be placed on both slopes of the median following the placement guidelines for a 6:1

negative roadside slope. Preliminary guidelines for the placement of dual-sided MGS on selected median configurations are summarized in Table 7.3 and Figure 7.12. Similarly, Table 7.4 and Figure 7.13 summarize the recommended placement locations for MGS on roadside slopes.

Table 7.3 Preliminary guideline for the placement of Midwest Guiderail System on median slopes.

Barrier Type	Median Width	Shoulder Width	Ditch Width	Slope	Acceptable barrier offset locations from slope break, X, "m" (ft)
Midwest Guardrail System	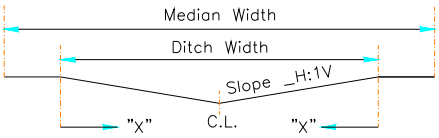				
	23.2 m (76 ft)	1.2 m (4')	20.7 m (68')	6:1	0-1.0 m (3.3'); 10.1 m (33.2')-C.L.
				8:1	0-1.6 m (5.25'); 6.6 m (21.6')-7.3 m (23.9'); 10 m (32.8') -C.L.
		1.8 m (6')	19.5 m (64')	6:1	0-1.0 m(3.3'); 9.5 m (31')-C.L.
				8:1	0-1.6 m (5.25'); 6.0 m(19.7')-6.6 m(21.6'); 9.4 m (30.8')-C.L.
	18.3 m (60 ft)	1.2 m (4')	15.9 m (52')	6:1	7.8 m (25.6')-C.L.
				8:1	0-0.9 m (2.9'); 3.9 m(12.8')-5 m(16.4'); 7.5 m (24.6')- C.L.
		1.8 m (6')	14.6 m (48')	6:1	7.25 m(23.8')-C.L.
				8:1	0-0.25 m (0.82'); 3.55 m (11.6')-4.5 m (14.7'); 7.0 m(23')-C.L.
	12.2 m (40 ft)	1.2 m (4')	9.8 m (32')	6:1	Not Recommended
				8:1	1.45 m (4.8')-1.5 m(4.92'); 4.8 m(15.75')-C.L.
		1.8 m (6')	8.5 m (28')	6:1	Not Recommended

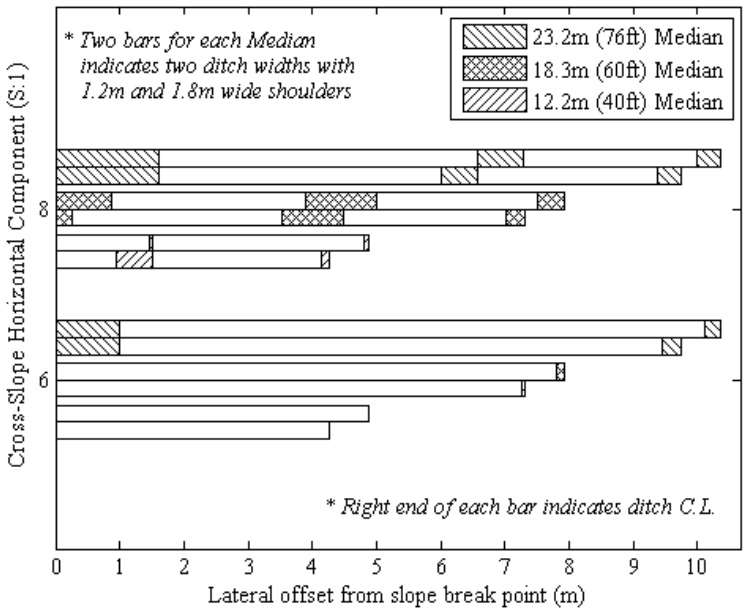

Figure 7.12 Preliminary guideline for the placements of Midwest Guardrail System on V-shaped median slopes.

Table 7.4 Preliminary guideline for the placements of Midwest Guardrail System on roadside slopes.

Barrier Type	Case	Slope	Acceptable guardrail offset locations from slope break, X, "m" (ft)
Midwest Guardrail System	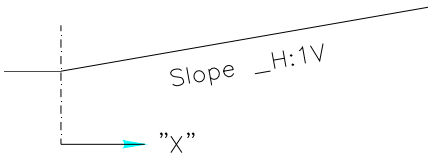 Roadside Positive Slope		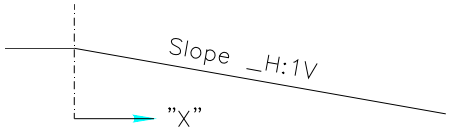 Roadside Negative Slope
	Positive (cut) Roadside slope	6:1	0-0.58 m (1.9'); 2.7 m(8.8')-5.2 m (17'); >6.4 m (21')
		8:1	0-0.8 m (2.6'); >2 m (6.5')
	Negative (fill) Roadside slope	6:1	0-1.0 m (3.3'); 4.95 m (16.2')-6.3 m (20.7'); >6.8 m (22.3')
		8:1	0-1.6 m (5.25'); >3.5 m (11.5')

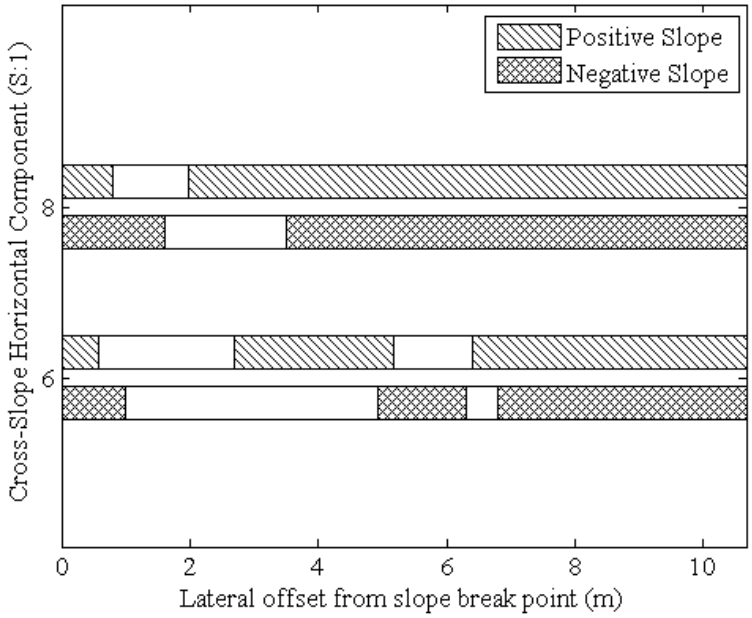

Figure 7.13 Preliminary guideline for the placements of Midwest Guardrail System on roadside slopes.

7.4. PLACEMENT GUIDELINE FOR MODIFIED THRIE-BEAM SYSTEM

Override and underride limits obtained for modified Thrie-beam guardrail are 830 mm (32.7″) and 315 mm (12.4″), respectively. As shown in Figure E.9 to Figure E.16 in appendix E, these limits were superimposed on the vehicle trajectory data to quantify performance of modified Thrie-beam barrier on the selected roadside and median slopes as a function of barrier offset. The acceptable lateral offset locations obtained from these figures were used to develop preliminary guidelines for the placement of modified Thrie-beam system on the selected median and roadside slopes. Preliminary guidelines for its placements on median slopes are summarized in Table 7.5 and Figure 7.14. Similarly, Table 7.6 and Figure 7.15 summarize the recommended placement locations for modified Thrie-beam guardrail on roadside slopes. Due to the presence of wider blockouts, wider Thrie-beam rail, and the highest rail mounting height, this guardrail performed satisfactorily for widest ranges of vehicle impact heights compared to all the

systems investigated in this study. Thus the system was found as the most suitable system for the placements on roadside and median slopes. However, as can be seen from Table 7.6 and Figure 7.14, when placed as a single system to protect the vehicle traveling from both directions, a dual-sided modified Thrie-beam barrier is not suitable for the placement on a 12.2 m (40 ft) wide median with 6:1 slope. The system however can be placed on a 6:1 negative roadside slope within 1.1 m (3.6') and anywhere beyond 4.88 m (16') from the slope break point. Thus instead of one dual-sided barrier, two single-sided guardrail systems can be placed near shoulder edge on both the foreslope and backslope of a 12.2 m (40 ft) wide median with 6:1 slope. The modified Thrie-beam guardrail can be effectively placed anywhere on an 8:1 positive roadside slope. On a 6:1 positive roadside slope vehicle override is expected only when the system is placed from 5.5 m (18') to 6.1 m (20') from the slope break point.

7.5. PLACEMENT GUIDELINES FOR MODIFIED WEAK POST W-BEAM SYSTEM

Override and underride limits obtained for modified weak post W-beam guardrail are 757 mm (29.8″) and 421 mm (16.5″), respectively. These limits were superimposed on vehicle trajectory data in Figure E.17 to Figure E.24 to determine acceptable lateral placement locations for the modified weak post W-beam system on roadside and median slopes. Preliminary guidelines for its placement on median slopes are summarized in Table 7.7 and Figure 7.16. Similarly, preliminary guidelines for the placements on roadside slopes are summarized in Table 7.8 and Figure 7.17. Although the system has a relatively high rail mounting height, absence of a blockout makes it less effective in successfully redirecting an airborne pickup. Relatively low override limit makes the system less effective, compared to an MGS and modified Thrie-beam guardrail system, for the placements on median and roadside slopes. Therefore, a narrower range of lateral offset locations can be recommended for the placements of this system on slopes.

Table 7.5 Preliminary guideline for the placements of modified Thrie-beam system on median slopes.

Median Width	Shoulder Width	Ditch Width	Slope	Acceptable barrier offset locations from slope break, X, "m" (ft)
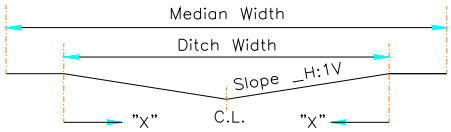				
23.2 m (76 ft)	1.2 m (4')	20.7 m (68')	6:1	0-1.12 m (3.67'); 7.31 m(24')-7.54 m(24.75'); 9.83 m (32.25')-C.L.
			8:1	0-1.8 m (5.91'); 6.5 m(21.33')-7.62 m (25'); 9.62 m (31.5')-C.L.
	1.8 m (6')	19.5 m (64')	6:1	0-1.09 m (3.58'); 6.8 m(22.3')-6.95 m(22.83'); 9.2 m (30.25')-C.L.
			8:1	0-1.65 m (5.41'); 5.94 (19.5') m-7.05 m (23.08'); 8.98 m (29.42')-C.L.
18.3 m (60 ft)	1.2 m (4')	15.9 m (52')	6:1	0-0.84 m(2.75'); 5.13 m(16.83')-5.5 m(18'); 7.47 m(24.5')-C.L.
			8:1	0-0.97 m(3.17'); 3.81 m(12.5')-5.64(18.5'); 7 m(23')-C.L.
	1.8 m (6')	14.6 m (48')	6:1	6.96 m (22.83') –C.L.
			8:1	0-0.33 m (1.08'); 3.35 m(11')-5 m (16.4'); 6.53 m (21.41')- C.L.
12.2 m (40 ft)	1.2 m (4')	9.8 m (32')	6:1	Not Recommended
			8:1	1.45 m (4.75') -1.7 m (5.58'); 4.42 m (14.5') -C.L.
	1.8 m (6')	8.5 m (28')	6:1	Not Recommended

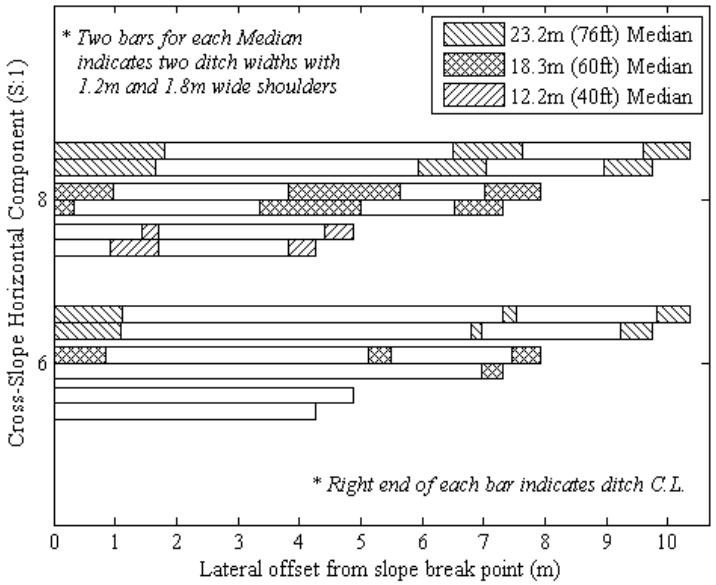

Figure 7.14 Preliminary guideline for the placements of modified Thrie-beam barrier on V-shaped median slopes.

Table 7.6 Preliminary guideline for the placements of modified Thrie-beam guardrail on roadside slopes.

Barrier Type	Case	Slope	Acceptable guardrail offset locations from slope break, X, "m" (ft)
Modif-ied Thrie-beam Guardrail System	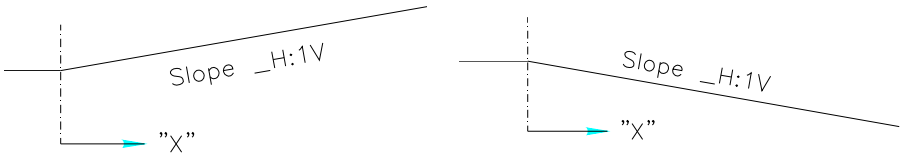 Roadside Positive Slope		Roadside Negative Slope
	Positive Roadside slope	6:1	0-5.5 m (18'); >6.1 m (20')
		8:1	Anywhere on the slope
	Negative Roadside slope	6:1	0-1.1 m (3.6'); >4.88 m (16')
		8:1	0-1.85 m (6'); >3.28 m (10.75')

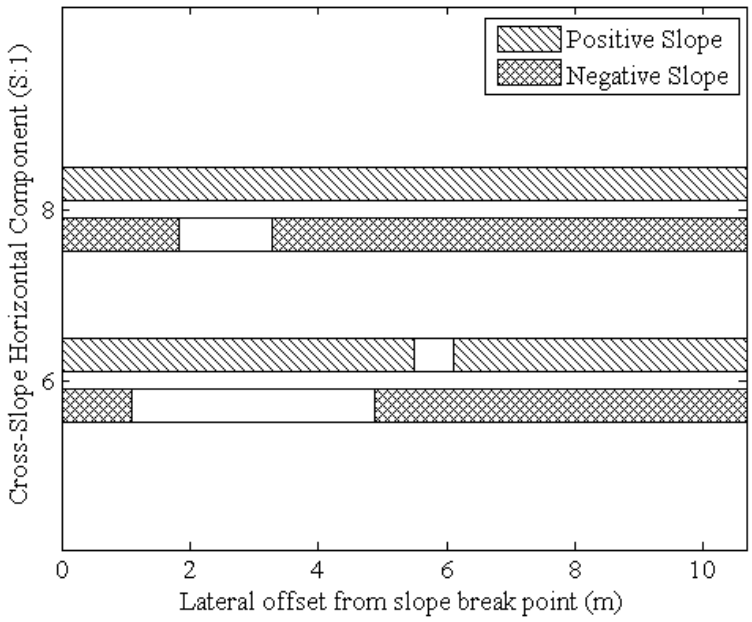

Figure 7.15 Preliminary guideline for the placements of modified Thrie-beam guardrail on roadside slopes.

Table 7.7 Preliminary guideline for the placements of modified weak-post W-beam barrier on median slopes.

Barrier Type	Median Width	Shoulder Width	Ditch Width	Slope	Acceptable barrier offset locations from slope break, X, "m" (ft)
Modified weak-post W-beam Guardrail System	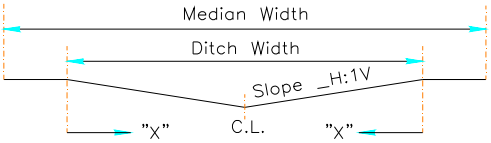				
	23.2 m (76 ft)	1.2 m (4')	20.7 m (68')	6:1	10.1 m (33') - C.L.
				8:1	0-0.86 m (2.83'); 7.19 m (23.58')-7.32 m (24'); 10 m (32.8') - C.L.
		1.8 m (6')	19.5 m (64')	6:1	0-0.62 m (2.0'); 9.5 m (31.16')-C.L.
				8:1	0-0.86 m (2.83'); 9.4 m (31.83') -C.L.
	18.3 m (60 ft)	1.2 m (4')	15.9 m (52')	6:1	7.82 m (25.67') –C.L.
				8:1	0-0.3 m (1'); 4.82 m (15.83') -5 m (16.41'); 7.52 m (24.67') -C.L.
		1.8 m (6')	14.6 m (48')	6:1	7.24 m (23.75')- C.L.
				8:1	4.26 m (14')-4.52 m (14.83'); 7.0 m (23')-C.L.
	12.2 m (40 ft)	1.2 m (4')	9.8 m (32')	6:1	Not Recommended
				8:1	4.8 m (15.75') - C.L.
		1.8 m (6')	8.5 m (28')	6:1	Not Recommended
				8:1	4.17 m (13.67') - C.L.

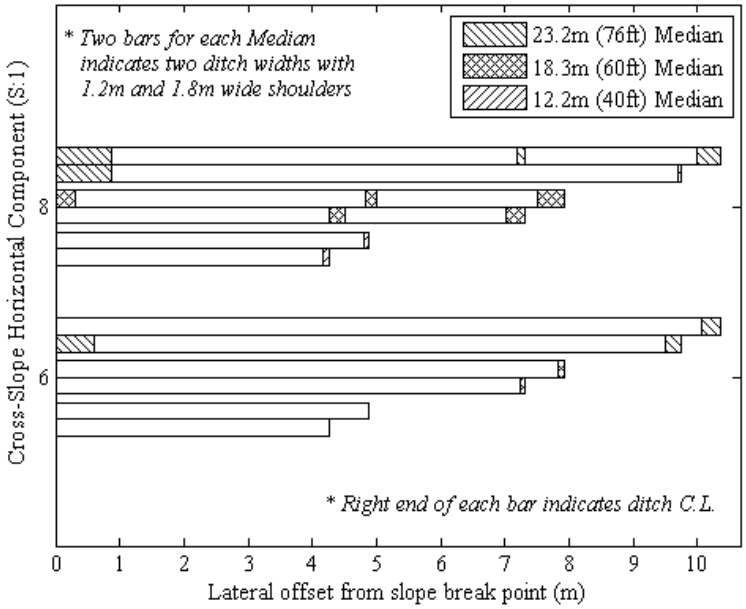

Figure 7.16 Preliminary guideline for the placements of modified weak-post W-beam barrier on V-shaped median slopes.

Table 7.8 Preliminary guideline for the placement of modified weak-post W-beam guardrail on roadside slopes.

Barrier Type	Case	Slope	Acceptable guardrail offset locations from slope break, X, "m" (ft)
Modified weak-post W-beam Guardrail System	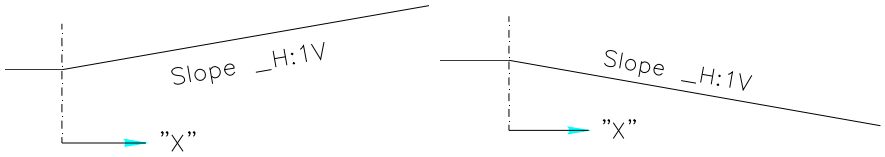 Roadside Positive Slope Roadside Negative Slope		
	Positive Roadside slope	6:1	0-0.56 m (1.83'); 2.7 m (8.83')-4 m (13.16'); > 7 m (23.25')
		8:1	0-0.66 m (2.17'); 2.1 m (6.9')-5.41 m (17.75'); >6 m (19.75')
	Negative Roadside slope	6:1	0-0.62 m (2.0'); 5.30 m (17.4')- 6.2 m (20.33'); >6.9 m (22.67')
		8:1	0-0.86 m (2.83'); >4.11 m (13.5')

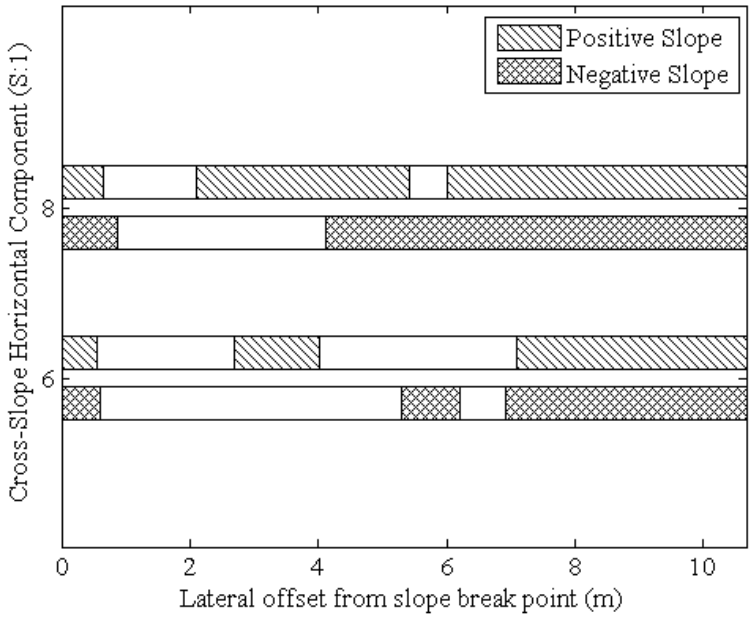

Figure 7.17 Preliminary guideline for the placements of modified weak-post W-beam guardrail on roadside slopes.

7.6. PLACEMENT GUIDELINE FOR BOX-BEAM SYSTEM

Override and underride limits obtained for Box-beam guardrail system are 764 mm (30″) and 384mm (15″), respectively. These limits were superimposed on vehicle trajectory data in Figure E.25 to Figure E.32 to determine acceptable lateral placement locations for Box-beam system on selected slope configurations. Preliminary guidelines for its placements on median and roadside slopes are summarized in Table 7.9, Figure 7.18, Table 7.10, and Figure 7.19. Lower rail base height coupled with readily detachable post-rail connection makes the box-beam system more effective in containing vehicles with compressed suspension. The lower underide limit allowed recommending wider ranges of acceptable lateral offset locations for the box-beam system compared to the modified G4(1S) and modified weak-post W-beam systems.

Table 7.9 Preliminary guideline for the placement of box-beam system on median slopes.

Barrier Type	Median Width	Shoulder Width	Ditch Width	Slope	Acceptable barrier offset locations from slope break, X, "m" (ft)
Box-beam Barrier	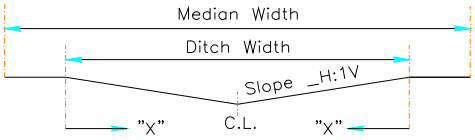				
	23.2 m (76 ft)	1.2 m (4')	20.7 m (68')	6:1	10 m (32.9') –C.L.
				8:1	0-.95 m (3.16'); 7 m (23')-7.4 m (24.25'); 9.86 m (32.3') -C.L.
		1.8 m (6')	19.5 m (64')	6:1	0-0.64 m(2.1'); 9.35 m (30.67')-C.L.
				8:1	0-0.95 m (3.16');6.5 m(21.33')-6.75 m(22.16'); 9.25 m (30.33')-C.L.
	18.3 m (60 ft)	1.2 m (4')	15.9 m (52')	6:1	0-0.3 m (1.0'); 7.7 m (25.3')-C.L.
				8:1	0-0.41 m (1.33'); 4.75 m (15.58')-5.2 m (17.0'); 7.4 m (24.25')-C.L.
		1.8 m (6')	14.6 m (48')	6:1	7.14 m (23.4')-C.L.
				8:1	4.1 m (13.41')-4.7 m(15.41'); 6.8 m (22.3')-C.L.
	12.2 m (40 ft)	1.2 m (4')	9.8 m (32')	6:1	Not Recommended
				8:1	4.66 m (15.25') -C.L.
		1.8 m (6')	8.5 m (28')	6:1	Not Recommended
				8:1	4.0 m (13.1') –C.L.

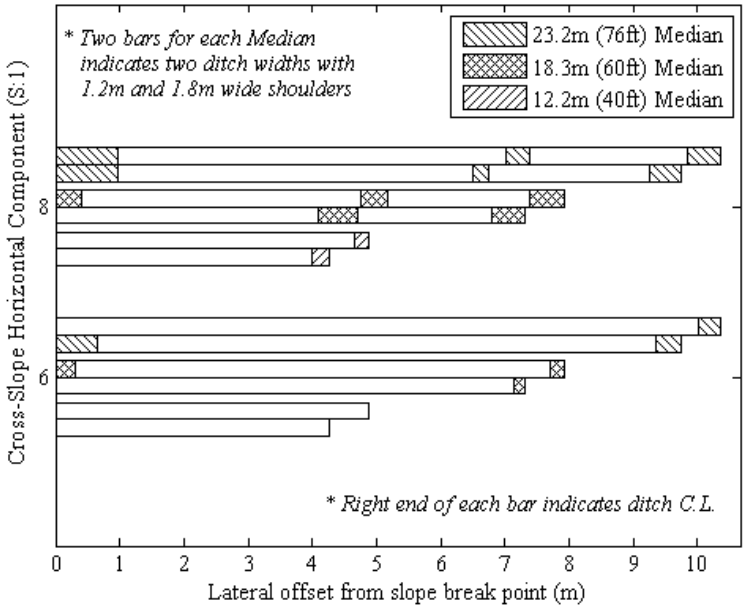

Figure 7.18 Preliminary guideline for the placements of box-beam system on V-shaped median slopes.

Table 7.10 Preliminary guideline for the placement of box-beam system on roadside slopes.

Barrier Type	Case	Slope	Acceptable guardrail offset locations from slope break, X, "m" (ft)
Box-beam Guardrail System	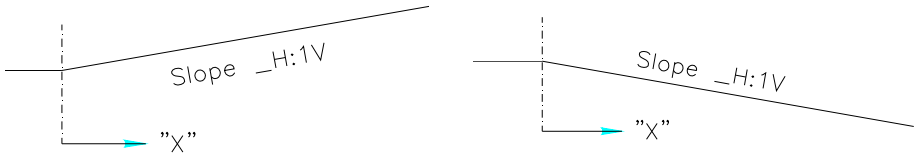 Roadside Positive Slope Roadside Negative Slope		
	Positive Roadside slope	6:1	0-0.79 m (2.58'); 1.78 m (5.83')-4.23 m(13.83'); >7.0 m(23.0')
		8:1	0-1.21 m (4'); >1.7 m (5.58')
	Negative Roadside slope	6:1	0-.64 m (2.1'); >5.3 m (17.4')
		8:1	0-0.95 m (0-3.1'); >4.0 m (13.1')

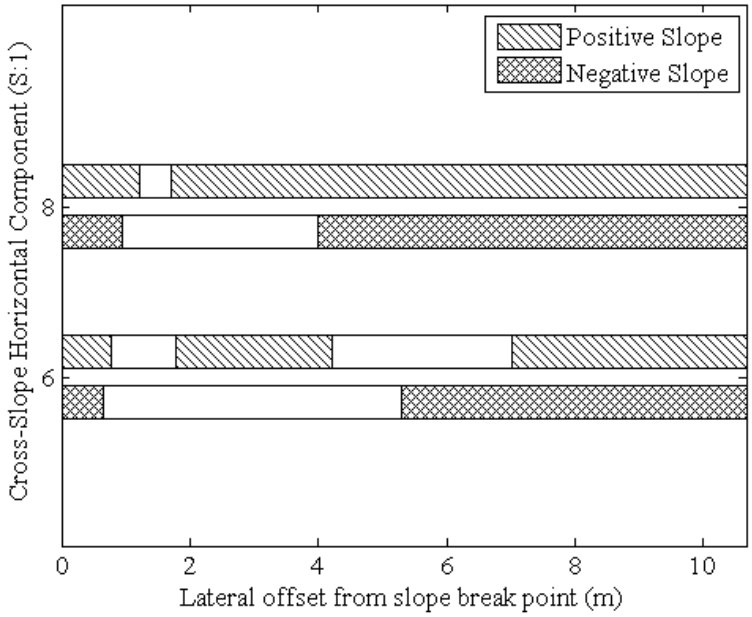

Figure 7.19 Preliminary guideline for the placements of box-beam system on roadside slopes.

7.7. CONCLUSIONS

Preliminary guidelines for the placement of barriers on selected roadside and median slopes were developed in this study using CARSIM generated vehicle trajectory data and acceptable vehicle impact height region for the barriers obtained using FE simulations. CARSIM utilizes computationally efficient multi-rigid body dynamic analysis technique to quantify the vehicle trajectory along ditch sections. There are some shortcomings to this approach. Depending on the slope configuration, the vehicle on a slope may become airborne upon entering the ditch, thus causing its suspension to extend (i.e., rebound). After some period of free flight, the vehicle eventually re-contacts the ground, resulting in a sudden compression (i.e., jounce) of the suspension. The vehicle frame undergoes some twists as it re-contacts the ground which dampens some of the reaction forces generated from the tire to ground impact. The overly rigid vehicle models used in CARSIM fails to capture this frame twist causing the vehicle rise higher than is expected

after the re-contact. Hence, the CARSIM predicted trajectory of the vehicle after the jounce on a depressed median is expected to be higher compared to an actual vehicle trajectory. This can produce a conservative guideline for the placement of barrier on the backslope of a depressed median. Vehicle model used in FE simulations, on the other hand, are more flexible and can capture the severe vehicle frame twists during a tire to ground contact after a free flight. Hence, to verify and refine the preliminary guidelines prepared using CARSIM generated trajectory, several acceptable and unacceptable cases on the guideline was simulated using LS-DYNA. The results of these simulations are presented in the next section.

8. VALIDATE AND REFINE THE PRELIMINARY GUIDELINES USING FE SIMULATIONS ON SLOPE

8.1. INTRODUCTION

The preliminary guidelines for the placement of barrier on slope, presented in the previous section, were developed based on the vehicle trajectory data obtained using a multi-rigid body dynamic analysis code (CARSIM) and the barrier performance limits obtained using a nonlinear FE analysis code (LS-DYNA). To verify, validate, and refine these guidelines, additional simulations were performed using LS-DYNA. These simulations captured the full encroachment event from departure of the vehicle off the traveled way through impact with the barrier. The total encroachment event is relatively long in duration and large computational times are required to capture both the encroachment and impact events using a single FE code. Hence, small number of cases with selected configurations of vehicle type, barrier type, barrier offset, and slope/ditch configuration were selected for the simulation. The matrix selected for the simulation included both the scenarios for which failure was expected and those for which successful containment was predicted. The terrain configurations simulated included vehicle encountering the barrier on a foreslope and on a backslope of the depressed median. Single dual-sided median barriers are generally used on V-shaped medians to protect errant vehicles traveling from either direction. To simulate these cases FE model of dual-sided systems were developed by adding extra rail and blockout elements to the single-sided guardrail models. The preliminary guidelines for guardrail/median barrier placement were refined and verified based on the results obtained from these simulations. This section discusses the cases selected for the comprehensive FE simulations and results obtained from these simulations. The section also presents the refined and finalized guidelines for the placements of traffic barriers on slope.

8.2. CASE SELECTION

As shown in Section 5, modified G4(1S) guardrail system has the lowest override limit compared to other systems investigated in this study. Similarly, modified G4(1S) w-beam, MGS, and modified weak post W-beam systems have high underride limits. Hence, the placements of modified G4(1S) system at offset locations controlled by its override and underride limits can be considered as worst case scenarios for a given slope. The preliminary guideline developed for the modified G4(1S) system was therefore thoroughly investigated using LS-DYNA simulations. Table 8.1 and Figure 8.1 shows the simulation cases selected to investigate the guidelines for the placement of modified G4(1S) system. The letter "P" in the case names indicates that the barrier is expected to pass the safety evaluation criteria set forth in report 350. The letter "F" indicates that the failure is expected according to the preliminary guideline. After investigating the vehicle trajectory data it was concluded that for negative (fill) roadside slopes and depressed medians, acceptable lateral offset areas near the base of the ditch are controlled by barrier underride limit, while the area near the edge of the shoulder is controlled by barrier override limit. Hence in the simulations on negative roadside slope and depressed medians, the small passenger car impacted the barrier at lateral offset locations near the center of the ditch and the pickup truck impacted the barrier at lateral offset locations near the shoulder edge. The first five cases in the table were selected for the roadside cases with negative cross-slope and the depressed median cases in which guardrails will be placed on both sides of the ditch. The guideline for the placement of a single dual-sided barrier on a depressed median, shown in Figure 8.1, is applicable for both the foreslope and backslope of the ditch. Cases P8 and P9 selected for the simulation included the lateral offsets of the barrier, controlled by its underrride limit, on the foreslope and backslope, respectively, of a 15.8 m (52 ft) wide ditch section.

Table 8.1 LS-DYNA simulation matrix for modified G4(1S) system on slope.

Case	Barrier Type	Terrain Type	Ditch Width	Slope	Offset from Slope Break	Vehicle Type	Impact Speed (km/h)	Impact Angle (deg.)	Guideline Predi-ction
P1	Modified G4(1S)	Median/ Roadside (Negative Slope)	14.63 m (48')	8:1	0.62 m (2.0') on foreslope	Chevy 2500	100	25	Pass
F2				8:1	1 m (3.28') on foreslope	Chevy 2500	100	25	Fail
P3			19.5 m (64')	6:1	0.45 m (1.5') on foreslope	Chevy 2500	100	25	Pass
F4				6:1	0.62 m (2.0') on foreslope	Chevy 2500	100	25	Fail
F5			--	6:1	9 m (29.5') on foreslope	Chevy 2500	100	25	Fail
F6		Median	8.54 m (28')	6:1	8.54 m (28') on backslope	Chevy 2500	100	25	Fail
F7			9.76 m (32')	6:1	9.76 m (32') on backslope	Chevy 2500	100	25	Fail
P8			20.7 m (68')	6:1	10.0 m (33') on foreslope	Geo Metro	100	20	Pass
P9					10.7 m (35') on backslope	Geo Metro	100	20	Pass

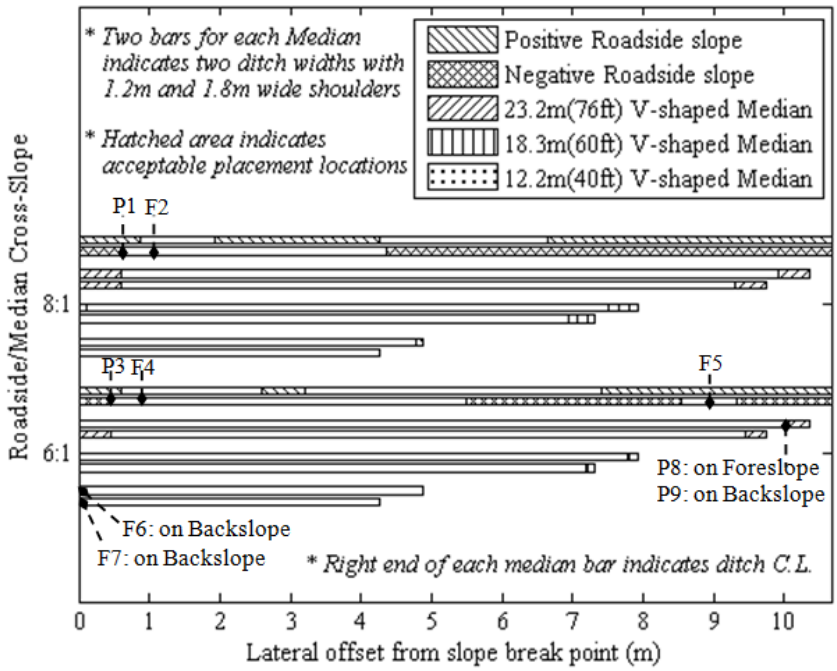

Figure 8.1 Simulation cases selected for modified G4(1S) system.

The preliminary guidelines were developed using vehicle trajectory data generated by CARSIM. Depending on the slope configuration, the vehicle traveling along a slope may become airborne upon entering the ditch, thus causing its suspension to extend (i.e., rebound). After some period of free flight, the vehicle eventually re-contacts the ground, resulting in a sudden compression (i.e., jounce) of the suspension. The vehicle frame undergoes some twists as it re-contacts the ground which dampens some of the reaction forces generated during the tire-ground impact. The overly rigid vehicle models used in CARSIM fails to capture this frame twist causing the vehicle rise higher than is expected after the re-contact. Hence, CARSIM generated trajectory of the vehicle on the backslope of a ditch is expected to be higher compared to its actual trajectory. In the preliminary guidelines for the placement of a single barrier on depressed medians, acceptable lateral offset area near a shoulder edge (e.g. cases F6 and F7) is controlled by the trajectory of the pickup on the backslope of the ditch. Thus the guidelines for these cases are expected to be overly conservative. Hence, two failure cases (case F6 and F7) were selected for further study where the pickup traveled both the foreslope and backslope of a depressed median before impacting the barrier placed on the opposite end of the ditch. For all the simulation cases selected for modified G4(1S) system, the encroachment speed and angle for the 2000-kg pickup were 100 km/h (62 mph) and 25 degrees, respectively. Similarly, the encroachment speed and angle for 820-kg Geo Metro car were 100 km/h (62 mph) and 20 degrees, respectively. These conditions conformed to the impact conditions specified for NCHRP report 350 Test Level 3 (TL-3).

As shown in Section 5, modified weak post W-beam guardrail system has the highest underride limit among the systems investigated in this study. Hence, three simulations cases were selected to investigate the preliminary placement guidelines controlled by the underride limit of this system. Table 8.2 and Figure 8.2 shows the simulation cases selected for the study. The trajectory envelopes developed in Section 7 showed that the underride limit of a given barrier controls the acceptable lateral offset areas near shoulder edge for a positive (cut) roadside slope and near the ditch bottom for

a depressed median. Hence, one case (Case P10) was selected where the small car impacted a single-sided guardrail placed on positive roadside slope near the shoulder edge. In the second case (Case P11), the small car impacted a dual-sided modified weak post W-beam barrier placed near the ditch bottom. Third case (Case P12) was selected to verify the recommended placement locations controlled by underride limit on a negative (fill) roadside slope. In this simulation, a small car impacted a single-sided modified weak-post W-beam guardrail placed on a 6:1 negative roadside slope at a lateral offset of 6.2 m (20') from slope break point. For all these cases, the small car exited the shoulder edge at a speed and angle of 100 km/h (62 mph) and 20 degrees, respectively.

8.3. LS-DYNA SIMULATIONS ON SLOPE

8.3.1. Case P1 and F2

For simulation cases P1 and F2, 2000-kg pickup model impacted the modified G4(1S) guardrail placed on a negative 8:1 roadside slope at two different offset locations near the slope break point. According to the preliminary guideline, the guardrail placed on the lateral offset location selected for case P1 is expected to successfully contain the vehicle. For lateral offset location selected for case F2 vehicle override is expected. Vehicle model, in the LS-DYNA simulation of off-road encroachments, should be initialized before exiting the roadway to minimize the effect of oscillation generated from initial tire to ground contact due to the sudden application of gravity load. In this study, the initialization was done by allowing the vehicle to travel some distance on flat terrain before reaching the slope break point. The tire-ground contact force and change in bumper top heights on the flat ground were monitored to determine a reasonable initialization time of 0.15 sec. In LS-DYNA simulation of cases P1 and F2, the pickup exited the road way at 0.15 sec at a speed and angle of 100 km/h (62 mph) and 25 degrees, respectively. The sequential images obtained from these simulations are shown in Figure 8.3. As can be seen from the figure, the pickup in case P1, impacted the

modified G4(1S) system at 0.18 sec with its bumper top below the guardrail override limit and was contained and redirected by the guardrail as predicted in the preliminary guideline. Similarly, in the simulation of case F2, the pickup overrode the system as expected. Thus results from both simulations matched preliminary guideline predictions.

Table 8.2 LS-DYNA simulation matrix for modified weak post W-beam system on slope.

Case	Barrier Type	Terrain Type	Ditch Width	Slope	Offset from Slope Break	Vehicle Type	Impact Speed (km/h)	Impact Angle (deg.)	Guideline Predi-ction
P10	Modified Weak post W-beam	Roadside (Positive Slope)	--	6:1	0.56 m (1.83') on Foreslope	Geo Metro	100	20	Pass
P11		Median	15.9 m (52')	6:1	8.03 m (26.3') on Backslope	Geo Metro	100	20	Pass
P12		Roadside (Negative Slope)	--	6:1	6.2 m (20') on Foreslope	Geo Metro	100	20	Pass

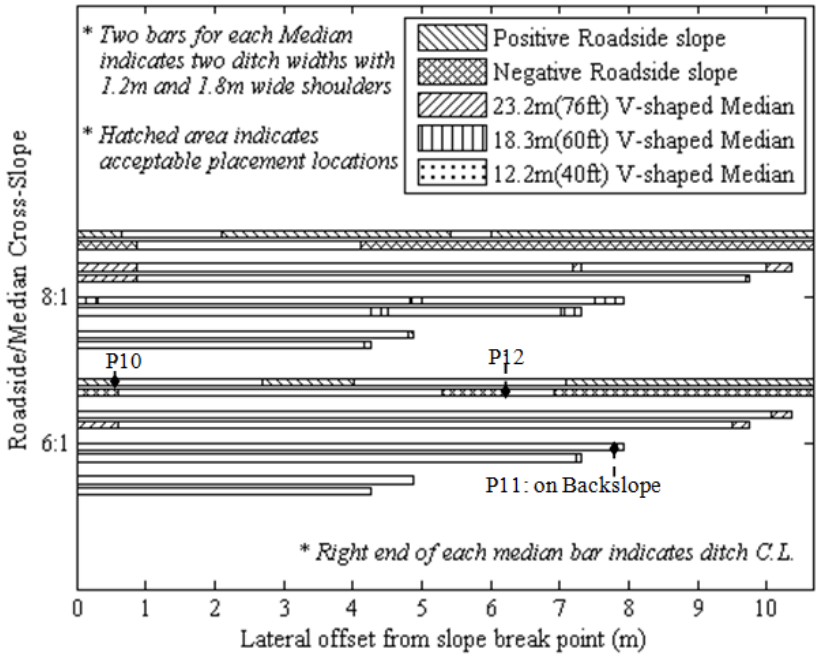

Figure 8.2 Simulation cases selected for modified weak post W-beam system.

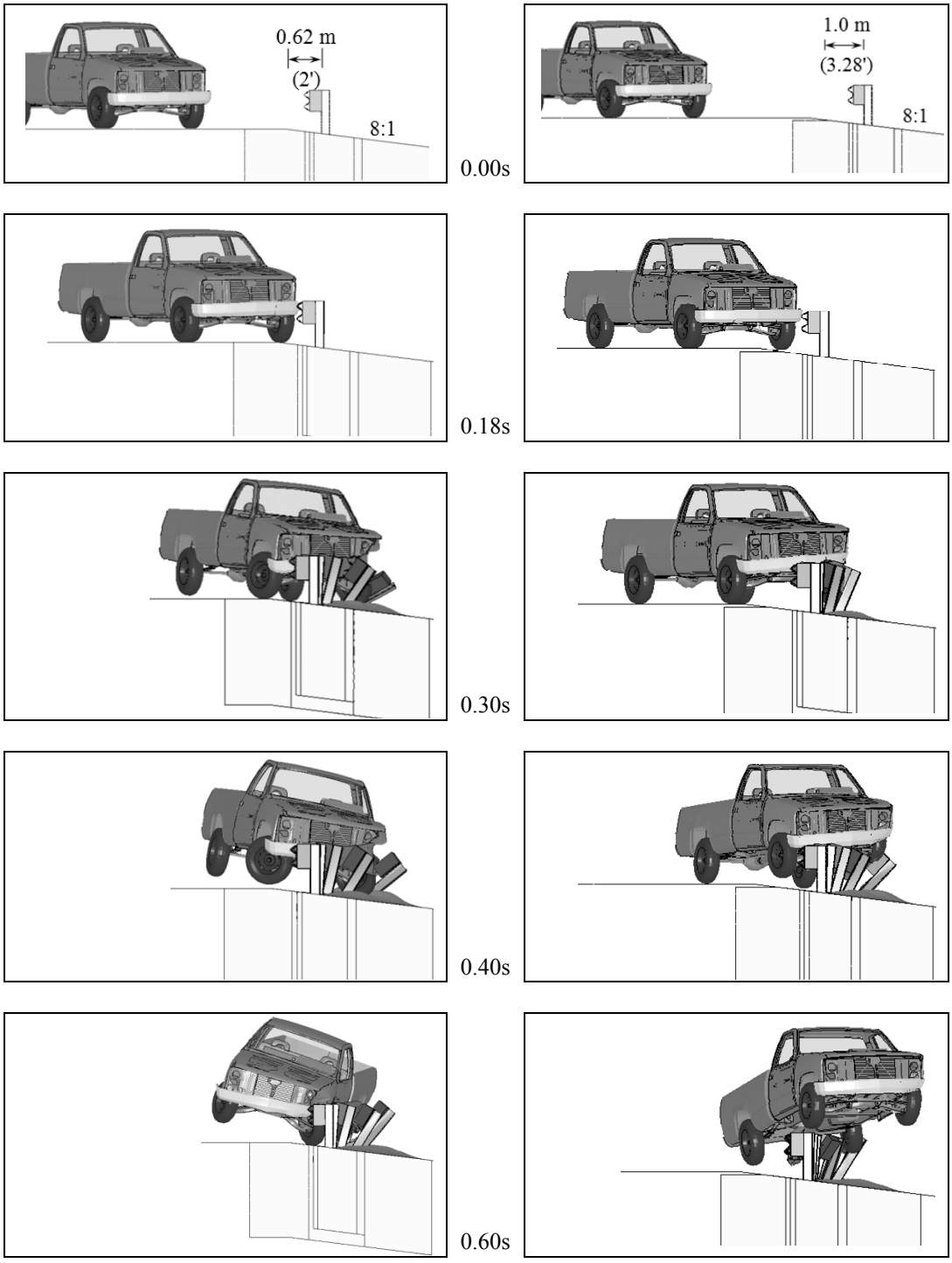

(a) Case: P1 (b) Case: F2

Figure 8.3 Sequential images obtained from the simulations of Case P1 and F2.

8.3.2. Case P3 and F4

In the simulation cases P3 and F4, the 2000-kg pickup impacted the modified G4(1S) system placed on a 6:1 negative roadside slope at two different lateral offset locations near slope break point. Figure 8.4 shows sequential images obtained from these simulations. As predicted in the preliminary guideline the pickup was contained and redirected in the simulation of case P3. Similarly, as predicted in the guideline, the pickup overrode the guardrail system in the simulation of case F4.

8.3.3. Case F5

In the simulation of case F5, the pickup traveled 9.0 m (29.5') off-road on a negative 6:1 roadside slope at a speed and angle of 100 km/h and 25 degrees, respectively, before impacting a single-sided modified G4(1S) system. The Figure 8.5 compares the trajectories of the pickup obtained from the LS-DYNA and CARSIM simulations. As can be seen from the figure, bumper top height at the impact location obtained from LS-DYNA was slightly higher compared to that obtained from CARSIM. According to the preliminary guideline prepared using CARSIM trajectories, vehicle in this simulation should override the system. Yet, the guardrail in LS-DYNA simulation was able to successfully contain and redirect the vehicle. The sequential images obtained from this simulation are shown in Figure 8.6. The override limit used to develop preliminary guideline was determined considering the changes in vehicle bumper height along the slope. The angular orientation of the vehicle associated with its trajectory on slope was not considered during these analyses. As shown in Figure 8.6, vehicle in the simulation impacted the guardrail above its override limit. However, the vehicle was successfully contained as it impacted the guardrail with around 10 degrees of negative pitch. Thus the selected placement location can be considered acceptable.

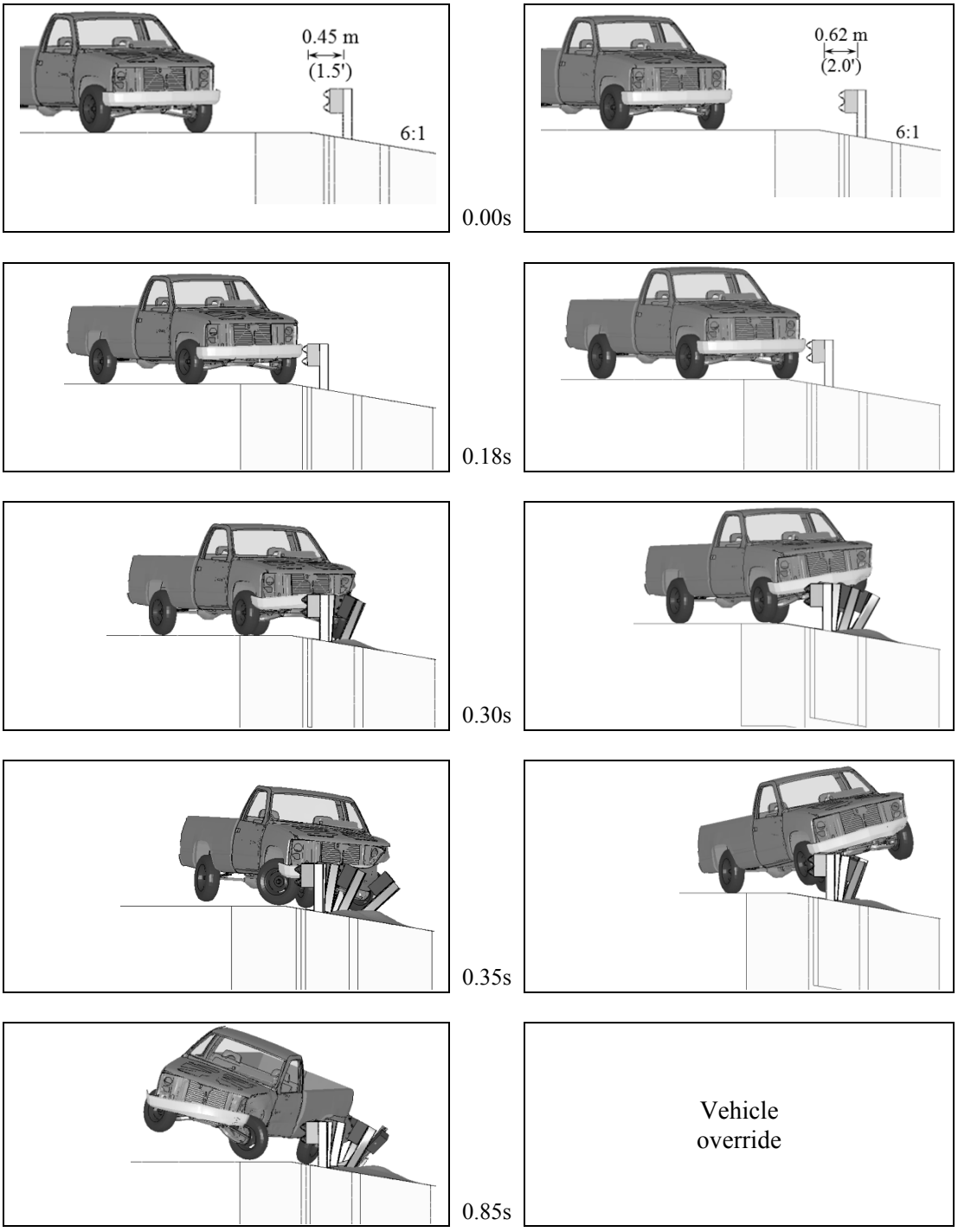

(a) Case: P3 (b) Case: F4

Figure 8.4 Sequential images obtained from the simulations of Case P3 and F4.

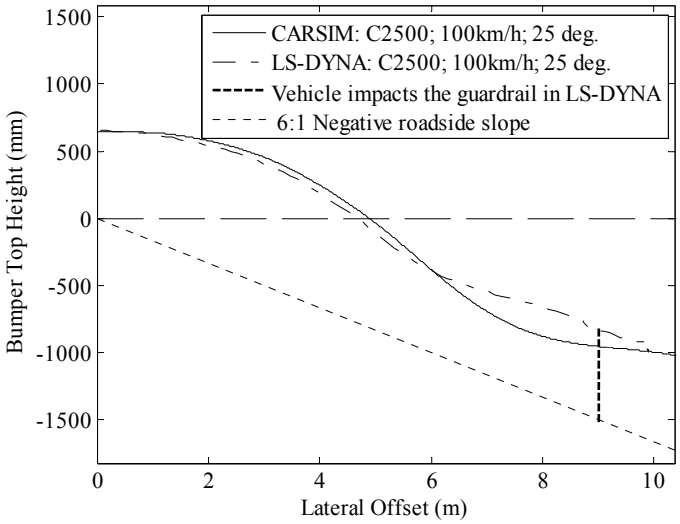

Figure 8.5 LS-DYNA and CARSIM generated trajectories of the C2500 pickup on 6:1 negative slope.

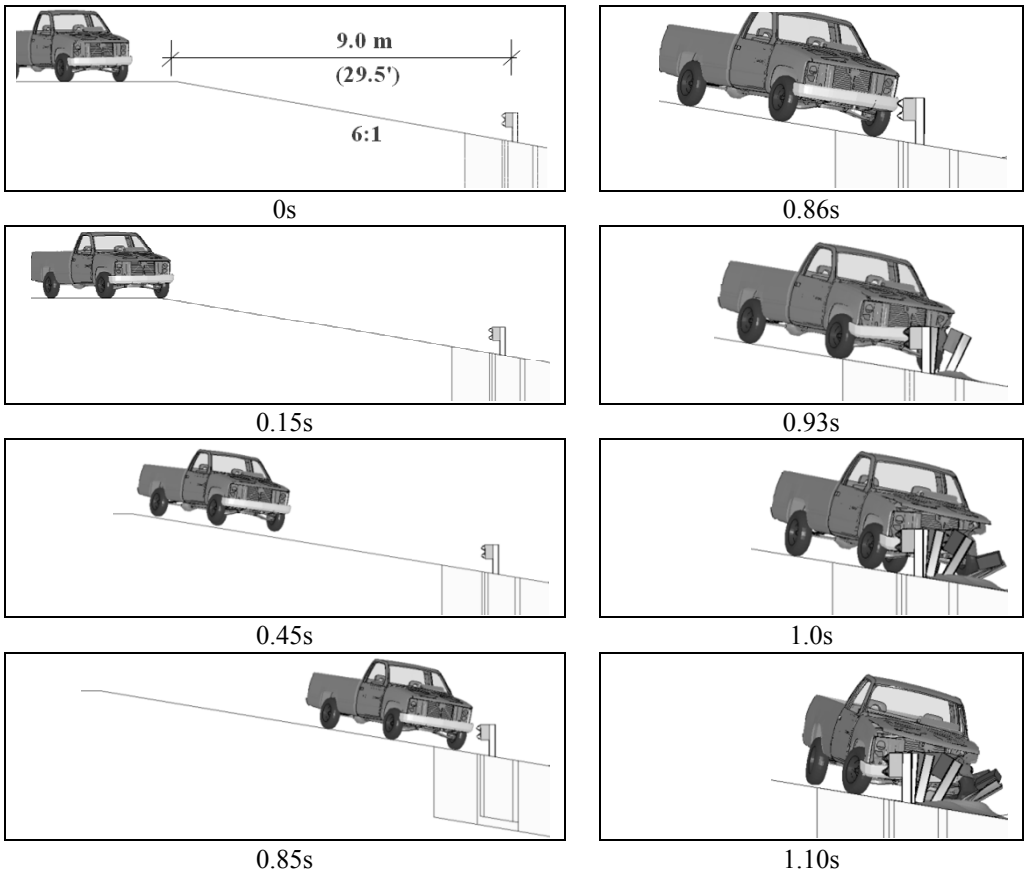

Figure 8.6 Sequential images obtained from the simulations of Case F5.

8.3.4. Case F6 and F7

For the placement of a single barrier on a depressed median, dual-sided barrier is used to protect the errant vehicle traversing from either direction. To simulate these cases, a dual-sided modified G4(1S) system model was developed by adding extra rail and blockout elements to the already developed and validated single-sided modified G4(1S) system. The detail of the 480,000 element FE model is shown in Figure 8.7.

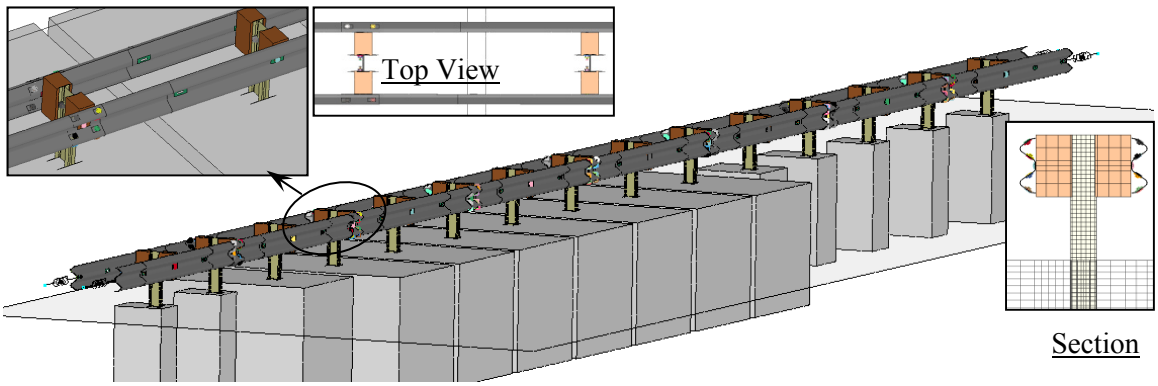

Figure 8.7 FE model for the dual-sided modified G4(1S) W-beam barrier used on median slopes.

In the LS-DYNA simulation of case F6 and F7, the C2500 pickup traveled both the foreslope and backslope of 8.54 m (28') and 9.76 m (32') wide ditches, respectively, before impacting a dual-sided modified G4(1S) system placed at the opposite end of the 6:1 slope ditch. Energy balance curves produced by LS-DYNA were analyzed as a measure of numerical stability of the simulation. As shown in Figure 8.8, the total energy curve did not vary more than 0.5% throughout the simulation for both cases. Figure 8.9 (a) and (b) compare the LS-DYNA and CARSIM generated trajectories of the pickup traversing these two ditches. These figures present relative heights of the bumper top assuming a reference line along the horizontal axis to identify the lateral offsets where a bumper height exceeds the barrier override limit. As can be seen from these

figures, CARSIM generated vehicle trajectories on the backslope of the ditch are more severe compared to those generated in LS-DYNA. The sequential images of the multi-rigid body pickup traversing two ditches obtained from CARSIM are shown in Figure 8.10. It can be seen that the vehicle traveling along the slope became airborne upon entering the ditch. After some period of free flight, the vehicle eventually re-contacted the ground. In reality, the vehicle frame undergoes some twists as it re-contacts the ground which dampens some of the reaction forces generated during the tire-ground impact. The overly rigid vehicle models used in CARSIM failed to capture this frame twist causing the vehicle rise higher than is expected after the re-contact. Vehicle models used in FE simulations, on the other hand, are more flexible and can capture the severe vehicle frame twists as shown in Figure 8.11. Figure 8.11 presents the sequential images obtained from the LS-DYNA simulations of case F6 and F7. These simulations captured the full encroachment event from departure of the vehicle off the traveled way through impact with the barrier. As can be seen from these figures, once the vehicle tires contacted the ground after the free flight, the more flexible FE vehicle model absorbed some portion of the energy through deformation which allowed it to rise lower than that predicted in CARSIM. According to the preliminary guidelines, the pickup should override the barrier placed at the end of the ditch for both case F6 and F7. Although the vehicle in LS-DYNA simulation seemed to rollover after impacting the system in case F6, it was successfully contained and redirected by the system placed at the end of the wider ditch (i.e. case F7). Hence, it was concluded that the CARSIM predicted vehicle trajectories produce an overly conservative guideline for the placement of barriers on the backslope of a depressed median. The FE simulations showed that for ditch widths greater than 8.54 m (28'), placement guidelines near the shoulder edge for a depressed median should be controlled by the trajectories of the pickup on the foreslope instead of those on the backslope of the ditch.

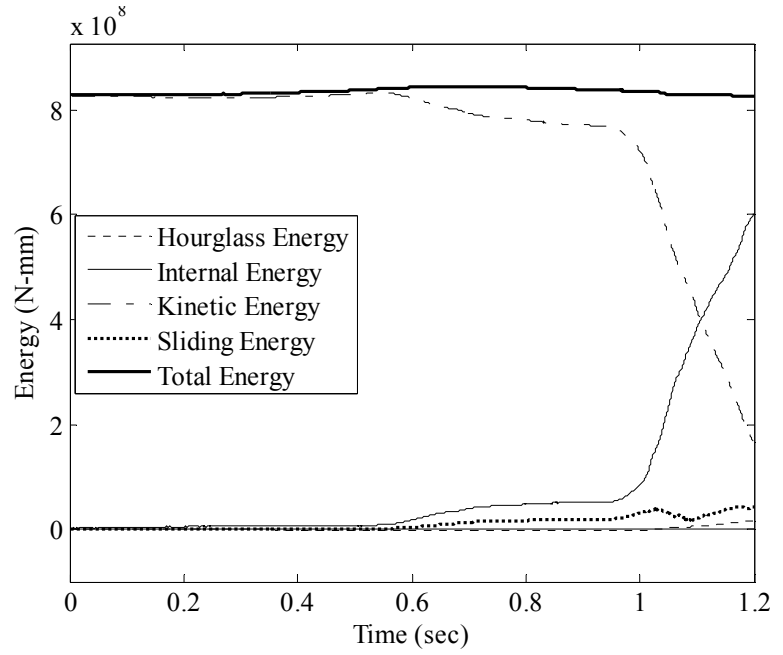

(a)

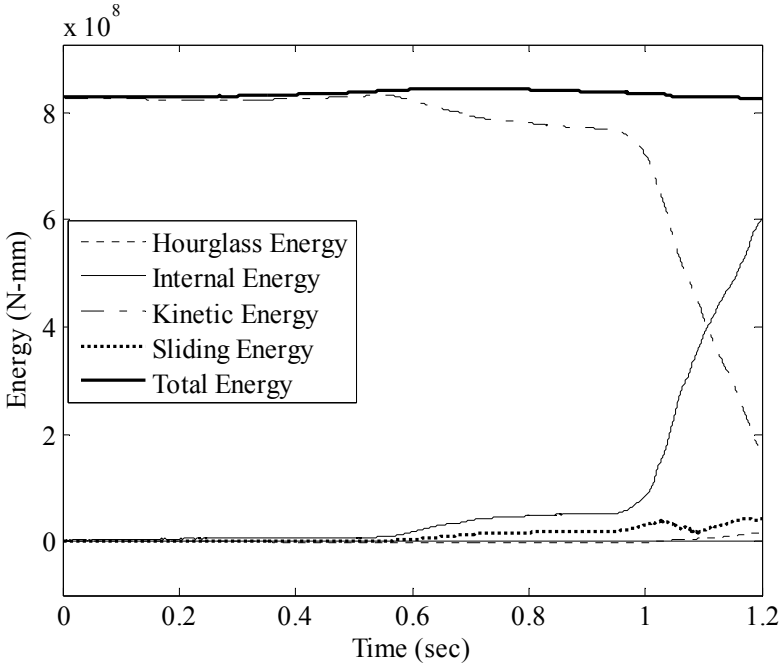

(b)

Figure 8.8 LS-DYNA generated energy balance curve for (a) Case F6 and (b) Case F7.

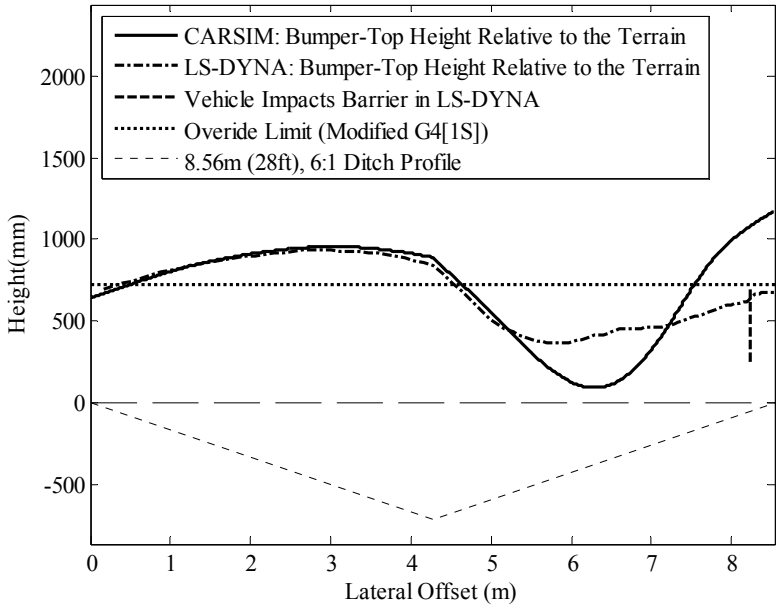

(a)

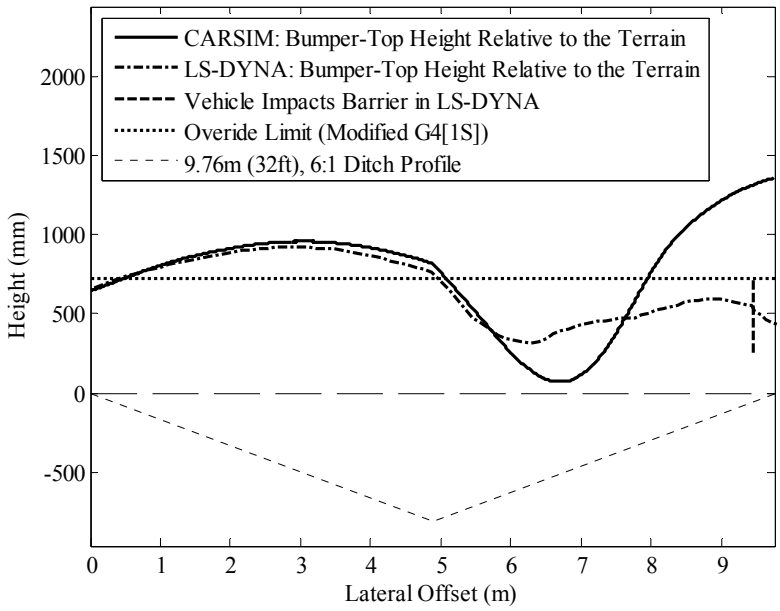

(b)

Figure 8.9 Comparison of LS-DYNA and CARSIM generated trajectories of the pickup traversing the depressed medians for (a) Case F6 and (b) Case F7.

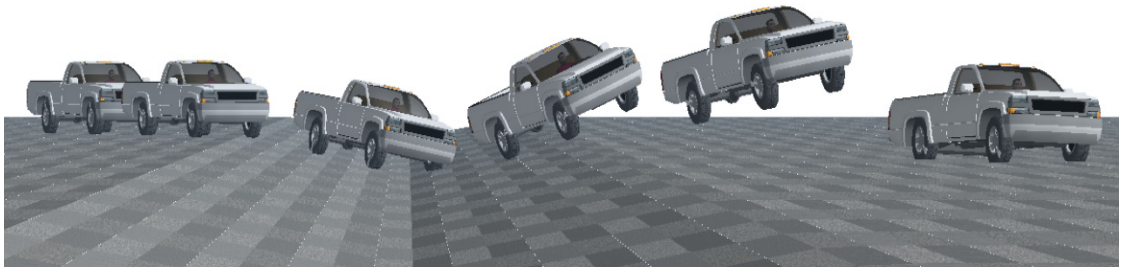

(a) 8.54 m (28') wide ditch

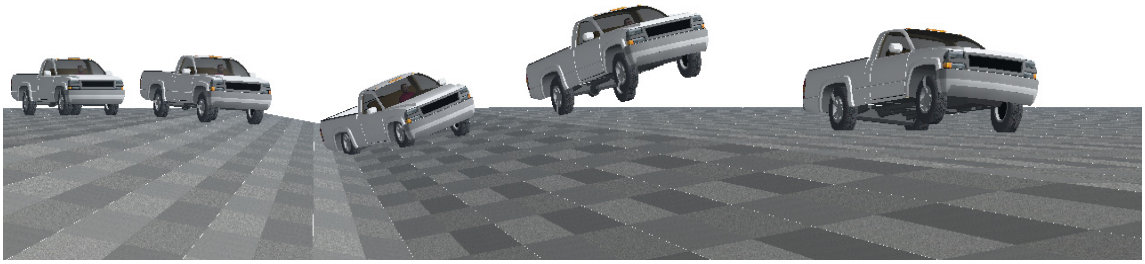

(b) 9.76 m (32') wide ditch

Figure 8.10 CARSIM generated sequential positions of the pickup traversing a 6:1 slope depressed median selected for (a) Case F6 and (b) Case F7.

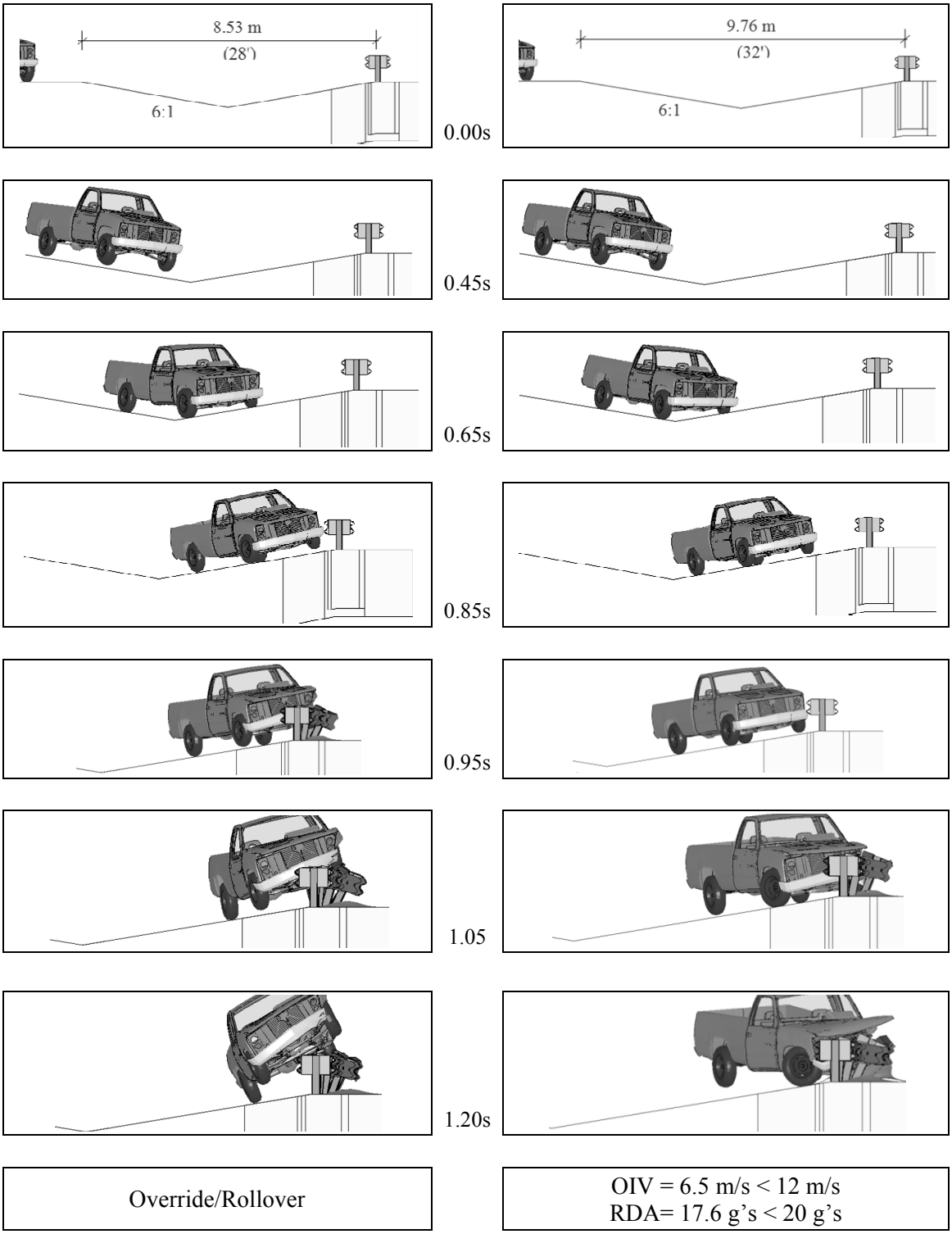

Figure 8.11 Sequential images obtained from the LS-DYNA simulation of (a) Case F6 and (b) Case F7.

8.3.5. Case P8 and P9

For simulation cases P8 and P9, a small passenger car impacted a dual-sided modified G4(1S) system placed on the foreslope and backslope, respectively, of a 20.7 m (68') wide ditch. For both cases the passenger car impacted the guardrail placed near the base of the ditch at a speed and angle of 100 km/h (62 mph) and 20 degrees, respectively. Energy balance curves produced by LS-DYNA, as shown in Figure 8.12, verifies the numerical stability of the simulation for both cases. According to the preliminary guideline, in each case the guardrail at the selected location should be impacted by the small car just above its underride limit and should be able to successfully contain the vehicle with no severe occupant injury. As shown in Figure 8.13, LS-DYNA generated trajectory of the small car traversing a ditch before impacting a barrier on the backslope closely matched the small car trajectory obtained from CARSIM. The sequential images and the occupant risk factors obtained from the LS-DYNA simulation of cases P8 and P9 are shown in Figure 8.14. It can be seen that for both cases the small car was successfully contained by the barrier. Also, the maximum occupant impact velocities (OIV) and ride down accelerations (RDA) were within acceptable limits. Outcomes of these simulations verify the preliminary guideline for the placement of barriers near underride limit controlled region (i.e. near the base of the ditch) on a depressed median. Among the systems studied, only the modified weak-post W-beam system with a higher underride limit has more potential for small car underride compared to the modified G4(1S) system. Hence, additional simulations were performed to verify the preliminary guidelines for the placements of modified weak-post W-beam barrier near its underride limit controlled region. Results of these simulations are discussed next.

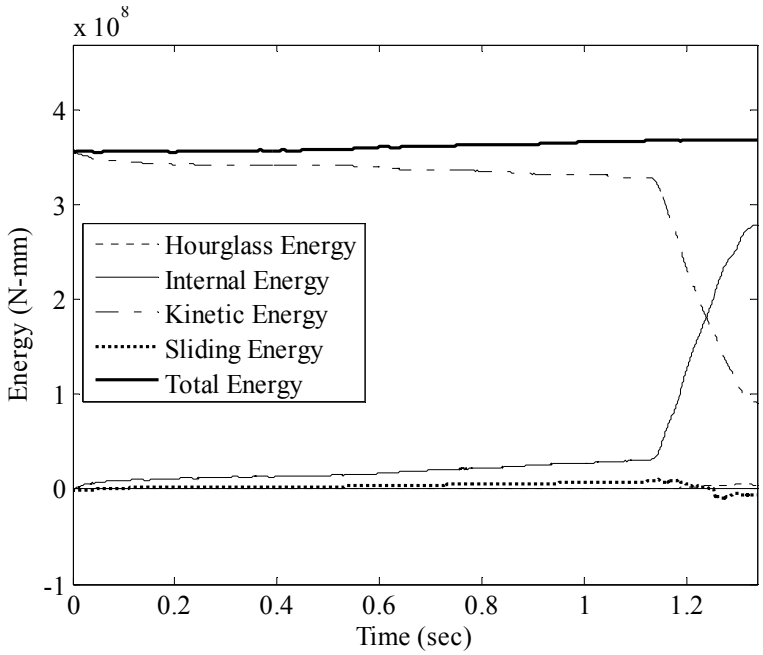

(a)

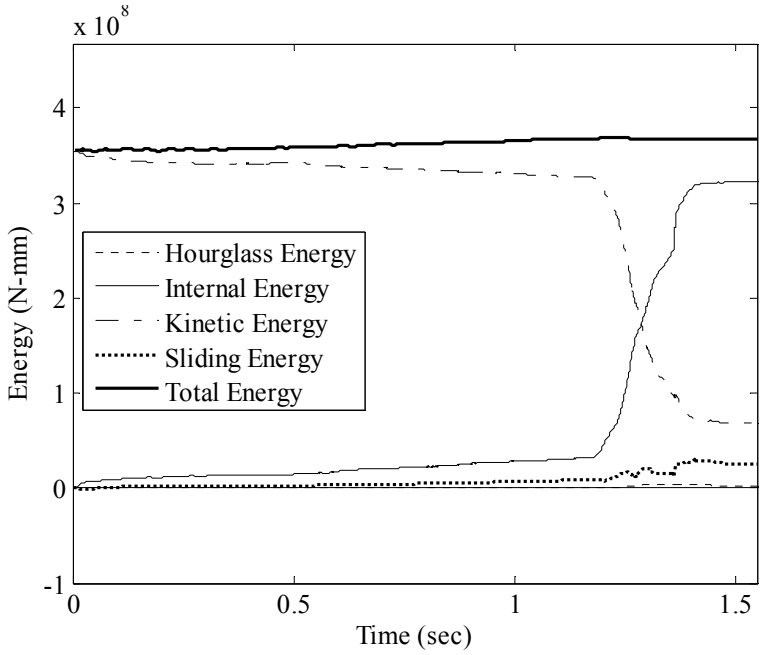

(b)

Figure 8.12 LS-DYNA generated energy balance curve for (a) Case P8 and (b) Case P9.

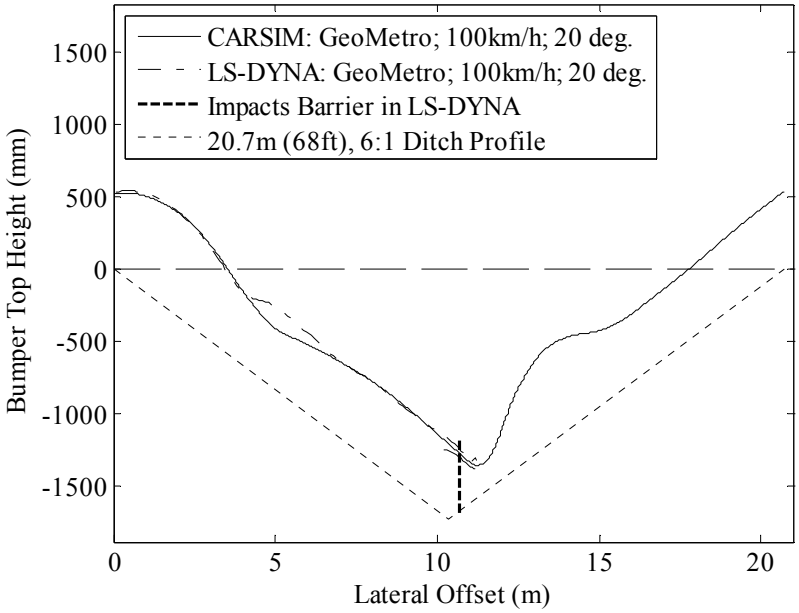

Figure 8.13 Comparison of LS-DYNA and CARSIM generated trajectories of the passenger car traversing a depressed medians for Case P9.

8.3.6. Case P10

For case P10, successful vehicle containment is predicted in the preliminary guideline. In the simulation of this case, a small car impacted a modified weak-post W-beam guardrail placed on a positive 6:1 roadside slope at an offset of 0.56 m (1.83') from the slope break point. The LS-DYNA generated energy balance curve, as shown in Figure 8.15, verifies the numerical stability of the simulation. Sequential images and occupant risk factors obtained from the simulations are shown in Figure 8.16. As can been seen from the figure, the guardrail successfully contained the small car and the occupant risk factors were within acceptable limits.

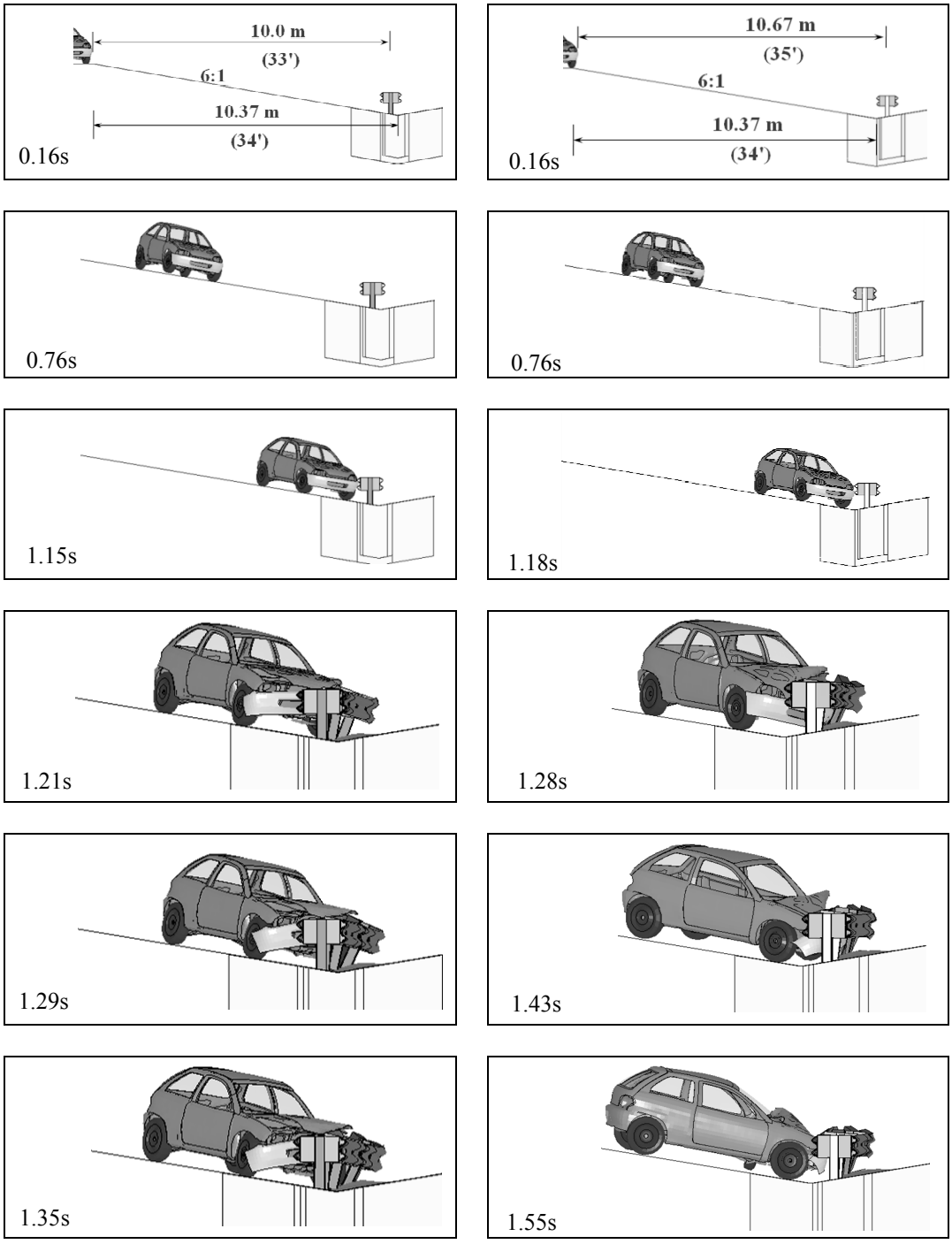

OIV=1.2m/s ≤ 12m/s;
RDA=14.7g's≤ 20g's

(a) Case P8

OIV=1.4 m/s ≤ 12m/s;
RDA=20.0g's ≤ 20g's

(b) Case P9

Figure 8.14 Sequential images obtained from LS-DYNA simulation of (a) Case P8 and (b) Case P9.

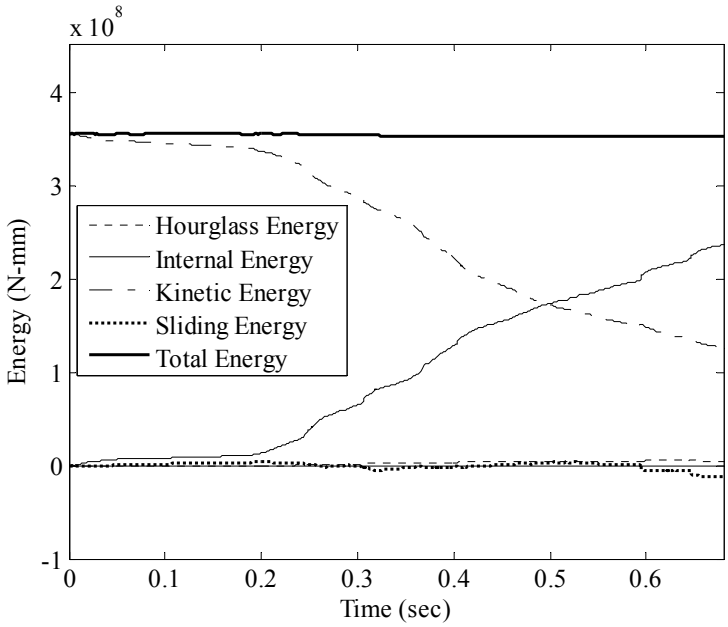

Figure 8.15 Energy curves obtained from LS-DYNA simulation for Case P10.

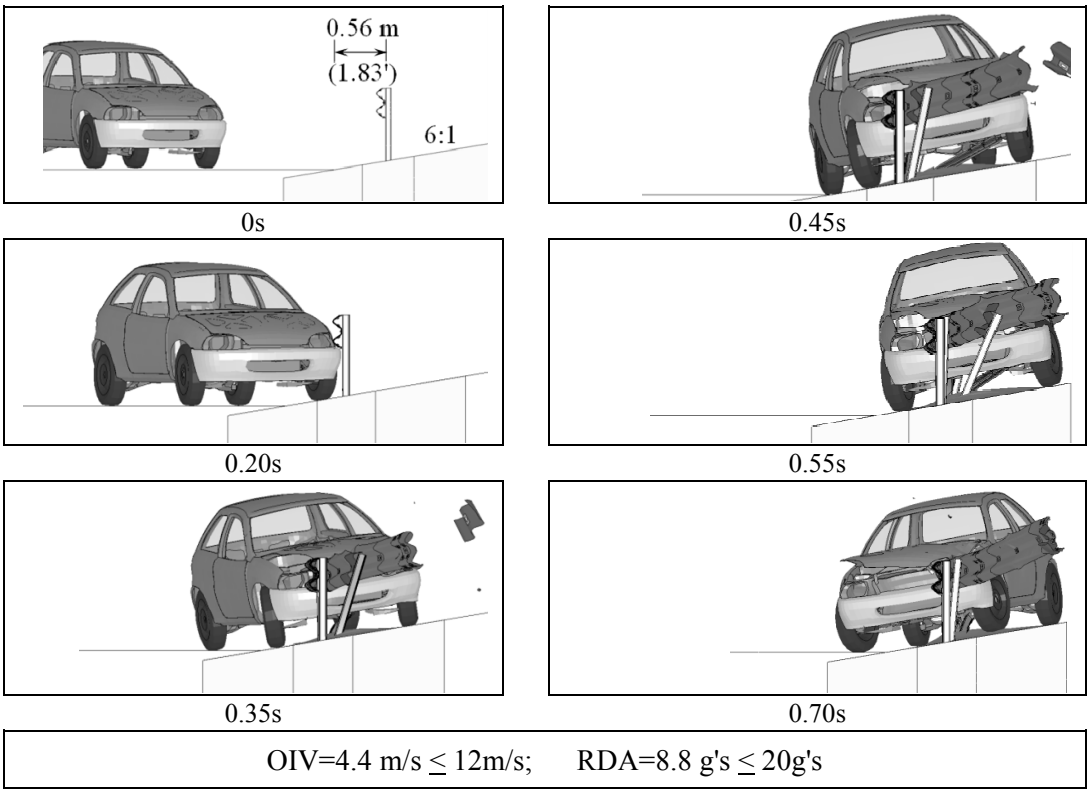

Figure 8.16 Sequential images obtained from LS-DYNA simulation of Case P10.

8.3.7. Case P11

To simulate case P11, an FE model for the dual-sided modified weak post W-beam barrier was developed by adding extra rail elements to the single-sided guardrail model. The model, as shown in Figure 8.17, consisted of 589,620 elements. In the simulation, a small car impacted the dual-sided modified weak-post W-beam barrier placed on the 6:1 backslope near the center of a 15.9 m (52') wide V-shaped ditch. Sequential images and occupant risk factors obtained from the simulation are shown in Figure 8.18. LS-DYNA generated energy balance curve, shown in Figure 8.19, verifies numerical stability of the simulation. According to the preliminary guideline, the barrier placed at the selected location should successfully contain the small car. As can be seen in Figure 8.18, small car seemed to underride the barrier at the end of the simulation. For this type of barrier with high rail mounting height, W-beam rail elements are easily detached from the posts thus allowing the small car underride the dual-sided rails with minimum effort. Hence, the placement of a single modified weak-post W-beam barrier should be avoided on the underride limit controlled region (i.e. near the base of the ditch) for all V-shaped medians.

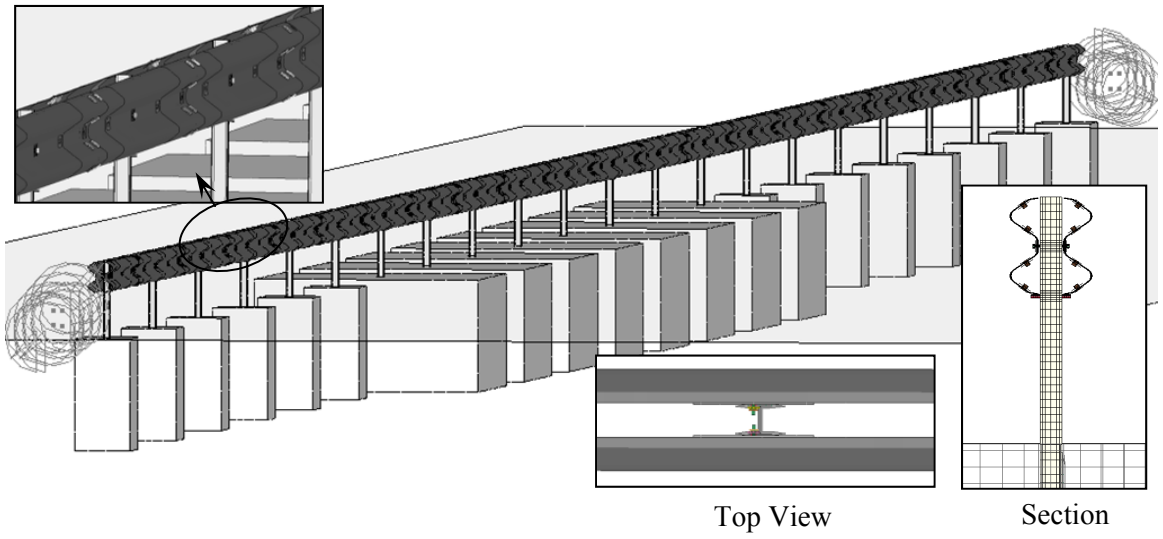

Figure 8.17 FE model for the dual-sided modified weak-post W-beam barrier.

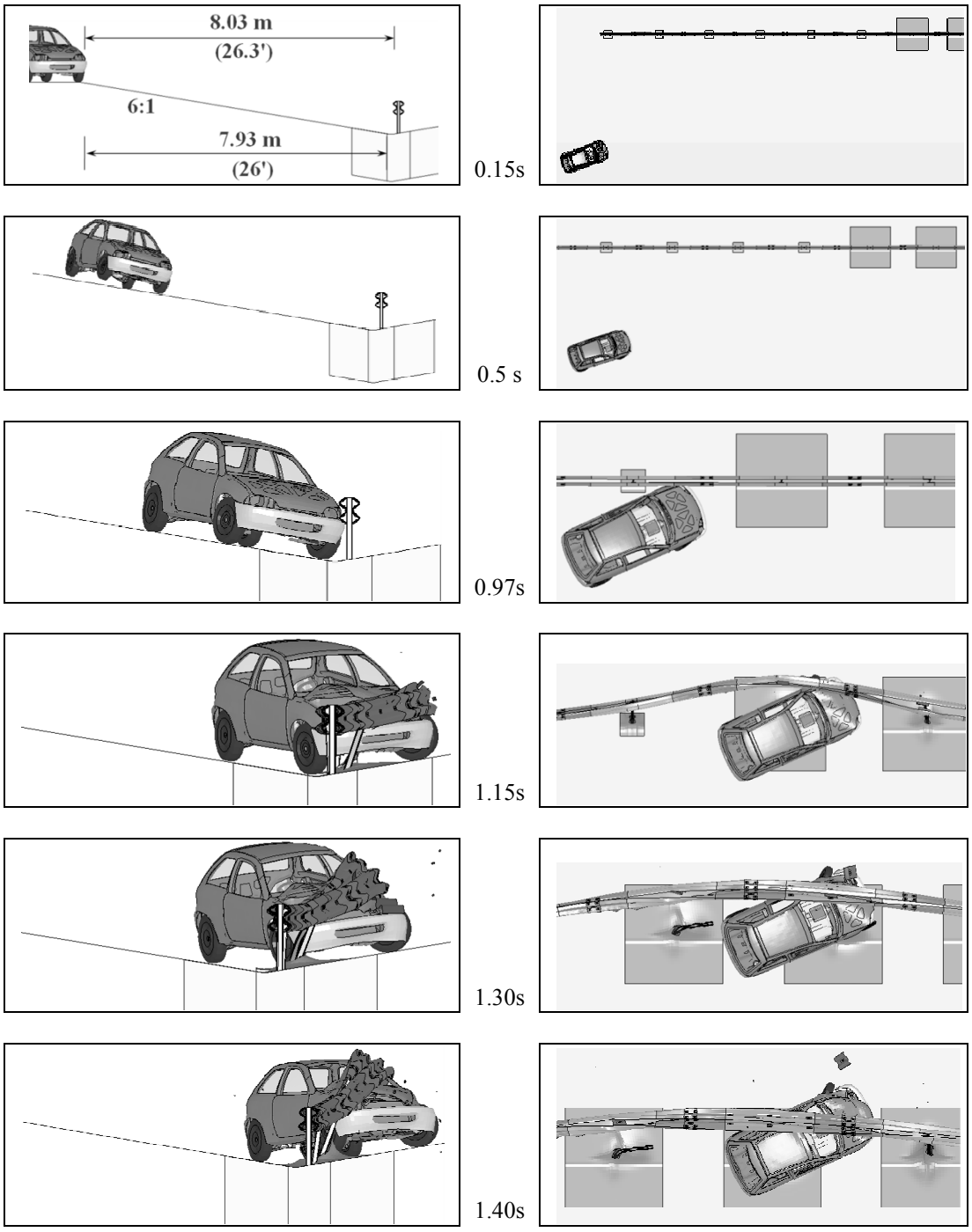

Figure 8.18 Sequential images obtained from simulation for Case P11.

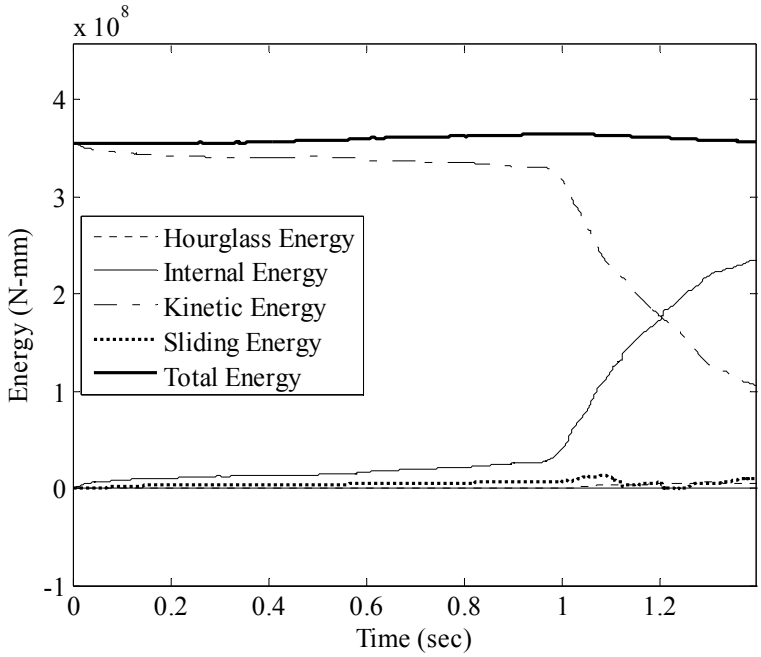

Figure 8.19 Energy curves obtained from LS-DYNA simulation for Case P11.

8.3.8. Case P12

In the simulation of case P12, the small car impacted a single-sided modified weak post W-beam guardrail model placed on a negative 6:1 roadside slope at a lateral offset of 6.2 m (20') from the slope break point. As shown in Figure 8.20, energy balance curves obtained from LS-DYNA verify numerical stability of the simulation. According to the preliminary guideline, guardrail placed at the selected location should be able to successfully contain the small car. Sequential images and occupant risk factors obtained from the simulation are shown in Figure 8.21. As can be seen from the figure, although the occupant risk factors obtained from the simulation were within acceptable limit, the small car seemed to partially underride the guardrail. The W-beam rail elements contacted top edge of the windshield frame at 1.10 sec. Compression and drag forces created by the rail elements on windshield during this contact can potentially shutter the windshield causing severe occupant injury. The report 350 safety evaluation criteria do

not permit any deformation of, or intrusion into, the occupant compartment that could cause serious occupant injury. The vehicle model used in this study does not have the capability to capture windshield damage and therefore it was uncertain whether the rail to windshield contact observed at 1.15 sec would cause occupant compartment intrusion. To remain on the safer side performance of the guardrail in the simulation was considered unacceptable. Placement guideline developed using a higher underride limit should allow avoiding these marginally unacceptable placement locations for the modified weak post W-beam system.

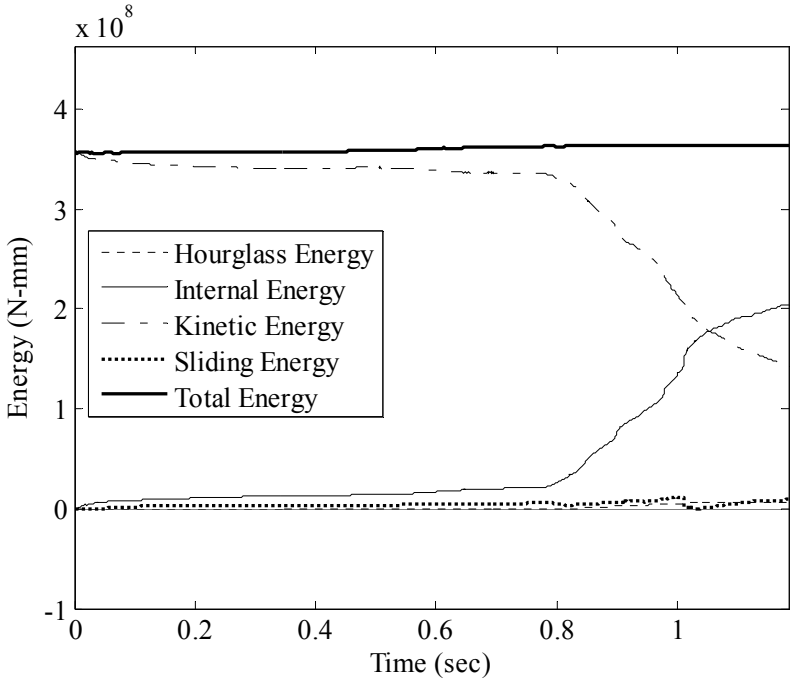

Figure 8.20 Energy curves obtained from LS-DYNA simulation of Case P12.

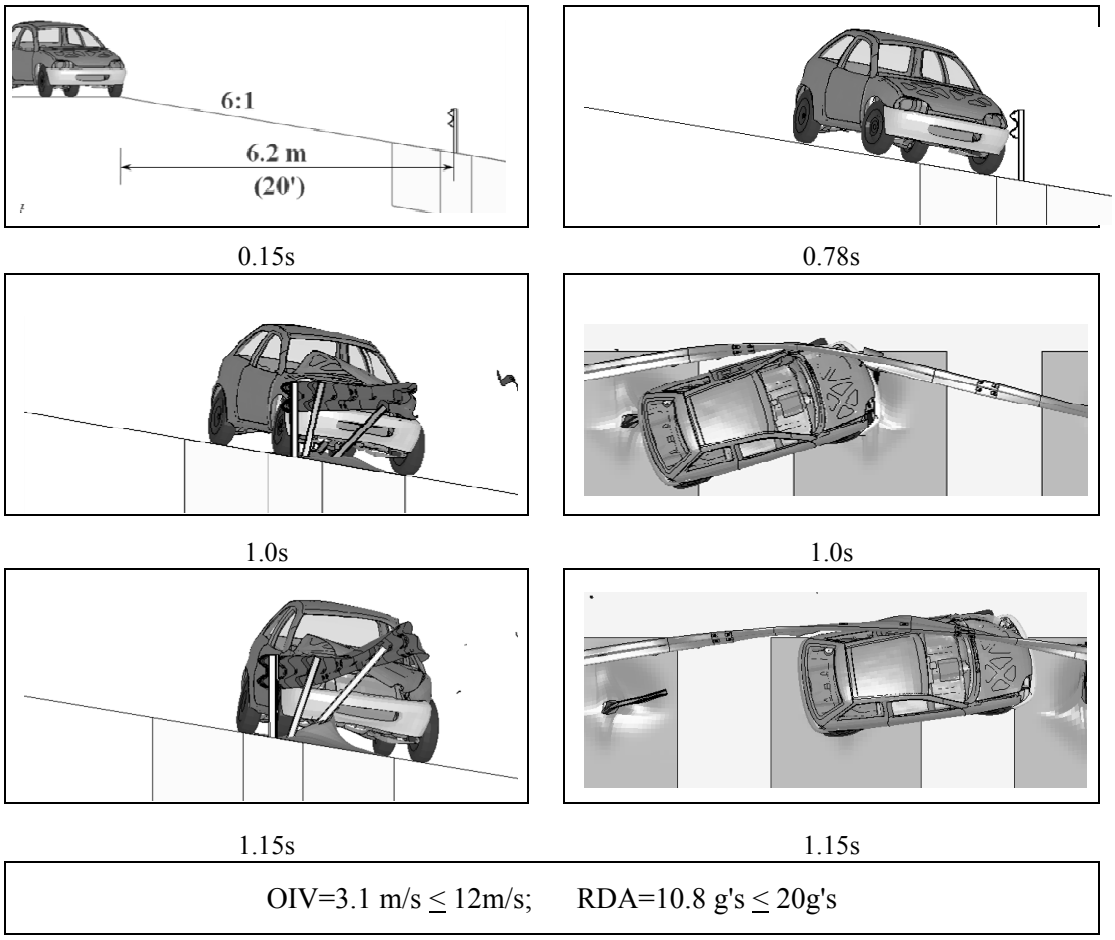

Figure 8.21 Sequential images obtained from simulation of Case P12.

8.4. FINALIZING THE GUIDELINE

To refine and validate the preliminary placement guidelines prepared using vehicle trajectories obtained from CARSIM and guardrail performance limits obtained from LS-DYNA impact analyses, LS-DYNA simulations were performed to capture full encroachment event from departure of the vehicle off the traveled way through impact with the barrier. Figure 8.22 and Figure 8.23 show the flow charts used to validate and refine preliminary guideline using the results obtained from these simulations. As can be seen from Figure 8.22, the simulations performed on the guardrails placed near the

shoulder edge (i.e. override limit controlled region) on a negative roadside slope matched the preliminary guideline predictions. However, the preliminary guideline permitting placement of the modified weak-post W-beam guardrail (Case P12) on a negative roadside slope or on the foreslope of a depressed median near its underride limit controlled region was found unacceptable. Hence to refine the preliminary guideline the underride limit of the modified weak-post W-beam guardrail was raised by 37.5 mm (1.5") to avoid the placement locations where small car windshield can potentially reach below the W-beam rail elements after an impact. The newly selected bumper top height at the time of impact (457 mm) successfully passed the safety criteria during the performance limit analyses as discussed in Section 5.

In the LS-DYNA simulations, the preliminary guideline permitting underride limit controlled placement locations near the base of a depressed median (case P8 and P9) were found acceptable for dual-sided modified G4(1S) barriers. Among the systems studied, only the modified weak-post W-beam system with a higher underride limit has more potential for small car underride compared to the modified G4(1S) system. For a dual-sided modified weak post W-beam system placed on a depressed median, results obtained from the simulation of the case (case P11) selected from underride limit controlled (i.e. near the base of the ditch) acceptable placement region were found unacceptable. It was therefore concluded that the placement of a single modified weak-post W-beam barrier should be avoided near the base of the ditch for all depressed medians.

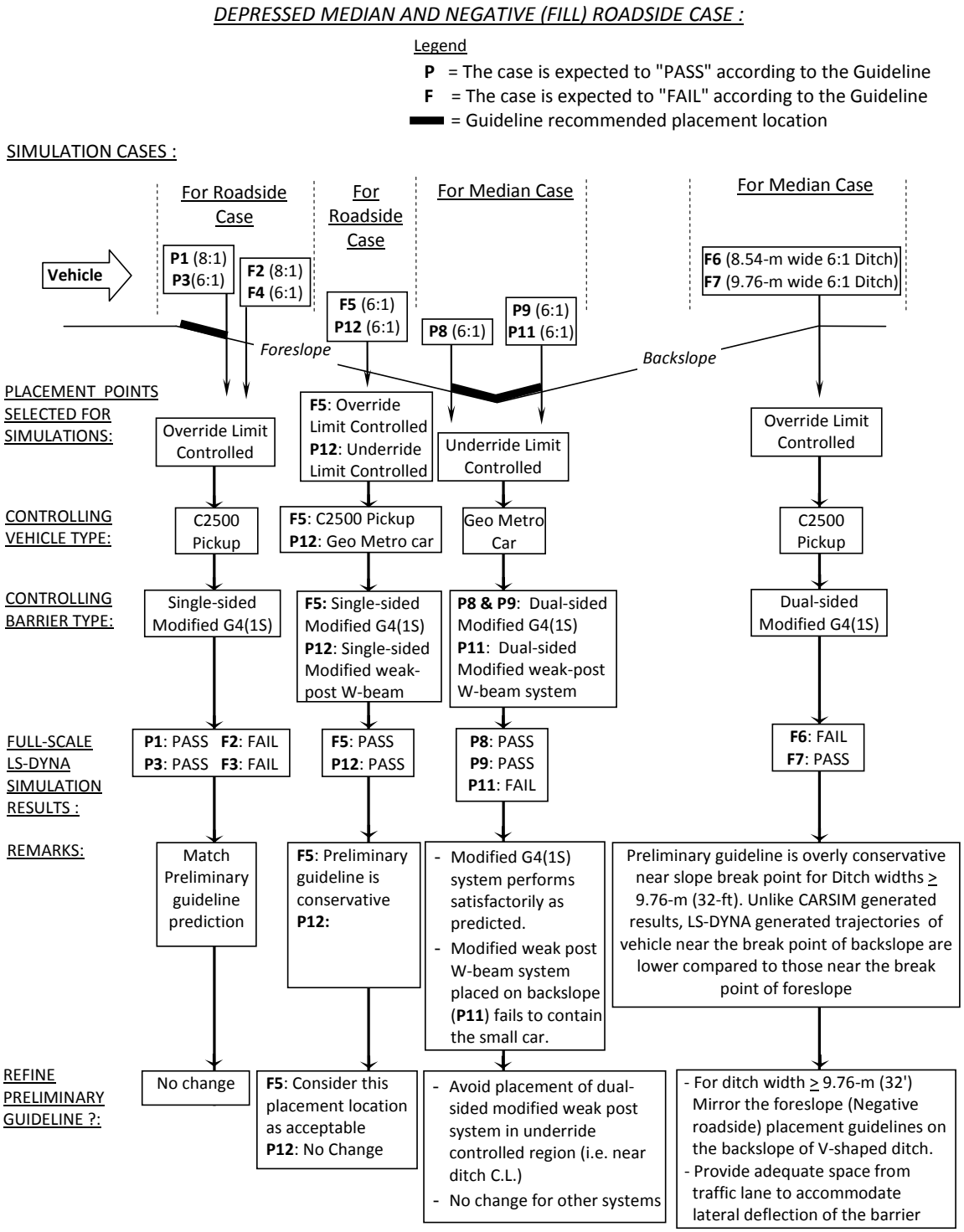

Figure 8.22 Flowchart for the validation and refinement of preliminary guidelines for the placements on median and negative roadside slopes using full-scale LS-DYNA simulations.

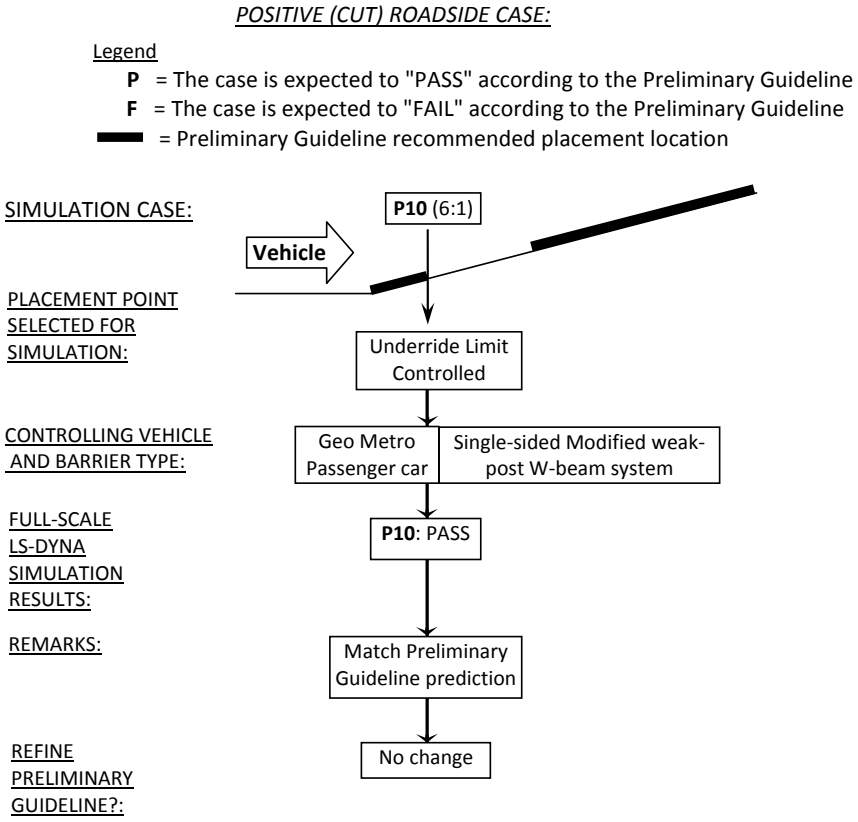

Figure 8.23 Flowchart for the validation and refinement of preliminary guidelines for the placements on positive roadside slope using full-scale LS-DYNA simulations.

The preliminary guidelines, prepared using CARSIM predicted vehicle trajectories, were found overly conservative for the placement of a single barrier near the shoulder edge of a depressed median. In the more justifiable LS-DYNA simulations, for ditches wider than 8.54 m (Case F7), trajectory of a pickup on the foreslope was found higher compared to that on the backslope of the ditch. Hence for the ditches wider than 8.54 m (28'), override limit controlled placement guidelines near the slope break point of a negative roadside slope (equivalent to the foreslope for a depressed median) can be used on either side of a depressed median. However, the systems investigated in this study are flexible and undergo large lateral deflections when impacted by a vehicle. In median installations, the dual-sided barriers should be placed such that the anticipated

deflection does not enter the opposing traffic lane. Table 8.3 presents the maximum dynamic deflections observed during the crash tests performed on single-sided guardrail systems placed on flat terrain. These values can be used conservatively for the stiffer dual-sided median barriers. In developing the final guideline for the placements of a single median barrier near the shoulder edge of a depressed median, spaces equivalent to these lateral deflections from the edge of the traffic lane were avoided to accommodate barrier deflections due to the impact by an errant vehicle traveling from the opposite end of the ditch. Table 8.3 shows the lateral placement region from slope break point that should be avoided to prevent intrusion of deflected barriers into the adjacent traffic lane for medians with 1.2 m (4') and 1.8 m (6') wide shoulders. As can be seen from the table, the dynamic deflection observed in a crash test performed on a modified weak post W-beam system exceeded both the 1.2 m (4') and 1.8 m (6') shoulder widths by 0.92 m (3') and 0.32 m (1'), respectively. Therefore, if a single dual-sided weak post system is placed within these distances from the shoulder edge, the impact from a vehicle traveling from the opposite end of the median may cause the barrier to deflect into the adjacent traffic lane. These lateral offsets were therefore avoided in the final placement guidelines. The dynamic deflections of other systems were contained within the distance equivalent to the smallest shoulder width. Hence, modification to the placement guidelines to accommodate barrier deflection was not needed for these systems.

Table 8.3 Maximum dynamic deflections observed in crash tests performed on single-sided guardrail systems placed on flat terrain.

Barrier Type	Crash Test		Maximum dynamic deflection	Unacceptable lateral offset length from slope break point to avoid intrusion into the adjacent traffic lane
	Testing Org.	Number		
Modified G4(1S) System	TTI	405421-01(*7*)	1.0 m (3.28')	0 for 1.2 m (4') shoulder 0 for 1.8 m (6') shoulder
Midwest Guardrail System	MwRSF	NPG-4(*14*)	1.09 m (3.5')	0 for 1.2 m (4') shoulder 0 for 1.8 m (6') shoulder
Modified Thrie-beam System	TTI	471470-30(*6*)	1.02 m (3.4')	0 for 1.2 m (4') shoulder 0 for 1.8 m (6') shoulder
Modified weak post W-beam System	TTI	473750-3(*3*)	2.12 m (6.95')	0.92 m (3') for 1.2 m shoulder 0.32 m (1') for 1.8 m shoulder
Box-beam System	TTI	471470-33(*6*)	1.15 m (3.8')	0 for 1.2 m (4') shoulder 0 for 1.8 m (6') shoulder

As shown in Figure 8.23, results obtained from the FE simulation of case P10, where a modified weak post W-beam guardrail was placed on a positive roadside slope at lateral offset controlled by its underride limit, matched preliminary guideline prediction. Hence preliminary guideline for the placements of each barrier on positive roadside slope can be considered acceptable. Most of these LS-DYNA simulations were performed on 6:1 slopes. The conclusions drawn based on the results obtained from the simulations performed on a steeper slope can be conservatively used to refine and validate the preliminary guidelines for the placements of barriers on a flatter (8:1) slope.

The preliminary guidelines were refined following the procedures discussed above to develop final guideline for the placement of traffic barriers on roadside and median slopes. The final guidelines for the placements of five barriers selected for this study are presented in Table 8.4, Table 8.5, and Figure 8.24 to Figure 8.28. The acceptable lateral offset distances, shown in Table 8.4 and Table 8.5, are calculated from the shoulder edge or slope break point. Hatched areas in the figures represent acceptable placement locations for the barriers on 6:1 and 8:1 slopes. Two bars for each depressed median indicate two ditch widths with 1.2 m (4') and 1.8 m (6') wide shoulders. Right end of each median bar represents the center of a symmetric ditch. Acceptable offset locations presented for depressed median are applicable for the placement of a single dual-sided barrier on either the foreslope or backslope of a median ditch. To use single-sided guardrails on both sides of a median ditch, guidelines for the negative roadside slope can be used.

Table 8.4 Final guideline for the placement of single dual-sided traffic barriers on depressed medians.

Barrier Type	Median Width	Shoulder Width	Ditch Width	Slope	Acceptable lateral offset distance from the shoulder edge, X, "m" (ft)
Modified G4(1S) System	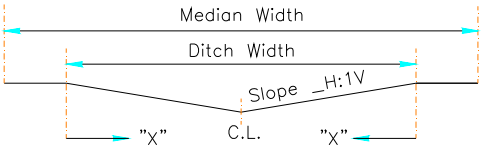				
	23.2 m (76 ft)	1.2 m (4')	20.7 m (68')	6:1	0-0.45 m (1.5'); 10.0 m (33') - C.L.
				8:1	0- 0.62 m (2.0'); 9.91m (32.5') - C.L.
		1.8 m (6')	19.5 m (64')	6:1	0-0.45 m (1.5'); 9.45 m (31')-C.L.
				8:1	0- 0.62 m (2.0′); 9.3 m (30.5′) -C.L.
	18.3 m (60 ft)	1.2 m (4')	15.9 m (52')	6:1	0-0.45 m (1.5'); 7.8 m (25.5′) -C.L.
				8:1	0-0.62 m(2.0'); 7.5 m (24.6')-C.L.
		1.8 m (6')	14.6 m (48')	6:1	0-0.45 m (1.5'); 7.2 m (23.6') - C.L.
				8:1	0-0.62 m(2.0'); 6.96 m (22.8') - C.L.
	12.2 m (40 ft)	1.2 m (4')	9.8 m (32')	6:1	0-0.45 m (1.5')
				8:1	0-0.62 m(2.0'); 4.8 m (15.7′) -C.L.
		1.8 m (6')	8.5 m (28')	6:1 & 8:1	Not recommended
Midwest Guardrail System	23.2 m (76 ft)	1.2 m (4')	20.7 m (68')	6:1	0-1.0 m (3.3'); 10.1 m (33.2')-C.L.
				8:1	0-1.6 m (5.25'); 6.6 m (21.6')-7.3 m (23.9'); 10 m (32.8') -C.L.
		1.8 m (6')	19.5 m (64')	6:1	0-1.0 m(3.3'); 9.5 m (31')-C.L.
				8:1	0-1.6 m (5.25'); 6.0 m(19.7')-6.6 m(21.6'); 9.4 m (30.8')-C.L.
	18.3 m (60 ft)	1.2 m (4')	15.9 m (52')	6:1	0-1.0 m (3.3'); 7.8 m (25.6')-C.L.
				8:1	0-1.6 m (5.25'); 3.9 m(12.8')-5 m(16.4'); 7.5 m (24.6')- C.L.
		1.8 m (6')	14.6 m (48')	6:1	0-1.0 m (3.3'); 7.25 m(23.8')-C.L.
				8:1	0-1.6 m (5.25'); 3.55 m (11.6')-4.5 m (14.7'); 7.0 m(23')-C.L.
	12.2 m (40 ft)	1.2 m (4')	9.8 m (32')	6:1	0-1.0 m (3.3')
				8:1	0-1.6 m (5.25'); 4.8 m(15.75')-C.L.
		1.8 m (6')	8.5 m (28')	6:1	Not recommended
				8:1	0.95 m (3.1')-1.5 m (4.95'); 4.15 m (13.6')-C.L.

Table 8.4 continued.

Barrier Type	Median Width	Shoulder Width	Ditch Width	Slope	Acceptable lateral offset distance from the shoulder edge, X, "m" (ft)
Modified Thrie-beam Guardrail System	23.2 m (76 ft)	1.2 m (4')	20.7 m (68')	6:1	0-1.1 m (3.67'); 7.31 m(24')-7.54 m(24.75'); 9.83 m (32.25')-C.L.
				8:1	0-1.85 m (6'); 6.5 m(21.33')-7.62 m (25'); 9.62 m (31.5')-C.L.
		1.8 m (6')	19.5 m (64')	6:1	0-1.1 m (3.67'); 6.8 m(22.3')-6.95 m(22.83'); 9.2 m (30.25')-C.L.
				8:1	0-1.85 m (6'); 5.94 (19.5') m-7.05 m (23.08'); 8.98 m (29.42')-C.L.
	18.3 m (60 ft)	1.2 m (4')	15.9 m (52')	6:1	0-1.1 m (3.67'); 5.13 m(16.83')-5.5 m(18'); 7.47 m(24.5')-C.L.
				8:1	0-1.85 m (6'); 3.81 m(12.5')-5.64 (18.5'); 7 m (23') – C.L.
		1.8 m (6')	14.6 m (48')	6:1	0-1.1 m (3.67'); 6.96 m (22.83') –C.L.
				8:1	0-1.85 m (6'); 3.35 m(11')-5 m (16.4'); 6.53 m (21.41')- C.L.
	12.2 m (40 ft)	1.2 m (4')	9.8 m (32')	6:1	0-1.1 m (3.67')
				8:1	0-1.85 m (6'); 4.42 m (14.5') -C.L.
		1.8 m (6')	8.5 m (28')	6:1	Not recommended
				8:1	0.91 m (3.0')-1.71 m (5.58'); 3.81 m (12.5') - C.L.
Modified weak post W-beam System	23.2 m (76 ft)	1.2 m (4')	20.7 m (68 ft)	6:1	Not recommended
				8:1	Not recommended
		1.8 m (6')	19.5 m (64 ft)	6:1	0.32 (1.0')-0.62 m (2.0')
				8:1	0.32 (1.0')-0.86 m (2.83')
	18.3 m (60 ft)	1.2 m (4')	15.9 m (52 ft)	6:1	Not recommended
				8:1	Not recommended
		1.8 m (6')	14.6 m (48 ft)	6:1	0.32 (1.0')-0.62 m (2.0')
				8:1	0.32 (1.0')-0.86 m (2.83')
	12.2 m (40 ft)	1.2 m (4')	9.8 m (32 ft)	6:1	Not recommended
				8:1	Not recommended
		1.8 m (6')	8.5 m (28 ft)	6:1	Not recommended
				8:1	Not recommended

Table 8.4 continued.

Barrier Type	Median Width	Shoulder Width	Ditch Width	Slope	Acceptable lateral offset distance from the shoulder edge, X, "m" (ft)
Box-beam System	23.2 m (76 ft)	1.2 m (4')	20.7 m (68 ft)	6:1	0-.64 m (2.1'); 10 m (32.9') –C.L.
				8:1	0-.95 m (3.1'); 7 m (23')-7.4 m (24.25'); 9.86 m (32.3') -C.L.
		1.8 m (6')	19.5 m (64 ft)	6:1	0-0.64 m(2.1'); 9.35 m (30.67')-C.L.
				8:1	0-0.95 m (3.1');6.5 m(21.33')-6.75 m(22.16'); 9.25 m (30.33')-C.L.
	18.3 m (60 ft)	1.2 m (4')	15.9 m (52 ft)	6:1	0-.64 m (2.1'); 7.7 m (25.3')-C.L.
				8:1	0-0.95 m (3.1'); 4.75 m (15.58')-5.2 m (17.0'); 7.4 m (24.25')-C.L.
		1.8 m (6')	14.6 m (48 ft)	6:1	0-.64 m (2.1'); 7.14 m (23.4')-C.L.
				8:1	0-0.95 m (3.1'); 4.1 m (13.41')-4.7 m(15.41'); 6.8 m (22.3')-C.L.
	12.2 m (40 ft)	1.2 m (4')	9.8 m (32 ft)	6:1	0-.64 m (2.1');
				8:1	0-0.95 m (3.1'); 4.66 m (15.25') -C.L.
		1.8 m (6')	8.5 m (28 ft)	6:1	Not recommended
				8:1	4.0 m (13.1') –C.L.

Table 8.5 Final guideline for the placement of single-sided guardrails on roadside slopes.

Barrier Type	Case	Slope	Acceptable lateral offset distance from the slope break point, X, "m" (ft)
	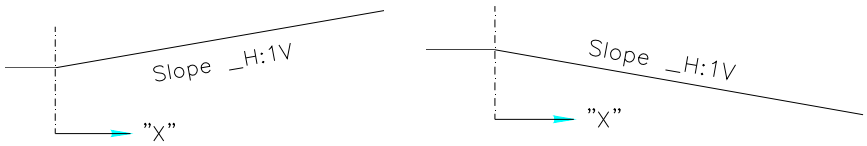 Roadside Positive Slope Roadside Negative Slope		
Modified G4(1S) System	Roadside Positive Slope	6:1	0-0.6 m (1.95'); 2.6 m (8.5')-3.2 m (10.5'); >7.4 m (24.3')
		8:1	0-0.9 m (2.9'); 1.9 m (6.3')-4.3 m (14'); >6.65 m (21.8')
	Roadside Negative Slope	6:1	0-0.45 m (1.5'); >5.5 m (18')
		8:1	0-0.62 m(2.0'); >4.4 m (14.3')
Midwest Guardrail System	Roadside Positive Slope	6:1	0-0.58 m (1.9'); 2.7 m(8.8')-5.2 m (17'); >6.4 m (21')
		8:1	0-0.8 m (2.6'); >2 m (6.5')
	Roadside Negative Slope	6:1	0-1.0 m (3.3'); 4.95 m (16.2')-6.3 m (20.7'); >6.8 m (22.3')
		8:1	0-1.6 m (5.25'); >3.5 m (11.5')
Modified Thrie-beam Guardrail System	Roadside Positive Slope	6:1	0-5.5 m (18'); >6.1 m (20')
		8:1	Anywhere on the slope
	Roadside Negative Slope	6:1	0-1.1 m (3.67'); >4.88 m (16')
		8:1	0-1.85 m (6'); >3.28 m (10.75')
Modified weak post W-beam System	Roadside Positive Slope	6:1	0-0.56 m (1.83'); 2.7 m (8.83')-4 m (13.16'); > 7 m (23.25')
		8:1	0-0.66 m (2.17'); 2.1 m (6.9')-5.41 m (17.75'); >6 m (19.75')
	Roadside Negative Slope	6:1	0-0.62 m (2.0'); >8.1 m (26.5')
		8:1	0-0.86 m (2.83'); >6.78 m (22.25')
Box-beam System	Roadside Positive Slope	6:1	0-0.79 m (2.58'); 1.78 m (5.83')-4.23 m(13.83'); >7.0 m(23.0')
		8:1	0-1.21 m (4'); >1.7 m (5.58')
	Roadside Negative Slope	6:1	0-.64 m (2.1'); >5.3 m (17.4')
		8:1	0-0.95 m (3.1'); >4.0 m (13.1')

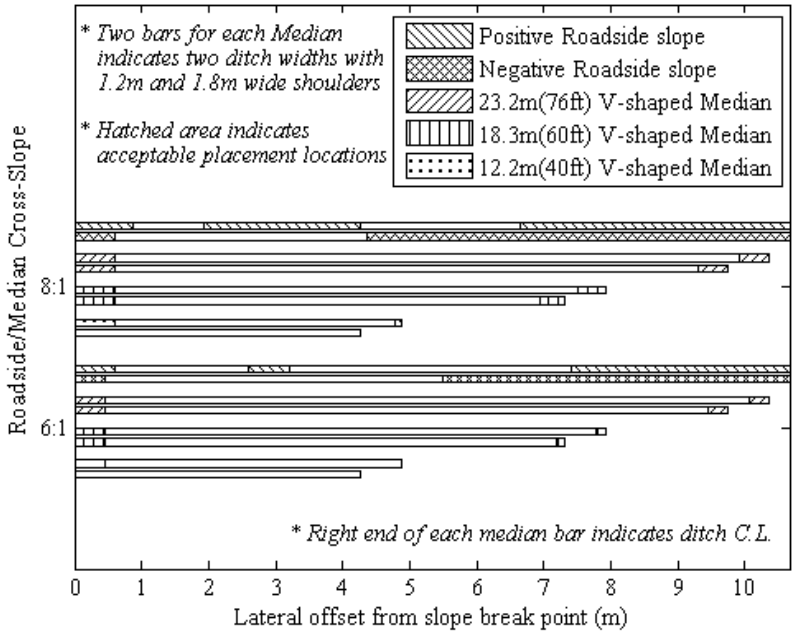

Figure 8.24 Final guideline for the placement of modified G4(1S) system on roadside and median slopes.

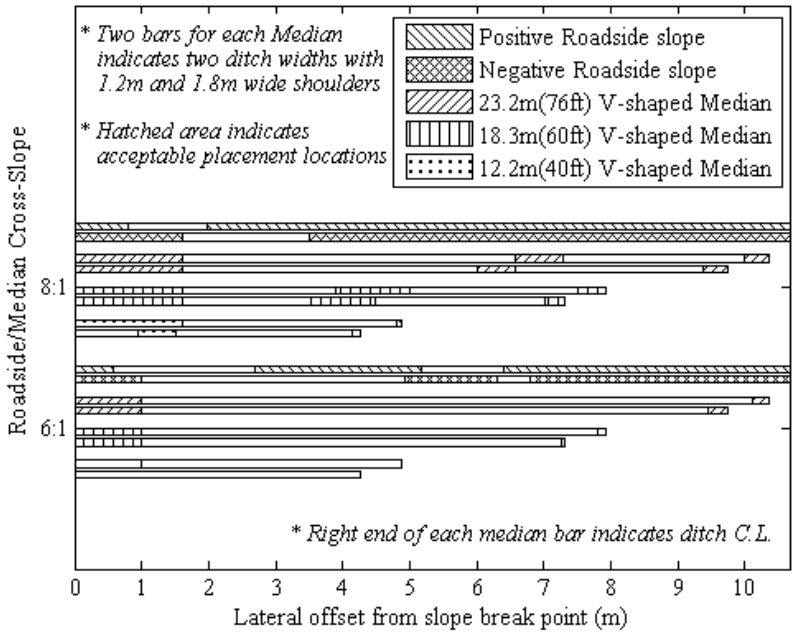

Figure 8.25 Final guideline for the placement of Midwest Guardrail system (MGS) on roadside and median slopes.

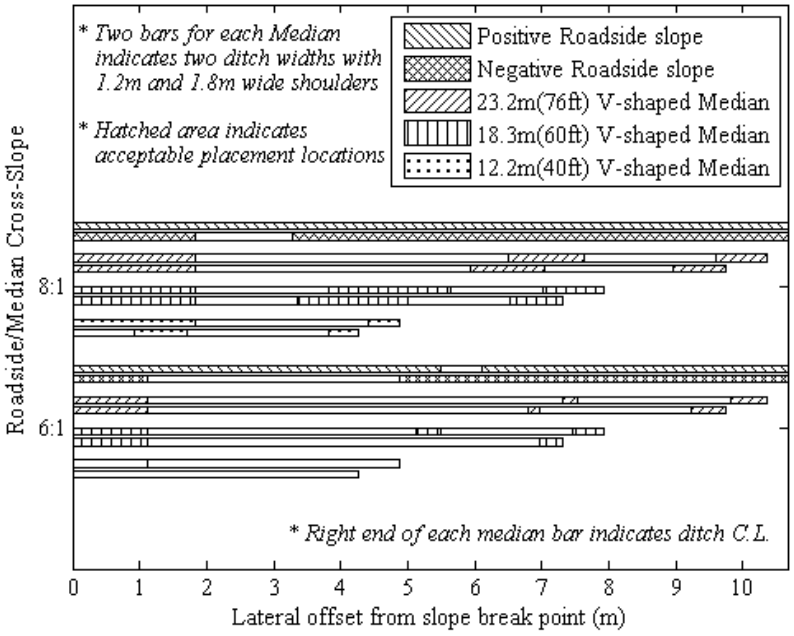

Figure 8.26 Final guideline for the placement of modified Thrie-beam system on roadside and median slopes.

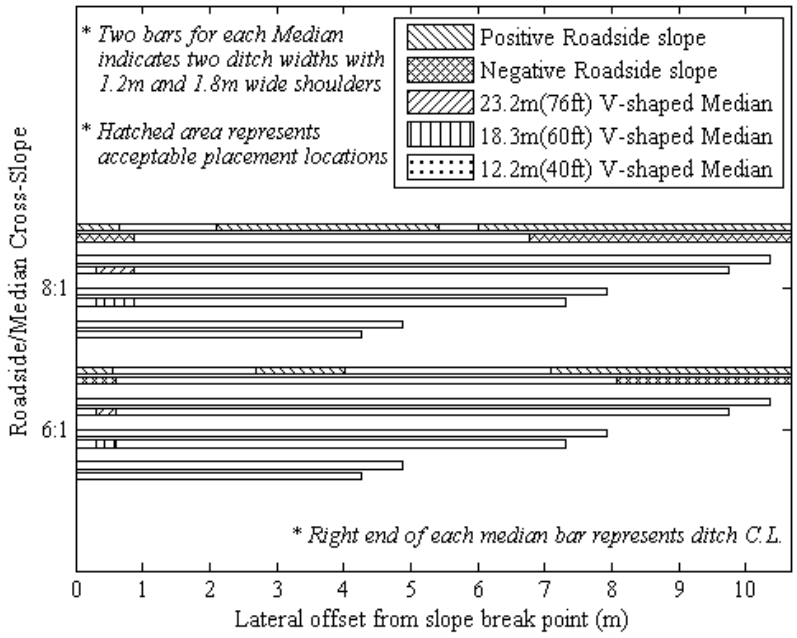

Figure 8.27 Final guideline for the placement of modified weak post W-bean system on roadside and median slopes.

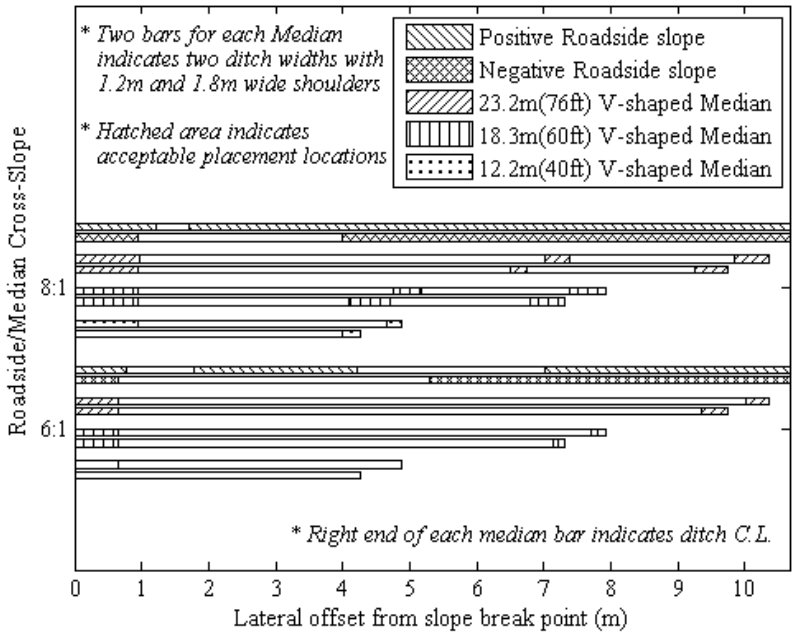

Figure 8.28 Final guideline for the placement of box-beam system on roadside and median slopes.

Figure 8.29 to Figure 8.36 compare the guideline recommended placement locations for the five traffic barriers investigated in this study. It can be seen that the modified Thrie-beam system has the widest range of acceptable placement locations among the systems studied. This system has the highest override limit due to its higher rail mounting height. It also has the lowest underride limit due to the presence of wider thrie-beam rails and wider blockouts. The modified G4(1S) system, on the other hand, has the lowest override limit due to its lower rail mounting height. Also, the presence of narrower blockout makes the system more susceptible to the vehicle-post snagging during the impacts with passenger car. High rail mounting height and the presence of wider blockouts make the MGS a better option for the placements on roadside and median slopes. The relatively low rail mounting height and substantial flexural and tensile strength of the tubular rail make the box-beam system more effective in containing the small car with compressed suspension. When placing near the shoulder edge on a depressed median, adequate space are provided for a dual-sided modified

weak-post W-beam barrier to accommodate its relatively large lateral deflections. High rail mounting height, easily detachable rail-post connections, and absence of spacers (blockout) make this system least effective in containing small cars with compressed suspension. Thus to avoid small car underride, the placement of single dual-sided modified weak-post W-beam system near the base of a ditch is not recommended in the guideline.

8.5. CONCLUSIONS

To verify and refine the preliminary guidelines, full-scale LS-DYNA simulations were performed that captured full encroachment event from departure of the vehicle off the traveled way through the impact with the barrier. Preliminary placement guidelines for the guardrail systems with lowest override limit and highest underride limit were selected for the study. The preliminary guidelines for all other barriers were modified and refined based on the results obtained from these simulations. The final guidelines for the placements of barriers on roadside and median slopes are presented in this section. Following key observation can be made from these guidelines. Placements of single dual-sided barrier should be avoided on a 6:1 ditch narrower than 9.76 m (32 ft). Two single sided guardrails on either side of the ditch should be used instead. Among the systems studied, modified thrie-beam system has the widest range of acceptable placement locations on all the slope configurations selected for this study. Unlike others, this system can be placed anywhere on an 8:1 positive roadside slope. Modified weak-post W-beam system was found unfit for the placements on depressed medians.

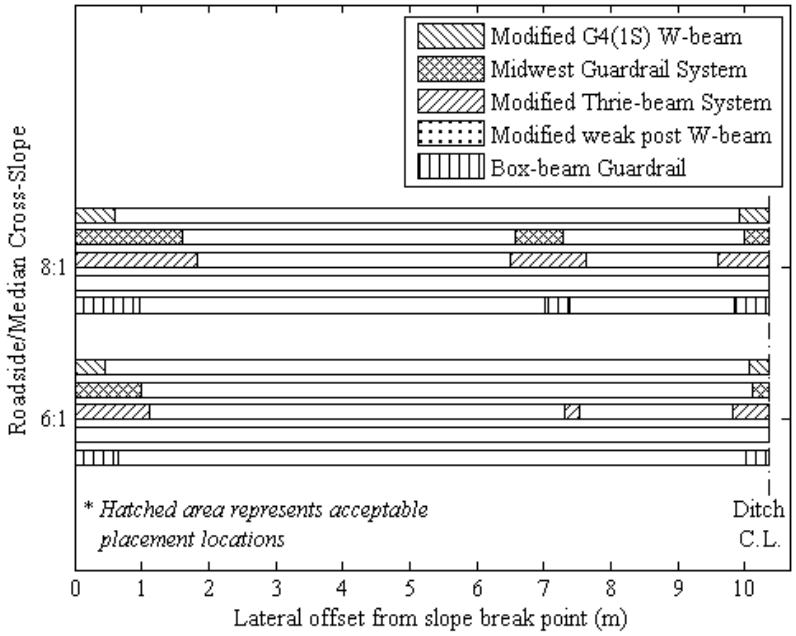

Figure 8.29 Final guideline for the placements of traffic barriers on 23.2 m (76ft) wide depressed median with 1.2 m (4ft) wide shoulder.

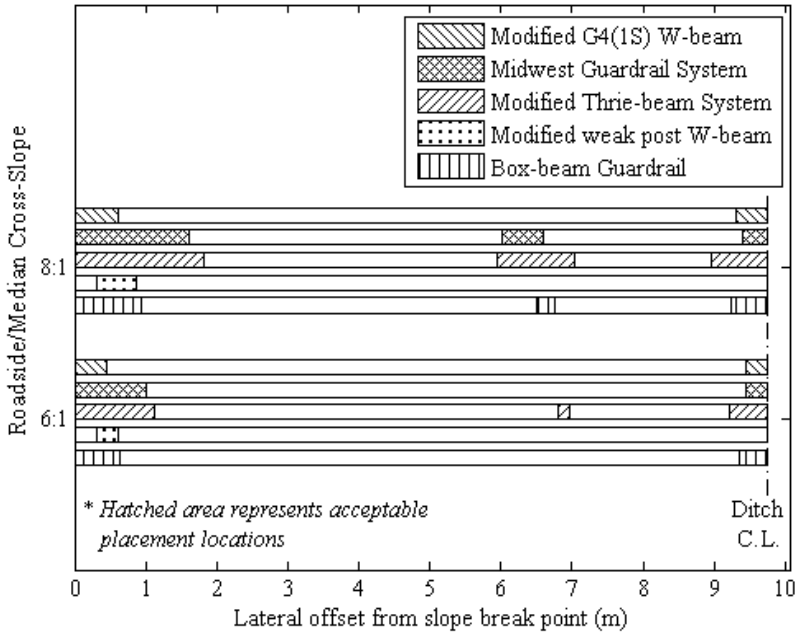

Figure 8.30 Final guideline for the placements of traffic barriers on 23.2 m (76ft) wide depressed median with 1.8 m (6ft) wide shoulder.

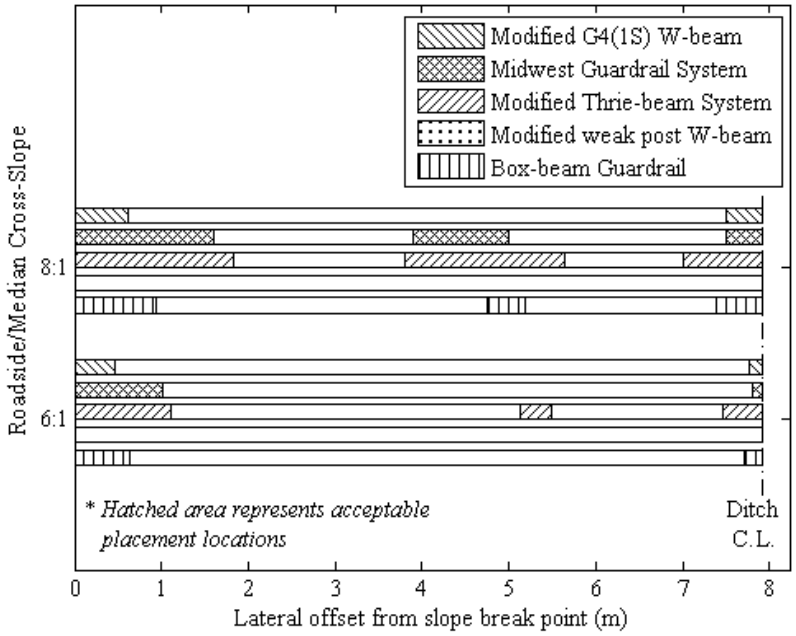

Figure 8.31 Final guideline for the placements of traffic barriers on 18.3 m (60ft) wide depressed median with 1.2 m (4ft) wide shoulder.

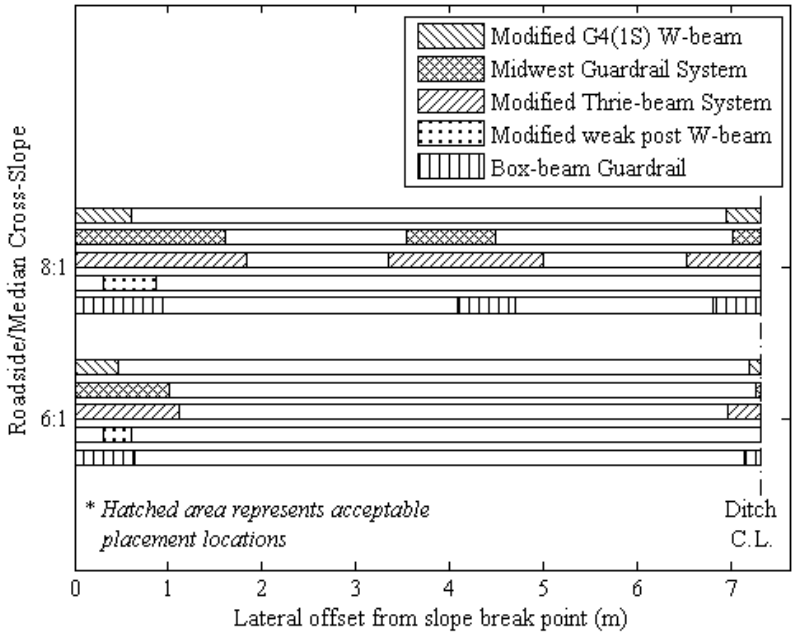

Figure 8.32 Final guideline for the placements of traffic barriers on 18.3 m (60ft) wide depressed median with 1.8 m (6ft) wide shoulder.

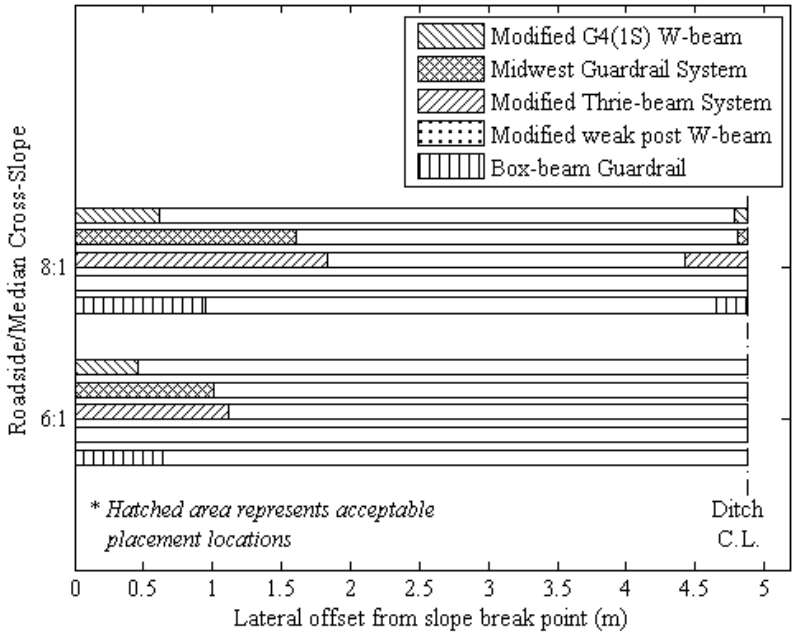

Figure 8.33 Final guideline for the placements of traffic barriers on 12.2 m (40ft) wide depressed median with 1.2 m (4ft) wide shoulder.

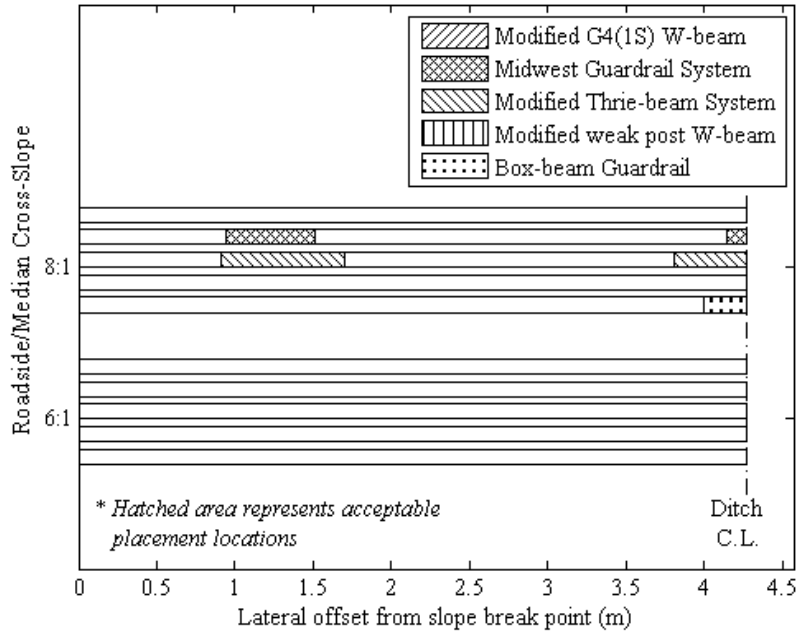

Figure 8.34 Final guideline for the placements of traffic barriers on 12.2 m (40ft) wide depressed median with 1.8 m (6ft) wide shoulder.

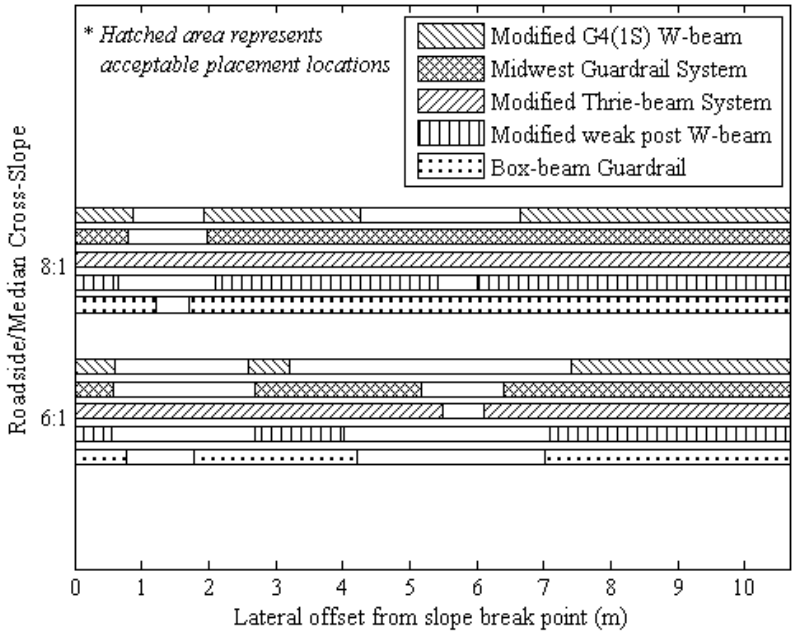

Figure 8.35 Final guideline for the placements of single-sided guardrail systems on positive (cut) roadside slopes.

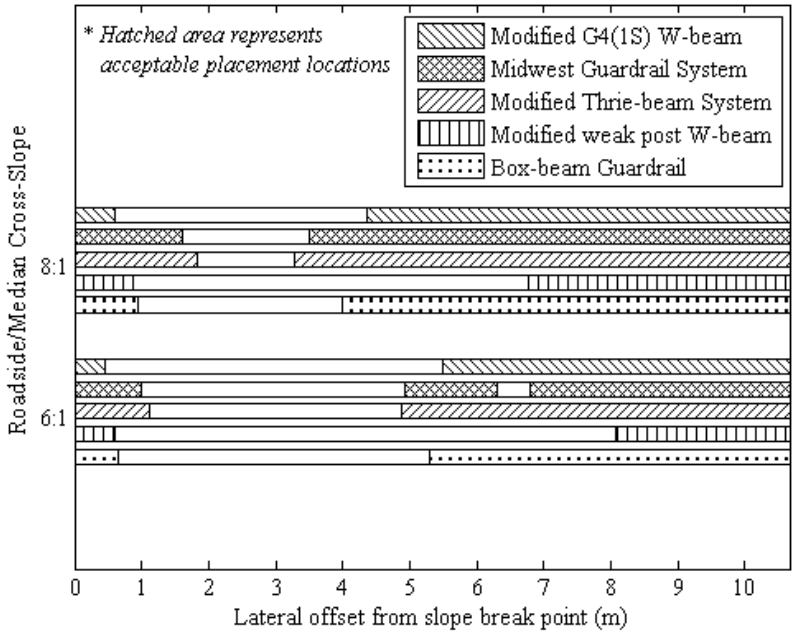

Figure 8.36 Final guideline for the placements of single-sided guardrail systems on negative (fill) roadside slopes.

9. CONCLUSIONS

9.1. SUMMARY

In this study, performances of modified G4(1S) W-beam, Midwest Guardrail System (MGS), modified Thrie-beam, modified weak post W-beam, and box-beam guardrail systems on roadside and median slopes were investigated using numerical simulations. These barriers were designed based on the finding obtained from crash tests performed on flat terrain. However, they are frequently placed on sloped terrains. For barriers placed on roadside and median slopes, vehicle impact height varies depending on the trajectory of the vehicle along the ditch section and lateral offset of the barrier. Thus depending on the placement location on slope, a barrier can be impacted by an errant vehicle at height and orientation more critical compared to those observed during the crash test performed on flat terrain. Hence, development of a guideline for the placement of these barriers on roadside and median slopes was undertaken.

The five guardrail systems used in this study successfully passed the safety evaluation criteria set forth in *NCHRP report 350* during the crash tests performed on flat terrain. The same *NCHRP report 350* evaluation criteria were used in this study to evaluate the performance of these barriers on sloped terrain. *Report 350* specified test vehicles were used to perform numerical simulations. Representative combinations of slope configurations and vehicle encroachment conditions, investigated in this study, were identified based on the existing guidelines.

To reduce the computational cost of running 112 long duration FE simulations of vehicles traversing various slope configurations, initial simulation analysis was divided into two parallel parts. One part of the simulation focused on developing performance envelopes in terms of vehicle containment heights for selected guardrail and median barrier systems installed on flat and level terrain. This part was executed using a non-linear finite element code capable of modeling vehicle to barrier contact. Finite element representation of each guardrail system was first prepared using LS-DYNA. While

public domain FE models for the needed vehicles exist, this is not the case for some of the selected guardrail systems. Although FE models for most of the components used in selected guardrail systems are readily available, preparing quality FE model for each system required component assembly, defining contact algorithms, and modifications to attain satisfactory simulation results. To ensure reliable results, model fidelity was assessed through comparison of simulated and measured responses reported in full scale crash test studies conducted on flat terrain. To develop the performance envelopes, thirty-one full-scale LS-DYNA simulations were performed on single-sided guardrail models. In these simulations, the vehicle impact height was parametrically varied to determine the performance limits of the barrier as defined by initiation of override or rollover for the pickup truck and underride for the small passenger car.

The other part of the initial analysis used a multi-rigid-body dynamics code, CARSIM, to quantify the trajectory of the vehicles across selected roadside and median configurations for different encroachment conditions. Multi-rigid-body code simulations significantly reduced computational effort and a large number of parametric variations could be evaluated. The pre-built A-Class hatchback and Full-size pickup models available in the CARSIM vehicle library were modified to represent the 820C and 2000P design test vehicles of *NCHRP Report 350*. Accurate suspension response was obtained by testing coil-springs and dampers from actual test vehicles. Properties obtained from these tests were used in the final vehicle models. The simulations were performed assuming a "free-wheeling" mode in which no steering, braking, or throttle inputs were applied to the vehicle as it encroached onto the roadside. One hundred and twelve CARSIM simulations were performed to quantify the trajectory envelopes for the vehicles traversing selected roadside and median configurations at different encroachment conditions.

Performance limits of the barriers obtained from LS-DYNA simulations were superimposed onto the trajectory envelopes developed from CARSIM simulations to develop a preliminary guideline for the placements of each barrier on roadside and median slopes. The lateral offset for a given barrier on slope was considered acceptable

where trajectories of the vehicles remained within its performance limit region. Preliminary guidelines were than verified and refined using full-scale LS-DYNA simulations. There are some shortcomings of using multi-rigid body dynamic analysis technique to quantify vehicle trajectory along off-road conditions. As the vehicle re-contacts the ground after a period of free flight on a ditch, its frame undergoes some twists and dampens some of the reaction forces generated from tire to ground impact. The overly rigid vehicle models used in CARSIM fails to capture this frame twist causing the vehicle rise higher than is expected after the re-contact. Also, as a vehicle travel on soft off-road grounds, the tires have a tendency to sink into the ground surface. This deep penetrating nature of the tires on soft ground causes a large difference in tire force during the vehicle traversal(*53*). To this date, there are no commercially available vehicle dynamic software package which have validated their tire model for soft soil traversal(*53*). Thus, CARSIM predicted trajectory of the vehicle after the jounce on a depressed median was higher compared to an actual vehicle trajectory. This produced a conservative guideline for the placement of barrier on the backslope of a depressed median

Vehicle model used in FE simulations are more flexible and can capture the severe vehicle frame twists during a tire to ground contact after a free flight. Hence, to verify, validate, and refine the preliminary guidelines developed from the superposition of the independent impact and trajectory analyses, twelve additional simulations were performed using LS-DYNA. These simulations captured the full encroachment event from departure of the vehicle off the traveled way through impact with the barrier. The matrix selected for the simulation included both the scenarios for which failure was expected and those for which successful containment was predicted. Single dual-sided median barriers are generally used on depressed medians to protect errant vehicles traveling from either direction. To simulate these cases, FE model of dual-sided systems were developed by adding extra rail and blockout elements to the single-sided guardrail models. During these simulations, the preliminary guidelines for the placements of barriers on depressed medians near its override limit controlled region (i.e. adjacent to

the shoulder edge) were found slightly conservative. However, the modified weak post W-beam barrier placed at a preliminary guideline recommended location near its underride limit controlled region (i.e. near bottom of the ditch) failed to successfully contain the small car. The preliminary guideline for the placements of barriers on slope was therefore refined based on the results obtained from these simulations. The final placement guidelines are presented in Section 8 of this report.

9.2. CONCLUSIONS

Following conclusions can be drawn from the guidelines presented in Section 8:

1. Modified Thrie-beam system has the widest range of acceptable placement locations among the systems studied. Unlike others, this system can be placed anywhere on an 8:1 positive roadside slope. The system has the highest override limit due to its higher rail mounting height. It also has the lowest underride limit due to the presence of wider thrie-beam rails and wider blockouts.
2. The modified G4(1S) system, on the other hand, has the lowest override limit due to its lower rail mounting height. Also, the presence of narrower blockout makes the system more susceptible to the vehicle-post snagging during the impacts with small car.
3. High rail mounting height and the presence of wider blockouts make the MGS a better option for the placement on roadside or median slopes.
4. The modified weak post W-beam system was found unfit for the placements on depressed medians. When placing near the shoulder edge on a depressed median, adequate space must be provided for a dual-sided modified weak-post W-beam barrier to accommodate its relatively large lateral deflections. The guideline also does not recommend the placement of this system near the base of a ditch since the high rail mounting heights, easily detachable rail-post connections, and absence of spacers (blockout) make this system least effective in containing small cars with compressed suspension.

5. The relatively low rail mounting height and substantial flexural and tensile strength of the tubular rail make the box-beam system more effective in containing the small car with compressed suspension.
6. Placements of single dual-sided barrier should be avoided on a 6:1 ditch narrower than 9.76 m (32 ft). Two single sided guardrails on either side of the ditch should be used instead.
7. Final barrier placement guideline for the symmetric depressed medians presented in Section 8 comprises the placement guideline from initial slope break point to the center of the ditch and is applicable on both the slopes of a V-shaped ditch.
8. The guidelines developed in this study can be applied on non-symmetric depressed median configurations by using the guidelines for symmetric medians with steeper cross-slope when determining the acceptable range to place a median barrier on the slope. For example if an 8:1 foreslope leads into a 6:1 backslope, the guideline for the 6:1 slope can be conservatively used.

9.3. RECOMMENDATIONS FOR FUTURE RESEARCH

In the present study, the guideline for the placements of barrier on slope were developed using numerical simulations. These guidelines require further validations using full-scale crash tests. The pickup truck tests should be used to evaluate impact performance of a selected barrier placed on both the foreslope and backslope of a median at an offset that the guidelines predict is near the override limit but for which successful containment and redirection is indicated. Small car tests should be performed for the placements near the bottom of the ditch since this is a likely scenario for underride. The guidelines presented in Section 8 should be revised as necessary to incorporate findings from the full-scale crash tests.

The present study investigated the performances of five commonly used barriers on 6:1 and 8:1 slopes. Use of these barriers on a more critical 4:1 slope requires further investigations. Similar study should be performed on other barrier systems. The F-shape

and single slope concrete barriers are widely used on roadside and median slopes. Pickup override is the only concern for the placement of these barriers on slope as there is no chance for small car underride.

In this study, no steering, breaking, or throttle input was applied on the vehicle during the CARSIM simulations to determine off-road vehicle trajectories. The panic "return-to-road steering" input may become more critical compared to a no steer input. In addition, when a vehicle departs the road surface with some degrees of sideslip, the sidewall forces of the tire tends to build up as the vehicle slides over the soft ground (*53*). These forces, often great enough to cause tripped rollover, was not considered in this study. Thus, the effect of driver response and the tripped phenomenon on the off-road vehicle trajectory should be investigated in future researches.

REFERENCES

1. Ross, H.E., and D.L. Sicking. Guidelines for Placement of Longitudinal Barriers on Slopes. *Transportation Research Record*, No. 974, 1984, pp. 3-9.
2. Ross, H.E., D.L. Sicking, R.A. Zimmer, and J.D. Michie. *NCHRP Report 350: Recommended Procedures for the Safety Performance Evaluation of Highway Features.* Transportation Research Board, National Research Council, Washington, D.C., 1993.
3. Buth, C.E., W.L. Menges, and S.K. Schoeneman. *NCHRP Report 350 Test 3-11 on the Modified Penn DOT Type 2 Guardrail.* TTI 473750-3. Texas Transportation Institute, Texas A&M University System, College Station, TX, 2000.
4. Bligh, R.P., S.P. Miaou, D. Lord, and S. Cooner. *Median Barrier Guidelines for Texas.* FHWA/TX-06/0-4254-1. Texas Transportation Institute, Texas A&M University, College Station, TX, 2006.
5. Faller, R.K., K.A. Polivka, B.D. Kuipers, B.W. Bielenberg, J.D. Reid, J.R. Rohde, and D.L. Sicking. Midwest Guardrail System for Standard and Special Applications. *Transportation Research Board, 83rd Annual Meeting*, 2003.
6. Mak, K.K., R.P. Bligh, and W.L. Menges. *Volume XI: Appendix J- Crash Testing and Evaluation of Existing Guardrail Systems.* TTI 471470. Texas Transportation Institute, Texas A&M University System, College Station, TX, 1998.
7. Bullard, D.L., D.C. Alberson, and W.L. Menges. *NCHRP Report 350 Compliance Test 3-11 of the Modified G4(1S) Guardrail with Timber Blockouts.* FHWA-RD-96-175. Texas Transportation Institute, Texas A&M University System, College Station, TX, 1996.
8. Gabauer, D.J., and H.C. Gabler. Methodology to Evaluate the Flail Space Model by Using Event Data Recorder Technology. *Transportation Research Record: Journal of the Transportation Research Board (TRB),* Vol. 1890, 2004, pp. 49-57.

9. Gabauer, D.J., and H.C. Gabler. Comparison of Roadside Crash Injury Metrics Using Event Data Recorders. *Accident Analysis and Prevention,* Vol. 40, 2008, pp. 548-558.
10. CasherTech., *Test Risk Assessment Program (TRAP). Version: 2.3.2.* Texas Transportation Institute, Texas A&M University, College Station, TX, 2010.
11. Michie, J.D. Collision Risk Assessment based on Occupant Flail-Space Model. *Transportation Research Record*, No. 796, 1981, pp. 1-9.
12. AASHTO, *AASHTO Roadside Design Guide Third Edition*. American Association of State Highway and Transportation Officials, Washington, D.C., 2006.
13. AASHTO, *AASHTO Guide to Standardized Highway Barrier Hardware*. AASHTO-AGC-ARTBA Joint Committee Task Force 13, 2000.
14. Polivka, K.A., R.K. Faller, D.L. Sicking, J.D. Reid, J.R. Rohde, J.C. Holloway, B.W. Bielenberg, and B.D. Kuipers. *Development of the Midwest Guardrail System (MGS) for Standard and Reduced Post Spacing and in Combination with Curbs.* TRP-03-139-04. Midwest Roadside Safety Facility, Uniersity of Nebraska-Lincoln, Lincoln, NE, 2004.
15. Sheikh, N.M., and R.P. Bligh. *Analysis of the Impact Performance of Concrete Median Barrier Placed on or Adjacent to Slopes.* Report 0-5206. Texas Transportation Institute, Texas A&M University System, College Station, TX, 2005.
16. Sheikh, N.M., R.P. Bligh, and W.L. Menges. *Crash Testing and Evaluation of F-shape Barriers on Slopes.* FHWA/TX-08/0-5210-3. Texas Transportation Institute, Texas A&M University System, College Station, TX, 2008.
17. Marzougui, D., P. Mohan, C.D. Kan, and K. Opilea. Performance Evaluation of Low-Tension, Three Strand Cable Median Barriers. *Transportation Research Record*, No. 2025, 2007, pp. 34-44.
18. NCAC. *Development of Guidance for the Selection, Use, and Maintenance of Cable Barrier Systems.* NCHRP 22-25 Qtr. Progress Report. National Crash Analysis Center, Ashburn, VA, 2009.

19. Johnson, E.A., K.A. Lechtenberg, J.D. Reid, D.L. Sicking, R.K. Faller, R.W. Bielenberg, and J.R. Rohde. *Approach Slope for Midwest Guardrail System.* Midwest Roadside Safety Facility, University of Nebraska-Lincoln, Nebraska, 2008.
20. Reid, J.D. Approach Slopes for Midwest Guardrail System. *Journal of Transportation Safety & Security,* Vol. 1, 2009, pp. 32-45.
21. Plaxico, C.A., F. Mozzarelli, and M.H. Ray. Tests and Simulation of a W-beam Rail-to-Post Connection. *International Journal of Crashworthiness,* Vol. 8, No. 6, 2003, pp. 543-551.
22. Marzougui, D., P. Mohan, C.D. Kan, and K. Opilea. *Evaluation of Rail Height Effects on the Safety Performance of W-beam Barriers.* NCAC 2007-W-002. National Crash Analysis Center, Ashburn, VA, 2007.
23. Ray, M.H., K. Engstrand, C.A. Plaxico, and R.G. McGinnis. Improvements to the Weak-Post W-Beam Guardrail. *Transportation Research Board, 80th Annual Meeting*, No. 1743, 2001, pp. 88-96.
24. Engstrand, K. *Improvements to the Weak-Post W-beam Guardrail*. Department of Civil Engineering, Worcester Polytechnic Institute, Worcester, MA, 2000.
25. Sonnenschein, U. Modeling of Bolts Under Dynamic Loads. *Crash II-Verbindungstechnik, Versagen*. LS-DYNA User Forum, Bamberg, 2008.
26. Hendricks, B., and J. Wekezer. Finite-Element Modeling of G2 Guardrail. *Transportation Research Record: Journal of the Transportation Research Board,* Vol. 1528, 1996, pp. 130-137.
27. Plaxico, C.A. *Design Guidelines for the Use of Curbs and Curb/Guardrail Combinations along High-Speed Roadways*. Department of Civil Engineering, Worcester Polytechnic Institute, Worcester, MA, 2000.
28. Patzner, G.S., C.A. Plaxico, and M.H. Ray. Effect of Post and Soil Strength on the Performance of the Modified Eccentric Loader Breakaway Cable Terminal. *Transportation Research Record*, No. 1690, 1999, pp. 78-83.
29. Hallquist, J.Q. *LS-DYNA Theory Manual*. Livermore Software Technology Corporation, Livermore, CA, 2006.

30. Uddin, W. Crashworthiness Analysis and Simulations of Vehicles Impacting a Roadside Guardrail. *CMES - Computer Modeling in Engineering and Sciences,* Vol. 5, No. 3, 2004, pp. 269-278.
31. Ray, M.H., C.A. Plaxico, and M. Anghileri. *Recommended Procedures for Verification and Validation of Computer Simulations Used for Roadside Safety Applications.* NCHRP 22-24. Worcester Polytechnic Institute, Worcester, MA, 2009.
32. Schwer, L.E. Validation Metrics for Response Histories: Perspectives and Case Studies. *Engineering with Computers,* Vol. 23, No. 4, 2007, pp. 295-309.
33. Ray, M.H. Repeatability of Full-Scale Crash Tests and Criteria for Validating Simulation Results. *Transportation Research Record*, No. 1528, 1996, pp. 155-160.
34. Mongiardin, M., and M.H. Ray. *Roadside Safety Verification and Validation Program User's Manual.* Worcester Polytechnic Institute, Worcester, MA, 2009.
35. Mechanical Simulation Corporation, *CARSIM. Version: 8.* Ann Arbor, MI, 1996.
36. Mechanical Simulation Corporation, *CARSIM Reference Manual.* Ann Arbor, MI, 2008.
37. Bligh, R.P., M.R. Ferdous, A. Abu-Odeh, and N.M. Sheikh. *Placements of Traffic Barriers on Roadside and Median Slopes.* NCHRP 22-22 Interim Report. Texas Transportation Institute, Texas A&M University, College Station, TX, 2009.
38. Mongiardin, M., and M.H. Ray, *Roadside Safety Verification and Validation Program. Version: 1.7.* Worcester Polytechnic Institute, Worcester, MA, 2009.
39. Gillespie, T.D. *Fundamentals of Vehicle Dynamics*. Society of Automotive Engineers Inc., Warrendale, PA, 1992.
40. National Crash Analysis Center. *NCAC Finite Element Model Archive*. http://www.ncac.gwu.edu/vml/models.html. Accessed: Dec 10, 2008.
41. LSTC, *LS-DYNA Keyword User's Manual (Version 971).* Livermore Software Technology Corporation, Livermore, CA, 2007.

42. Reid, J.D., and B.W. Bielenberg. Using LS-DYNA Simulation to Solve a Design Problem: Bull-nose Guardrail Example. *Transportation Research Record*, No. 1690, 1999, pp. 95-102.
43. American Society of Testing and Material, *Annual Book of ASTM standards (Part 4) : Steels- Structural, Reinforcing, Pressure Vessel, Railway, Fasteners.* West Conshohocken, PA, 1978.
44. Abu-Odeh, A., R.P. Bligh, and M.E. Hamilton. *Analysis and Design of the Texas T-6 Breakaway Bridge Railing System Using Finite Element Methodology.* TTI 473210-3. Texas Transportation Institute, Texas A&M University System, College Station, TX., 2001.
45. Mongiardin, M. *Development of a Computer Program for the Verification and Validation of Numerical Simulation in Roadside Safety*. Department of Civil Engineering, Worcester Polytechnic Institute, Worcester, MA, 2010.
46. Ray, M.H., A.O. Atahan, M. Mongiardin, C.A. Plaxico, and M. Anghileri. *Development of Verification and Validation Procedures for Computer Simulations Used in Roadside Safety Application.* NCHRP 22-24 Interim Report. Worcester Polytechnic Institute, Worcester, MA, 2007.
47. Heydinger, G.J., R.A. Bixel, W.R. Garrot, M. Pyne, J.G. Howe, and D.A. Guenther. Measured Vehicle Inertia Parameters - NHTSA's Data through November 1998. *Society of Automotive Engineers-Paper 1999-01-1336*, 1999.
48. Enders, J. *Personal Communication: Tests Performed on Coil Springs and Shock Absorbers of a Chevy 2500 Pickup and a Geo Metro Passange Car.* RE Suspension Inc., Mooresville, NC, 2009.
49. Harris, W. *How Car Suspension Works?* http://auto.howstuffworks.com/car-suspension.htm/printable. Accessed: Nov, 2010.
50. NCAC. *Development of Guidance for the Selection, Use, and Maintenance of Cable Barrier Systems.* NCHRP 22-25 Qtr. Prog. Report. National Crash Analysis Center, Ashburn, VA, 2009.

51. Reid, J.D., D.A. Boesch, and R.W. Bielenberg. Detailed Tire Modeling for Crash Applications. *International Journal of Crashworthiness,* Vol. 12, No. 5, 2007, pp. 521-529.
52. Orengo, F., M.H. Ray, and C.A. Plaxico. *Modeling Tire Blow-out in Roadside Hardware Simulations Using LS-DYNA*. 2003 ASME International Mechanical Engineering Congress, November 15, 2003 - November 21, 2003, Washington, DC, 2003.
53. Stine, J.S. *Analyzing Highway Median Safety through Vehicle Dynamic Simulations*. Department of Mechanical and Nuclear Engineering, Pennsylvania State University, University Park, PA, 2009.

APPENDIX A. IMPORTANT TABLES AND FIGURES

Table A.1 Safety Evaluation guideline for test designation 3-10 and 3-11 (Table 5.1 in NCHRP Report 350)

<table>
<tr><th>Evaluation Factors</th><th>Evaluation Criteria</th><th>Applicable tests</th></tr>
<tr><td>Structural Adequacy</td><td>A. Test article should contain and redirect the vehicle; the vehicle should not penetrate, underride, or override the installation although controlled lateral deflection of the test article is acceptable</td><td>10, 11, 12, 20, 21, 22, 35, 36, 37, 38</td></tr>
<tr><td rowspan="5">Occupant Risk</td><td>D. Detached elements, fragments or other debris from the test article should not penetrate or show potential for penetrating the occupant compartment, or present an undue hazard to other traffic, pedestrians, or personnel in a work zone. Deformation of, or intrusion into, the occupant compartment that could cause serious injuries should not be permitted.</td><td>All</td></tr>
<tr><td>F. The vehicle should remain upright during and after the collision although moderate roll, pitchin, and yawing are acceptable.</td><td>All except those listed in criterion G.</td></tr>
<tr><td>G. It is preferable, although not essential, that the vehicle remain upright during and after collision.</td><td>12, 22, 30[b], 31[b], 32[b], 33[b],34[b],35[b],36[b],37[b], 38[b],39[b], 40[b], 41[b],42[b], 43[b],44[b].</td></tr>
<tr><td>H. Occupant Impact Velocities should satisfy the followings
<table>
<tr><th colspan="3">Occupant Impact Velocity Limits</th></tr>
<tr><td>Component</td><td>Preferred</td><td>Maximum</td></tr>
<tr><td>Longitudinal and Lateral</td><td>9 m/s (30 ft/s)</td><td>12 m/s (40 ft/s)</td></tr>
</table></td><td>10, 20, 30, 31, 32, 33, 34, 36, 40, 41, 42, 43, 50, 51, 52, 53, 80, 81.</td></tr>
<tr><td>I. Occupant Ridedown Acceleration should satisfy the followings
<table>
<tr><th colspan="3">Occupant Ridedown Acceleration (G’s)</th></tr>
<tr><td>Component</td><td>Preferred</td><td>Maximum</td></tr>
<tr><td>Longitudinal and Lateral</td><td>15</td><td>20</td></tr>
</table></td><td>10, 20, 30, 31, 32, 33, 34, 36, 40, 41, 42, 43, 50, 51, 52, 53, 60, 61, 70, 71, 80, 81</td></tr>
<tr><td rowspan="3">Vehicle Trajectory</td><td>K. After collision it is preferable that the vehicle’s trajectory not intrude into adjacent traffic lanes.</td><td>All</td></tr>
<tr><td>L. The occupant impact velocity in the longitudinal direction should not exceed 12 m/s and the occupant ridedown acceleration in longitudinal direction should not exceed 20 G’s</td><td>11, 21, 35, 37, 38, 39</td></tr>
<tr><td>M. The exit angle from the test article preferably should be less that 60 percent of test impact angle, measured at time of vehicle loss of contact with test device</td><td>10, 11, 12, 20, 21, 22, 35, 36, 37, 38, 39</td></tr>
</table>

Table A.2 Properties of common barrier rail elements (Table A3.1 in NCHRP Report 350)

Rail[a]	Elastic Section Modulus (cm^3)	Form Factor	Plastic Section Modulus (cm^3)	Plastic Moment (kN-m)
12 ga. W-beam	22.5	1.41	31.6	10.9
10 ga. W-beam	28.8	1.41	40.6	14.0
12 ga. Thrie-beam	35.7	1.40	50.0	17.2
10 ga. Thrie-beam	45.9	1.40	64.2	22.1
W6×15	159	1.11	177	43.9
TS 6×6×3/16 Box Beam	134	1.16	156	49.5
TS 6×6×3/8 Box Beam	244	1.20	293	93.0
TS 8×6×1/14	257	1.19	306	97.1

[a] Post Sizes are in English units

Table A.3 Dynamic Yield forces of posts embedded in strong soil (Table A3.3 in NCHRP Report 350)

Post Type[a]	Embedment Depth (m)	Maximum Soil Limit (kN)	Maximum Post Limit (kN)
6 inch × 8 inch Wood Post	0.91	50.2	72.1
8 inch × 8 inch Wood Post	0.91	55.2	101.0[b]
10 inch × 10 inch Wood Post	0.91	72.5	205.0[b]
W6×9 Steel Post	1.12	55.2	65.0
W6×15 Steel Post	1.12	81.4	105.2

[a] Post Sizes are in English units
[b] Estimated for Douglas Fir using Equation A3.1

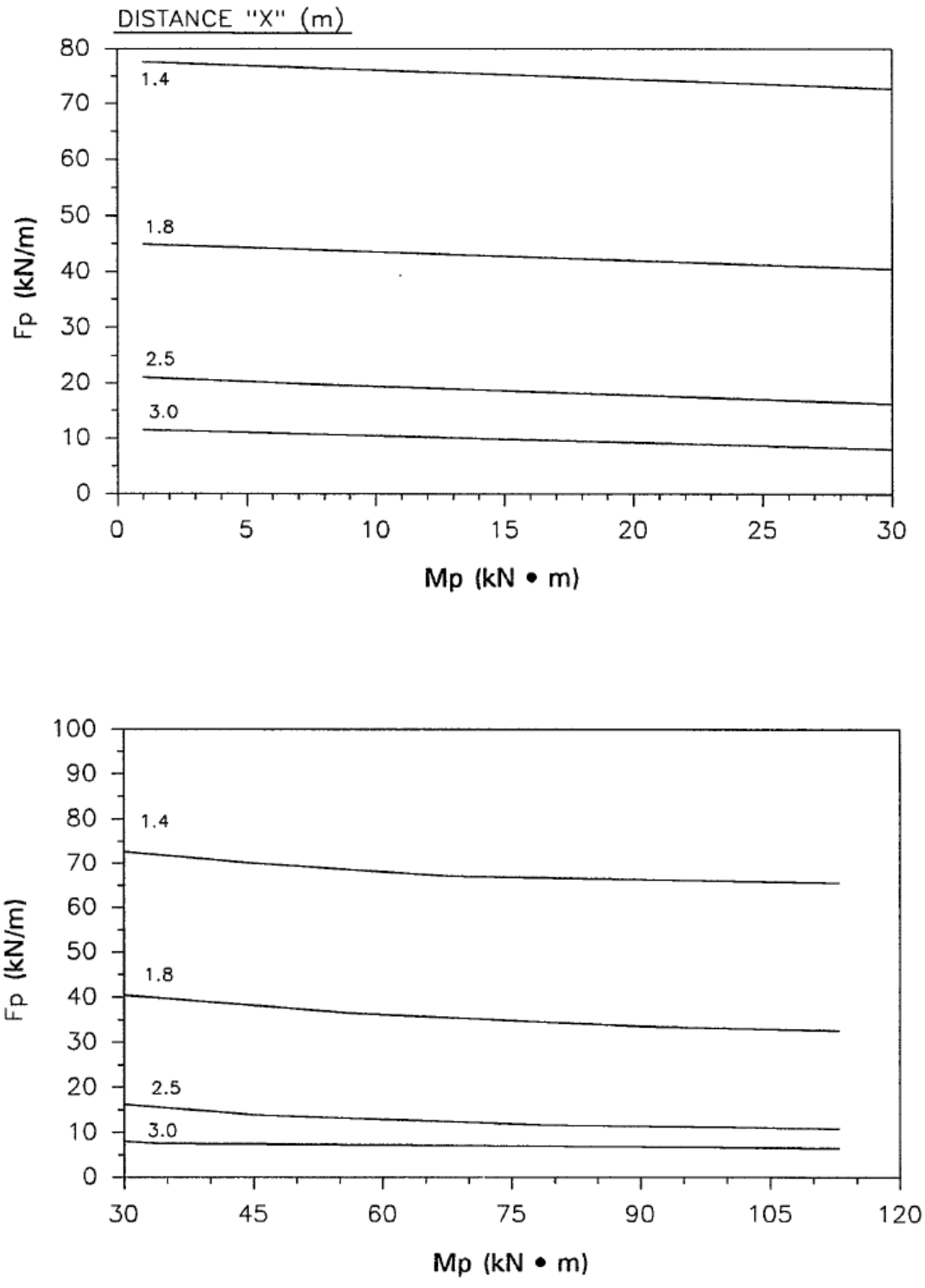

Figure A.1 Critical impact point for Test 10, levels 3, 4, 5, and 6 (Figure 3.8 in NCHRP Report 350)

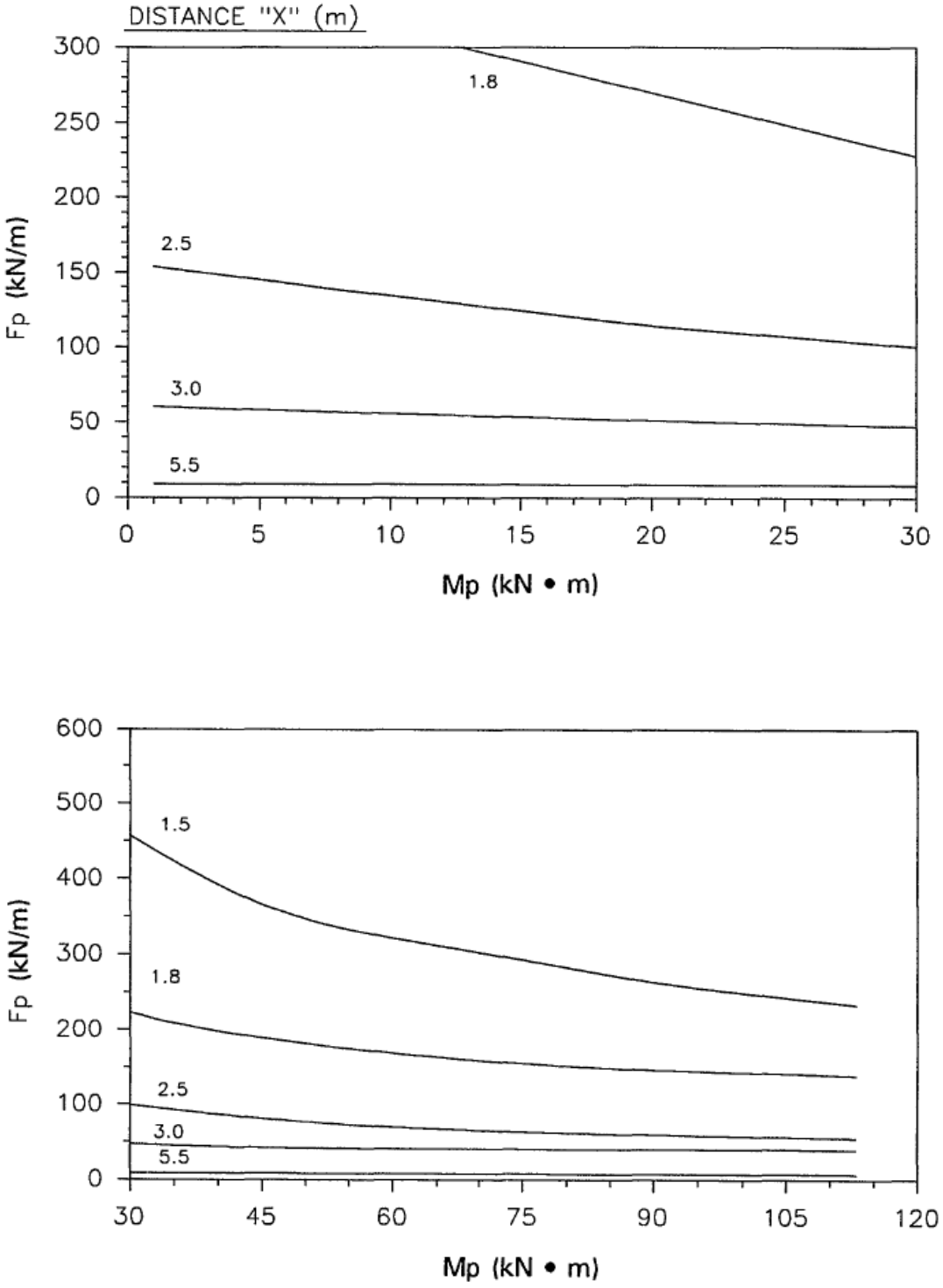

Figure A.2 Critical impact point for Test 11, levels 3, 4, 5, and 6 (Figure 3.10 in NCHRP Report 350)

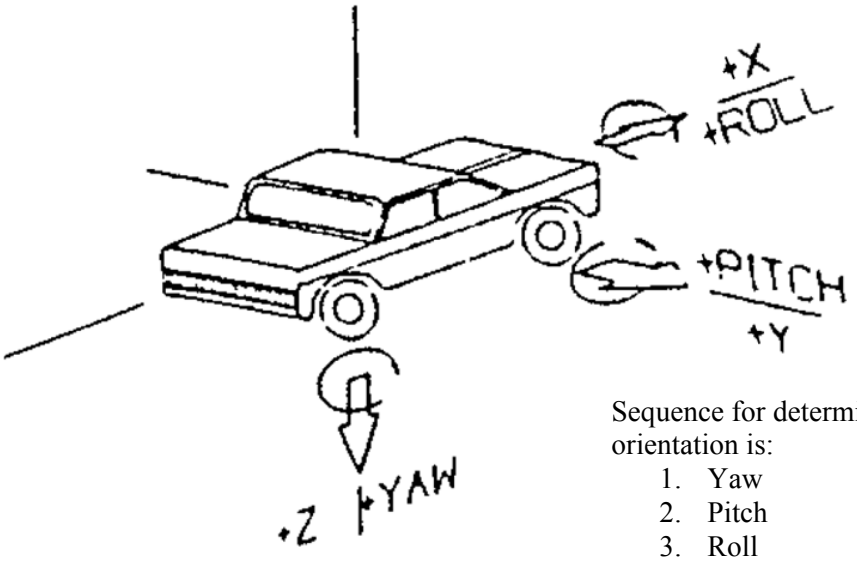

Sequence for determining orientation is:

1. Yaw
2. Pitch
3. Roll

Figure A.3 Vehicle Fixed Coordinate System

APPENDIX B. THIRD-PARTY TEST RESULTS

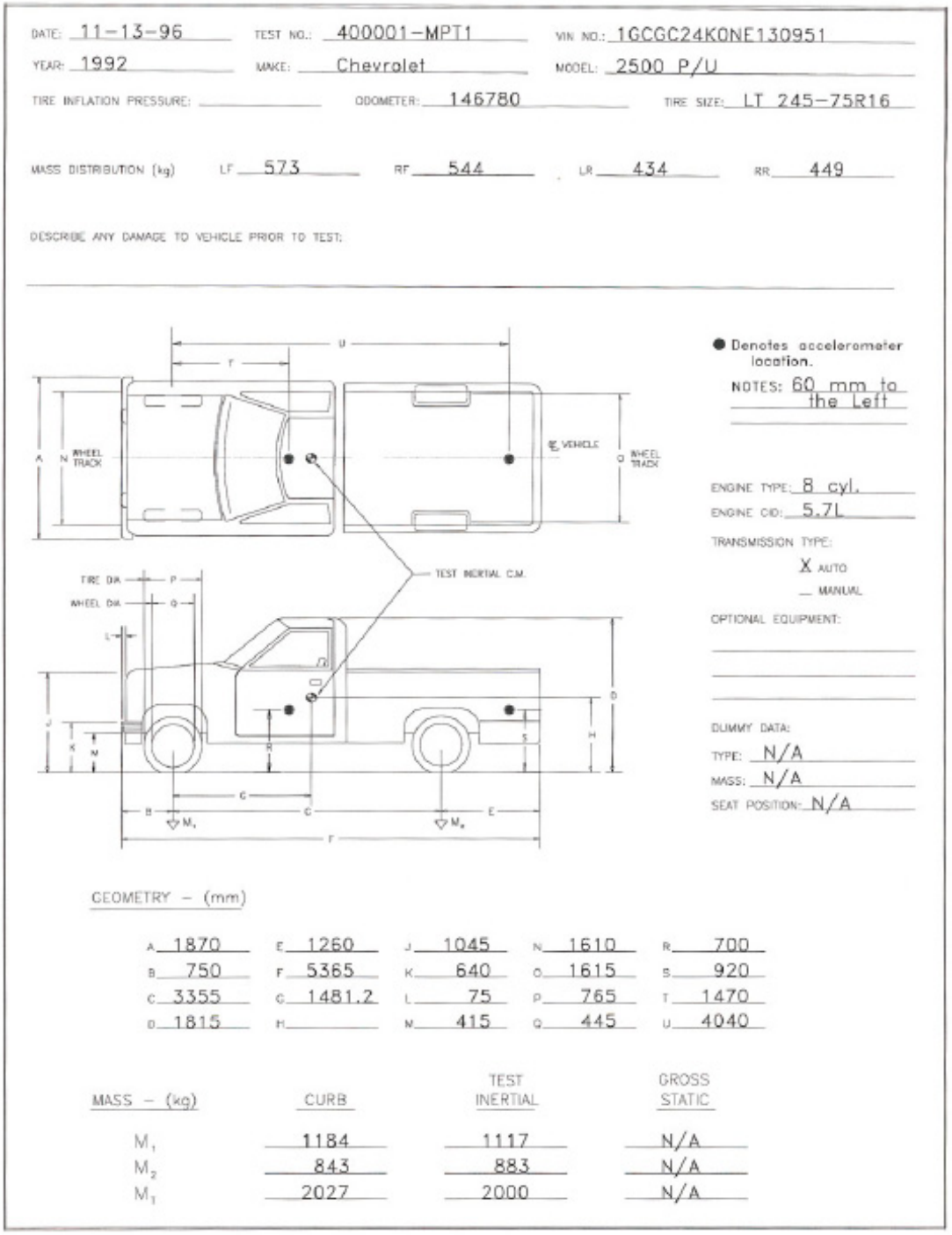

DATE: 11-13-96 TEST NO.: 400001-MPT1 VIN NO.: 1GCGC24K0NE130951

YEAR: 1992 MAKE: Chevrolet MODEL: 2500 P/U

TIRE INFLATION PRESSURE: ____ ODOMETER: 146780 TIRE SIZE: LT 245-75R16

MASS DISTRIBUTION (kg) LF 573 RF 544 LR 434 RR 449

DESCRIBE ANY DAMAGE TO VEHICLE PRIOR TO TEST:

● Denotes accelerometer location.

NOTES: 60 mm to the Left

ENGINE TYPE: 8 cyl.

ENGINE CID: 5.7L

TRANSMISSION TYPE:

X AUTO

__ MANUAL

OPTIONAL EQUIPMENT:

DUMMY DATA:

TYPE: N/A

MASS: N/A

SEAT POSITION: N/A

GEOMETRY – (mm)

A	1870	E	1260	J	1045	N	1610	R	700
B	750	F	5365	K	640	O	1615	S	920
C	3355	G	1481.2	L	75	P	765	T	1470
D	1815	H		M	415	Q	445	U	4040

MASS – (kg)	CURB	TEST INERTIAL	GROSS STATIC
M_1	1184	1117	N/A
M_2	843	883	N/A
M_T	2027	2000	N/A

Figure B.1 Vehicle measurement sheet developed at TTI for a 2000-kg Pickup

Date: 04-07-2006 Test No.: RF474970-1 VIN No.: 2C1MR2294T6717573

Year: 1996 Make: Chevrolet Model: Metro

Tire Inflation Pressure: 32 psi Odometer: 125329 Tire Size: P155/80R13

Describe any damage to the vehicle prior to test:

⌖ Denotes accelerometer location.

NOTES:

Engine Type: 4 cylinder
Engine CID: 1.3 liter
Transmission Type:
X Auto
___ Manual
Optional Equipment:

Dummy Data:
Type: 50th percentile male
Mass: 74 kg
Seat Position: Driver

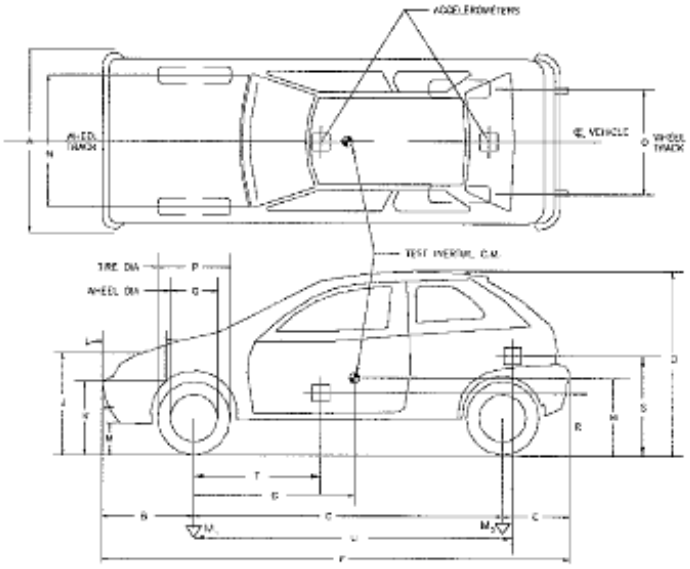

Geometry (mm)

A	1590	E	600	J	850	N	1385	R	420
B	790	F	3755	K	515	O	1350	S	550
C	2365	G	879.8	L	102	P	570	T	950
D	1410	H	513	M	400	Q	365	U	2420

Mass (kg)	Curb	Test Inertial	Gross Static
M_1	532	525	562
M_2	300	311	348
M_{Total}	832	836	910

Mass Distribution (kg): LF 266 RF 259 LR 156 RR 155

Figure B.2 Vehicle measurement sheet developed at TTI for 820-kg Geo-Metro car

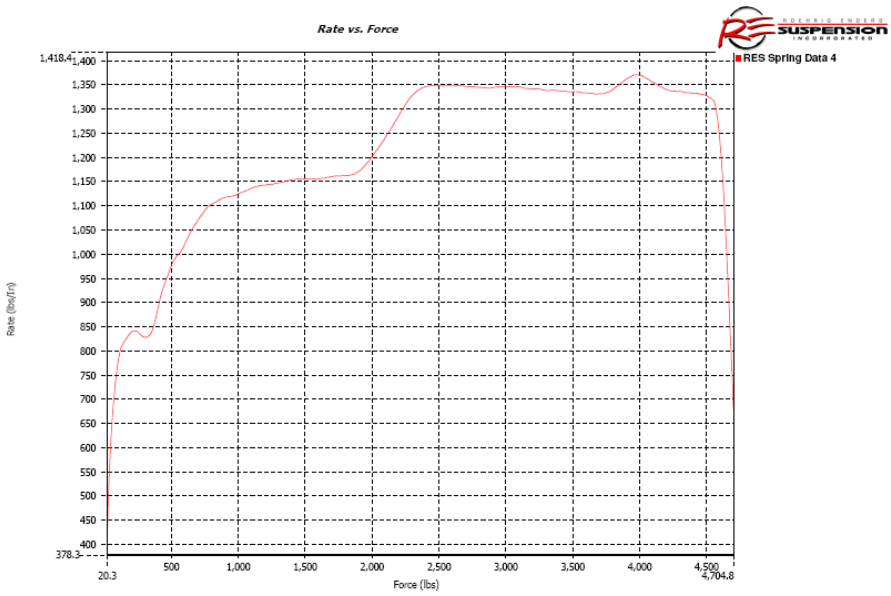

HeightForce: 10.00 lbs
ZeroForceLength: 14.925 in
TestedAverageRateExtension: 1,111.04 lbs/In
TestedAverageRateAverage: 1,110.67 lbs/In
TestedEndPointRateAverage: 1,111.16 lbs/In
MaxTravel: 3.787 in
TestedStartPoint: 500.00 lbs

TestedEndPointRateExtension: 1,110.27 lbs/In
FreeLength: 14.911 in
CoilBind: 11.124 in
TestedEndPoint: 1.000 in
TestedEndPointRelativeToStart: True
TestedAverageRateCompression: 1,111.48 lbs/In
TestedEndPointRateCompression: 1,112.22 lbs/In

Displacement (in)	Force (lbs)	Rate (lbs/In)
11.100	4,531.21	1,322.69
11.200	4,398.15	1,332.20
11.300	4,264.69	1,336.97
11.400	4,130.79	1,350.54
11.500	3,994.46	1,370.87
11.600	3,857.37	1,352.89
11.700	3,723.82	1,331.81
11.800	3,590.62	1,333.28
11.900	3,457.18	1,336.14
12.000	3,323.38	1,338.43
12.100	3,189.44	1,342.14
12.200	3,054.99	1,346.22
12.300	2,920.25	1,345.15
12.400	2,785.92	1,345.32
12.500	2,651.16	1,348.37
12.600	2,516.40	1,347.74
12.700	2,381.58	1,344.71
12.800	2,247.81	1,308.55
12.900	2,119.93	1,249.97
13.000	1,997.33	1,200.52
13.100	1,879.46	1,167.50
13.200	1,763.32	1,161.83
13.300	1,647.18	1,157.40
13.400	1,531.71	1,155.13
13.500	1,416.06	1,154.24
13.600	1,300.89	1,147.33
13.700	1,186.46	1,142.42
13.800	1,072.38	1,133.11
13.900	959.87	1,120.50
14.000	848.08	1,110.61
14.100	737.81	1,086.01
14.200	630.92	1,039.61
14.300	529.76	992.23
14.400	432.35	924.68
14.500	345.18	835.61
14.600	263.36	835.01
14.700	178.56	831.64
14.800	97.09	771.19
14.900	26.65	484.58

Figure B.3 Compression test results for the front coil spring of a 2000-kg Chevrolet C2500 pickup (source: RE suspension Inc.)

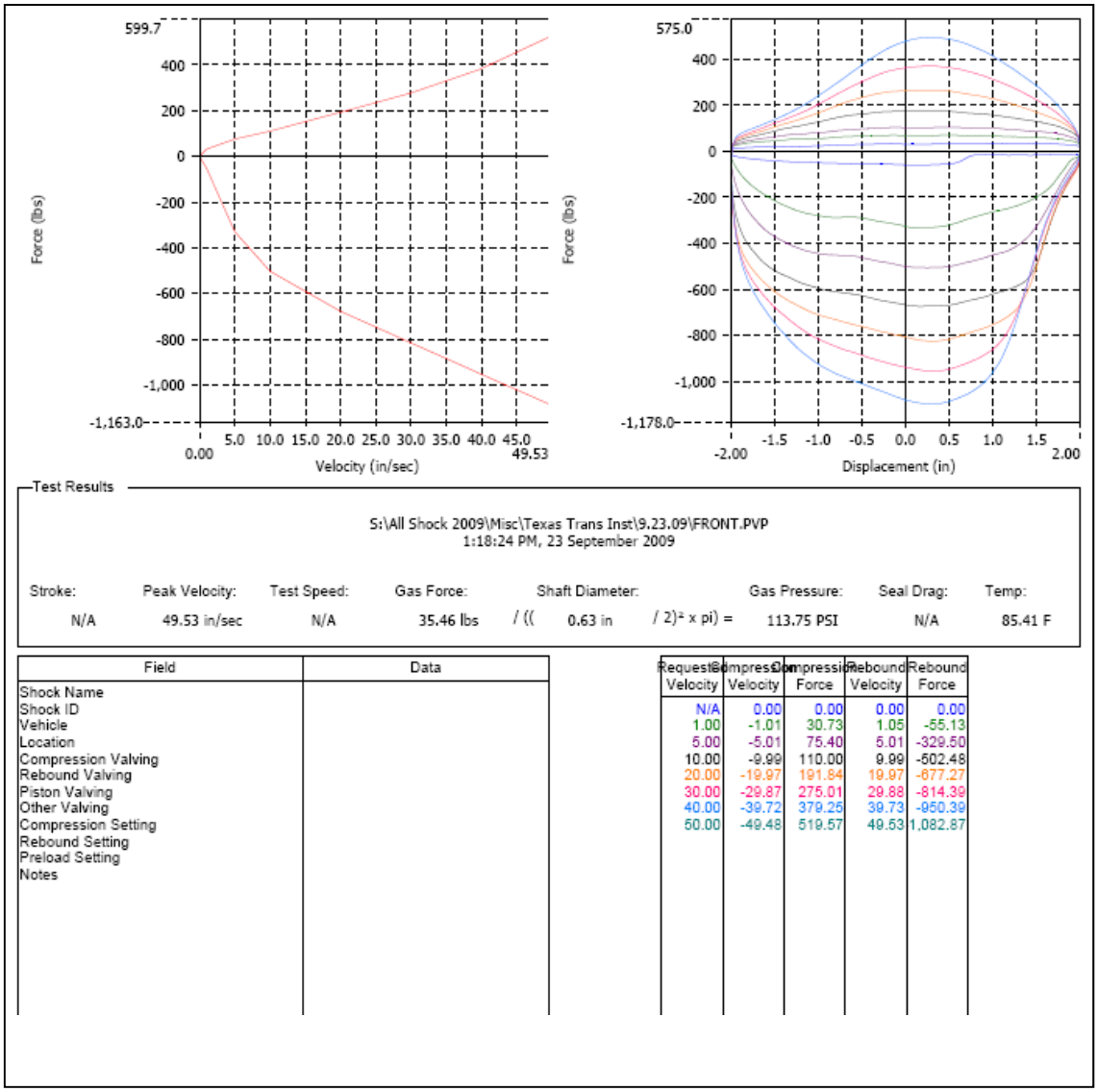

Figure B.4 Dynamometer test results for the front dumper of a 2000-kg Chevrolet C2500 pickup (source: RE suspension Inc.)

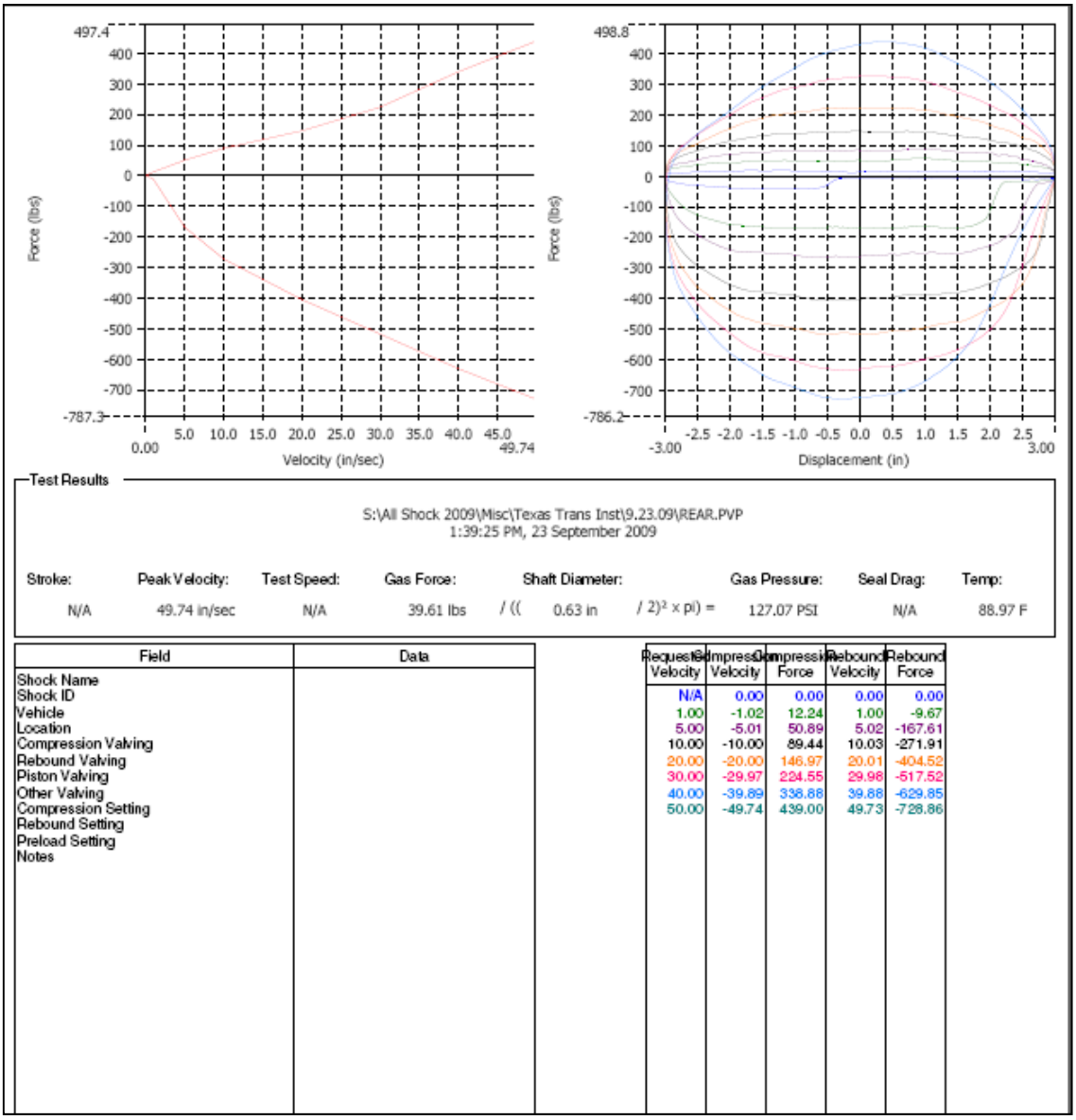

Figure B.5 Dynamometer test results for the rear dumper of a 2000-kg Chevrolet C2500 pickup (source: RE suspension Inc.)

Table B.1 Compression test results for the front coil spring of an 820-kg Geo-Metro (source: RE suspension Inc.)

Displacement (in)	Force (lbs)	Rate(lbs/in)	Displacement (in)	Force (lbs)	Rate(lbs/in)
3.5	933.1	129.16	7.5	455.56	123.68
3.6	919.85	118.95	7.6	443.52	130.61
3.7	908.23	120.47	7.7	431.28	128.31
3.8	896.86	109.81	7.8	419.14	126.77
3.9	884.97	119.82	7.9	407.01	121.34
4	873.28	113.68	8	395.25	115.14
4.1	861.52	115.93	8.1	383.43	112.85
4.2	849.98	128.3	8.2	371.56	122.12
4.3	837.91	117.45	8.3	359.56	126.74
4.4	826.12	116.74	8.4	347.95	116.71
4.5	814.36	122.94	8.5	336.16	119.07
4.6	802.08	118.27	8.6	324.57	122.93
4.7	790.78	116.79	8.7	313.55	91.98
4.8	778.43	119.76	8.8	302.18	110.51
4.9	766.36	117.49	8.9	290.45	116.7
5	754.36	118.28	9	279.12	118.25
5.1	742.3	122.1	9.1	267.95	117.5
5.2	730.16	117.41	9.2	256.23	114.38
5.3	717.88	117.42	9.3	245.03	121.35
5.4	705.98	128.42	9.4	233.76	115.18
5.5	693.88	122.11	9.5	221.94	114.4
5.6	681.71	120.59	9.6	210.63	106.68
5.7	669.57	129.84	9.7	198.98	121.34
5.8	657.01	121.35	9.8	187.92	121.34
5.9	644.98	125.93	9.9	176.06	111.31
6	633.5	108.23	10	164.55	119.81
6.1	621.74	110.55	10.1	153.17	112.84
6.2	609.54	117.49	10.2	142.67	119.03
6.3	598.37	125.97	10.3	131.72	112.04
6.4	586.54	122.9	10.4	120.86	113.63
6.5	574.41	118.28	10.5	110.12	117.5
6.6	562.79	122.9	10.6	99.19	108.99
6.7	551	116.76	10.7	88.1	112.07
6.8	539.1	115.92	10.8	77.84	104.34
6.9	527.45	122.11	10.9	67.06	111.3
7	515.31	117.47	11	56	106.66
7.1	503.24	116.71	11.1	45.67	115.16
7.2	491.28	124.44	11.2	35.02	102.79
7.3	479.28	117.46	11.3	24.31	101.25
7.4	467.35	121.37	11.4	14.54	85.03

Table B.2 Compression test results for the rear coil spring of a 820-kg Geo-Metro (source: RE suspension Inc.)

Displacement (in)	Force (lbs)	Rate(lbs/in)
3.7	2395.36	6907.51
3.8	2044.11	4671.81
3.9	1794.26	1084.46
4	1725.36	633.81
4.1	1661.95	636.84
4.2	1608.62	442.94
4.3	1571.99	305.09
4.4	1544.42	269.02
4.5	1518.13	254.13
4.6	1491.93	269.15
4.7	1465.6	261.05
4.8	1439.43	264.7
4.9	1413.54	271.48
5	1387.15	268.97
5.1	1360.74	269.53
5.2	1334.31	265.88
5.3	1307.84	266.05
5.4	1281.28	262.41
5.5	1254.91	263.79
5.6	1228.16	261.38
5.7	1201.76	271.08
5.8	1175.19	263.38
5.9	1148.74	270.26
6	1121.56	269.96
6.1	1095.02	268.74
6.2	1069.23	242.29
6.3	1044.38	242.66
6.4	1019.67	242.27
6.5	994.91	251.58
6.6	970.23	249.06
6.7	946.02	245.34
6.8	921.54	245.74
6.9	896.71	250.22
7	871.6	241.73
7.1	846.74	246.92
7.2	822.01	245.17
7.3	796.85	244.67
7.4	772.39	252.54

Displacement (in)	Force (lbs)	Rate(lbs/in)
7.5	747.59	250.02
7.6	722.61	257.93
7.7	697.47	246.89
7.8	672.48	245.97
7.9	647.03	251.95
8	623.04	249.01
8.1	597.71	253.46
8.2	572.87	248.99
8.3	547.56	239.78
8.4	522.56	251.73
8.5	497.05	244.23
8.6	472.48	250.97
8.7	447.12	247.32
8.8	422.04	253.64
8.9	397.14	238.99
9	372.69	238.65
9.1	348.39	248.22
9.2	324.17	242.39
9.3	300.79	239.42
9.4	276.9	230.32
9.5	252.6	243.81
9.6	228.85	237.64
9.7	204.66	244.35
9.8	180.64	248.52
9.9	156.54	237.28
10	133.09	231.67
10.1	109.37	235.14
10.2	85.82	234.72
10.3	63.1	223.72
10.4	40.26	213.18
10.5	25.36	148.4
10.6	11.84	129.25

Table B.3 Dynamometer test results for the front damper of an 820-kg Geo-Metro (source: RE suspension Inc.)

Compression Velocity	Compression Force	Rebound Velocity	Rebound Force
in/sec	Lbs	lbs	lbs
0	0.000004	0	0.000004
-1.001036	12.53389	1.001254	-21.0618
-5.002568	26.33237	5.000133	-112.901
-10.00116	40.15339	10.00044	-137.312
-19.99821	64.71188	19.99514	-181.936
-29.96299	93.82364	29.97183	-233.194
-39.91637	122.7546	39.93626	-293.163
-44.92518	140.2531	44.89177	-319.073
-49.90936	159.2723	49.86916	-347.834

Table B.4 Dynamometer test results for the rear damper of an 820-kg Geo-Metro (source: RE suspension Inc.)

Compression Velocity	Compression Force	Rebound Velocity	Rebound Force
in/sec	lbs	lbs	lbs
0	0	0	0
-1.00331	16.63718	1.003136	-20.7103
-5.01693	39.57695	5.015253	-153.771
-10.0295	56.52112	10.02827	-186.831
-20.0534	81.28629	20.05562	-248.095
-30.0731	110.0402	30.06435	-318.756
-40.0592	141.9512	40.05983	-407.679
-45.0393	159.6826	45.07288	-456.252
-50.0137	179.5159	50.06487	-512.953

APPENDIX C. COMPUTER CODES TO PRE-AND POST- PROCESS CARSIM DATA

C.1 PROGRAM SOURCE CODE

```
%% Singlerun.m
%% script to run CARSIM Median Study
%% Oct 21st, 2009
cd ('D:/_users/r-ferdous/carsim data');
close all
clear all
clc
bdclose  %Close any or all SIMULINK system windows unconditionally
tic

%%%%%% INPUT parameters%%%%%%%%%%%%%%%
Encroach_Ang=[25];      speed =[100];
DitchWidth=[64];       Slope=[6];
RdFriction=[0.85;0.3];
%%%%%%%%%%%%%%%%%%%%%%%%%%%%%%%%%%%%

Nang=size(Encroach_Ang,1);  Nspeed=size(speed);
NDW=size(DitchWidth,1);    Nslope=size(Slope,1);
unit_con=3.28;  %%converts ft to m.....1m=3.28ft
%%% For Ditch configuration
%%LL= length of each line ; Offset= starting point(in lateral dir) for
%%entrance line
XP2=250; LL=30; Offset=3.428;

for dd = 1:Nspeed %%  Speed
    for cc = 1:Nang %%1-6 encroachment angle
        for aa = 1:NDW  %Ditch Width
            for bb = 1:Nslope   % Slope
%% write the Simulink import pars file
                fid = fopen('Sim_ICs.par', 'wt');
                fprintf(fid,'PARSFILE \n\n');
                fprintf(fid,'OPT_INIT_ROAD 0\n');
                fprintf(fid, 'SPEED %3.2f\n',speed(dd));
                fprintf(fid, 'END\n');
                fclose(fid);
                %%convert ft to m.....1m=3.28ft
%% Calculate Ditch Profile
                MWm=DitchWidth(aa)/unit_con;    slope=Slope(bb);
                ditch_offset=-MWm/2*1/slope;     Ang=-Encroach_Ang(cc)*pi/180;
                cd ('D:\_users\r-ferdous\carsim data\MatlabCode');
                [Xcrd,Ycrd,Xoff,Yoff,S]=Carsim_Ditchprofile(Ang,MWm,...
                    ditch_offset,XP2,Offset);
                cd('D:\_users\r-ferdous\carsim data\External Parsfile');
%% write the XY coordinate for the road
                fid = fopen('RoadXY.par', 'wt');
                fprintf(fid,'PARSFILE \n');
                fprintf(fid,'#Approach Angle:%d degree\n\n',Encroach_Ang(cc));
                fprintf(fid,'SPATH 0\n');
                fprintf(fid,'OPT_ROAD_LOOP 0\n');
                fprintf(fid,'OPT_ROAD 1\n');

                fprintf(fid,'YIN_TABLE\n');
                for i=1:6
                   fprintf (fid, ' %10.3f %10.3f %10.3f\n',Xcrd(i),Ycrd(i),S(i));
                end
                fprintf(fid, 'ENDTABLE\n');
                fprintf(fid, 'END\n');
```

```
                fclose(fid);
%% write the Off center Elevation map data
                fid = fopen('Road.par', 'wt');
                fprintf(fid,'PARSFILE \n');
                fprintf(fid,'#DitchWidth:%dft, Slope: %dH:1V\n\n',...
                    DitchWidth(aa),Slope(bb));
                fprintf(fid, '*3D_XLabel Lateral coordinate (m)\n');
                fprintf(fid, '*3D_YLabel Station (m)\n');
                fprintf(fid, '*3D_ZLabel Incremental elevation (m)\n\n');

                fprintf(fid, '*3D_DATA 5, 6 ! columns x rows\n');
                fprintf(fid, 'ROAD_DZ_CARPET\n');
        fprintf (fid, '%10.3f %10.3f %10.3f  %10.3f %10.3f %10.3f \n'...
                      ,Yoff(1),Yoff(2),Yoff(3),Yoff(4),Yoff(5),Yoff(6));
                for i=1:6
        fprintf (fid, '%10.3f %10.3f %10.3f  %10.3f %10.3f %10.3f \n'...
                      ,Xoff(i,1),Xoff(i,2),Xoff(i,3),Xoff(i,4),Xoff(i,5),Xoff(i,6));
                end
                fprintf(fid, 'ENDTABLE\n');
                fprintf(fid, 'END\n');
                fclose(fid);
%% write the Median Friction Data
                fid = fopen('RdFric.par', 'wt');
                fprintf(fid,'PARSFILE \n');
                fprintf(fid,'#Ditch Friction:%d\n\n',RdFriction(2));
                fprintf(fid,'MU_ROAD_CARPET VAR_WIDTH\n');
                fprintf(fid,'%4.3f %4.3f %4.3f %4.3f %4.3f %4.3f %4.3f\n',...
                    0,1,2,3,4,5,6);
                fprintf(fid,'%4.3f %4.3f %4.3f %4.3f %4.3f %4.3f,... %4.3f\n',S(1),...
                    RdFriction(1),RdFriction(1),RdFriction(2),RdFriction(2),...
                    RdFriction(1),RdFriction(1));
                fprintf(fid,'%4.3f %4.3f %4.3f %4.3f %4.3f %4.3f %4.3f\n',S(6),...
                    RdFriction(1),RdFriction(1),RdFriction(2),RdFriction(2),...
                    RdFriction(1),RdFriction(1));
                fprintf(fid,'ENDDATA\n');
                fprintf(fid,'%4.3f %4.3f %4.3f %4.3f %4.3f %4.3f
%4.3f\n',0,1,2,3,4,5,6);
                fprintf (fid, '%4.3f %4.3f %4.3f  %4.3f %4.3f %4.3f %4.3f \n'...
                      ,S(1),Yoff(2),Yoff(3),Yoff(3)+.1,Yoff(5)-.1,Yoff(5),Yoff(6));
                fprintf (fid, '%4.3f %4.3f %4.3f  %4.3f %4.3f %4.3f %4.3f \n'...
                      ,S(6),Yoff(2),Yoff(3),Yoff(3)+.1,Yoff(5)-.1,Yoff(5),Yoff(6));
                fprintf(fid,'ENDCOLS\n');
                fprintf(fid,'ENDTABLE\n\n');
                fprintf(fid,'RdTb1_CARPET\n');
                fprintf(fid,'%4.3f %4.3f %4.3f %4.3f %4.3f %4.3f
%4.3f\n',0,1,2,3,4,5,6);
                fprintf(fid,'%4.3f %4.3f %4.3f %4.3f %4.3f %4.3f %4.3f\n',S(1),...
                    RdFriction(1),RdFriction(1),RdFriction(2),RdFriction(2),...
                    RdFriction(1),RdFriction(1));
                fprintf(fid,'%4.3f %4.3f %4.3f %4.3f %4.3f %4.3f %4.3f\n',S(6),...
                    RdFriction(1),RdFriction(1),RdFriction(2),RdFriction(2),...
                    RdFriction(1),RdFriction(1));
                fprintf(fid,'ENDTABLE\n');
                fprintf(fid,'RdTb2_CARPET\n');
                fprintf(fid,'%4.3f %4.3f %4.3f %4.3f %4.3f %4.3  %4.3f\n'...
                             ,0,1,2,3,4,5,6);
                fprintf (fid, '%4.3f %4.3f %4.3f  %4.3f %4.3f %4.3f %4.3f\n'...
                      ,S(1),Yoff(2),Yoff(3),Yoff(3)+.1,Yoff(5)-.1,Yoff(5),Yoff(6));
                fprintf (fid, '%4.3f %4.3f %4.3f  %4.3f %4.3f %4.3f %4.3f \n'...
                      ,S(6),Yoff(2),Yoff(3),Yoff(3)+.1,Yoff(5)-.1,Yoff(5),Yoff(6));
                fprintf(fid, 'ENDTABLE\n');
                fprintf(fid, 'END\n');
                fclose(fid);
%% %%%%*************************************************************%%%%% %%
%% RUN UPTO THIS POINT TO UPDATE THE ROAD GEOMETRY AND OTHER PARAMETERS
%% -THEN PRESS SEND TO SIMULINK BUTTON TO SEND THE Run***.par FILE TO THE
%% SIMULINK MODEL 'PARAMETRIC STUDY'
```

```
%% -THEN RUN THIS PROGRAM ('Singlerun) FROM THE OTHER MATLAB WINDOW
%% %%%%************************************************************%%%% %%
                cd ('D:\_users\r-ferdous\carsim data');
%                pause(5)
                sim('Paramatric_study');
                bdclose
%
%                 %% Saving data from each run
                      yaw=Yaw;        roll=Roll;
                      pitch=Pitch;
                      Xcar=X_RP1;     Ycar=Y_RP1;
                      Zcar=Z_RP1;
            cd ('D:\_users\r-ferdous\carsim data\MatlabCode');
[norm_Xt,norm_Zt,norm_Zadj,norm_Xditch,norm_Zditch]=Extract_Bumperprofile(yaw, ...
roll,pitch,Xcar,Ycar,Zcar,XP2,LL,Offset,MWm,slope,Ang,unit_con);

%% %%%%%%%%%%%%%%%%%%%%%%%   Writing the OUTPUT  %%%%%%%%%%%%%%%%%%%%%%%%%%%
%% %%%%%%%%%%%%%%%%%%%%%%%     =============   %%%%%%%%%%%%%%%%%%%%%%%%%%%
cd ('D:\_users\r-ferdous\carsim data\Data_Batches\Bumper Profile\Chevy2500\64ft_6H');
%%Write Bumper profile data on a txt file
%For X-Y Coordinates of centerline
%Open the file

filename = sprintf('Bump_prof%3.1fDeg%3.1fkph%dft%dH.txt',Encroach_Ang(cc),...
    speed(dd),DitchWidth(aa),Slope(bb));
fid = fopen( filename, 'wt' );
% Print the title of the table.
fprintf(fid, 'Bumper profile (Normalized) FPS unit \n');
% Print column headings
fprintf(fid, 'X (ft), Z-ft(from Ditch), norm.Z-ft(from horz) \n');
n=size(norm_Zt,2);
for i=1:n
fprintf (fid, ' %10.3f %10.3f %10.3f \n',norm_Xt(i),norm_Zt(i), norm_Zadj(i));
end
status = fclose( fid );
%%% Plot The Bumper Profile
x=[0,DitchWidth(aa)+1]; y=[0,0]; ymin=ditch_offset*unit_con-1; ymax=(max(norm_Zt)+3);
figure;
plot (norm_Xt,norm_Zt*12,'g-',norm_Xt,norm_Zadj*12,'r-',norm_Xditch,...
    norm_Zditch*12,'b-',x,y,'k-');...
    legend('Z (from actual Ditch Proile)','Z (when Horz. axis is ditchproile)',...
    'Normalized Ditch','Location','NE');
    xlabel('Lateral Offset(ft)'),ylabel('Height (in)');
    set(gca,'FontName','Times','FontSize',8,'FontUnits','points');
    %set(gca,'FontName','Helvetica','FontSize',10,'FontUnits', ...
    %'points','FontWeight','bold','FontAngle','oblique')
    axis([0 DitchWidth(aa)+1 ymin*12 ymax*12]);
    cd ('D:\_users\r-ferdous\carsim data\Data_Batches\Bumper Profile\Chevy2500\Plots')
    filename = sprintf('PlotProfile%dDeg%dkph%dft%dH',Encroach_Ang(cc),...
        speed(dd),DitchWidth(aa),Slope(bb));
    print ('-dmeta',filename);
    cd ('D:/_users/r-ferdous/carsim data')
%% %%%%%%%%%%%%%%%%%%%%%%%     =============   %%%%%%%%%%%%%%%%%%%%%%%%%%%
%% %%%%%%%%%%%%%%%%%%%%%%%     =============   %%%%%%%%%%%%%%%%%%%%%%%%%%%
            end
        end
    end
    cd ('D:/_users/r-ferdous/carsim data');
end
toc
```

C.2 SOURCE CODE FOR THE SUBROUTINES

```
function[norm_Xt,norm_Zt,norm_Zadj,norm_Xditch,norm_Zditch]=...
    Extract_Bumperprofile(yaw,roll,pitch,Xcar,Ycar,Zcar,XP2,LL,Offset,...
    MWm,slope,Ang,unit_con);
%%LL= length of each line ; Offset= starting point(in lateral dir) for
%%entrance line
NoD=size(Xcar,1);
ditch_offset=-MWm/2*1/slope;

%%Ditch Profile
%%X-Y Geometry
[Refline_A,Refline_B,Entrance_A,Entrance_B,Center_A,Center_B,Exit_A,Exit_B]...
    =Ditch_profile(Ang,MWm,ditch_offset,XP2,LL,Offset);
%%%%DO NOT NEED TO Update X, Y, Z coordinate of the trackpoint on the vehicle considering
%%%% the yaw,pitch,roll and Xcg,Ycg,Zcg (@Veh CG(at GL)for carsim )obtained
%%%% form carsim since we can get the X Y Z coordinates from the reference
%%%% point (in carsim) assigned at bumper location

for i=1:NoD
    %%convert yaw pitch roll into radian
    yaw(i)=yaw(i)*pi/180;pitch(i)=pitch(i)*pi/180;roll(i)=roll(i)*pi/180;
%%%% Update X, Y, Z coordinate of the ref.point on the vehicle
    Xt(i)=Xcar(i);
    Yt(i)=Ycar(i);
    Zt(i)=Zcar(i);
end

%%This gives the (x,y,z) coordinate of track point over the global
%%terrain..However Z coordinate is calculated form ground and hence it must
%%be adjusted again to account for ditch profile.
%%%%
```

```
Z_ditch=[0;0;ditch_offset;0];

%%% Convert all data into FPS unit and Normalize the coordinate such that the (0,0) is at
the entrance line
[norm_Xditch,norm_Zditch,norm_Xt,norm_Zt,norm_Zadj,norm_Zdrop]...
    =normalize_data(X_ditch,Z_ditch,Xt,Zt,Zadj,Z_D2H,Offset,MWm,unit_con,NoD);
end
_____________________________________________________________________________

%%%%%%%%%%%%%%%%%%%%%%%%Calculate and rotate the ditch profile%%%%%%%%%
function [Refline_A,Refline_B,Entrance_A,Entrance_B,Center_A,Center_B,...
    Exit_A,Exit_B]=Ditch_profile(Ang,MWm,ditch_offset,XP2,LL,Estart)
YP2=XP2*tan(Ang);
X=[0;XP2];Y=[0;YP2];
x=[0;LL+5];y=[0,0];
%%%%Initial Ditch Profile (|| to X axis)
Refline_A=[0;0;0];Refline_B=[LL;0;0];
Entrance_A=[0;Estart;0];Entrance_B=[LL;Estart;0];
Center_A=[0;(Estart+MWm/2);ditch_offset];
Center_B=[LL;(Estart+MWm/2);ditch_offset];
Exit_A=[0;Estart+MWm;0];Exit_B=[LL;Estart+MWm;0];

%%Rotate Ditch Profile
[Refline_A,Refline_B]=Rotate_line(Refline_A,Refline_B,Ang);
[Entrance_A,Entrance_B]=Rotate_line(Entrance_A,Entrance_B,Ang);
[Center_A,Center_B]=Rotate_line(Center_A,Center_B,Ang);
[Exit_A,Exit_B]=Rotate_line(Exit_A,Exit_B,Ang);

ReflineX=[Refline_A(1);Refline_B(1)];ReflineY=[Refline_A(2);Refline_B(2)];
ReflineZ=[Refline_A(3);Refline_B(3)];
EntranceX=[Entrance_A(1);Entrance_B(1)];EntranceY=[Entrance_A(2);Entrance_B(2)];
EntranceZ=[Entrance_A(3);Entrance_B(3)];
CenterX=[Center_A(1);Center_B(1)];CenterY=[Center_A(2);Center_B(2)];
CenterZ=[Center_A(3);Center_B(3)];
ExitX=[Exit_A(1);Exit_B(1)];ExitY=[Exit_A(2);Exit_B(2)];
ExitZ=[Exit_A(3);Exit_B(3)];

%%Write ditch profile for carsim
%For X-Y Coordinates of centerline
%Open the file
fid = fopen( 'Ditchoffcenter.txt', 'wt' );
% Print the title of the table.
fprintf(fid, ' CARSIM: Road:  X-Y Coordinates of centerline\n\n');
% Print column headings
fprintf(fid, ' PathProfile: X(m),Y(m)\n');

Xcrd(1)=-1;Xcrd(2)=0;Xcrd(3)=XP2/1000;Xcrd(4)=XP2/100;Xcrd(5)=XP2/10;Xcrd(6)=XP2;
for i=1:6
Ycrd(i)=Xcrd(i)*tan(Ang);
fprintf (fid, ' %10.3f %10.3f \n',Xcrd(i),Ycrd(i));
end
fprintf(fid, '\n\n');

%For Offcenter elevation map
Yoff(1)=0;Yoff(2)=Estart-53.28;Yoff(3)=Estart;Yoff(4)=Estart+MWm/2;
Yoff(5)=Estart+MWm;Yoff(6)=-Yoff(2);
Xoff=zeros(6);
Xoff(:,1)=Xcrd(:);Xoff(:,4)=ditch_offset;

fprintf(fid, ' CARSIM: Road: Off center elevation Map Data (in S-L Coordinate)\n\n');
% Print column headings
fprintf(fid, ' Top row: Lateral Coordinate in Ascending order\n');
fprintf(fid, ' Xaxis: Station (m), Rest: incremental elvation\n');
fprintf (fid, '%10.3f %10.3f %10.3f  %10.3f %10.3f %10.3f \n'...
    ,Yoff(1),Yoff(2),Yoff(3),Yoff(4),Yoff(5),Yoff(6));
for i=1:6
fprintf (fid, '%10.3f %10.3f %10.3f  %10.3f %10.3f %10.3f \n'...
```

```
    ,Xoff(i,1),Xoff(i,2),Xoff(i,3),Xoff(i,4),Xoff(i,5),Xoff(i,6));
end
status = fclose( fid );
end
```

```
%%%Function used to rotate a single line Q--->R of the ditch profile about
%%% the origin P(0,0,0) with an angle theta (+ve CCW)
function [Q1,R1]=Rotate_line(Q,R,theta);
%%call rotation matrix @Z
Rz= Rot_Z(theta);
Q1=Rz*Q; QR=R-Q;
R1=Q1+Rz*QR;
end
```

```
function[Rz]= Rot_Z(a);
Rz=[cos(a),-sin(a),0;sin(a),cos(a),0;0,0,1];
end
```

```
%%Obtain Z_D2H= the distance from ditch to horizon at track point projection and
%adjust the Zt(w r to ditch profile) to get the height of tr pt w r to horizontal plane
Z_adjusted
    %%%% step1: Test the coordinate of the trackpoint
    %%%%to check the projected plane on use [ckpl] from function check_plane
    %%%% Step2: determine the Delta Z= distance of ditch from the horizontal
    %%% line... Use the function Equation_plane
function [Z_D2H,Z_adjusted]=adjust_forditchoffset(Entrance_A,...
    Entrance_B,Center_A,Center_B,Exit_A,Exit_B,Xt,Yt,Zt,NoD);

%%determine normals to the planes 1,2 &3
[n1]=normal(Entrance_A,Entrance_B,Exit_A);
[n2]=normal(Entrance_A,Entrance_B,Center_A);
[n3]=normal(Center_A,Center_B,Exit_A);
for i=1:NoD
    %%%% tracking the plane the trackpoint is on
    %test the coordinate of the trackpoint to check the projected plane
[ckpl]=check_plane(Entrance_A,Entrance_B,Center_A,Center_B,...
    Exit_A,Exit_B,Xt(i),Yt(i));
%plane(i)=ckpl;
%%% determine the Delta Z= distance of ditch from the horizontal line...
if (ckpl==1)
    [DeltaZ]=Equation_plane(Xt(i),Yt(i),n1,Entrance_A);
elseif (ckpl==2)
    [DeltaZ]=Equation_plane(Xt(i),Yt(i),n2,Entrance_A);
else
    [DeltaZ]=Equation_plane(Xt(i),Yt(i),n3,Center_A);
end
%%Z_D2H=distance from ditch to horizon at track point preojection
Z_D2H(i)=-DeltaZ;
Z_adjusted(i)=Zt(i)+Z_D2H(i);
end
end
```

```
%%determine normal to the plane
function [n]=normal(P,Q,R)
PQ=Q-P;PR=R-P;
n=cross(PQ,PR);
end
```

```
function [ckpl]=check_plane(A1,A2,C1,C2,E1,E2,xactual,yactual);
[mA,bA]=eq_line(A1,A2);
[mC,bC]=eq_line(C1,C2);
```

```
[mE,bE]=eq_line(E1,E2);
ytest1=mA*xactual+bA;ytest2=mC*xactual+bC;ytest3=mE*xactual+bE;
if (yactual<ytest1)
    ckpl=1;
elseif ((yactual>ytest1)&(yactual<ytest2))
    ckpl=2;
elseif ((yactual>ytest2)&(yactual<ytest3))
    ckpl=3;
else
    ckpl=1;
end
end
```

```
function [m,b]=eq_line(A,B)
m=(B(2)-A(2))/((B(1)-A(1)));
b=A(2)-m*A(1);
end
```

```
function[z]=Equation_plane(x,y,n,P);
z=P(3)-(n(1)*(x-P(1))+n(2)*(y-P(2)))/n(3);
end
```

```
function [X,Y,Z]=transfor2_ditchcoord(Xt,Yt,Zt,Ang,NoD);
if (Ang<0)
    beta=-pi/2-Ang;
else
    beta=pi/2-Ang;
end
for i=1:NoD
Coord=[Xt(i);Yt(i);Zt(i)]; tr_Coord=Rot_Z(beta)*Coord;
X(i)=tr_Coord(1);Y(i)=tr_Coord(2);Z(i)=tr_Coord(3);
end
end
```

```
%%% Convert all data into FPS unit and Normalize the coordinate such that the (0,0) is at
the entrance line
function [norm_Xditch,norm_Zditch,norm_Xt,norm_Zt,norm_Zadj,norm_Zdrop]...
   =normalize_data(X_ditch,Z_ditch,Xt,Zt,Zadj,Z_D2H,Offset,MWm,unit_con,NoD);
%%Normalized Ditch and convert to FPS unit
for i=1:3
norm_Xditch(i)=(X_ditch(i+1)-Offset)*unit_con;
norm_Zditch(i)=Z_ditch(i+1)*unit_con;
end
%%Filter/Normalize the data..and convert it into FPS unit...
j=1;
for i=1:NoD
     if (Xt(i)>Offset)& (Xt(i)<Offset+MWm)
        norm_Xt(j)=(Xt(i)-Offset)*unit_con;
        norm_Zt(j)=Zt(i)*unit_con;
        norm_Zadj(j)=Zadj(i)*unit_con;
        norm_Zdrop(j)=-Z_D2H(i)*unit_con;
        j=j+1;
     end
end
end
```

APPENDIX D. VEHICLE TRAJECTORY DATA

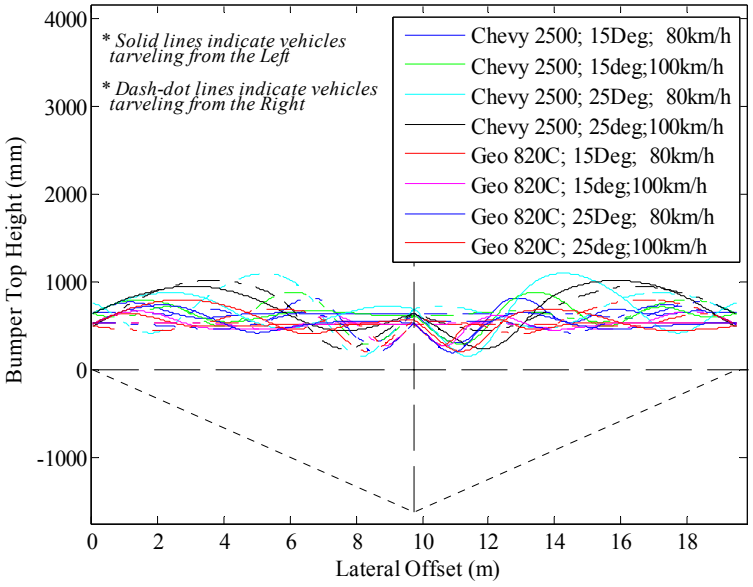

(a)

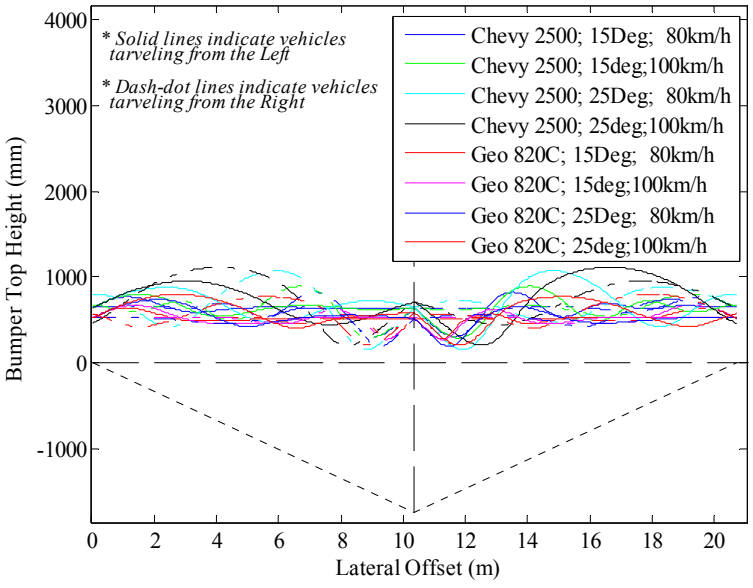

(b)

Figure D.1 Vehicle trajectory (relative) data for depressed median case: 6:1 slope, and 23.2 m (76') wide median with (a) 1.8 m (6') and (b) 1.2 m (4') wide shoulders.

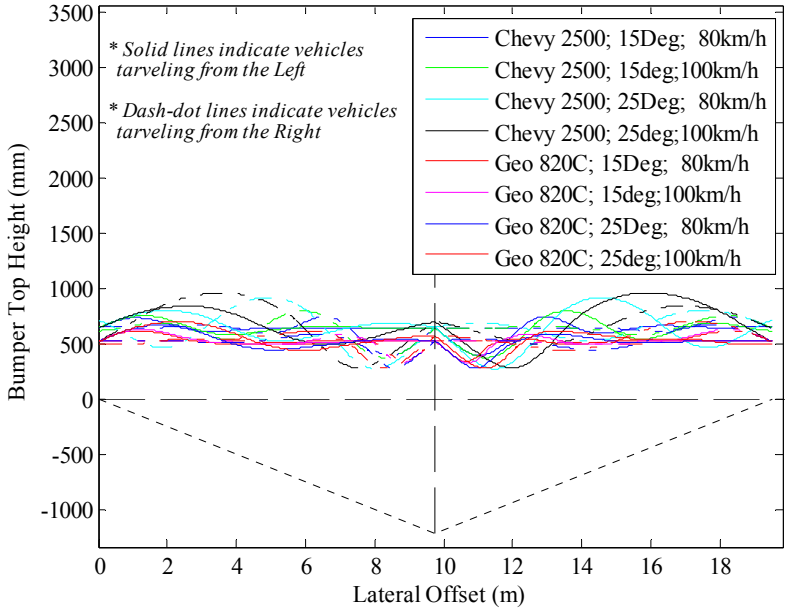

(a)

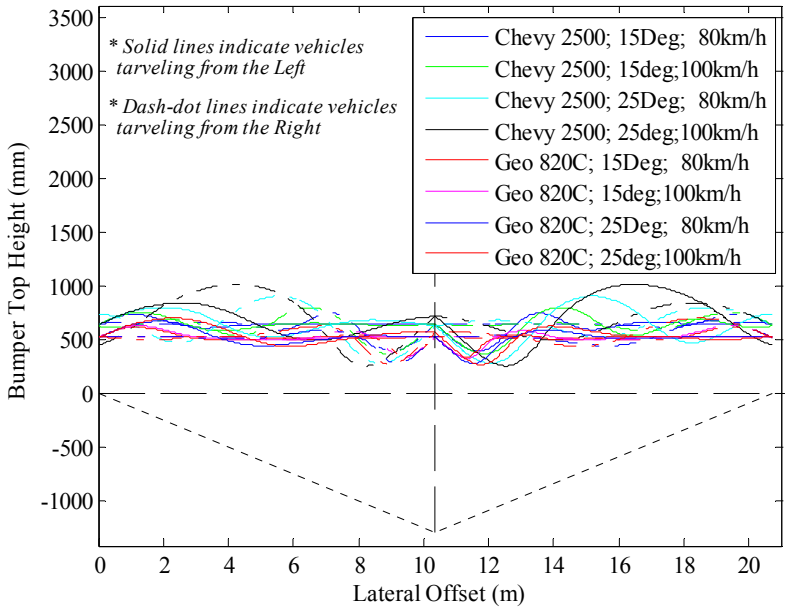

(b)

Figure D.2 Vehicle trajectory (relative) data for depressed median case: 8:1 slope, and 23.2 m (76') wide median with (a) 1.8 m (6') and (b) 1.2 m (4') wide shoulders.

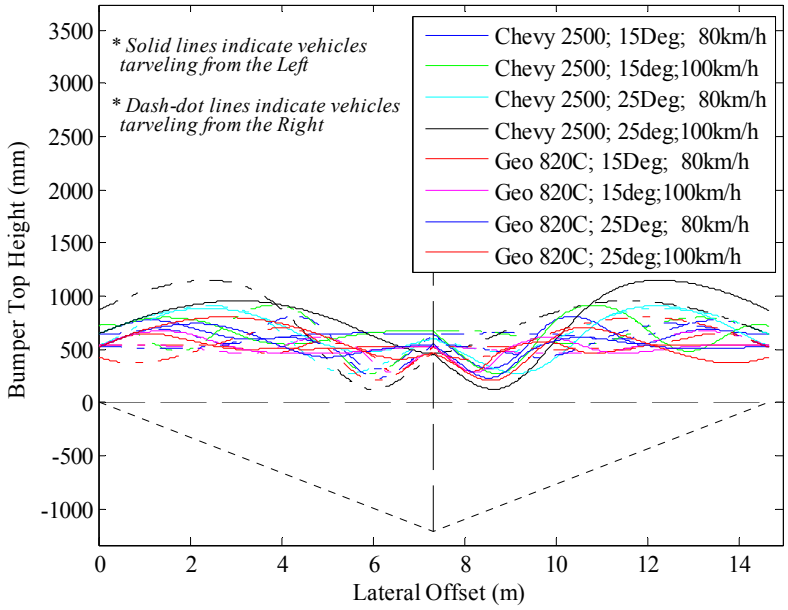

(a)

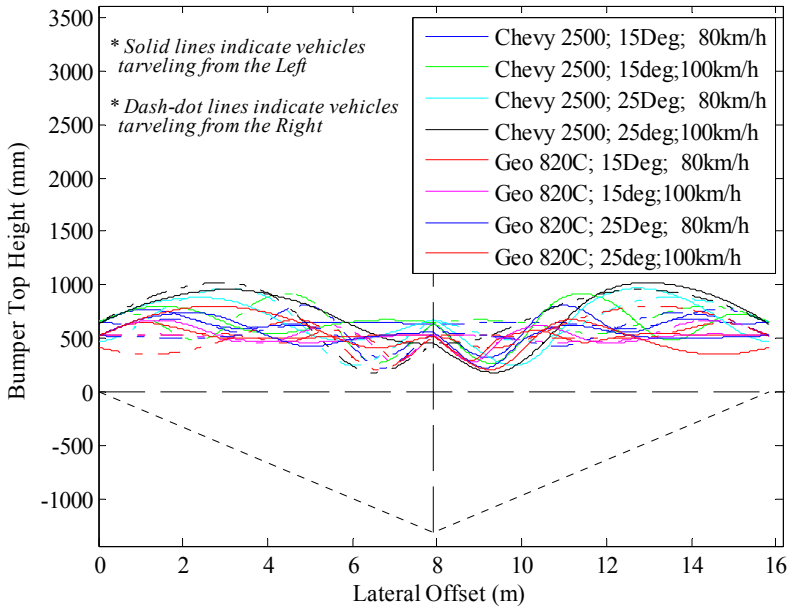

(b)

Figure D.3 Vehicle trajectory (relative) data for depressed median case: 6:1 slope, and 28.3 m (60') Median width with (a) 1.8 m (6') and (b) 1.2 m (4') wide shoulders.

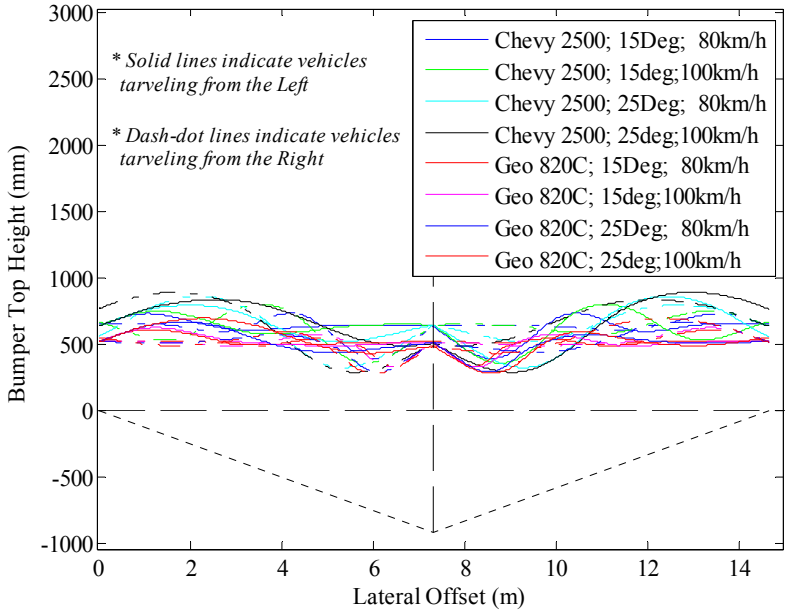

(a)

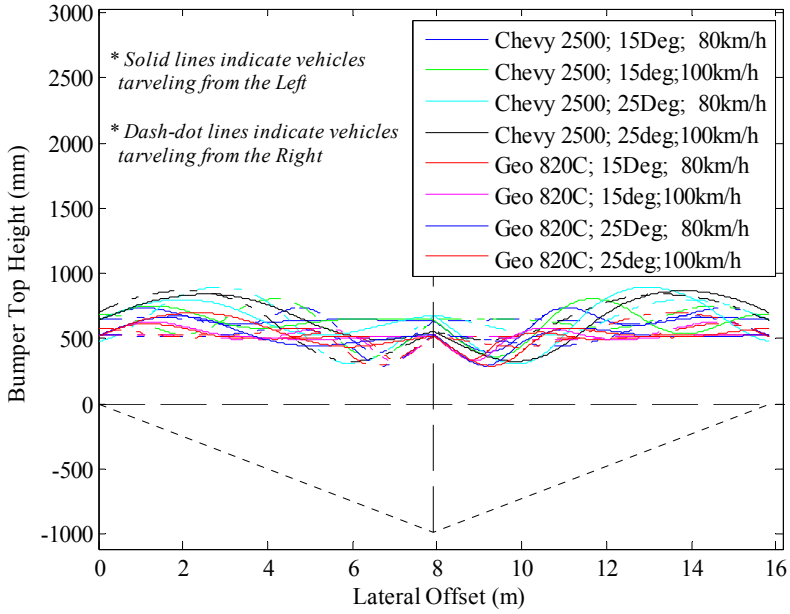

(b)

Figure D.4 Vehicle trajectory (relative) data for depressed median case: 8:1 slope, and 28.3 m (60') wide median with (a) 1.8 m (6') and (b) 1.2 m (4') wide shoulders.

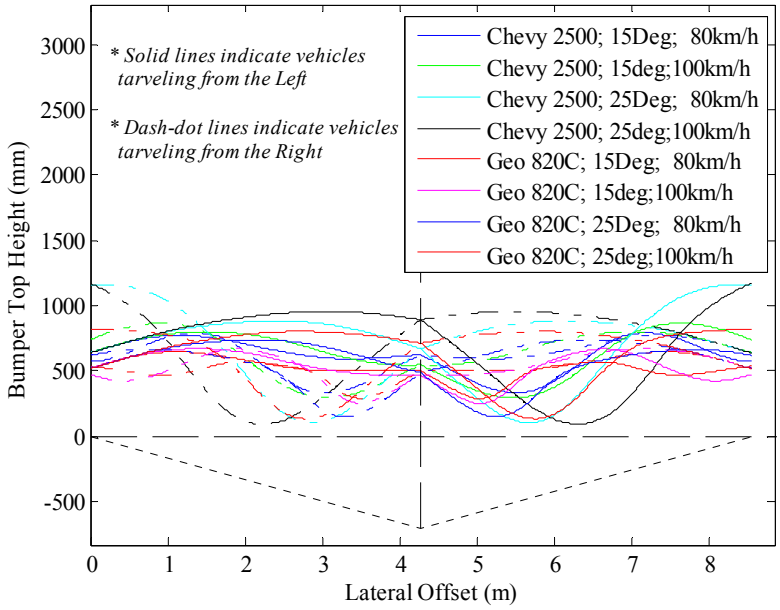

(a)

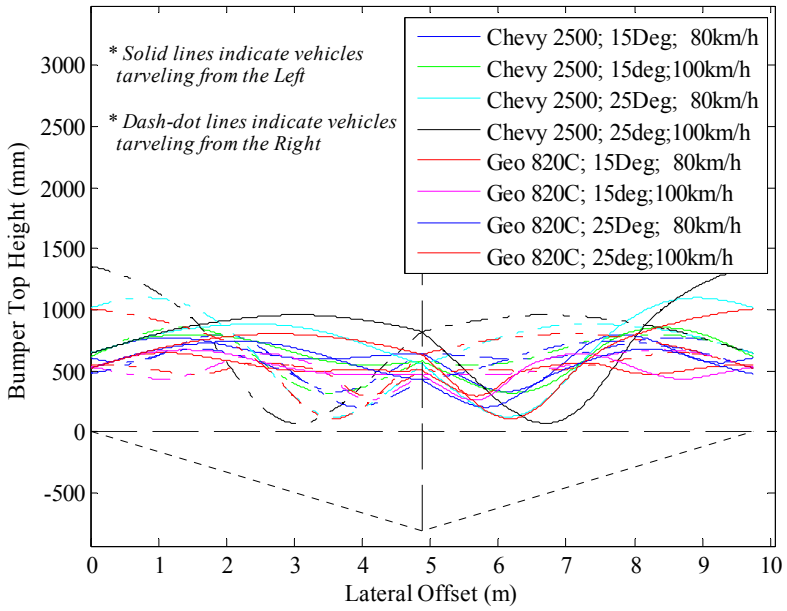

(b)

Figure D.5 Vehicle trajectory (relative) data for depressed median case: 6:1 slope, and 28.3 m (60') Median width and (a) 1.8 m (6') and (b) 1.2 m (4') wide shoulders.

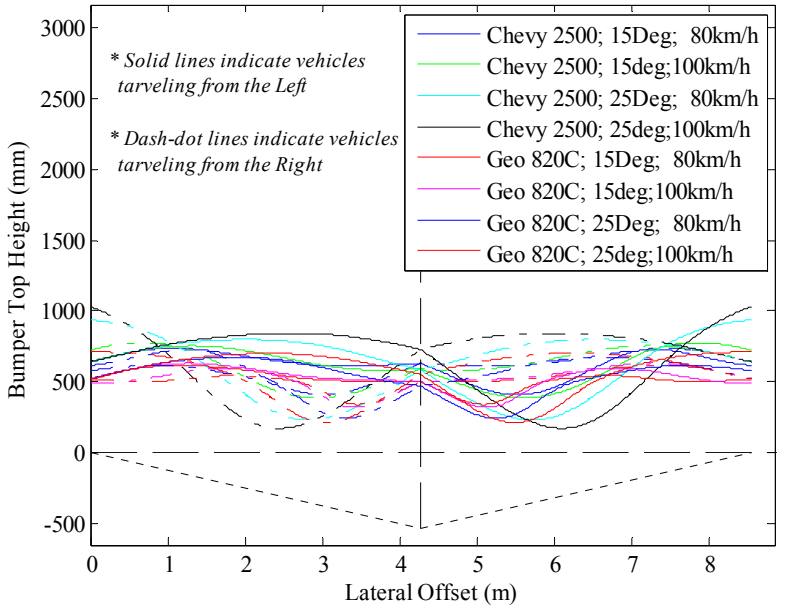

(a)

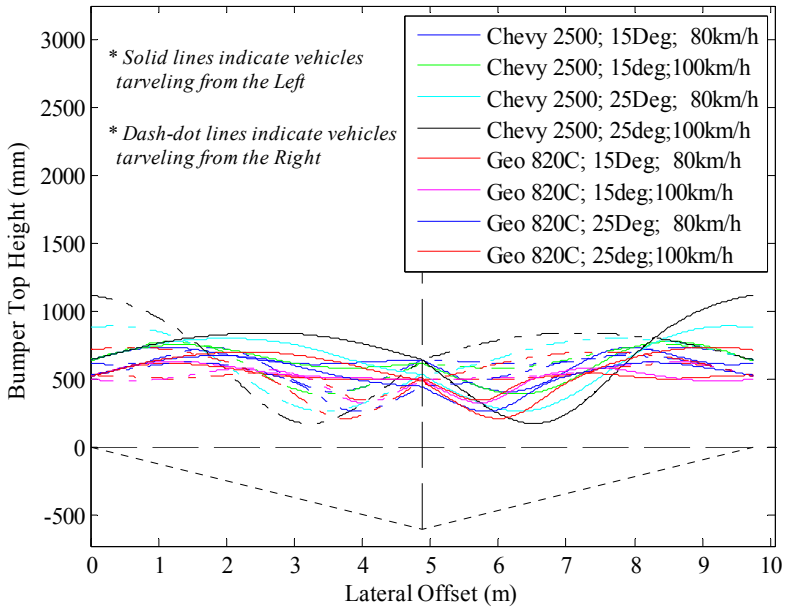

(b)

Figure D.6 Vehicle trajectory (relative) data for depressed median case: 8:1 slope, and 12.2 m (40') wide median with (a) 1.8 m (6') and (b) 1.2 m (4') wide shoulders.

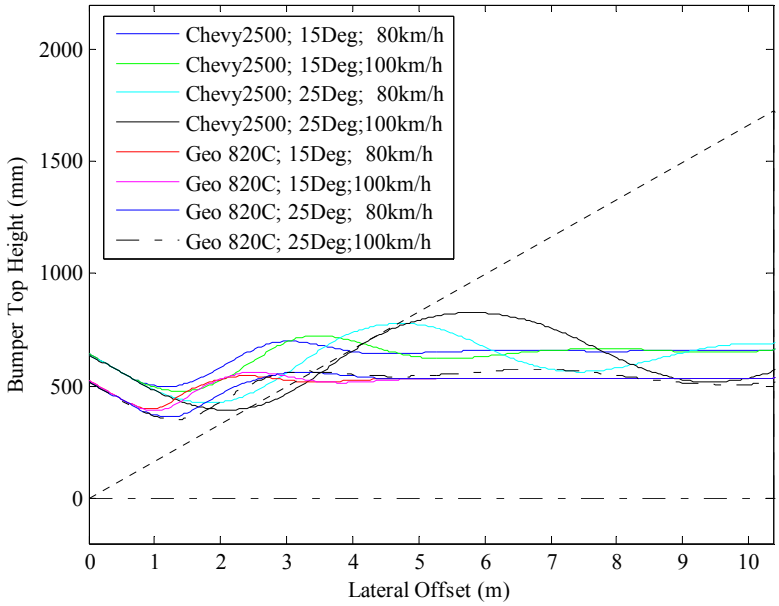

(a)

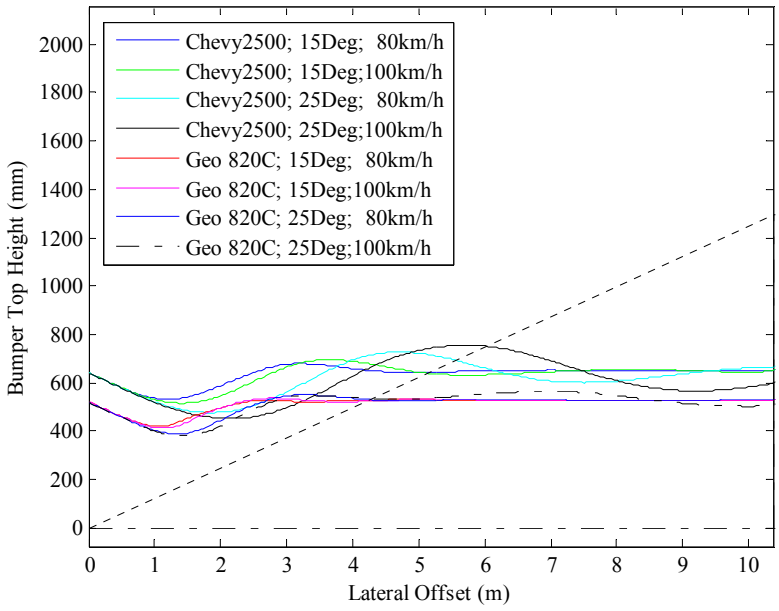

(b)

Figure D.7 Vehicle trajectory (relative) data for roadside case with (a) 6:1 and (b) 8:1 positive cross-slopes.

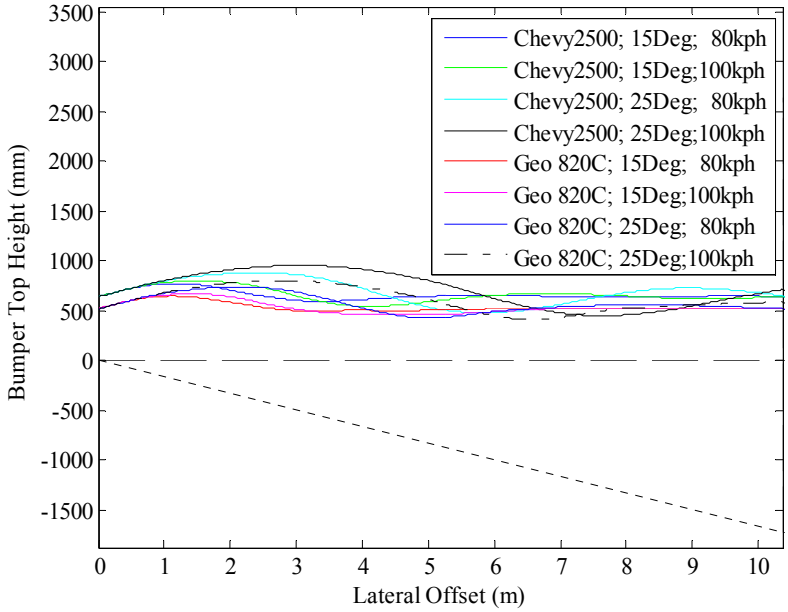

(a)

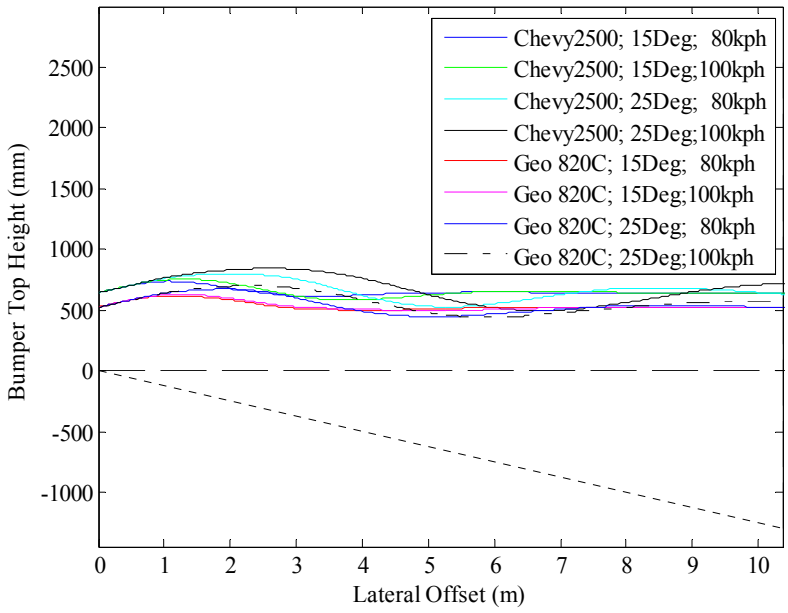

(b)

Figure D.8 Vehicle trajectory (relative) data for roadside case with (a) 6:1 and (b) 8:1 negative cross-slopes.

APPENDIX E. DETERMINING ACCEPTABLE BARRIER PLACEMENT LOCATIONS

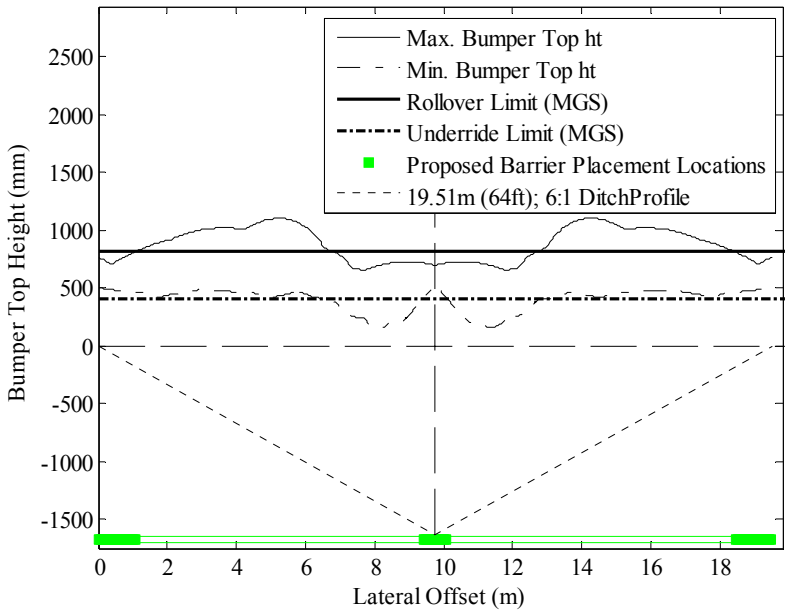

(a)

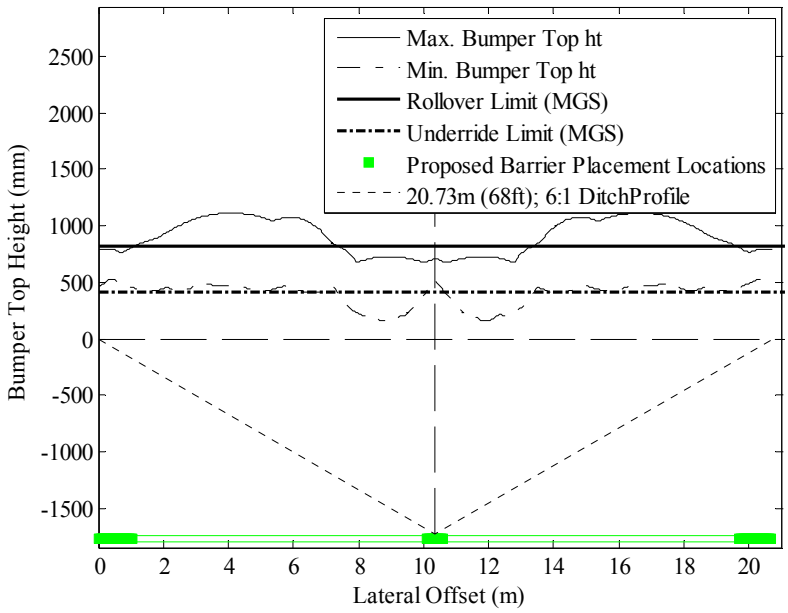

(b)

Figure E.1 Determining placement locations: Midwest Guardrail System (MGS) on a 6:1, 23.2 m (76') wide depressed median with (a) 1.8 m (6') and (b) 1.2 m (4') wide shoulders.

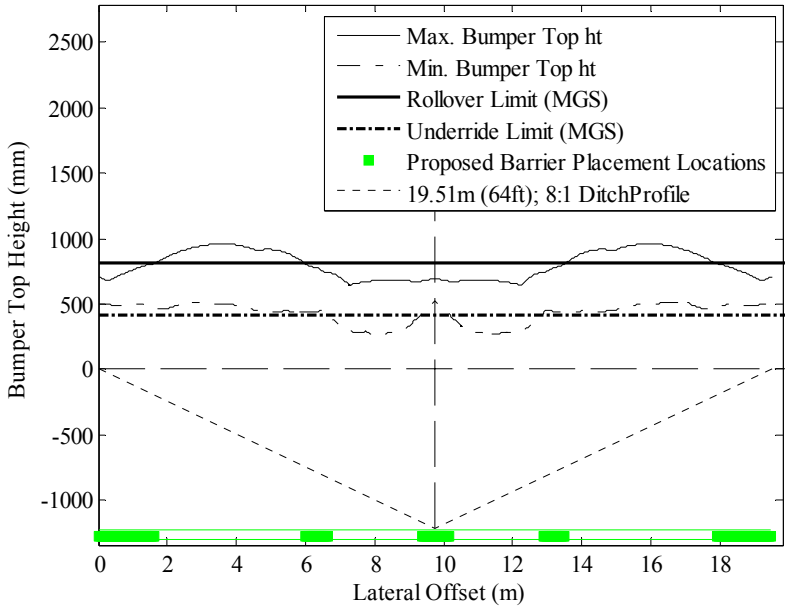

(a)

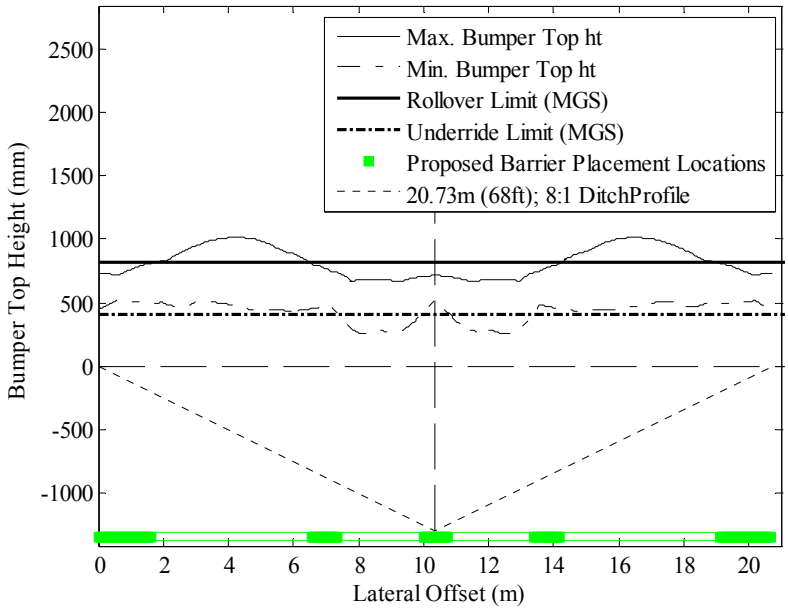

(b)

Figure E.2 Determining placement locations: Midwest Guardrail System (MGS) on a 8:1, 23.2 m (76') wide depressed median with (a) 1.8 m (6') and (b) 1.2 m (4') wide shoulders.

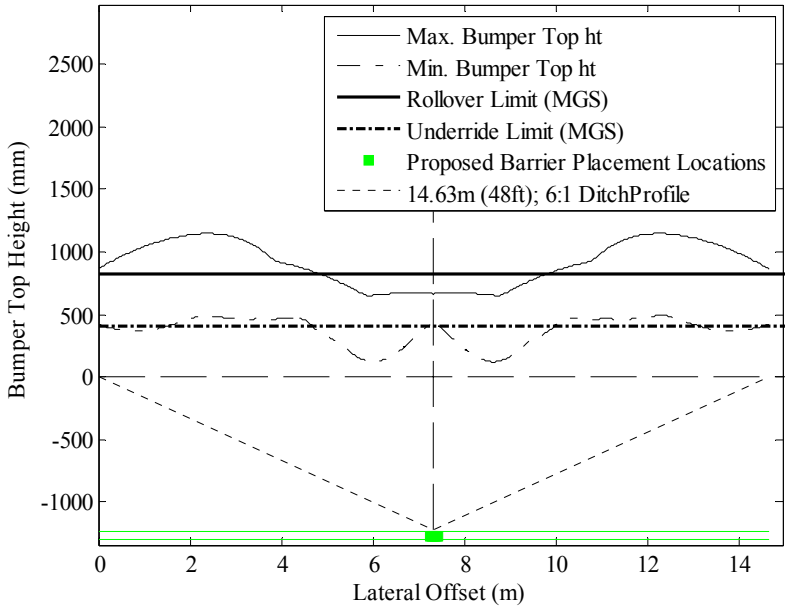

(a)

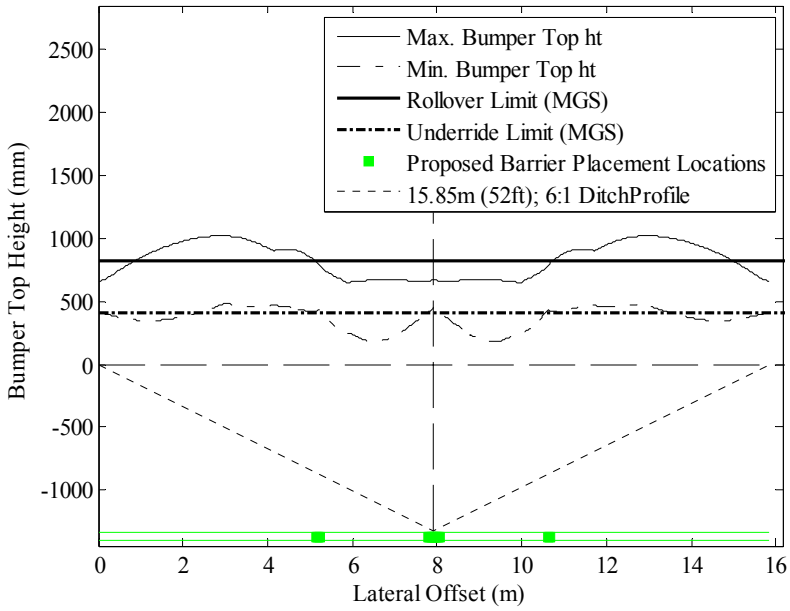

(b)

Figure E.3 Determining placement locations: Midwest Guardrail System (MGS) on a 6:1, 18.3 m (60') wide depressed median with (a) 1.8 m (6') and (b) 1.2 m (4') wide shoulders.

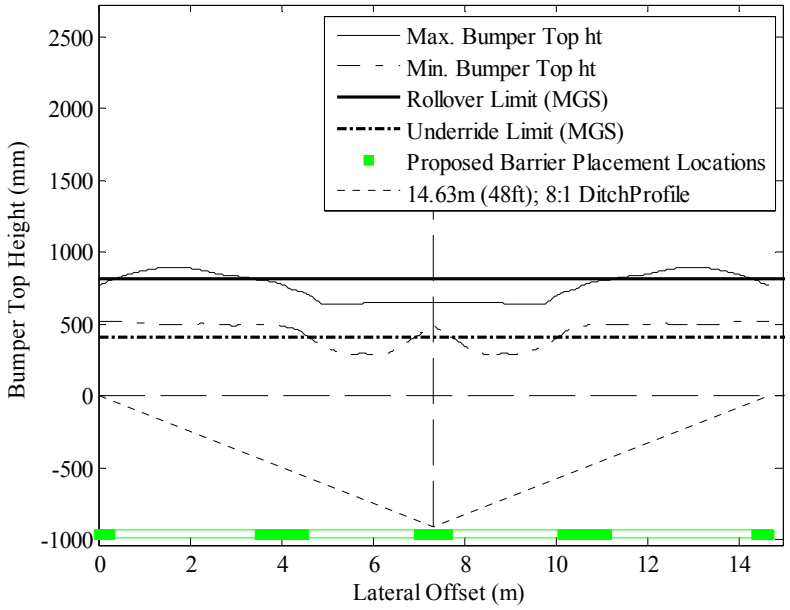

(a)

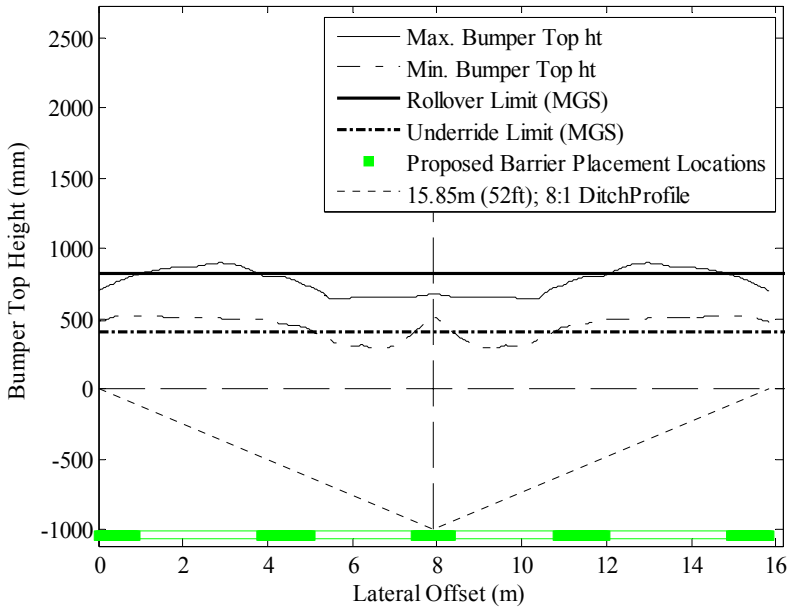

(b)

Figure E.4 Determining placement locations: Midwest Guardrail System (MGS) on an 8:1, 18.3 m (60') wide depressed median with (a) 1.8 m (6') and (b) 1.2 m (4') wide shoulders.

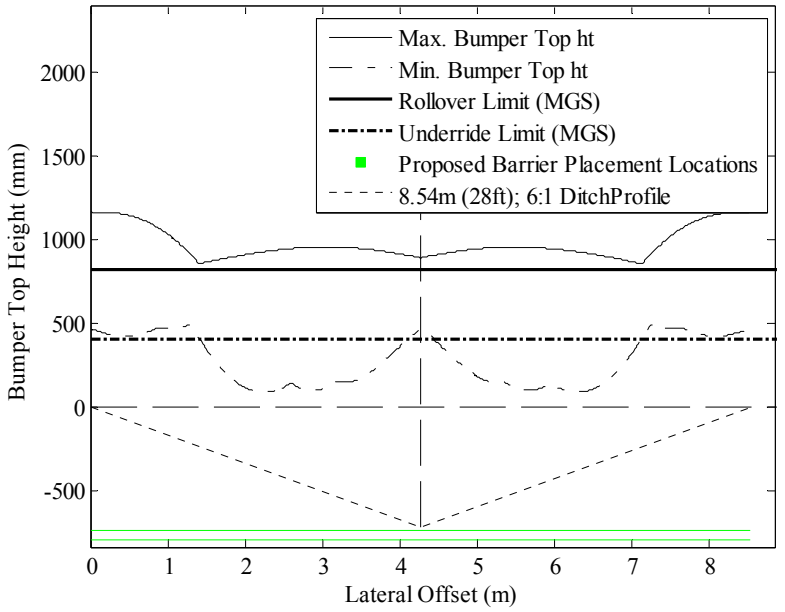

(a)

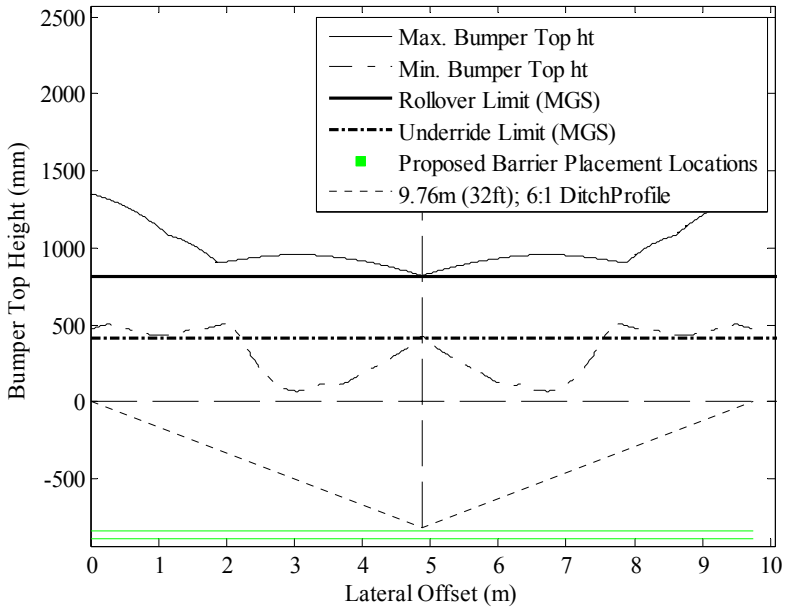

(b)

Figure E.5 Determining placement locations: Midwest Guardrail System (MGS) on a 6:1, 12.2 m (40') wide depressed median with (a) 1.8 m (6') and (b) 1.2 m (4') wide shoulders.

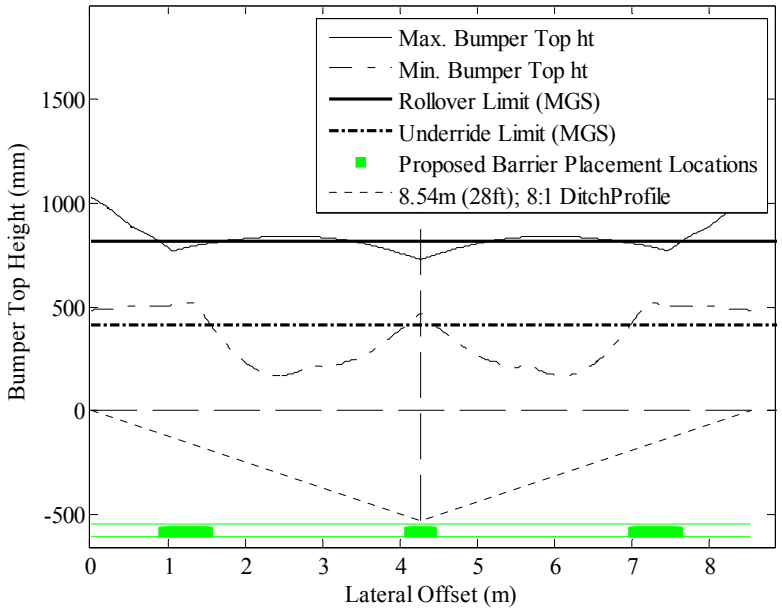

(a)

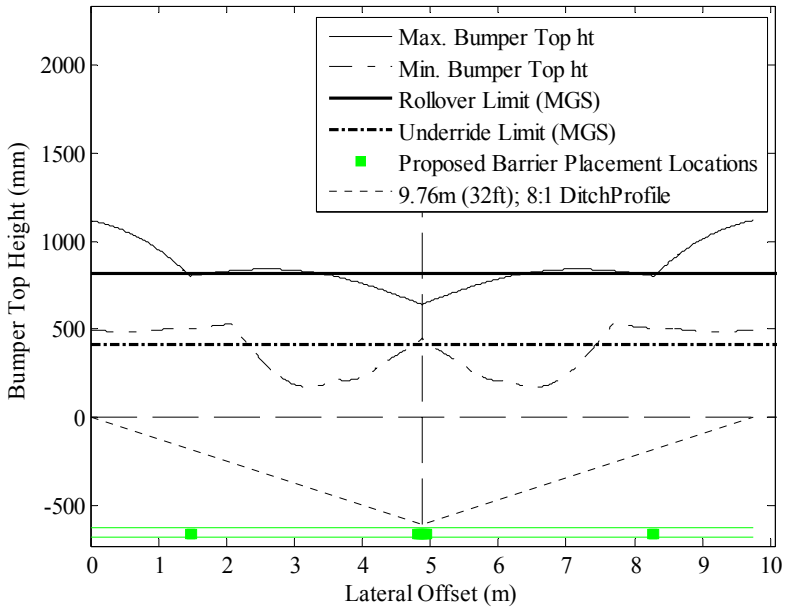

(b)

Figure E.6 Determining placement locations: Midwest Guardrail System (MGS) on an 8:1, 12.2 m (40') wide depressed median with (a) 1.8 m (6') and (b) 1.2 m (4') wide shoulders.

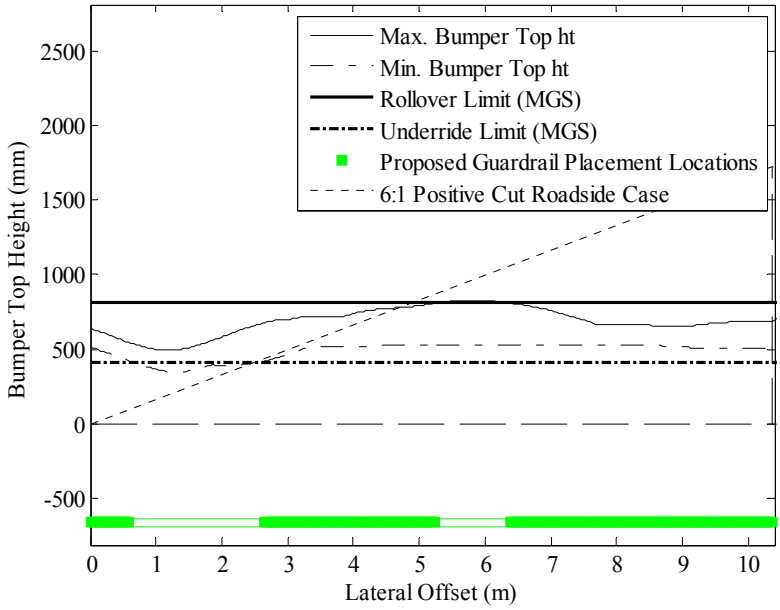

(a)

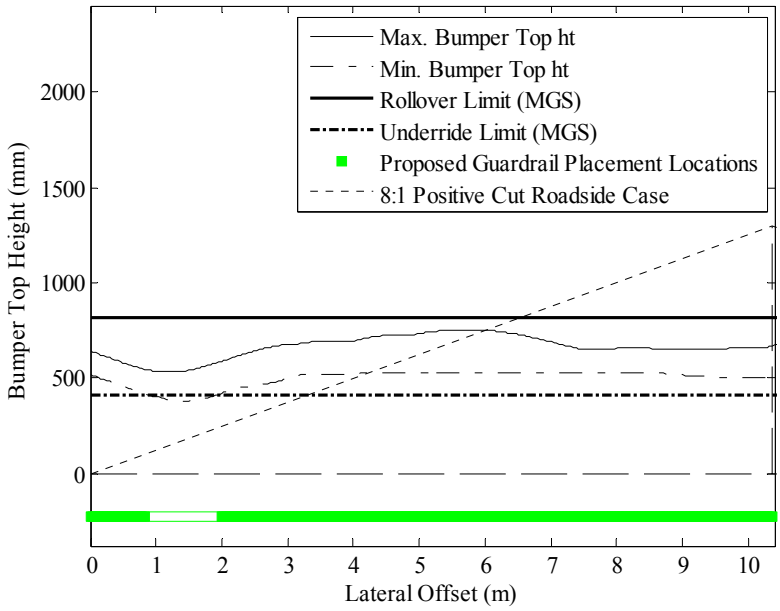

(b)

Figure E.7 Determining placement locations: Midwest Guardrail System (MGS) on positive (cut) (a) 6:1 and (b) 8:1 roadside slopes.

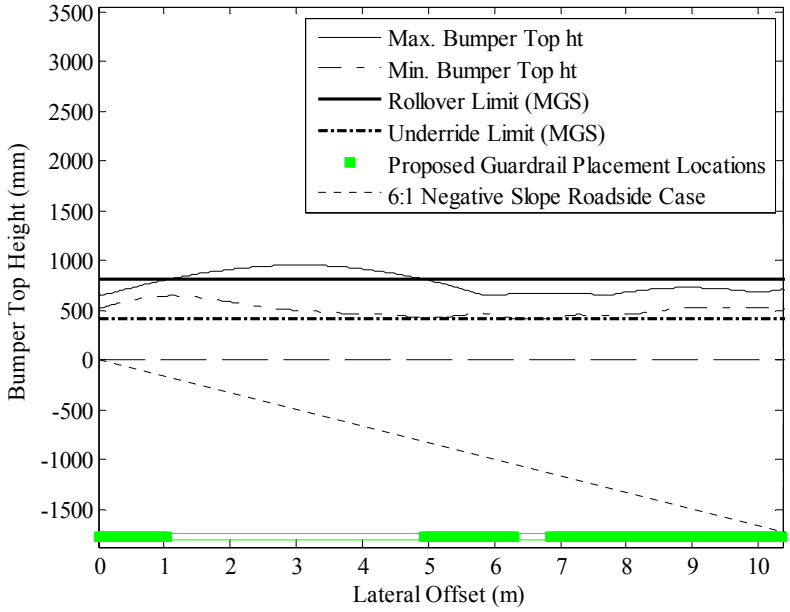

(a)

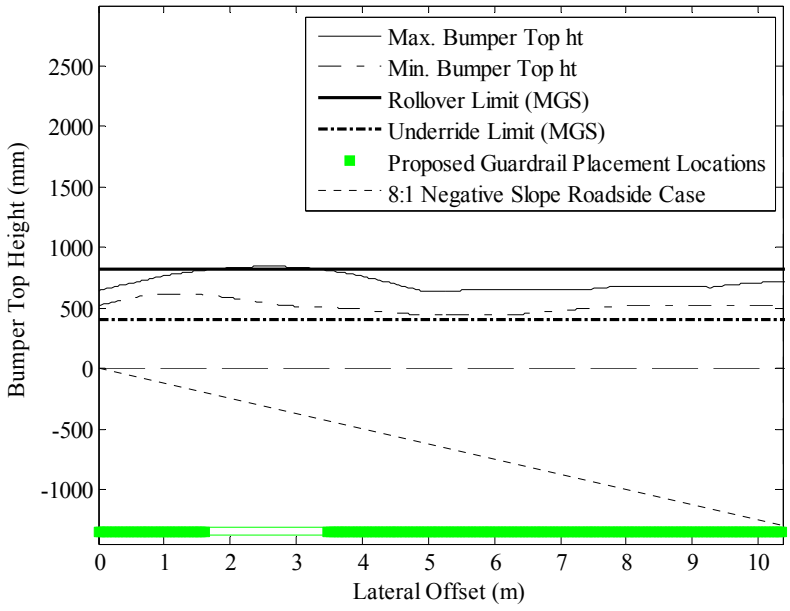

(b)

Figure E.8 Determining placement locations: Midwest Guardrail System (MGS) on negative (fill) (a) 6:1 and (b) 8:1 roadside slopes.

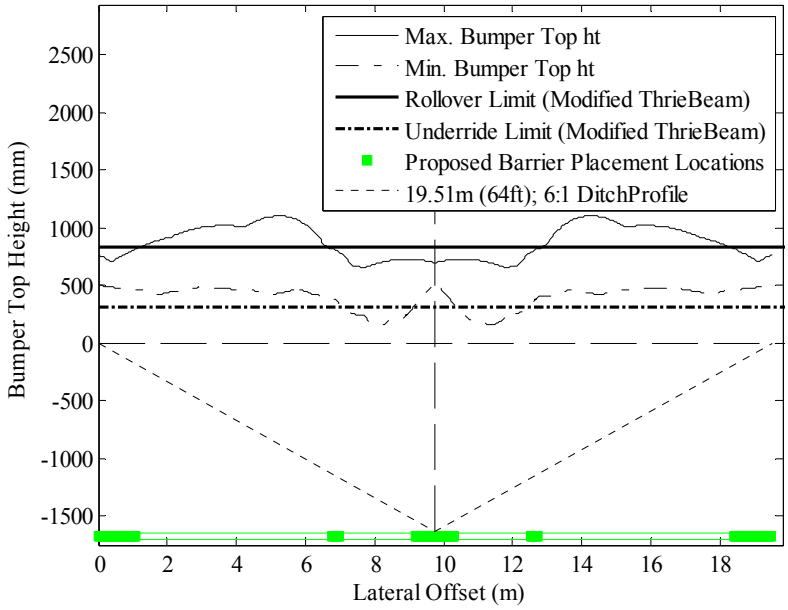

(a)

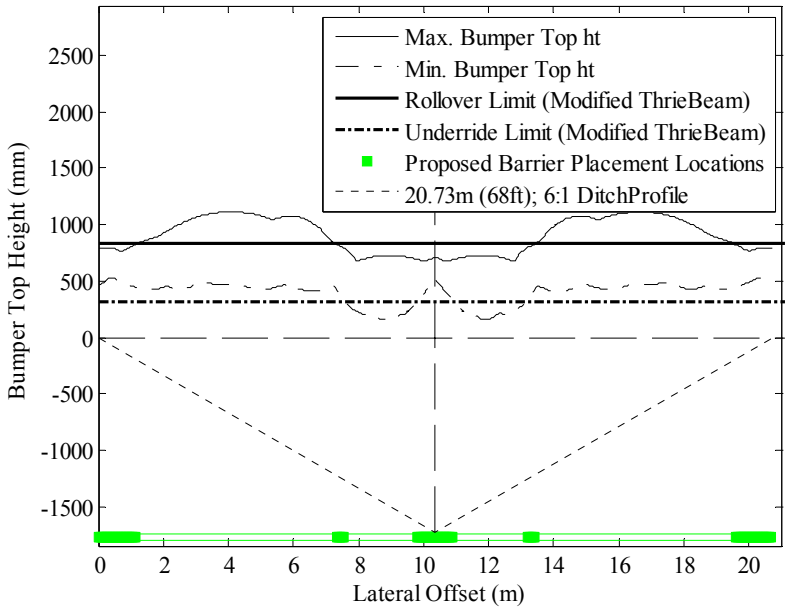

(b)

Figure E.9 Determining placement locations: Modified Thrie-beam System on a 6:1, 23.2 m (76') wide depressed median with (a) 1.8 m (6') and (b) 1.2 m (4') wide shoulders.

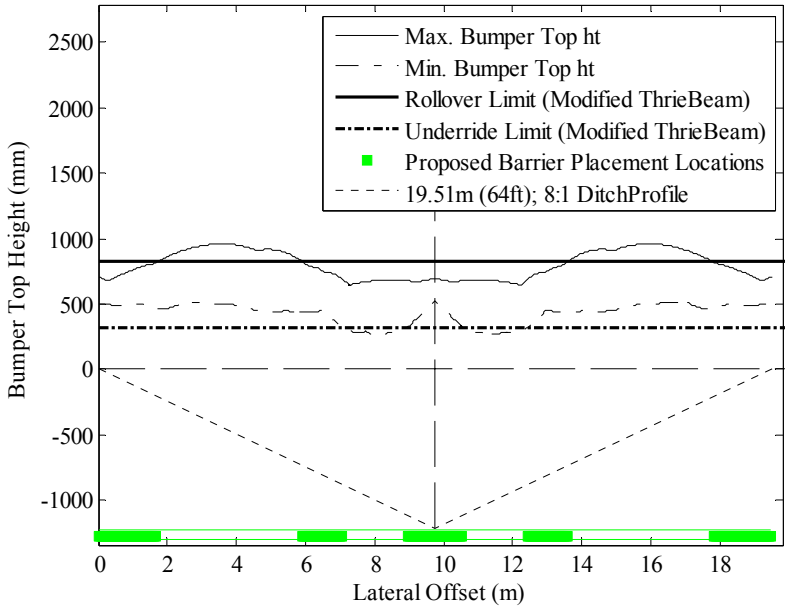

(a)

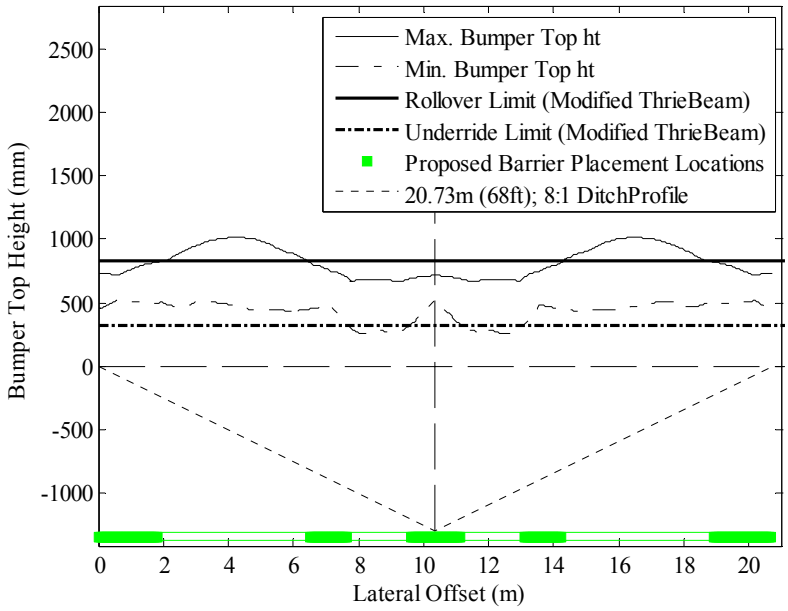

(b)

Figure E.10 Determining placement locations: Modified Thrie-beam System on an 8:1, 23.2 m (76') wide depressed median with (a) 1.8 m (6') and (b) 1.2 m (4') wide shoulders.

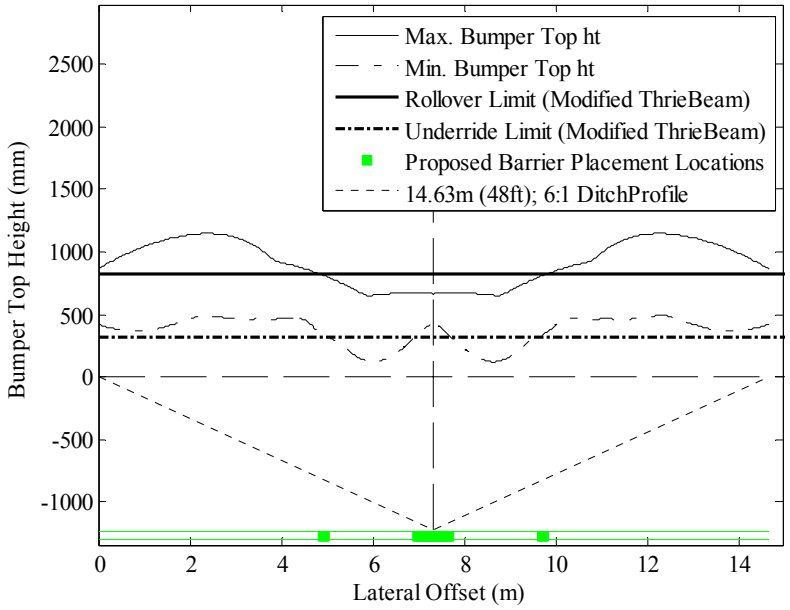

(a)

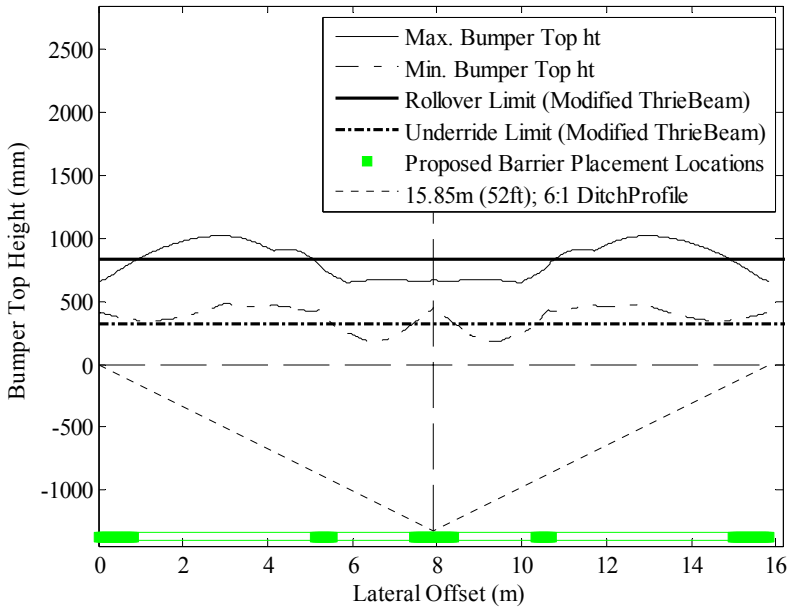

(b)

Figure E.11 Determining placement locations: Modified Thrie-beam System on a 6:1, 18.3 m (60') wide depressed median with (a) 1.8 m (6') and (b) 1.2 m (4') wide shoulders.

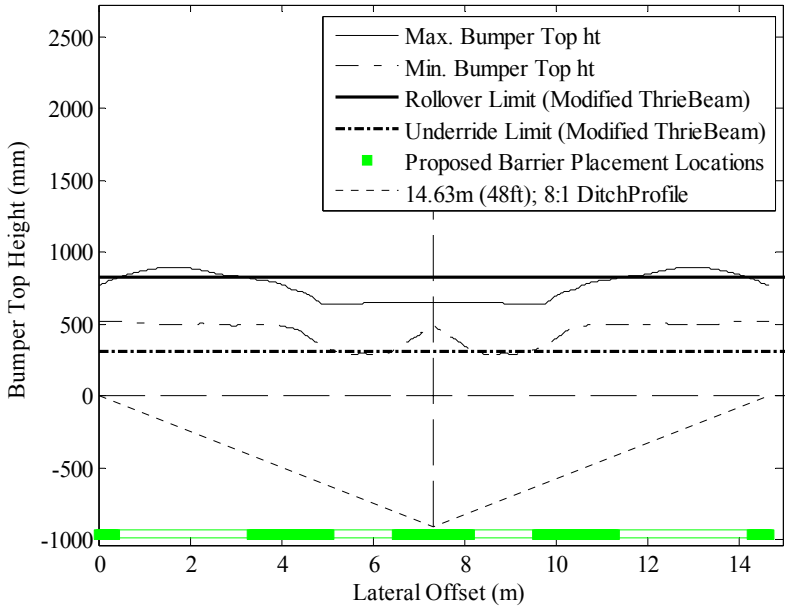

(a)

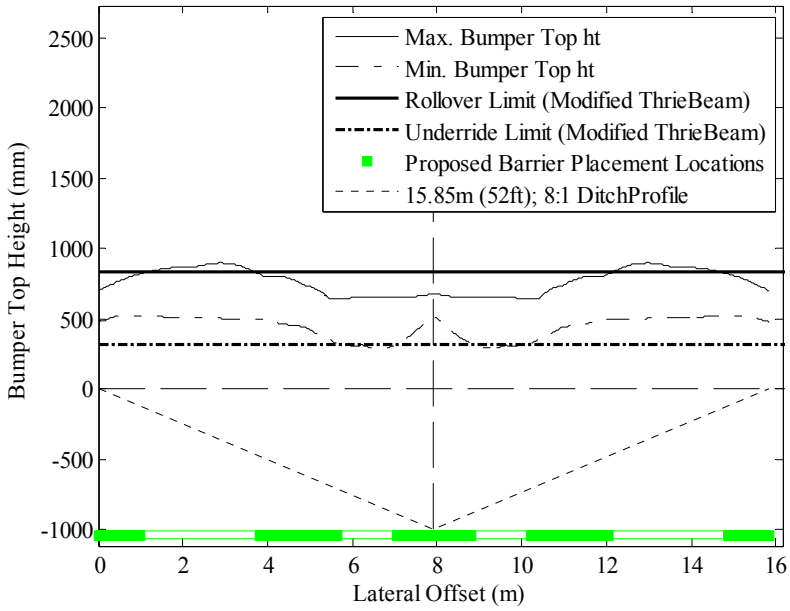

(b)

Figure E.12 Determining placement locations: Modified Thrie-beam System on an 8:1, 18.3 m (60') wide depressed median with (a) 1.8 m (6') and (b) 1.2 m (4') wide shoulders.

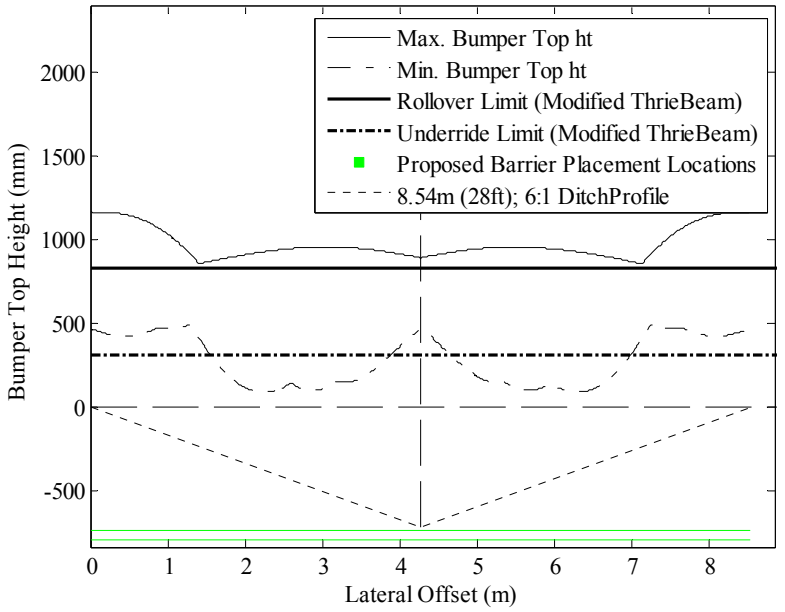

(a)

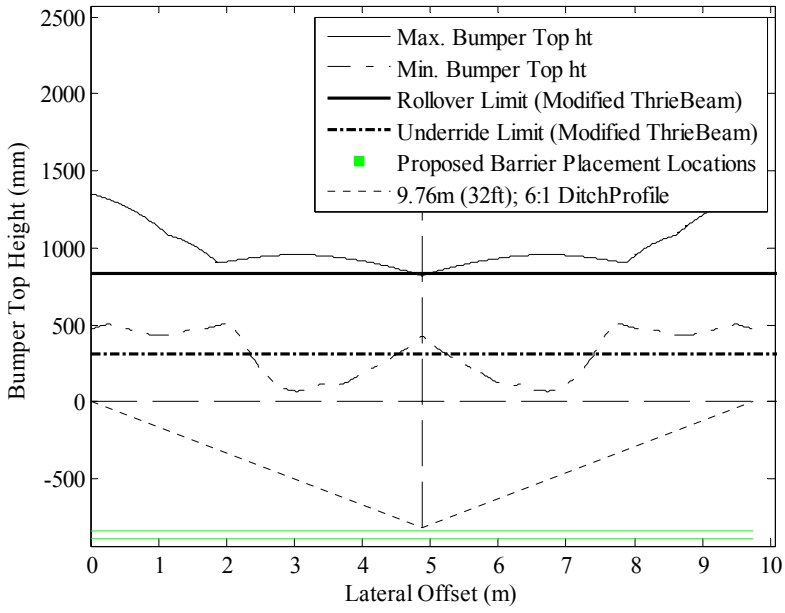

(b)

Figure E.13 Determining placement locations: Modified Thrie-beam System on a 6:1, 12.2 m (40') wide depressed median with (a) 1.8 m (6') and (b) 1.2 m (4') wide shoulders.

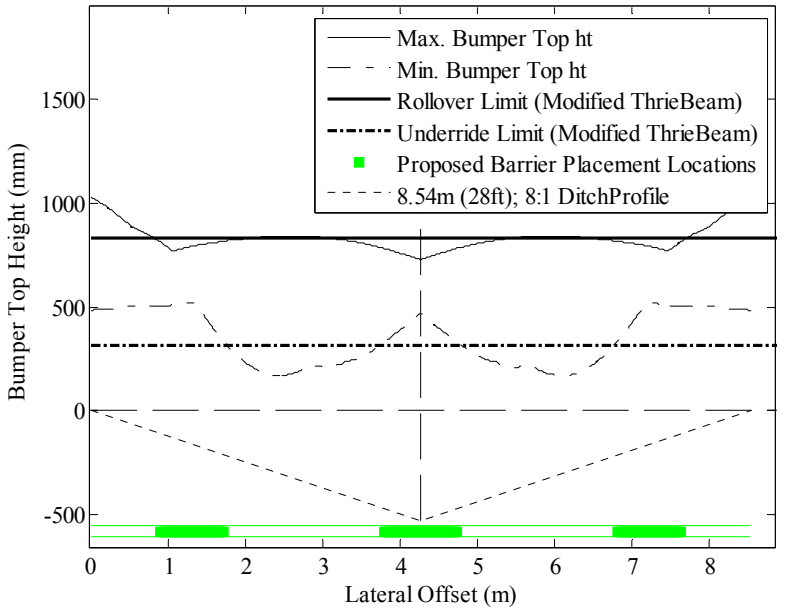

(a)

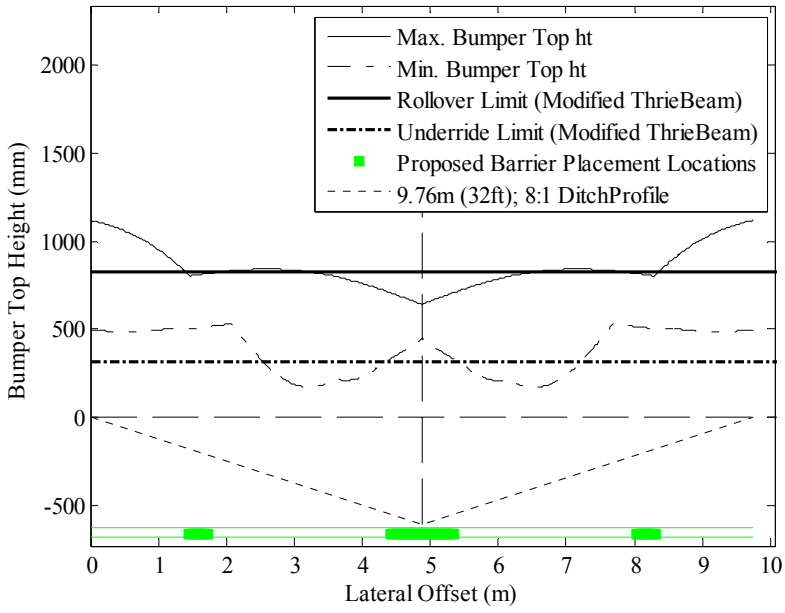

(b)

Figure E.14 Determining placement locations: Modified Thrie-beam System on an 8:1, 12.2 m (40') wide depressed median with (a) 1.8 m (6') and (b) 1.2 m (4') wide shoulders.

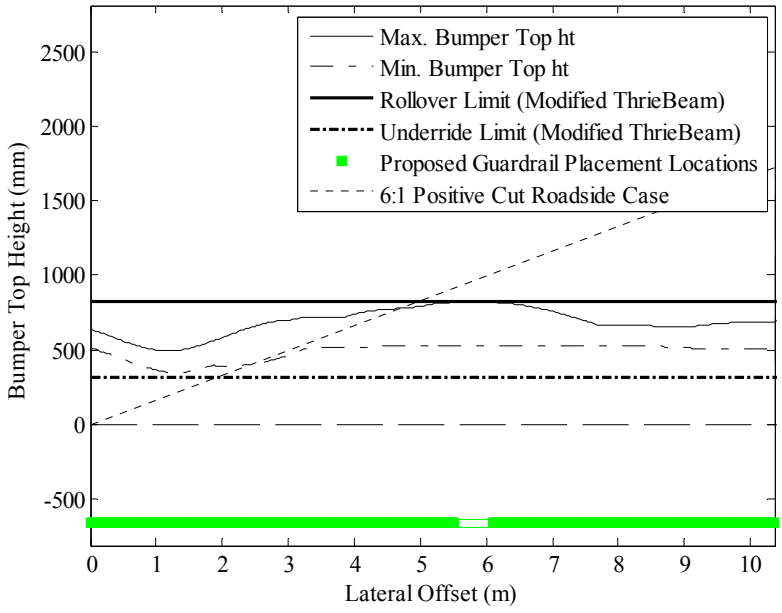

(a)

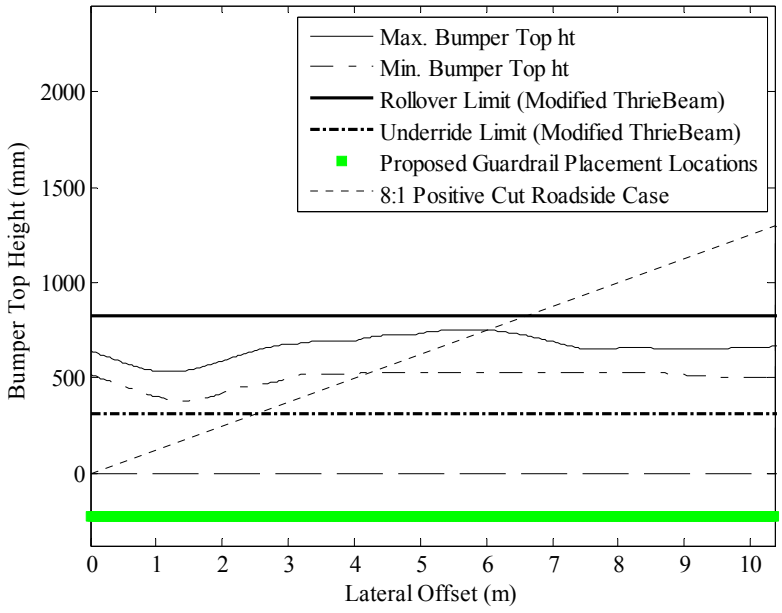

(b)

Figure E.15 Determining placement locations: Modified Thrie-beam system on positive (cut) (a) 6:1 and (b) 8:1 roadside slopes.

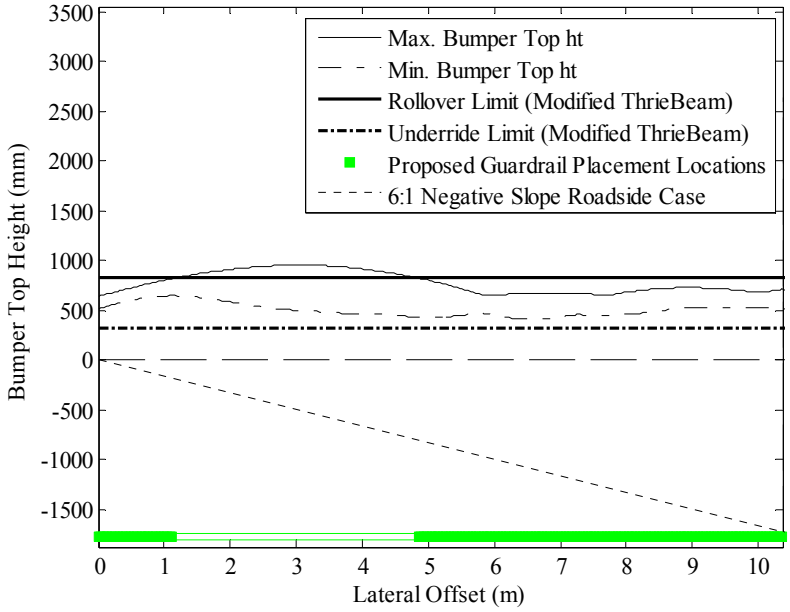

(a)

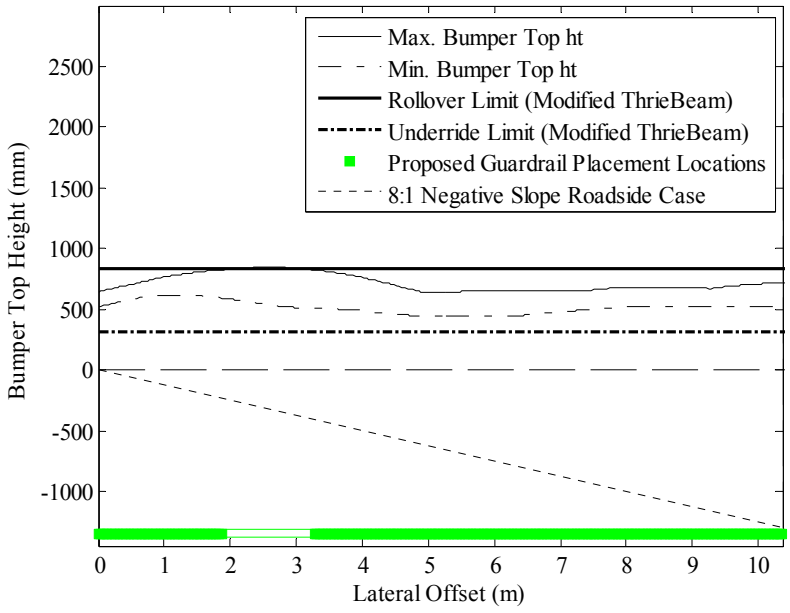

(b)

Figure E.16 Determining placement locations: Modified Thrie-beam system on negative (fill) (a) 6:1 and (b) 8:1 roadside slopes.

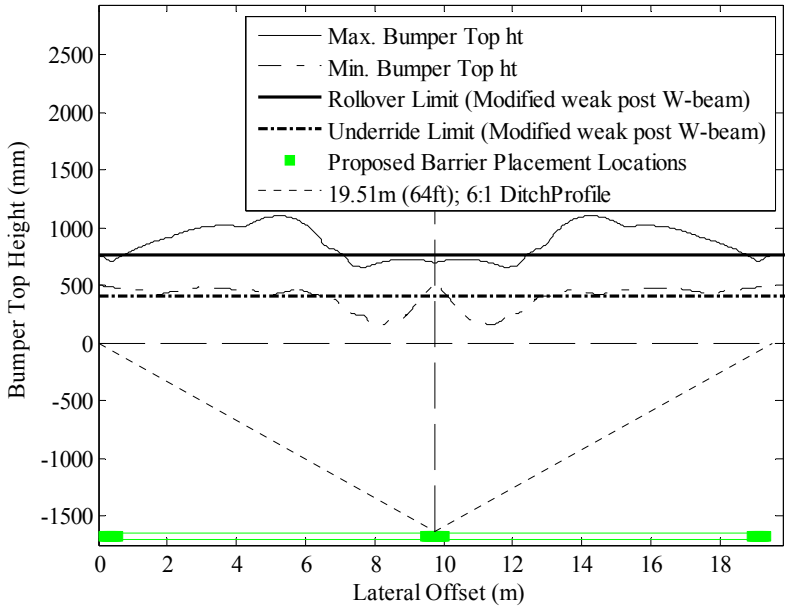

(a)

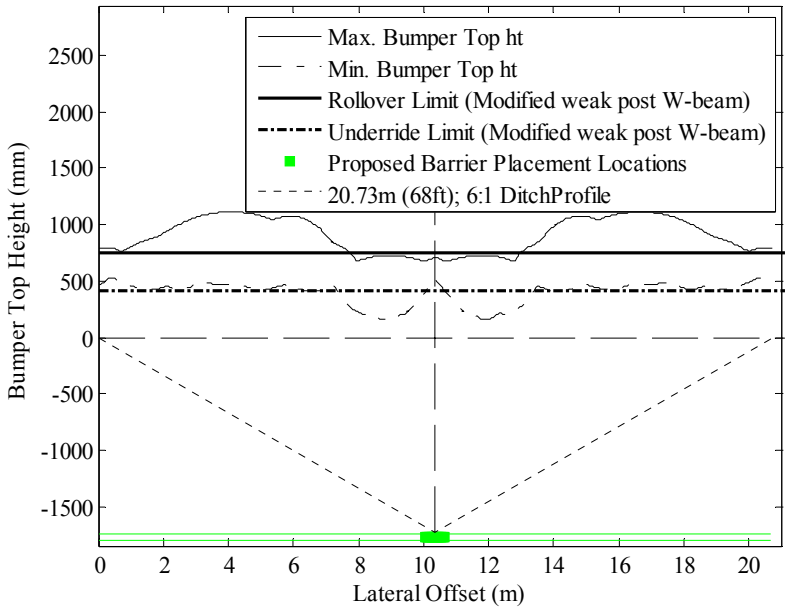

(b)

Figure E.17 Determining placement locations: Modified weak post W-beam system on a 6:1, 23.2 m (76') wide depressed median with (a) 1.8 m (6') and (b) 1.2 m (4') wide shoulders.

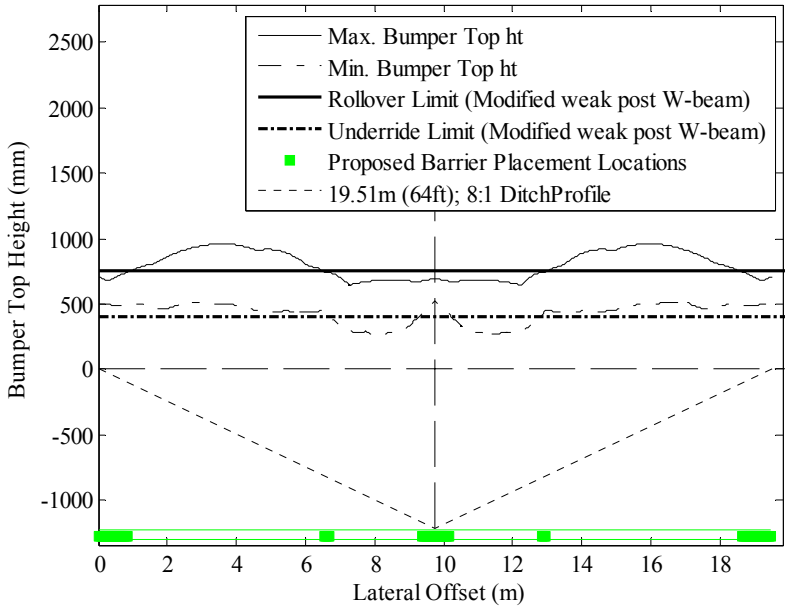

(a)

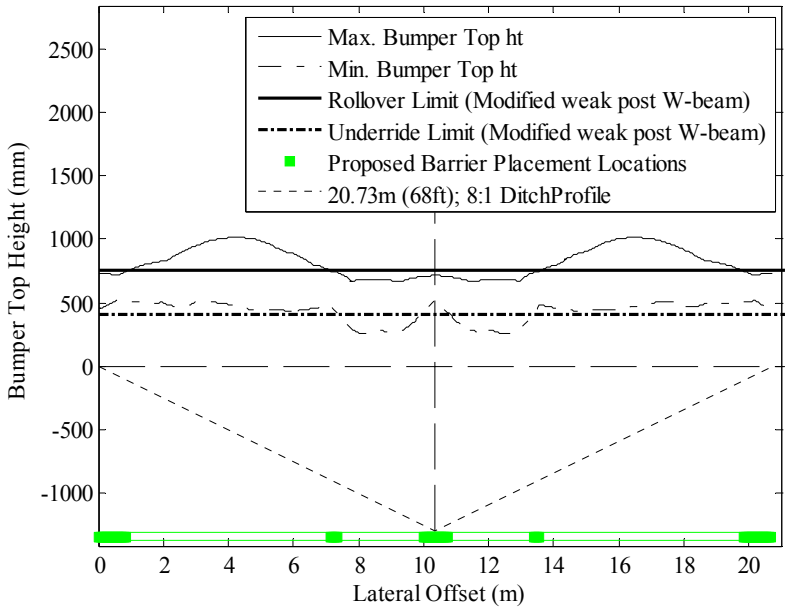

(b)

Figure E.18 Determining placement locations: Modified weak post W-beam system on an 8:1, 23.2 m (76') wide depressed median with (a) 1.8 m (6') and (b) 1.2 m (4') wide shoulders.

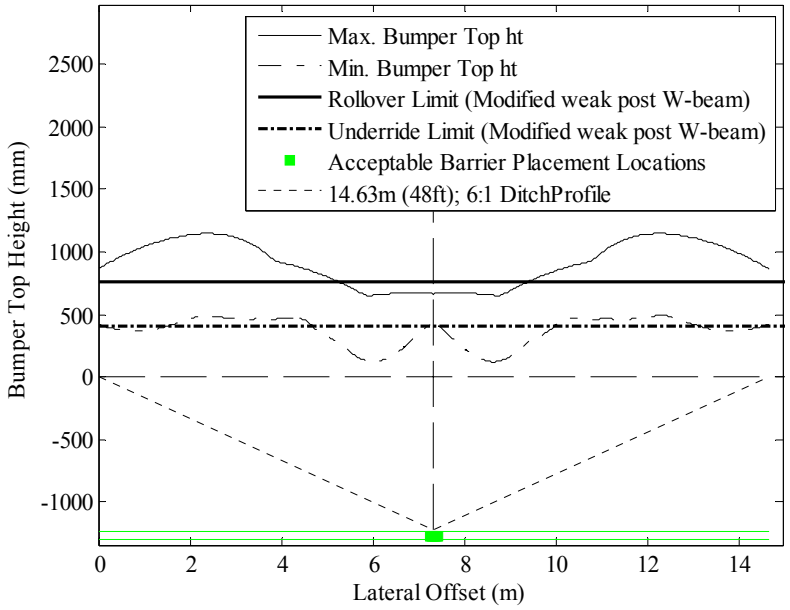

(a)

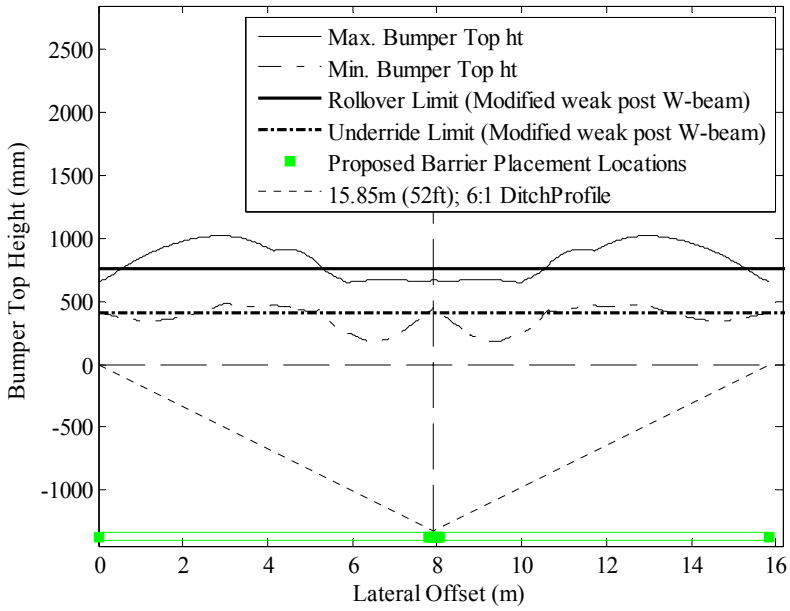

(b)

Figure E.19 Determining placement locations: Modified weak post W-beam system on a 6:1, 18.3 m (60') wide depressed median with (a) 1.8 m (6') and (b) 1.2 m (4') wide shoulders.

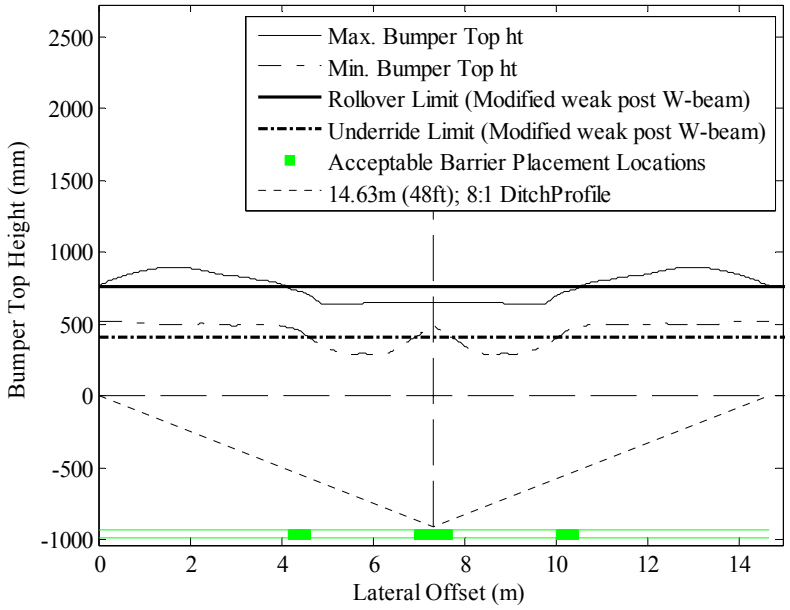

(a)

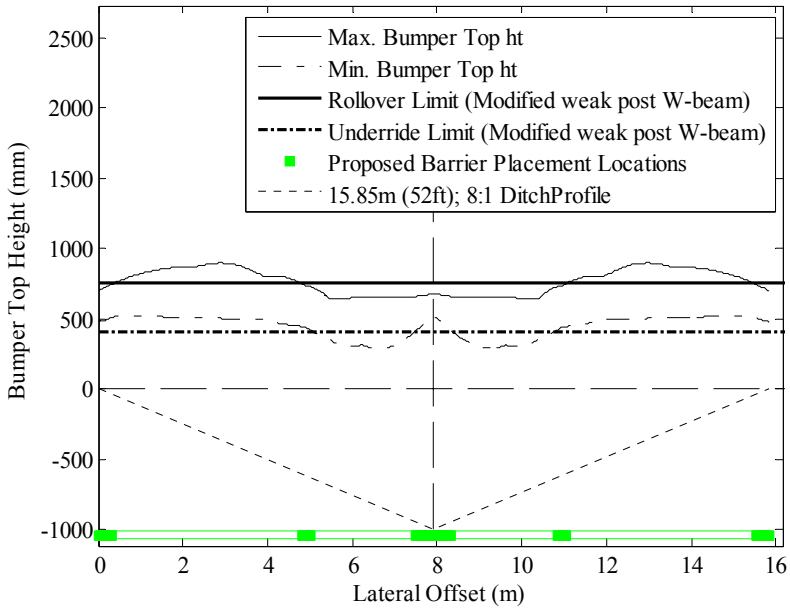

(b)

Figure E.20 Determining placement locations: Modified weak post W-beam system on an 8:1, 18.3 m (60') wide depressed median with (a) 1.8 m (6') and (b) 1.2 m (4') wide shoulders.

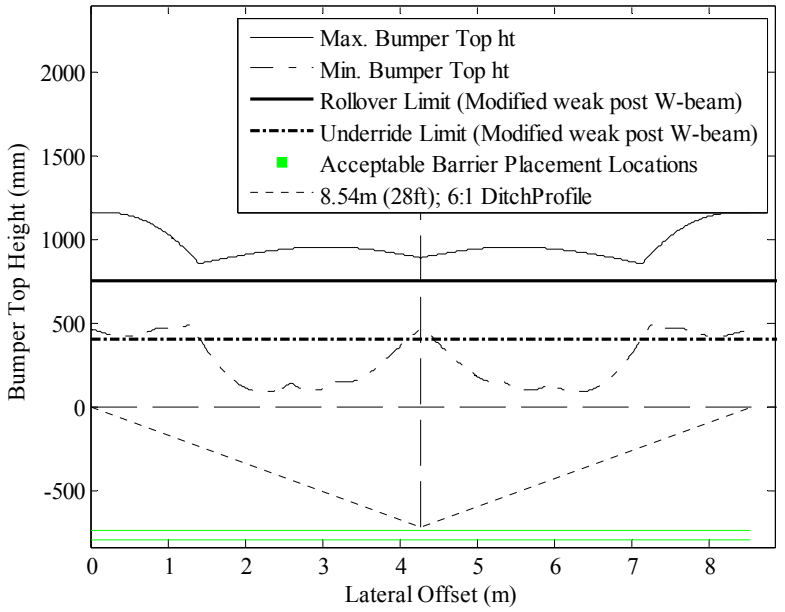

(a)

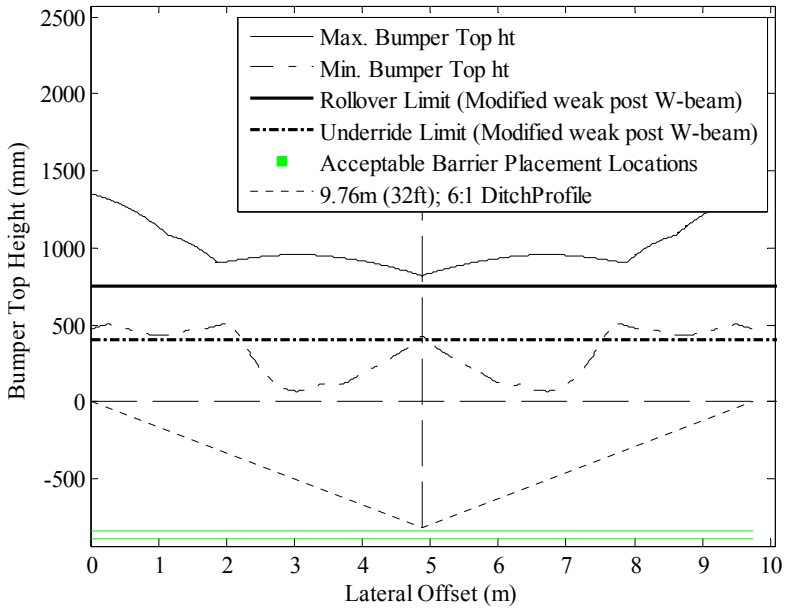

(b)

Figure E.21 Determining placement locations: Modified weak post W-beam system on a 6:1, 12.2 m (40') wide depressed median with (a) 1.8 m (6') and (b) 1.2 m (4') wide shoulders.

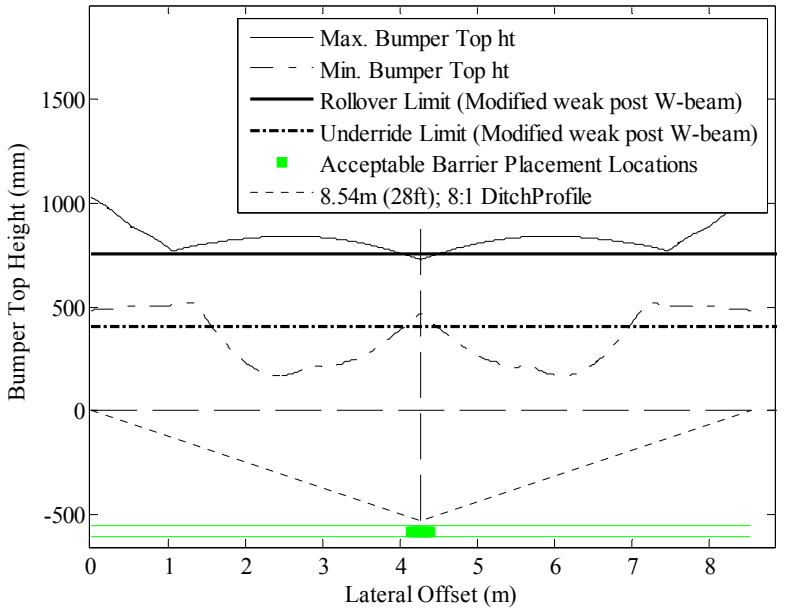

(a)

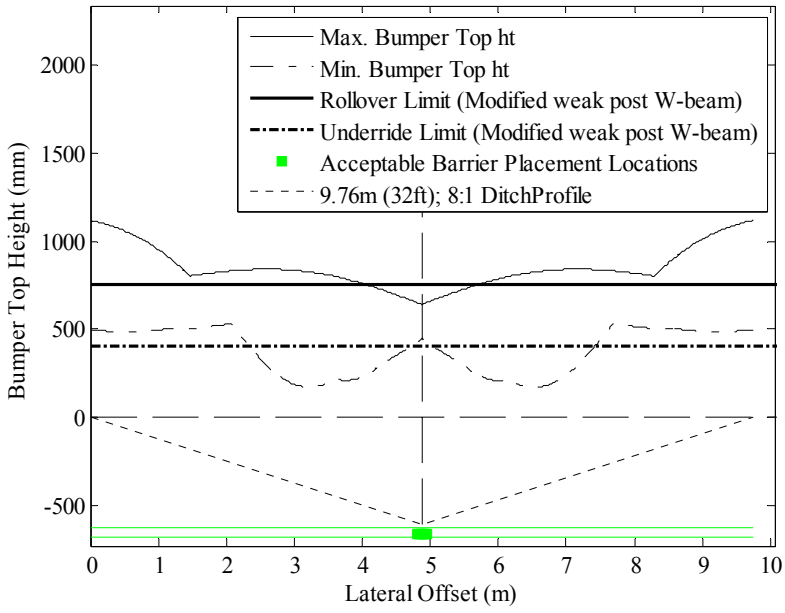

(b)

Figure E.22 Determining placement locations: Modified weak post W-beam system on an 8:1, 12.2 m (40') wide depressed median with (a) 1.8 m (6') and (b) 1.2 m (4') wide shoulders.

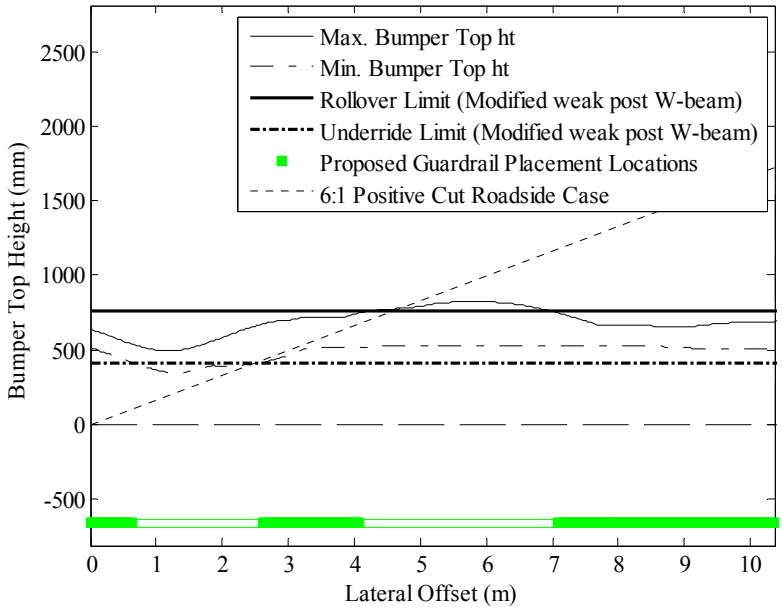

(a)

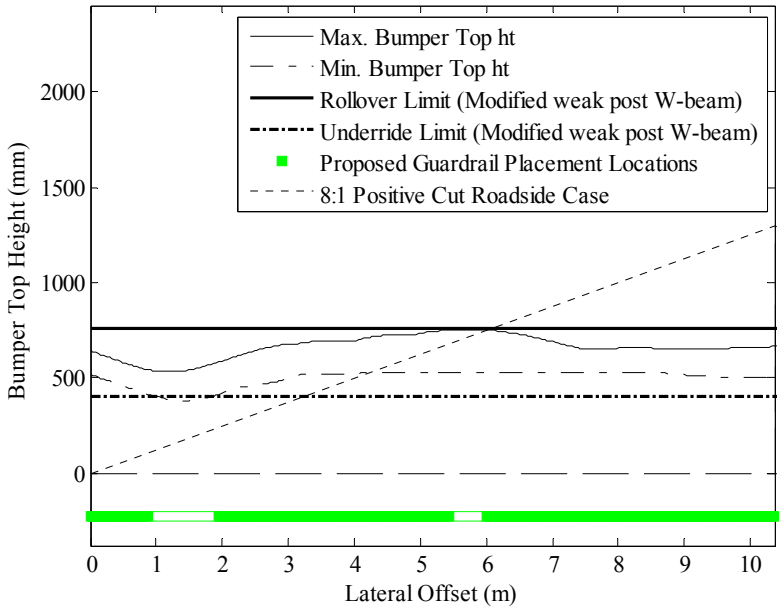

(b)

Figure E.23 Determining placement locations: Modified weak post W-beam system on positive (cut) (a) 6:1 and (b) 8:1 roadside slopes.

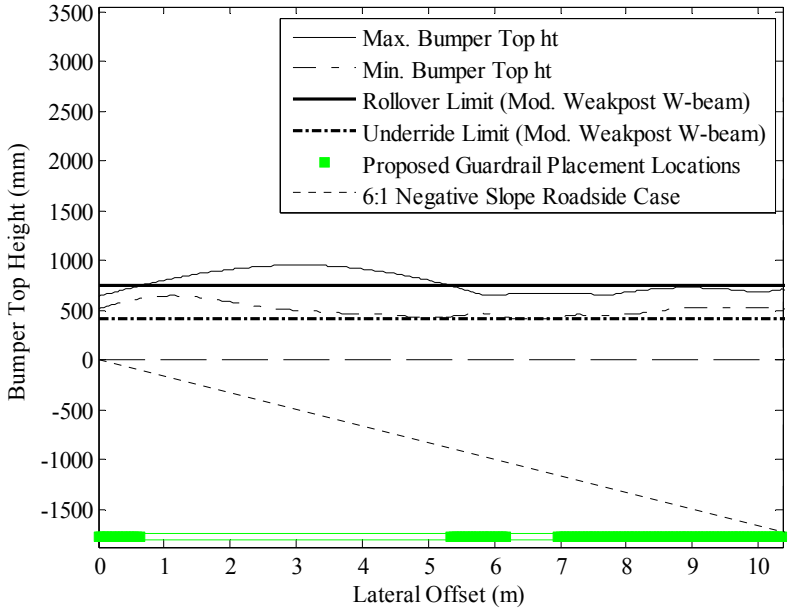

(a)

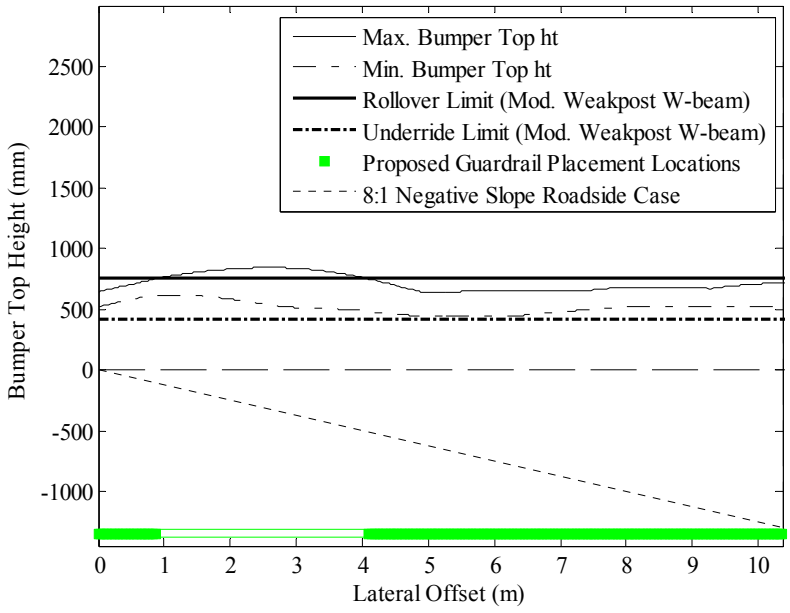

(b)

Figure E.24 Determining placement locations: Modified weak post W-beam system on negative (fill) (a) 6:1 and (b) 8:1 roadside slopes.

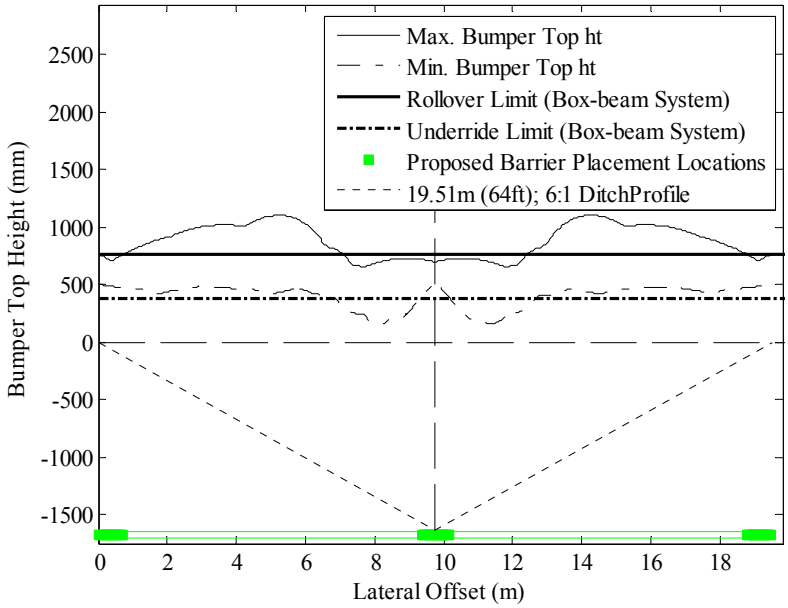

(a)

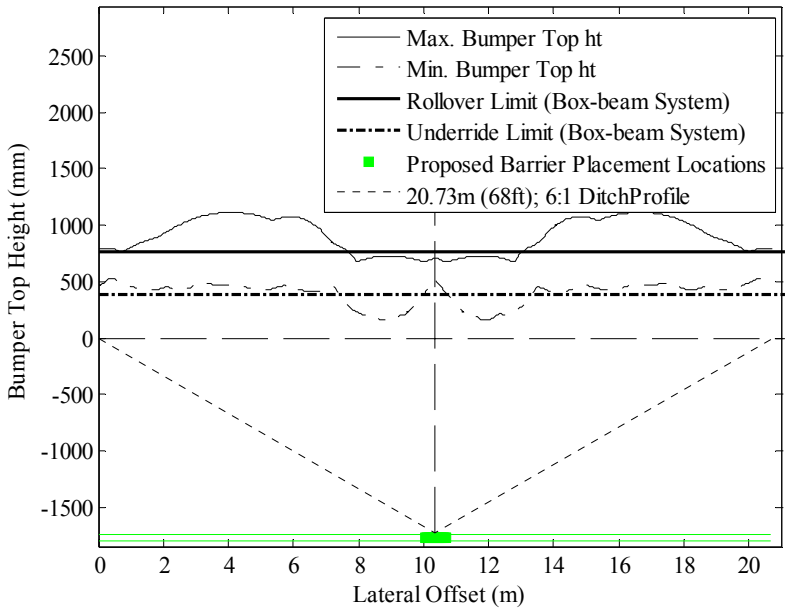

(b)

Figure E.25 Determining placement locations: Box-beam system on a 6:1, 23.2 m (76') wide depressed median with (a) 1.8 m (6') and (b) 1.2 m (4') wide shoulders.

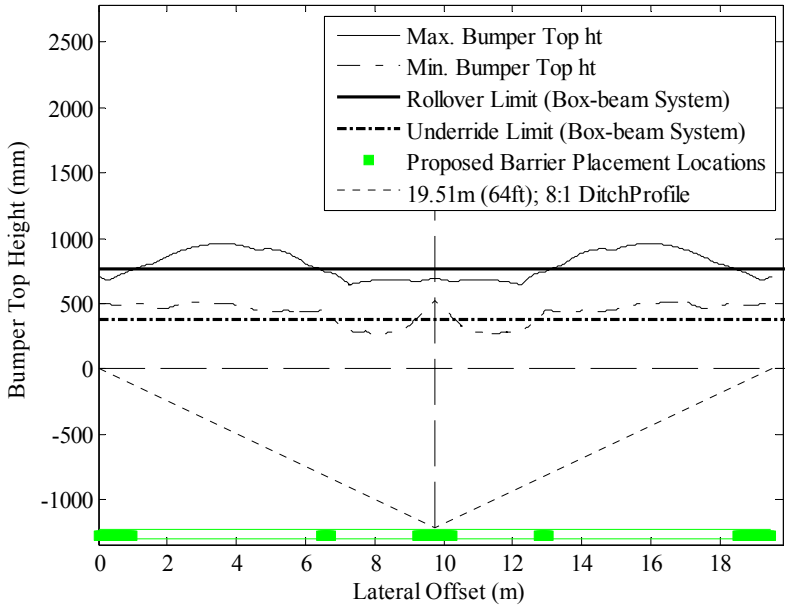

(a)

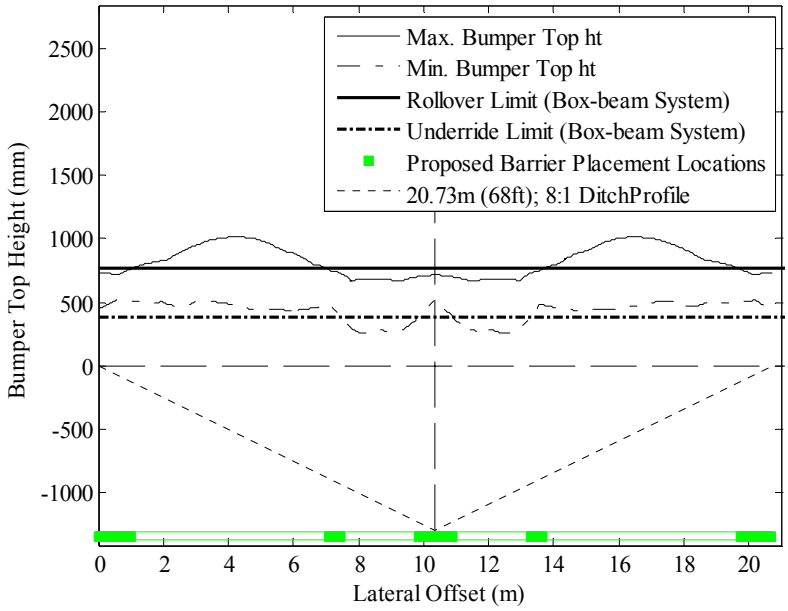

(b)

Figure E.26 Determining placement locations: Box-beam system on an 8:1, 23.2 m (76') wide depressed median with (a) 1.8 m (6') and (b) 1.2 m (4') wide shoulders.

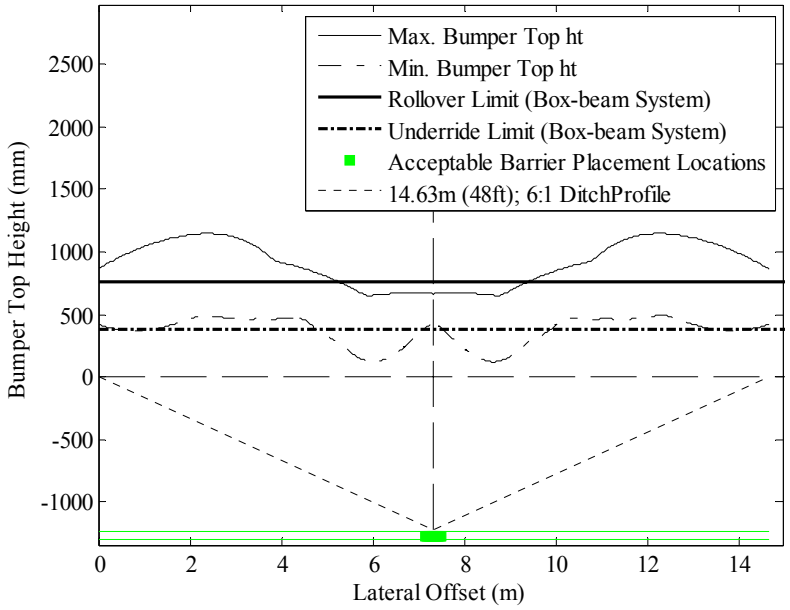

(a)

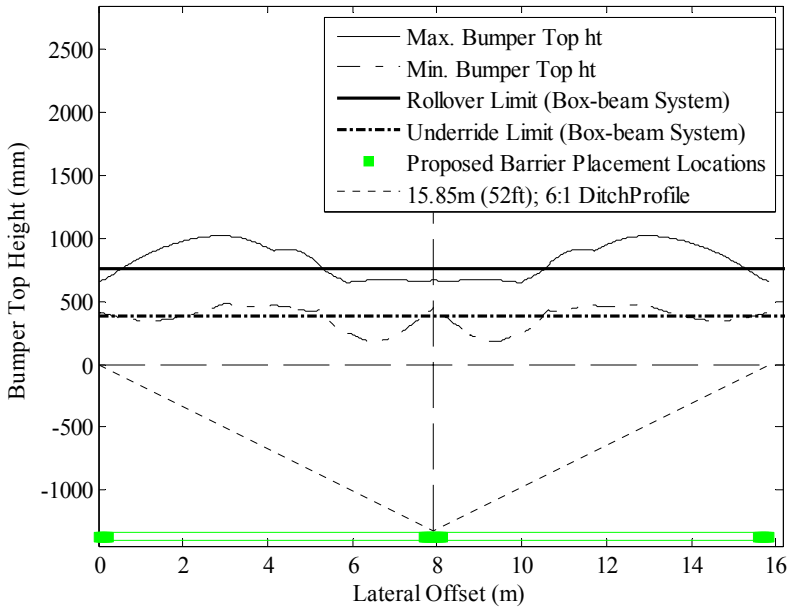

(b)

Figure E.27 Determining placement locations: Box-beam system on a 6:1, 18.3 m (60') wide depressed median with (a) 1.8 m (6') and (b) 1.2 m (4') wide shoulders.

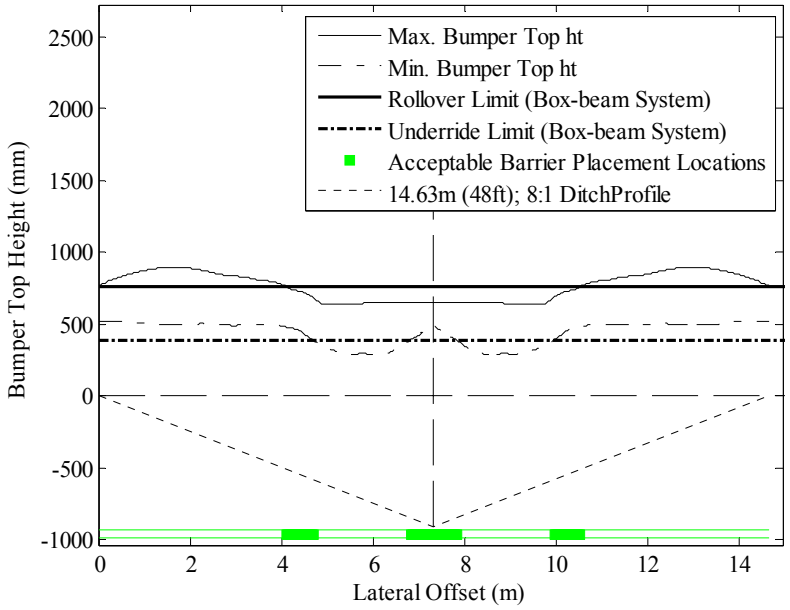

(a)

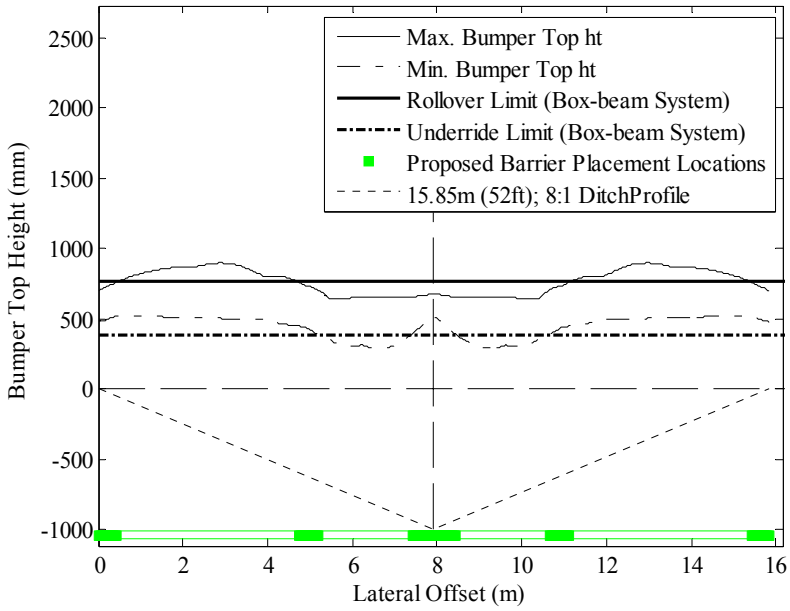

(b)

Figure E.28 Determining placement locations: Box-beam system on an 8:1, 18.3 m (60') wide depressed median with (a) 1.8 m (6') and (b) 1.2 m (4') wide shoulders.

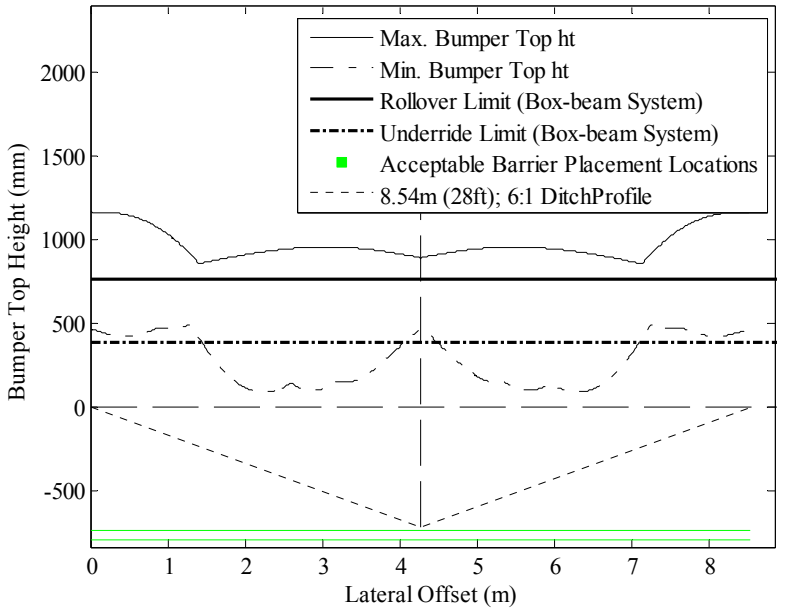

(a)

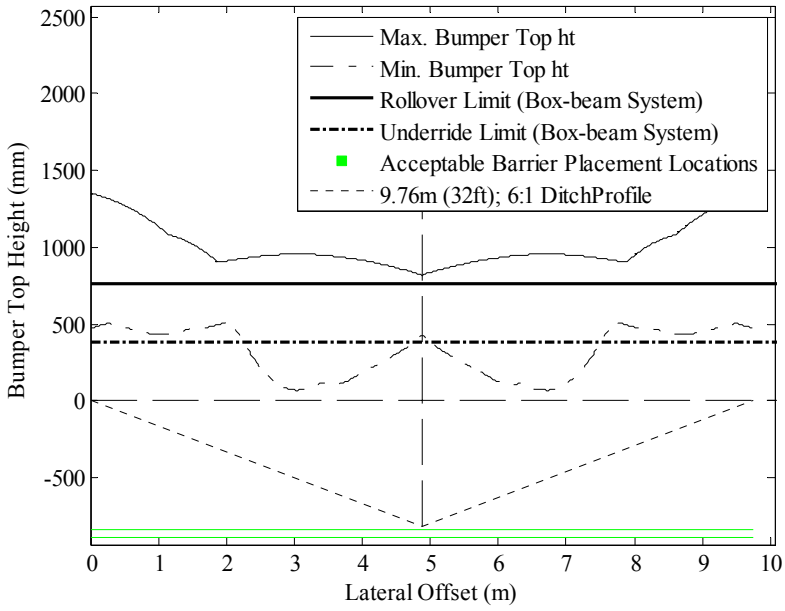

(b)

Figure E.29 Determining placement locations: Box-beam system on a 6:1, 12.2 m (40') wide depressed median with (a) 1.8 m (6') and (b) 1.2 m (4') wide shoulders.

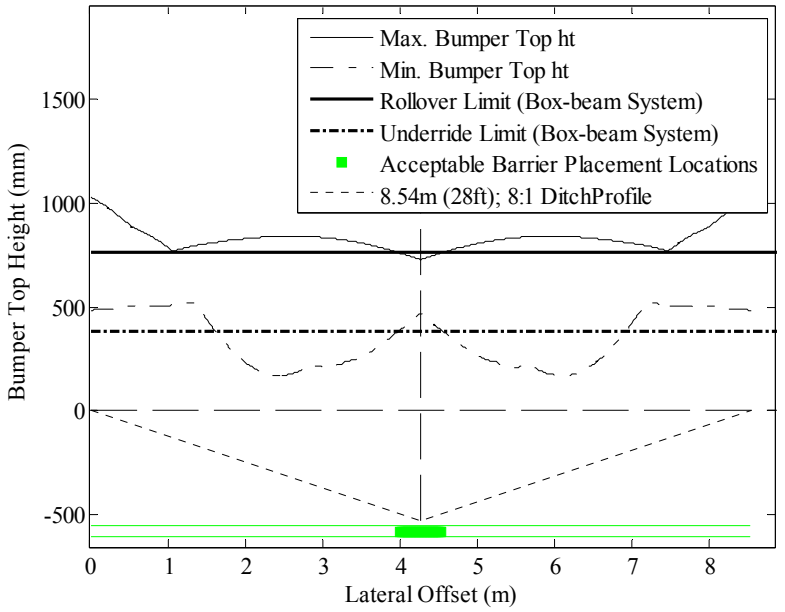

(a)

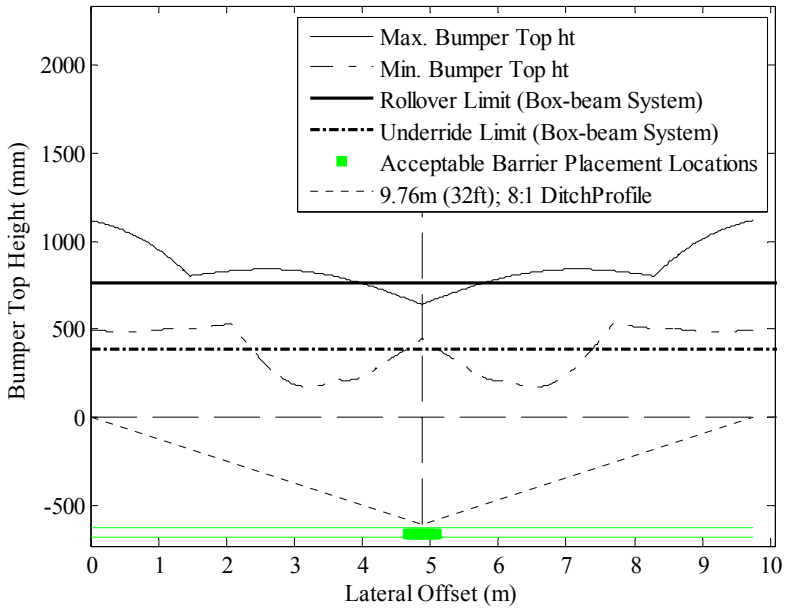

(b)

Figure E.30 Determining placement locations: Box-beam system on an 8:1, 12.2 m (40') wide depressed median with (a) 1.8 m (6') and (b) 1.2 m (4') wide shoulders.

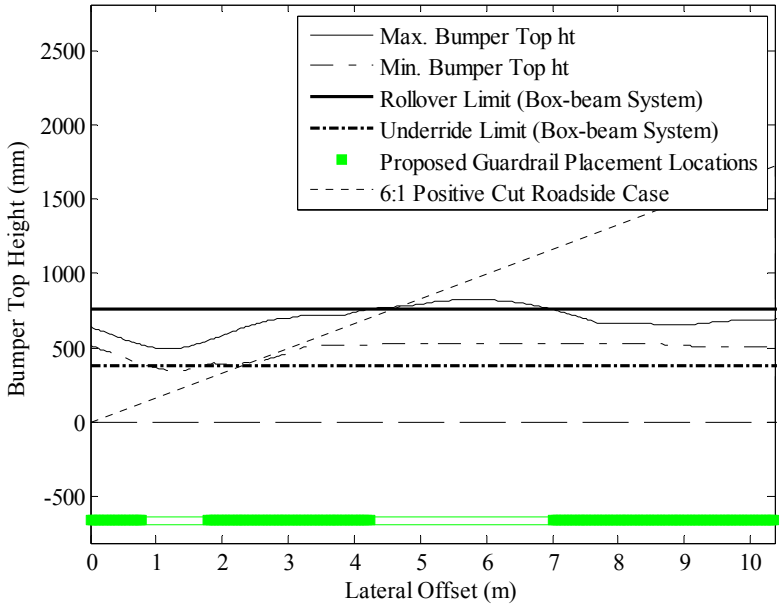

(a)

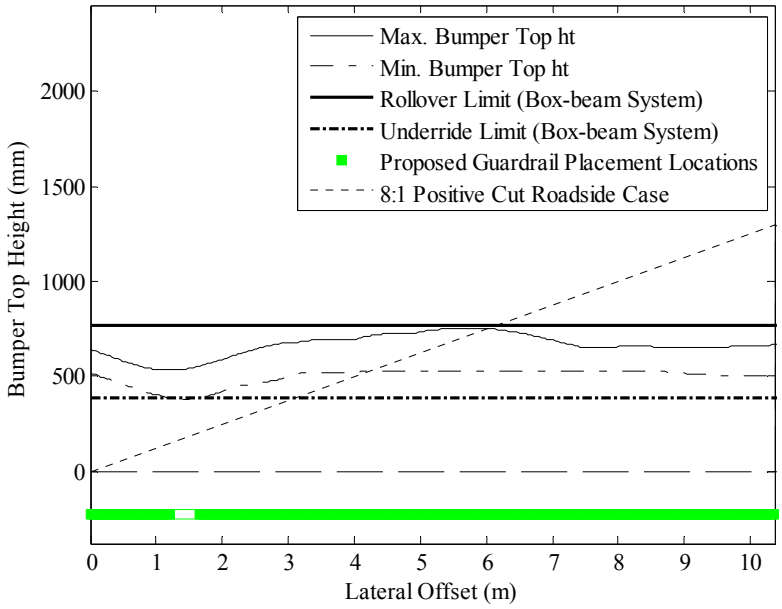

(b)

Figure E.31 Determining placement locations: Box-beam system on positive (cut) (a) 6:1 and (b) 8:1 roadside slopes.

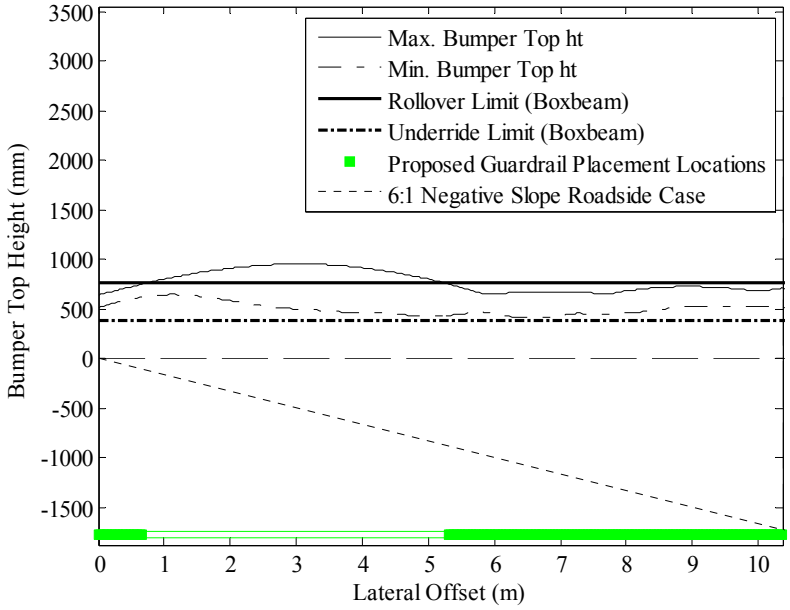

(a)

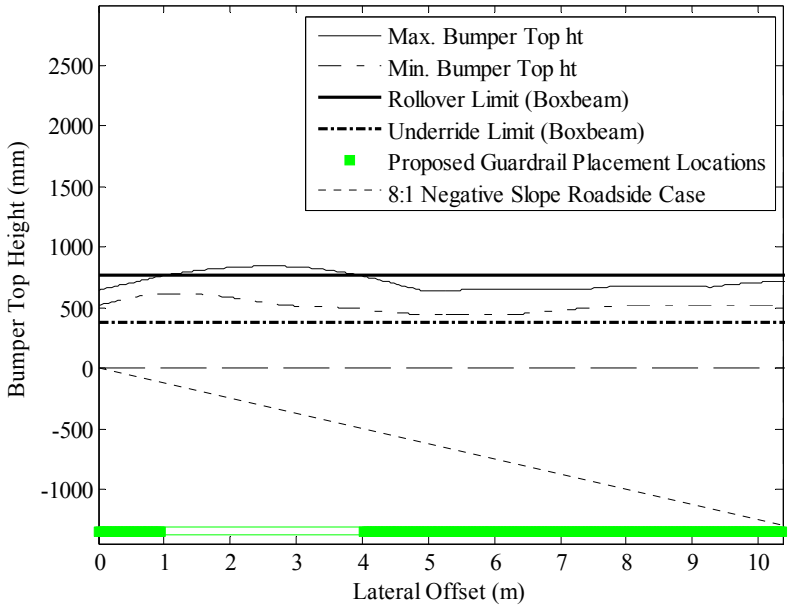

(b)

Figure E.32 Determining placement locations: Box-beam system on negative (fill) (a) 6:1 and (b) 8:1 roadside slopes.

VITA

Md Rubiat Ferdous received his Bachelors of Science degree in Civil Engineering from Bangladesh University of Engineering and Technology, Dhaka, Bangladesh in February 2003. He received his Master of Science degree in Civil Engineering with emphasis in structural engineering from Louisiana State University, Baton Rouge, LA in August 2007. After that, he joined the Zachry Department of Civil Engineering at Texas A&M University in August 2007 and received his Doctor of Philosophy degree in May 2011. His research interest includes structural mechanics, structural dynamics, finite element analysis of structural systems, roadside safety structures, and vehicle dynamics.

He can be reached at the following address:

Roadside Safety Program- Riverside 7091
Texas Transportation Institute
The Texas A&M University System
3135 TAMU
College Station, TX 77843-3135
Email: r-ferdous@ttimail.tamu.edu